Development and Characterization of Novel Nanofibrous Metal–Organic Framework Adsorption Membranes for Water Treatment

uOttawa

Johnson Effoe Efome

Thesis submitted

in partial fulfillment of the requirements for the degree of

Doctor of Philosophy in Chemical Engineering

Department of Chemical and Biological Engineering

Faculty of Engineering

University of Ottawa

19th June 2018

This work is dedicated to my grandparents

Mrs. Mary Embelle, Ikome

&

Mr. Teke Henry, Ngange

Abstract

Membrane technology has become a predominant process in providing one of the key components of life (water), either through water and wastewater treatment for water quality purposes or desalination as seen in Ultra-filtration, Nano-filtration, Reverse osmosis, Membrane distillation, Pervaporation, among others. With the ever-increasing demand for portable water due to population increase, constant research has focused on the improvements of the performances of the different water treatment systems including enhancing the performance of the membrane. Among all the different membrane performance enhancement techniques exploited, incorporation of filler has gained much grounds in the last decades. Traditional fillers like silica gel, activated carbon, metal oxides and zeolites are now being challenged by the recent class of mesoporous materials known as Metal Organic Frameworks (MOFs), which are built of metal ions or metal ion clusters linked together by organic ligands giving these materials tunable pore geometries and pore volume, greatly improved surface area with extraordinary adsorptive properties. The membrane incorporating MOFs demonstrate enhance performances more than the other fillers due to the good coordination of the organic moiety and polymers.

The overall objective of this project is to develop and study a membrane incorporated MOFs nanofiber system vis-à-vis their applications in heavy metal contaminated water treatment, stability in aqueous media and the advantages and drawbacks of these composite membranes with regards to the quality of the water produced. The developed materials were characterized by SEM, FTIR, TEM, XPS, DSC, and TGA. The heavy metals earmarked for this study include; Lead, Mercury, Cadmium, and Zinc and were studied using flame atomic absorption spectrometry (FAAS). Upon successful fabrication of the nanofiber membranes, detailed adsorption studies were conducted (pristine MOF, pristine nanofibers, enmeshed MOFs) to establish adsorption kinetics and isotherm, which were used further to select the best performing membranes for filtration application. Two different MOFs were used, MOF808; made

of Zirconium and Benzene Tricarboxylate) and MOF F300; made of Iron and Benzene Tricarboxylate) The adsorption capacities of the MOFs for the different heavy metal analyzed were; MOF 808 (Pb-170.74 mg g^{-1}, Zn-287 mg g^{-1}, Cd-225.05 mg g^{-1}, Hg-276.96 mg g^{-1}) and MOF F300 (Pb-148.13 mg g^{-1}, Hg-229.66 mg g^{-1}), while the membrane adsorption capacities were; PA808 (MOF 808 embedded within polyacrylonitrile (PA) nanofibers, (Pb-23.98 mg g^{-1}, Hg-50.88 mg g^{-1}), PA300, MOF F300 embedded within polyacrylonitrile nanofibers, (Pb-30.19 mg g^{-1}, Hg-53.09 mg g^{-1}). Upon activation of MOF 808 by water (hydractivation), the removal efficiency of MOF 808 was improved by 10% while the MOF membrane efficiency was increased by 30%. Filtration experiments could produce 577.5 L of treated water with a single layer of PAN/ MOF808 membrane at 0.1 bar using a 50 ppb Pb ion feed solution.

Résumé

La technologie de membrane est devenue un processus prédominant en fournissant une des composantes clés de la vie (l'eau), par le traitement de l'eau pour la qualité de l'eau ou par le traitement des eaux résiduaires ou le dessalement comme vu dans l'ultra-filtration, Nano-filtration, osmose d'inversion, Pervaporation notamment. Des différentes techniques d'amélioration de comportement des membranes exploitées, l'incorporation du remplisseur a gagné beaucoup des raisons pendant les dernières décennies. Les remplisseurs traditionnels aiment le silicagel, charbon actif, des oxydes métalliques et les zéolites maintenant sont contestés par la classe récente des matériaux mesoporous connus sous le nom de cadres organiques en métal (MOFs) qui sont établis des ions en métal ou des groupes d'ion en métal liés ensemble par les ligands organiques donnant à ces matériaux les géométries de pore et le volume réglables de pore, superficie considérablement améliorée avec les propriétés adsorptives extraordinaires. En raison de la bonne coordination de la partie organique et des polymères, MOF a basé des membranes tournent pour augmenter des représentations davantage que les autres remplisseurs.

L'objectif global de ce projet, est de développer et étudier les membranes polymères de nanofibre basées par MOF vis-à-vis leurs demandes de traitement d'eau contaminée de métaux lourds, de leur stabilité dans le media aqueux, d'avantages et d'inconvénients de ces membranes composées quant à la qualité de l'eau produite. Les métaux lourds affectés à cette étude incluent ; Plomb, Mercury, cadmium, et zinc. Sur la fabrication réussie des membranes de nanofibre, des études détaillées d'adsorption ont été entreprises (MOF original, nanofibres original, MOFs emmêlé) pour établir la cinétique et l'isotherme d'adsorption, qui ont été employées plus loin pour sélectionner les membranes les plus performantes pour l'application de filtration. En outre, une compréhension en profondeur du mécanisme d'adsorption a été établie et plusieurs paramètres de processus affectant le processus de filtration sur membrane ont été étudiés le long du côté.

Statement of contributions

I solemnly declare that this thesis was written by me including the designing and management all of the experimentations, characterizations and performance testing therein. All experimental setups for this project were designed, constructed and troubleshot by myself for all data collections.

My supervisors provided with concept development and experimentation guidance.

Dr. Dipak Rana provided with manuscripts revisions and submissions.

All my supervisors contributed in data analysis, discussion of results, reviewing and responding to comments from editors to produce final accepted manuscripts including this thesis.

Acknowledgement

My supervisors and co-supervisors Prof. Christopher Lan and Prof. Takeshi Matsuura and Dr. Dipak Rana have supported me in this journey through their invaluable and unmeasurable contributions from master's through Ph.D. They gave me the opportunity to stretch and test my capabilities in areas of my career I never thought of. Sincere gratitude to them for believing so much in me and putting their time and energy in this project.

Special thank you to the National Science and Research Council (NSERC) and the Fund for research, nature and technology (FRQNET) of Quebec for their financial support.

Not forgetting the works of all the Undergraduate and Graduate students through experimentations and thanks to my colleagues of the industrial membrane research institute.

I wish to extend special thanks to my friends and family for their unconditional support over the course of this journey. In particular, my wife (Sally Kange) and my daughters (Margaret, Kerry-Johnson and Eva-Johnson). The Diabe, Ngaajieh and Asonganyi families are sincerely appreciated for all the encouragements and support. Sincere gratitude to Miss H. Efange, Miss C. Mojoko and Mr. W. Mfonyo-Oben and thanks to all the members of the First Baptist Church, Ottawa for their prayers.

Finally, I am grateful to the Almighty God, through HIM wisdom, good health and Love was showered to all the participants of this project to see it to the end.

List of published and ongoing manuscripts

1) ***J. E. Efome, D. Rana, T. Matsuura, C. Q. Lan,*** Metal-organic framework supported on nanofibers to remove heavy metals, *J. Mater. Chem. A,* 2018, 6, 4550-4555
2) ***J. E. Efome, D. Rana, T. Matsuura, C. Q. Lan,*** Insight Studies on Metal-Organic Framework Nanofibrous Membrane Adsorption and Activation for Heavy Metal Ions Removal from Aqueous Solution, *ACS Appl. Mater. Interfaces: 2018, 10* (22), 18619–18629
3) ***J. E. Efome, D. Rana, T. Matsuura, C. Q. Lan,*** Effects of operating parameters and co-existing ions on the efficiency of lead removal by Nano-fibrous MOF membrane filtration process-Under Review, Chem. Eng. Jour. Manuscript #: CEJ-D-18-09723
4) ***J. E. Efome, D. Rana, T. Matsuura, C. Q. Lan,*** Experimental and modeling for flux and permeate concentration of heavy metal ion in adsorptive membrane filtration using a metal-organic framework incorporated nanofibrous membrane, *Chem. Eng. Jour*. 352 (2018) 734-744

Table of Contents

List of Figures

List of Tables

Abbreviations

PVDF	Poly (vinylidene fluoride)
PAN	Polyacrylonitrile
MOF	Metal-Organic Framework
BTC	Benzene 1,3,5 tricarboxylate
UiO-66	Universitet i Oslo-66
MIL	Material of Institute Lavoisier
PDMS	Polydimethylsiloxane
PEBA	Poly (ether-block-amide)
DMF	Dimethylformamide
DMSO	Dimethyl sulfoxide
NMP	N-Methyl-2-pyrrolidone
DMAc	Dimethylacetamide
TEOS	Tetraethyl orthosilicate
DBTDL	Dibutyltin dilaurate
HKUST	Hong Kong University of Science and Technology
NFM	Nanofiber membrane.
NMOM	Nanofibrous MOF membranes

Chapter 1: Introduction

1.1 Background

With the steady rise in global population and the associated need for continuous industrialization, pollution and contamination of water have been on the forefront, compromising essentials of life like water. Water contamination is a growing cause of degrading public health as more attention has been drawn to the anthropogenic sources of contamination. Among the contaminants of air, land and water, heavy metals have showed their omnipresence across land and water with relatively severe negative health impacts. These heavy metals have challenged the water treatment industry for decades because they cannot be degraded by natural biological mechanisms, as such, solid phase sorbents have been developed for the remediation of contaminated water. With only 3% of the available global water being fresh water, the World Health Organisation (WHO) has estimated that about 1.2 billion people live in areas were water is physically scarce and another 1.6 billion are suffering from economic water shortage where nations lack the necessary infrastructure to process ground water, river water, etc. [1]. The WHO has also set strict guidelines that water quality must meet including heavy metal ion content. For example, the maximum allowable concentrations (MAC) include; Pb (10 pbb), Hg (1 ppb), Cd (3 ppb), As (10 ppb) [2].

Technologies that are currently available for heavy metal removal include adsorption, advanced oxidation processes (AOP) [3,4] and membrane separation. For the removal of trace metals from water by conventional adsorption techniques, a relatively large quantity of the sorbent is required. Also, AOPs usually produce unwanted by-products and are substance specific. Membrane technology have proven to be a more reliable tool for water treatment, but the challenges that it is facing include inadequate removal of trace heavy metals, the effects of background or co-existing ions, membrane fouling, the low fluxes, among others.

Nanofiber membranes (NFMs) adsorption has the advantage of high surface to volume ratio which greatly enhances adsorption efficiency compared to conventional adsorption processes for an equivalent dose of adsorbent. The resistance to water flow in NFMs processes is negligible hence much higher fluxes are attainable. Compared to conventional membranes, NFMs have higher porosity, interconnected open pore structure and tailored thickness. These makes them an easy target for low pressure processes and hence avoidance of high cost high pressure operations. It is thus evident that NFMs systems are expected to be a viable and inexpensive process for the removal of heavy metal contaminants in water compared to competing technologies.

1.2 Project objectives

This project has been designed with the overall goal of developing high flux adsorptive nanofiber membranes enmeshed with metal organic frameworks (MOFs) for the treatment of heavy metal contaminated water. NFMs are chosen because of their easy preparation procedure and they have been considered as relatively high flux membranes and MOFs for their superb adsorption capacities and fast kinetics towards heavy metal ions. The treated water is expected to meet drinking water standards guidelines for Canada in terms of the heavy metal content and easy scale up for industrial purposes are to be considered as well. The required route that will be pursued to arrive at these goals are outlined in Figure 1-1 below.

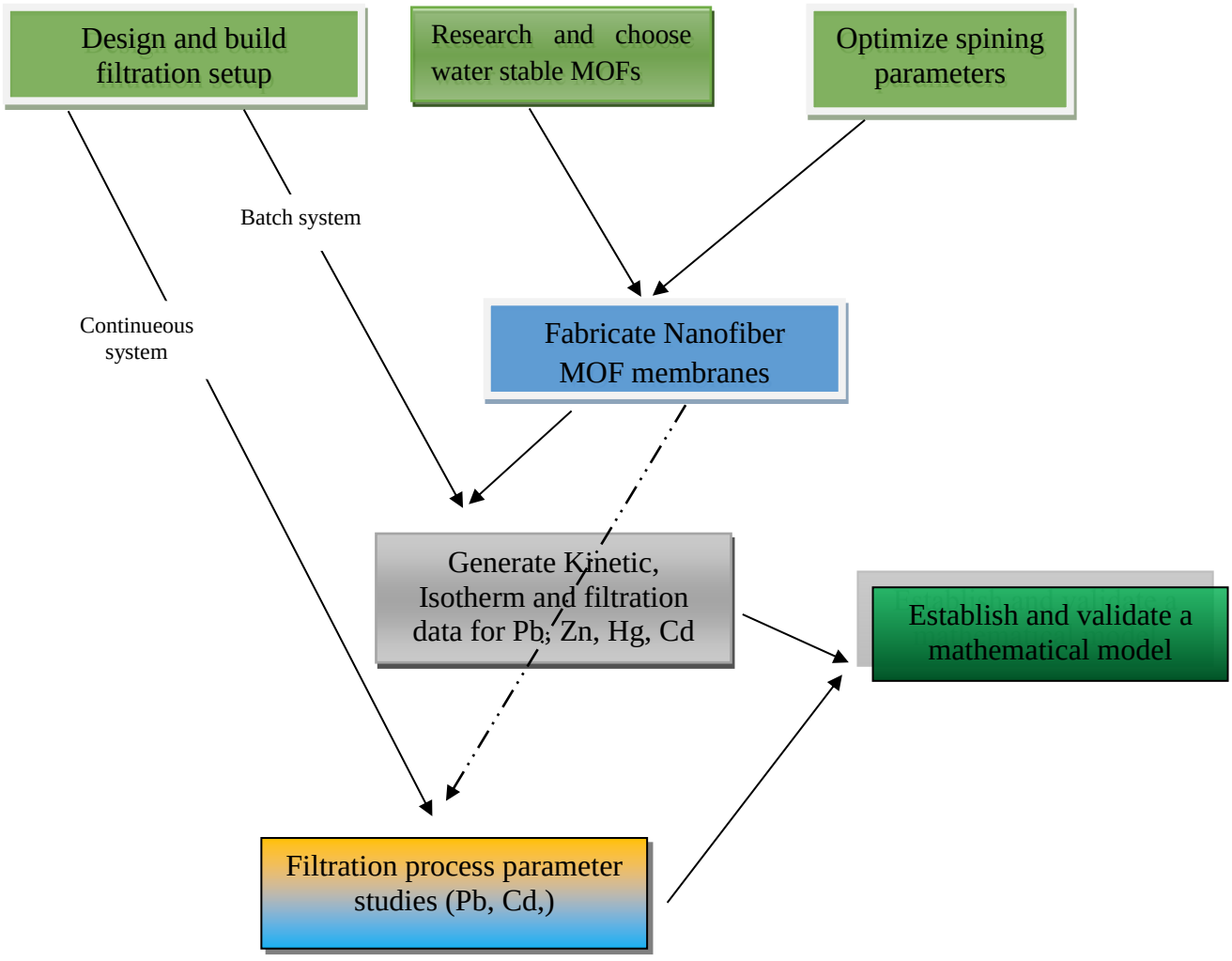

Figure 0-1.Flow sheet demonstrating the various routes to achieve project goals.

1.3 Thesis structure

Chapter 2 of this work introduces MOFs as materials for adsorption and the different routes that have been employed for their synthesis and their incorporation as fillers into polymer matrix for membrane adsorption purposes and the various techniques involved in the fabrication of MOFs membranes.

Chapter 3 builds on a proof of concept where MOFs are synthesized then incorporated into the polymer and one of the techniques discussed in chapter 2 is used in preparing MOF nanofibrous membranes to be applied for the treatment of heavy metal ion contaminated water. Two specific MOFs are targeted for preparation with two different polymers and both MOFs and MOF embedded membranes are tested for their efficiencies focusing on two specific heavy metal ions. The pristine MOF and their corresponding membranes were characterized as much as possible and an optimal membrane was selected for targeted performance experimentation.

Chapter 4 seeks to establish an in-depth understanding of the adsorption mechanism earlier discussed in chapter 3 by looking more closely at the MOF material. This chapter is intended to create a deeper understanding of the removal principles in order to be able to create room for improvement through activation of MOFs by removal of entrapped pore solvent to enhance the performances reported in chapter 3.

Chapter 5 attempts to show a mathematical model based on some performance results from prior two chapters and the following chapter 6. It tries to show a model capable of predicting the quality of the membrane filtrate when certain parameters are specified. A simple to apply yet robust model was established capable of predicting the permeate quality as filtration time changes.

Chapter 6 discusses the effect of some process parameters and how they affect the filtration process in terms of the volume of treated feed. This chapter targets specific and important parameters and shows the role they play in the volume of the sufficiently treated water, to enable treatment facilities to understand the capacity of the membrane relative to process parameters and adjust accordingly based on the process parameter been considered at the time of operation.

Finally, chapter 7 presents a conclusion of this study and proposes a road map for going forward and looking at areas where improvements could be attained, and some suggestions are made on future works.

Chapter 2: Literature review

Adsorption of heavy metals from waste and contaminated water has been achieved conventionally by use of adsorbents such as activated carbon and metal oxides in a fixed bed. The metal oxides commonly used are manganese oxide, ferric oxides, titanium oxides, aluminium oxides, and cerium oxides[5–9]. These adsorbents are well known for their high adsorption capacity and selectivity for heavy metals. However, they easily aggregate due to weak van der Waals forces and thus adsorption capacities may decrease. Also, in the fixed bed, the excessive pressure drop and the adsorbents' poor mechanical stability make them less suitable for treatment processes.

Natural adsorbents like paddy husk, corn cob, wheat bran, orange peel, coconut husk and saw dust[10] have been used for the removal of heavy metals such as Cd, Pb, Ni, and Zn. Their low adsorption capacities, slow kinetics and difficulty of regeneration limits their use for water treatment processes.

Metal organic frameworks (MOFs) are a recently developed class of materials gaining much attention as standalone adsorbents and fillers for mixed matrix membrane fabrication. This class of materials are made of inorganic metal ions or clusters linked together by organic moieties (Fig. 2-2). With diverse metal and organic combinations possible, MOFs turn out to show varied structural morphology (2D and 3D) with tunable pore geometry, exceptionally high porosity hence large surface areas, resulting in profoundly large adsorptive properties[11] . MOFs have been used as adsorbents in the adsorptive removal of various heavy metals in wastewater with high adsorption capacities and relatively fast kinetics[12]. However, much more research has been done on gas separation than on aqueous phases most likely due to the instability of most MOFs material in water. For the MOFs that have showed hydro-stability, the linkers have most often taken the credit. These linkers also play a vital role in cases where the MOFs are used in composite with other materials like polymers. Since MOF linkers are mainly organic chains, coordination bonding with the polymer is stronger, which further leads to enhancement

of selectivity and stability by preventing micro-gap formation [13]. Thus, MOFs are potentially suitable as fillers to be embedded in polymeric membranes.

2.1 Structure of MOFs

MOFs are made of two distinctive components: the secondary building units (SBU) which are the metal ions or metal clusters and the organic molecules that link the SBUs to create a 3D (Fig. 2-1) periodic meso-porous structure. The metal ion or cluster and the linkers could be substituted to produce a vast array of different MOFs. A variety of SBU could be substituted with the same linker to produce different MOFs (Fig. 2-1)

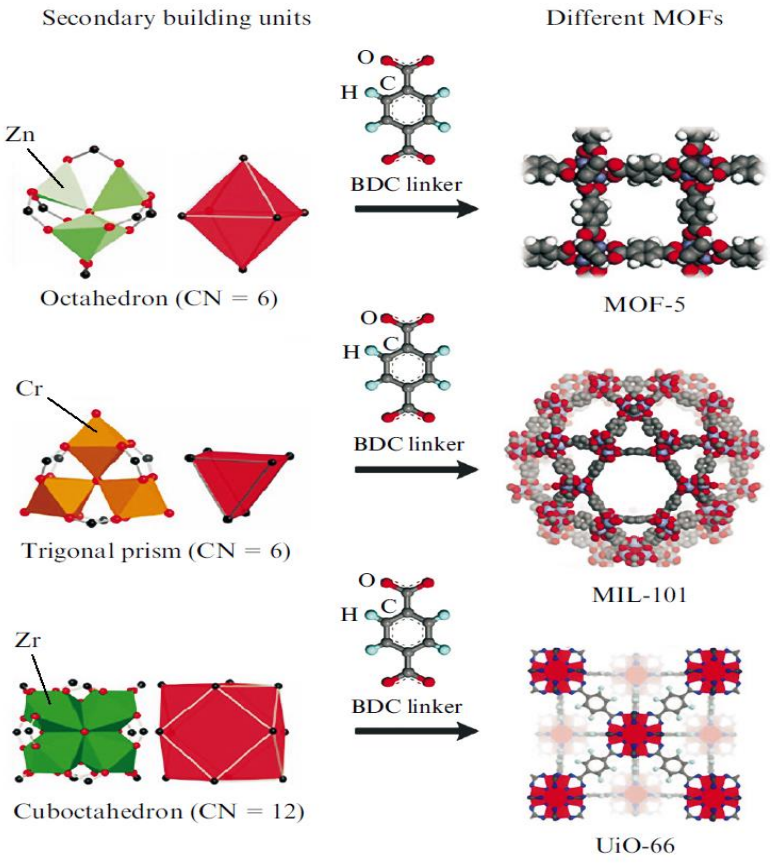

Figure 2-1. MOF structures from different metal clusters with same linker (BDC; terephthalate) [14]

A

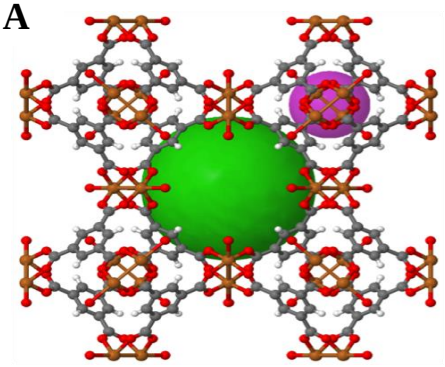

HKUST-1 (Hong Kong University of Science and Technology) is a metal organic framework (MOF) made up of copper nodes with 1,3,5-benzenetricarboxylic acid struts between them. The spheres represent the pore sizes within the framework. which can be used for heavy metal adsorption.

B

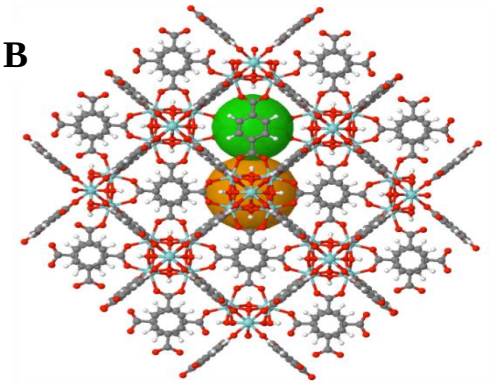

UiO-66 (Universitet i Oslo) is a metal organic framework made up of $[Zr_6O_4(OH)_4]$ clusters with 1,4-benzodicarboxylic acid struts. The orange sphere shows the primary pore size and the green sphere shows the secondary pore size, both of which can be used for heavy metal ion adsorption.

C

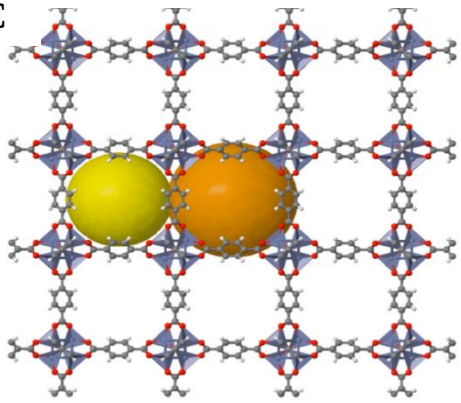

MOF-5 (sometimes called IRMOF-1) is a metal organic framework (MOF) formed from Zn_4O nodes with 1,4-benzodicarboxylic acid struts between the nodes. The spheres represent the pore size that can be used for heavy metal ion adsoprtion.

D

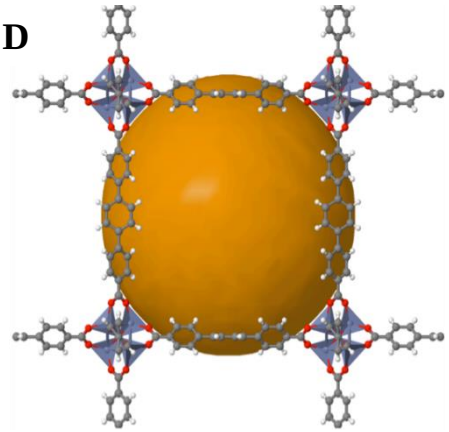

IRMOF-10, also known as MOF-10, is part of an IRMOF series based on MOF-5

(IR stands for isoreticular = based on the same net, having the same topology)

It is formed from Zn_4O nodes with 4,4'-biphenyldicarboxylate (BPDC) struts between the nodes.

Figure 2-2. Structural representation of different MOFs (CAS-Princeton University database)

Although it has been seen in gas phase separation that MOF incorporated mixed matrix membranes (MMMs) pose great potentials, other schools of thought have presented opinions that the potentials of MOFs embedded in a polymer matrix will not be completely accessible since there is a possibility of a thin polymer film build up around the MOFs particles[15]

Our interest is primarily on the use of MOF incorporated MMMs for the treatment of aqueous solutions, the different techniques which have been employed are for the preparation of MOF incorporated MMMs, a systematic analysis on the MOF stability in aqueous media, and the advantages and drawbacks associated with the use of MOF incorporated MMM for treatment of water and wastewater.

2.2 MOFs Synthesis

MOFs usually were prepared by conventional electric heating with the reaction temperature as the key parameter for synthesis. Two temperature ranges defined as solvothermal and non-solvothermal have been used to distinguish the reaction setups. Solvothermal reactions could be defined as those syntheses occurring in closed vessels under autogenous pressure and above the boiling point of the solvent. Non-solvothermal reactions occur below or at the boiling point of the solvent under ambient pressure thus simplifying the synthetic requirements.

A summary of the various synthesis routes for MOFs is shown in Fig. 2-3. The two most important and widely used techniques (microwave assisted and electrochemical synthesis) shall be discussed briefly.

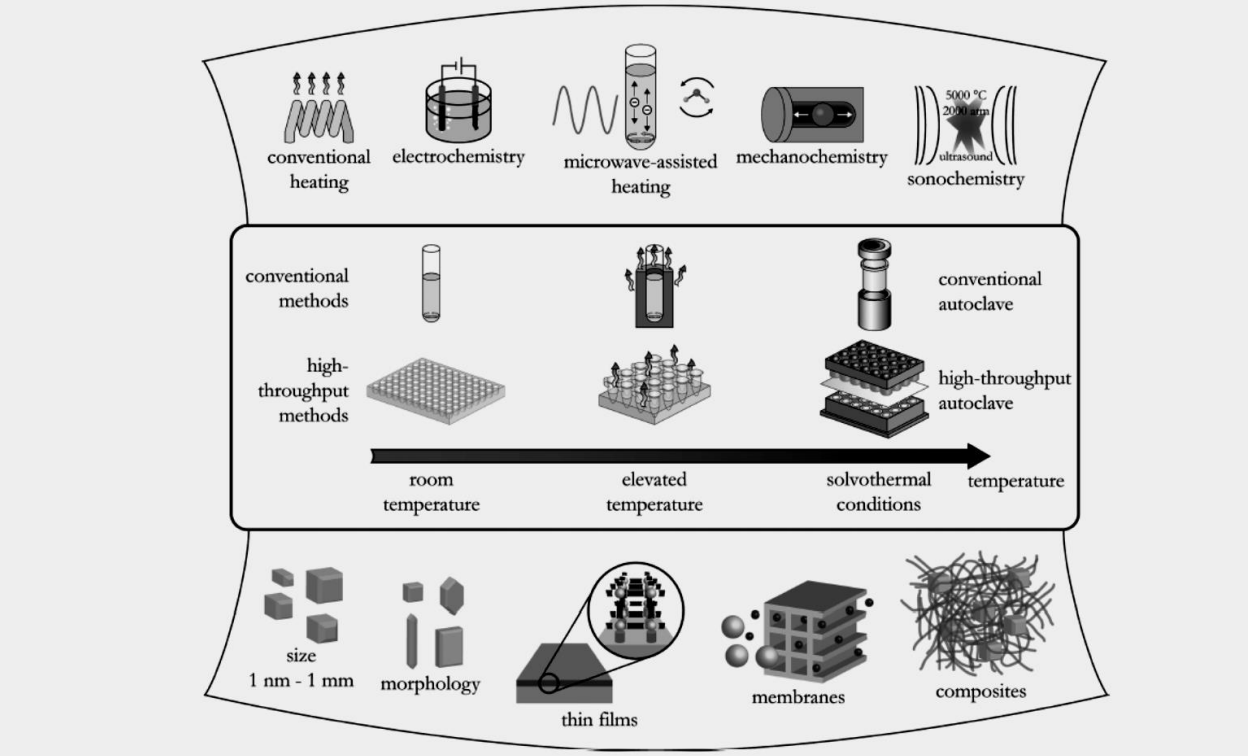

Figure 2-3. Overview of different synthesis routes for MOFs [14]

2.2.1 Microwave (MW)-Assisted synthesis

This synthesis route depends greatly on the interaction of mobile electric charges with electromagnetic waves. The electric charges could come from electron/ions in a solid or from polar solvents molecules/ions in a solution. The polar molecules in the solution will try to align themselves with the electromagnetic field as such they change their original orientations permanently. Heating in the solid is mostly due to electric resistance as an electric current is applied. In both systems, when an appropriate frequency difference is applied, it increases the oscillation and collision, hence increasing the kinetic energy of the system, i.e., temperature. Since the solution/reactants interact directly with the radiation,

MW heating is no doubt a very energy efficient means of heating. As such, MW heating provides high heating temperatures and homogeneous heating of the sample is achieved. Temperatures of MW assisted synthesis are usually above 100 ^{o}C and total reaction time not exceeding 1 h. Here, the choice of solvent and energy input should be taken into consideration since initial materials could interact with the MW radiation. This method of MW assisted synthesis has an advantage of accelerated crystallization and the formation of nanoscale products but it is also known for the purity of its products. Several MOFs of the metal (III/VI) carboxylate base have been prepared by this route especially those for Fe, Al, Cr, Ce, and Zr [16–21].

2.2.2 Electrochemical synthesis

For large scale and continuous synthesis of MOFs, researchers turn to electrochemistry for the formation of crystalline powders as first accomplished by BASF researchers in 2005 [22]. In this technique, metal ions rather than metal salts are used and introduced continuously through anodic dissolution to the reaction environment containing a conducting salt and dissolved linker molecules. Solvents like acrylonitrile, acrylic acid and other protic solvents are used to prevent deposition of metal on the cathode. The performance of MOFs produced by electrochemistry is inferior to their solvothermal counterparts due to incorporation of linker molecules and/or conducting salts in the pores of the MOF during crystallization. That notwithstanding, this synthesis route can best be used to produce MOF thin films by carefully adjusting and fine tuning the reaction conditions to grow films in the range of 2-50 μm [23].

2.3 Mechanism of Heavy metal adsorption by MOF

Several mechanisms have been reported for MOF/heavy metal ion adsorption, some of which will be discussed here and summarized in Fig. 2-4.

2.3.1 Electrostatic interactions

This is the most dominant mechanism in heavy metal adsorption using MOFs. Depending on the type of the ion being treated (Anion or Cation) the surface charge of the MOF plays a key role in the removal process. The isoelectric point (iep) will determine the pH at which the MOF carries no net surface charge. Lin et al., studied the adsorptive behaviour of Cu-BTC over methylene blue (MB). They demonstrated that, the iep of the MOF was pH 4 ±0.4, implying below this pH, the zeta potential of the MOF was positive and above pH 4, it was negative. For improved adsorption, therefore, the removal was conducted at a higher pH. In aqueous medium, MOFs usually undergo deprotonation which exposes their anionic groups for easy electrostatic interaction with cationic groups. This concept was further proven [24] during the studies of removal of dyes; methyl red, Nile red (NR) and Nile blue (NB) using the cationic MOF ($Cu(Imid)(H_2O)^+$). Since NB exists in anionic form, the cationic MOF could adsorb NB but not positive NR although NB and NR are structurally similar. This selectivity was attributed to electrostatic interactions.

2.3.2 Hydrogen bonding

Adsorption by H-bonding also occurs in removal of contaminants by MOFs which is common with organics. Several MOF/adsorbate systems have been studied to understand the H-bonding concept as seen in the studies conducted by Xie et al. [25]. Two Al-based MOFs (CAU-1 and MIL-68-Al) were used for adsorption of nitrobenzene. The presence of the μ-OH in both MOF group (Al-O-Al units) enables the H-bond formation with the nitrogen atom of the nitrobenzene. Hasan et al., [26] also studied

the pyridine adsorption over UiO-66 and NH_2-UiO-66. It was seen that there existed a preferential adsorption of pyridine to the functionalized NH_2-UiO-66 compared to the UiO-66. The N on the pyridine could form H-bonds with the H on the amino group of NH_2-UiO-66.

2.3.3 Influence of framework metal

Adsorption by analogous MOFs has been reported to show varied adsorption capacities in gas-phase and non-aqueous liquid phase adsorption systems. This influence was studied by Tong et al., [27] when they used MIL-100-Fe/Cr for the adsorption of dyes. Both of them have similar surface area (1770 and 1760 m^2/g, respectively) and pore volumes (0.76 and 0.75 cm^3/g) but in the adsorption of methyl orange (MO) in water, MIL-100-Fe showed significantly higher adsorption capacities (1045 mg/g) compared to MIL-100-Cr (211.8 mg/g). This difference could be explained in terms of the competitive adsorption of MO and water at the surface of the MOF. Adsorption of water molecules generally occurs at the aperture of pentagonal and hexagonal windows, which turns to reduce the accessibility of the MIL-100-Cr cages for the MO.

2.3.4 Pore/size-selective adsorption

MIL-101-Cr is a highly crystalline MOF material and has unique properties with the ability to tune their pore size without any significant effect on its structural properties. As a result, size selective adsorption plays a role in the adsorption to the MOFs. In the adsorption of methylene blue (MB) over MIL-101-Cr and meso-structured MIL-101-Cr [28] complete adsorption of MB was noticed with meso-structured MIL-101-Cr within 2 h, while no adsorption occurred with the pristine MIL-101-Cr over the same time frame. This clearly shows the effect of mesopores in enhancing the adsorption process. Adsorption of MB, malachite green (MG) and rhodamine B (RB) were also studied by Yao et al [29]. The neutral MOF could adsorb MB and MG but not RB due to the large size of RB creating steric hindrance and restricting the passage through the small pores of the MOF.

Other mechanism of adsorption includes pi-pi interactions brought about through the interactions of the benzene sea of electrons on the MOF with an adjacent ring from the adsorbate molecule. Also, acid-base and hydrophobic interactions have been proposed as possible adsorption mechanisms for heavy metal ions.

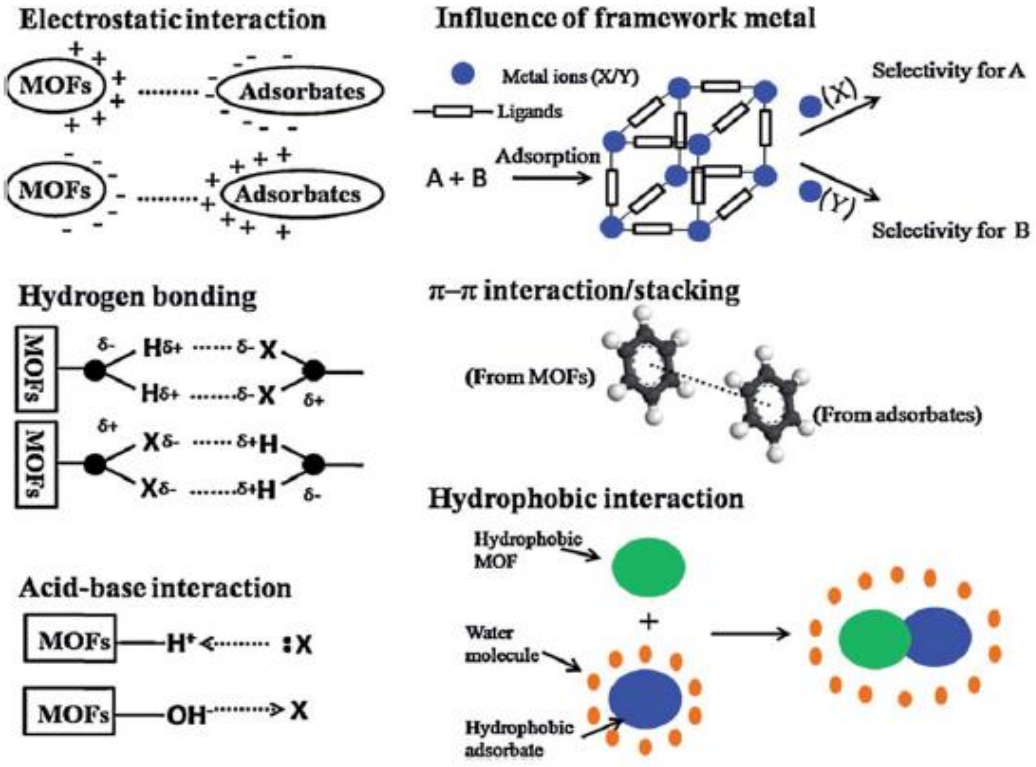

Figure 2-4. Schematic of plausible mechanism of removal of heavy metals by MOFs[30]

2.4 Structural stability of MOF in aqueous media

The first generation of porous metal-organic materials synthesized, MOF-5 and HKUST-1 showed relatively strong sensitivities to moisture making them inappropriate for use in processes that involve moisture and water. This instability mechanism has thus been studied in greater details to understand the interactions in order to develop more water and moisture resistant MOF materials applicable in both

direct and indirect water related processes. But the lack of predictive models of water adsorption is posing a challenge in the design of water resistant MOFs [31]. Fig. 2-5 below shows the comparative stability of different MOFs under varied steam conditions conducted by Low and colleagues [32].

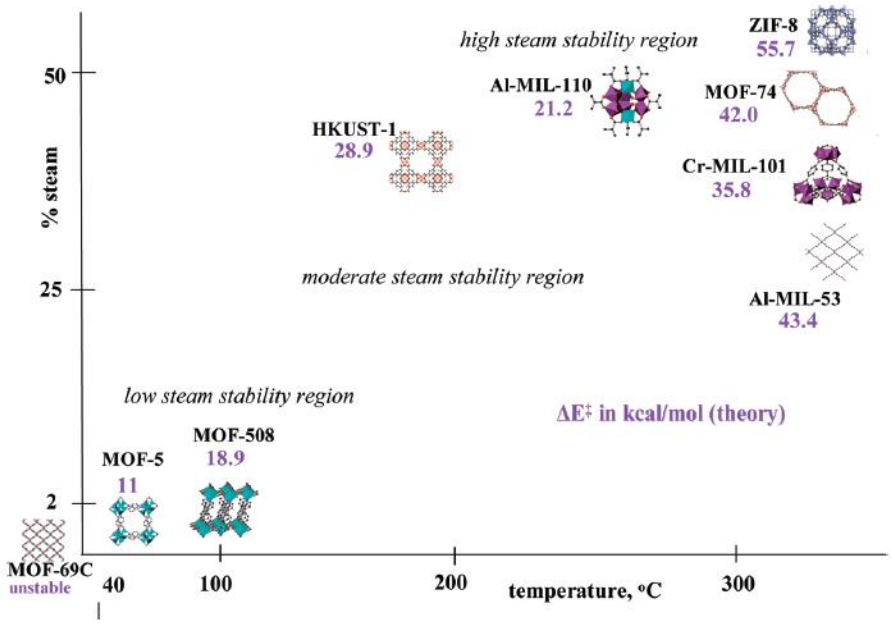

Figure 2-5. Steam stability map of MOFs. The position of the structure for a given MOF represents its maximum structural stability as probed by XRD measurements, while the energy of activation for ligand displacement by a water molecule as determined by molecular magenta numbers (kcal/mol) [32]

It is observed from the figure that, some of the MOFs fall on the higher steam stability region, at high water loading as is the case with water treatment application, the MOF is unstable.

Since this discussion focuses on the use of MOFs as candidates for water treatment processes, this section will dwell more on the stability of the MOF when applied to aqueous systems. The crystallinity, pore volume along with the adsorption potentials when exposed to water (liquid) shall be reviewed.

It is of utmost importance that during the water treatment process, the stability of the MOF should not be compromised. This could either lead to the central metal ion displacement causing leakage into the

process stream or the MOF could lose its adsorption ability earlier than presumed. These adversely affects the amount of feed the process can treat, resulting from structure collapse (pore volume shrinkage). The structural stability of MOFs in water and water vapor depends on several factors, which this section will try to outline in an un-exhaustive representation (Fig. 2-6).

2.4.1 Metal-ligand bond strength

The stability of any compound has always been linked to the bond strength of the elements that make up the compound. In MOFs, the center metal ion is always bonded to the ligand through a ligand oxygen /nitrogen moiety. As already known in bond chemistry that bond length in most cases determines the bond strength (the shorter the bond, the more stable it is). The stability of MOFs in water has also been associated to the metal-oxygen or metal-nitrogen bond strength and the ability of the ligand to shield the inorganic metal node from direct attack by water molecules. A comparison of some metal-ligand bond energies of divalent metals explains why MOF-5 is unstable in water compared to HKUST-1 while MIL-101 is more stable than HKUST-1. MOF-5: (Zn-O, 365 kJ/mol) < HKUST-1: (Cu-O, 372 kJ/mol) < MIL-101: Fe-O (468 kJ/mol).

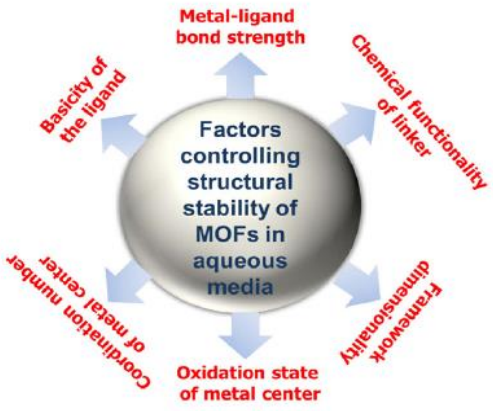

Figure 2-6. Factors controlling the structural stability of MOFs in aqueous media [33]

2.4.2 Ligand basicity

The research into MOFs has seen tremendous improvement to the extent that many different ligands have been developed to produce MOFs to suit varied purposes (Fig. 2-1). The structural stability of a MOF has also been associated to the basicity of the ligand with the more basic linkers capable of forming stronger metal-ligand bonds than less basic linkers. The imidazole linkers (p*K*a ≈ 18.6) and pyrazole linkers (p*K*a ≈ 19.8) with relatively higher pKa values turn to be more hydrothermally stable than the carboxylates (p*K*a ≈ 5) and pyridine (p*K*a ≈ 5) due to the higher p*Ka* of nitrogen-based linkers found in the imidazole and pyrazole (ZIFs) compared to the weaker p*Ka* oxygen-based linkers of the carboxylates. Certain members of the carboxylate based MOFs like UiO-66 (Zr), MIL-101(Fe), MIL-125(Ti), MIL-53(Al) and MIL-101(Cr) have also been proven to be structurally stable in aqueous media[34,35], which implies not only does the basicity of the linker and strength of the metal-ligand bond affects the structural stability of the MOF, and other factors also play key roles in aqueous media stability (Fig. 2-7).

2.4.3 Metal center and coordination number

It is very much understood that compounds with high coordination number metal ions are more stable than those with lower coordination number metal ions. MOFs metal ion coordination numbers are usually 4 (tetrahedral) and 6-8 (octahedral) Fig. 2-7. In the octahedral state, the metal ion is saturated thus posing a higher energy barrier for a water molecule to react with the metal as opposed to a lower energy barrier in a tetrahedral unsaturated state, thus leading to linker displacement in aqueous media.

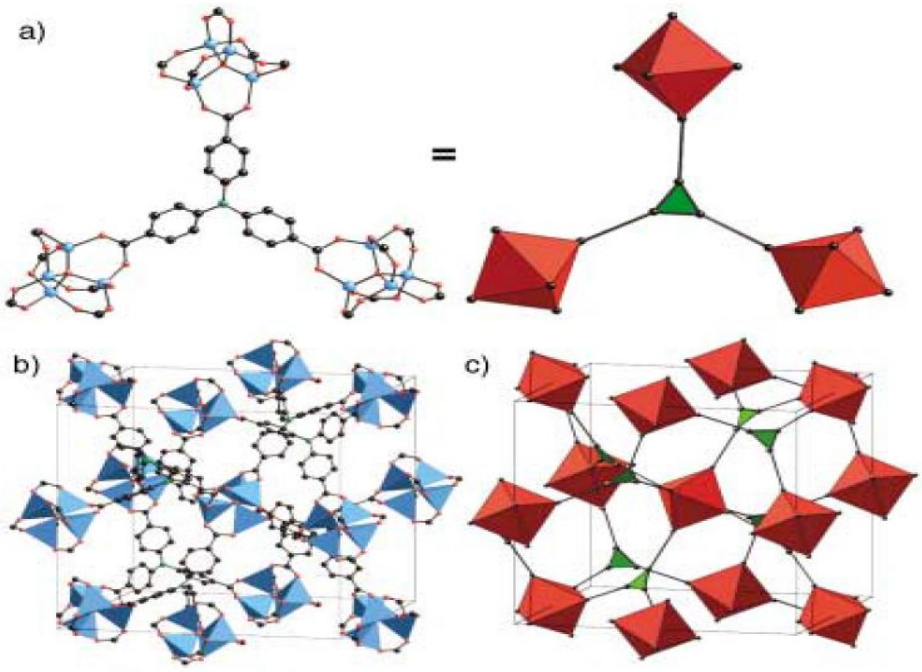

Figure 2-7. a) DCA unit linked to three octahedral SBUs. Zn blue, O red, N green, C black. b) One net of MOF-150 with ZnO_4 tetrahedral (blue) filled in c) as (b) but stylized [36]

This phenomenon has prevailed in the explanation of the unstable nature of Cu-BTC in aqueous medium and high stability of UiO-66 in aqueous medium. Liu and coworkers [37], studied UiO-66 stability in aqueous media for a period of 100 days. The PXRD data showed a highly stable MOF (Fig. 2-8). Cu-BTC has two central Cu ions bonded to four of the tri-carboxylates resulting in a tetrahedral coordination similar to Fig. 2-7a above. It is thus evident that, the unsaturated Cu ions are susceptible to attacks by water molecules and other small molecules with free electrons to form other complexes.

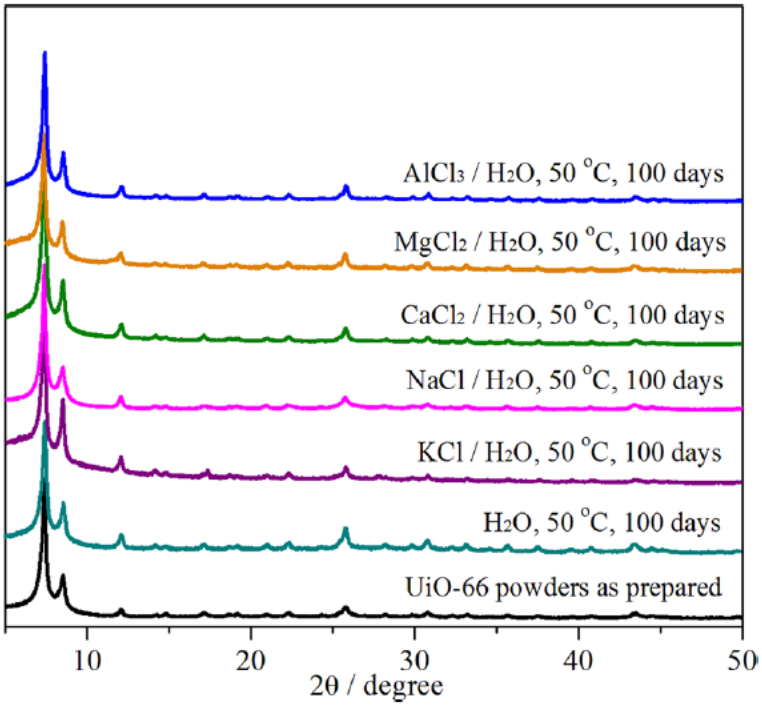

Figure 2-8. PXRD pattern of UiO-66 powders, as-prepared and after stability test [37].

On the other hand, UiO-66 is very much water stable due to the saturated nature of the Zr metal ion. UiO MOF lineage has twelve- $Zr_6O_4(OH)_4$ coordinated to terephthalate ligand as shown in (Fig. 2-7a). The Zr central metal in this MOF thus has a coordination number of 8, hence saturated, making it difficult for water and other small molecules to access the metal.

The type of central metal ion carried by the MOF has also been studied for stability in aqueous medium. A series of frameworks M(BDC)(TED) were studied [38] to better understand the role played by the central metal ion. (M=Cu, Zn, Ni, Co, BDC= 1,4 benzene-di-carboxylate, TED = tri-ethylenediamine). Experimental analysis using PXRD of these MOF after interaction with water revealed that the central metal ion was a contributor to the decomposition of the MOF. In the case of Cu $(BDC)(TED)_{0.5}$, a hydrolysis reaction of the Cu-O-C group was observed to induce the paddle-wheel structural decomposition. In the case of the other MOFs (Zn and Co frameworks), the water molecules gradually

replaced the TED pillars and bonds to the apical sites of the paddle-wheel $Zn_2(COO)_4$ and $Co_2(COO)_4$. It was further concluded that the trend observed in the MOF series followed the bond dissociation energies of the diatomic metal-oxygen complexes and the metal-amine complex stability constants. Thus, the isostructural MOF hydrothermal stability follows the order of Co-MOF > Zn-MOF > Ni-MOF > Cu-MOF.

2.4.4 Metal oxidation state

Metal ion or metal clusters with higher oxidation state or numbers generally form stable compounds when bonded. Serre et al., (2002) demonstrated that the Cr^{3+} ion found in MIL-53-Cr contributed in the structural stability of the MOF when compared to the Cr^{2+} contained in MIL-101-Cr. It must be noted that, the oxidation state on its own has relatively little effect on the stability but for the fact that M^{3+} metals usually form octahedral bridges with the linkers hence making the M-O bond very water resistant. This hypothesis was studied by comparing the isostructural MOF MIL-53-(Al, Cr) [34] and found that the Al-O bond strength (514 kJ/mol) was similar to the Cr-O bond strength (514 kJ/mol) but further analysis revealed that, the activation energy for displacement of the linker by hydrolysis was 43.5 kcal/mol for Al^{3+} and 30.4 kcal/mol for Cr^{3+} proving why MIL-53-Al turns to be hydrothermally stable than MIL-53-Cr. This concept was further validated [39] using two different Al based MOFs (MIL-53 and MIL-110). Since the Al in the MIL-110 is linked through an octahedral lattice to the BTC linker, it showed enhance hydrothermal stability than MIL-53-Al.

2.5 MOF incorporated membrane synthesis for liquid phase applications

While most MOF incorporated membranes have been applied for gas separation, several MOF incorporated membranes have been applied in the treatment of aqueous and non-aqueous liquids. Irrespective of the technique and process, membrane dope always comprises of a suitable polymer, suitable solvent and the filler (MOFs). Several polymers including Polyvinylidene fluoride (PVDF), Polyvinyl alcohol (PVA), Polydimethylsiloxane (PDMS), Polyacrylonitrile (PAN), and polyether block amide (PEBA) are the most common because of the chemical and mechanical stability, the ease at which they dissolve in most solvents like Dimethylacetamide (DMAc), N-Methyl-2-pyrrolidone (NMP), Dimethyl sulfoxide (DMSO) and Dimethyl formamide (DMF).

Considering the flexibility and the ease of application, non-solvent phase inversion separation is among the common techniques for preparing MOF-MMM for liquid phase treatment. Here, a coagulation bath, usually water is used to induce a solvent/non-solvent exchange with the end point being the solidification of the polymer to form porous flat sheets. Three different MOFs (based upon Iron, aluminum and copper) [40] were used to prepare ultrafiltration membranes by phase inversion (precipitation immersion) method shown in Fig. 2-9. 1 wt. % MOF was dispersed in the polymer /solvent mixture, followed by sonication and immersion into a coagulation water bath. The resulting membranes showed good porosity (>80%), enhanced rejection with dextran and also a permeability of up to 260 L/m^2 h bar.

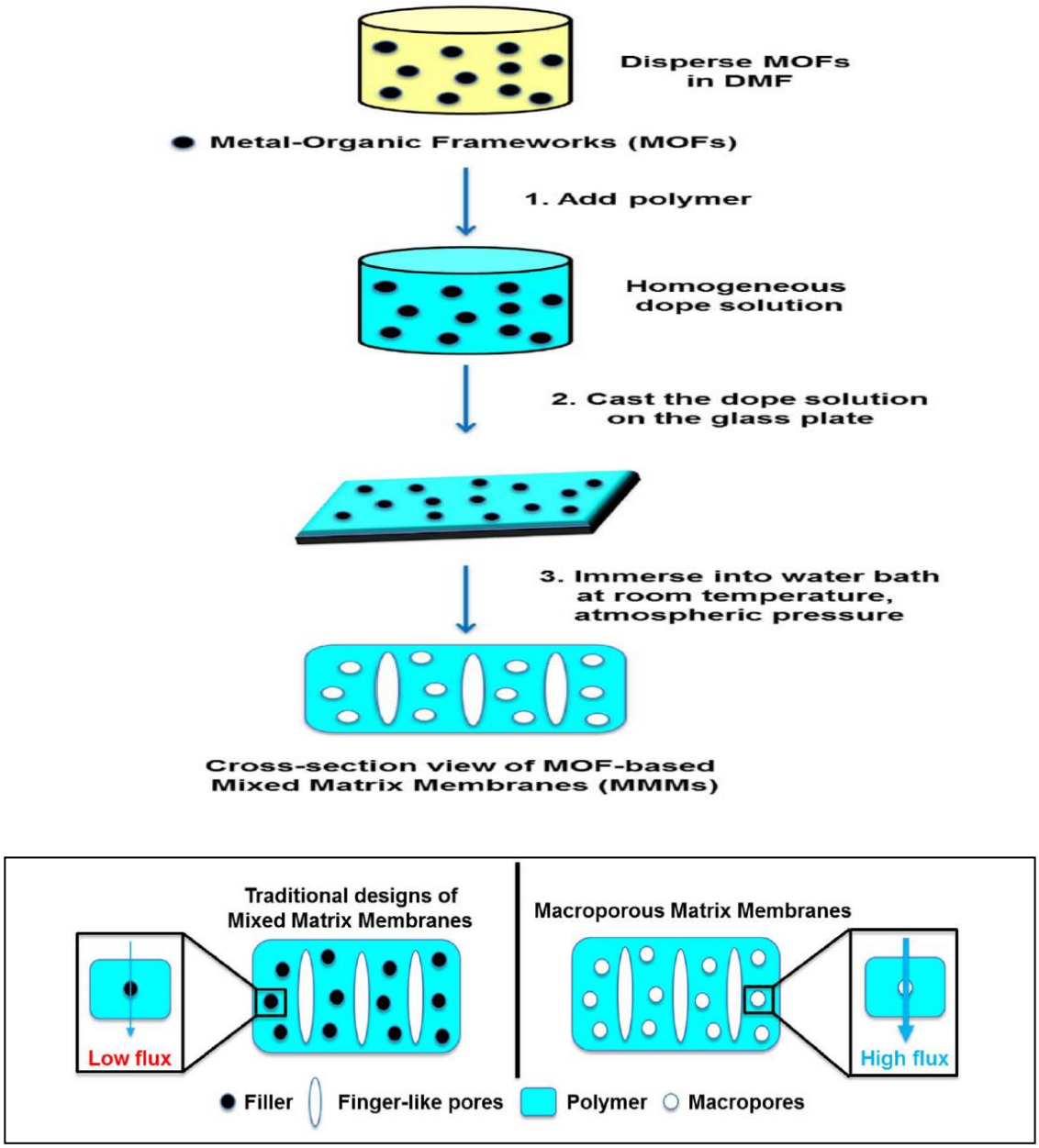

Figure 2-9. Schematic preparation of Porous matrix membrane by phase inversion precipitation immersion method [40]

A traditional technique mostly used in preparing dense membranes for pervaporation has also been used in preparing MOF-MMM for pervaporation treatment of aqueous and non-aqueous liquids. The MOF is added and ultra-sonicated into the polymer mixture to attain homogeneity. Usually low filler concentrations are used to prevent particle aggregation. Hua et al. [41] used this method to prepare

pervaporation membranes for dehydration of isopropanol using ZIF-90/P84/DMF mixed matrix membrane. In this fabrication route, the total mass fraction of ZIF-90/P84 in DMF was about 17 wt. %. The solution was cast using a casting knife (250 µm) on a glass plate which was then placed in an oven for solvent evaporation as opposed to the immersion precipitation method earlier discussed where the plate is immersed in a coagulation bath. After drying for 13h at 60 ^{o}C, the membrane was peeled off and then subjected to solvent-exchange using methanol for 24h to effectively remove residual solvent from membrane pores. Thereafter, the membrane is ready for further characterization and pervaporation performance test.

For pressure driven separation processes like nanofiltration and ultrafiltration, the membranes fabricated from the above techniques suffer from mechanical instability and thus synthesis has been improved by casting the MOF-polymer solution on a support. Instead of casting on a glass plate and peeling off, the dope is casted on a support (usually porous) for extra mechanical strength. We believe that this method of membrane fabrication can be a great and simple tool for fabricating durable membranes when the dope solution is allowed to penetrate the pores of the support, during the optimized contact period, with neither completely filling the pores nor floating on the outside. Thus, the membrane performance could be greatly improved in terms of flux, porosity and mechanical strength. This optimization will therefore be greatly influenced by dope viscosity and the tortuosity of the support material pores and therefore a concise systematic study is required.

Ceramic substrates are one of the most common substrates used in the fabrication of support-based MOF membranes. The choice of this support is due to its highly porous surface and chemical resistance. Tubular ceramic substrates were used in an in-situ layer-by-layer (LbL) (Fig. 2-10) preparation of ZIF8/poly (sodium 4 styrenesulfonate) (PSS) membrane for removing MB dye from water by nanofiltration [42]. The substrate surface is first functionalized by (3-Aminopropyl) triethoxysilane

(APTES) and then grafted with PSS by immersing in 0.3 wt.% PSS solution for 30 min at 60 ºC followed by immersion in Zn $(NO_3)_2$ methanol solution for the same period and at the same temperature. A final stage involved immersion of the tubular ceramic membrane in a solution mixture of Zn $(NO_3)_2$ and Hmim in methanol ($C_{Zn(NO3)2}$: C_{Hmim}, 1:4).

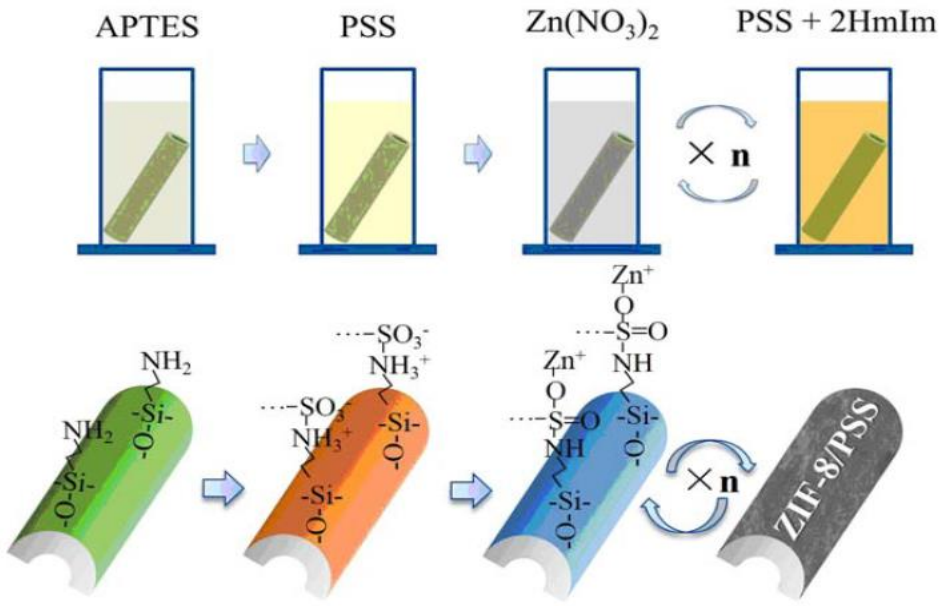

Figure 2-10. Schematic representation of the preparation of ZIF8/PSS membrane on tubular ceramic membrane by a layer-by-layer assembly method [42]

The membrane was then rinsed with methanol for 10 min and dried at 60 ºC for 1h. The last stage as shown on the figure could be repeated based upon the number of layers of ZIF-8/PSS required. This LbL technique proves efficient since the MOF is produced in-situ and deposited on the surface at same time, hence a more uniform distribution is achieved. Depending upon the number of layers, the flux could be greatly reduced due the increased dense nature of membrane with increasing layers (resistance to mass transfer). The initial grafting stage turned to be the main determinant for the long- term use of such

membranes because if the grafting should become unfavorable, the top MOF membrane could peel off. The stability of such grafted membrane has to be tested further for reliability and compatibility for long term processes.

Whenever porous or nano-scaled or metal oxide materials are used as the filler in the composite membrane, there is always the issue of agglomeration. Agglomeration is known to increase the size of these particles from the usual nano-scale to micro levels. Preparing MOF incorporated membranes also suffers from the same issues but with techniques like the in-situ preparation discussed above, the agglomeration effects can be reduced. Co-blend simultaneous spraying was proven to reduce aggregation of MOF particles even at high loadings of 40 wt.% [43]. This technique was used in preparing ZIF-8/PDMS membrane for biobutanol permselective pervaporation. Here, ZIF-8/PDMS solution were loaded in one nuzzle and a cross-linking agent tetraethyl orthosilicate (TEOS) and catalyst dibutyltin dilaurate (DBTDL) was loaded onto another nozzle (Fig. 2-11). Both the nozzles were then pressurized simultaneously to spray both solutions on a porous substrate. XRD and SEM analysis of the resulting membrane showed uniformly dispersed ZIF-8 particles.

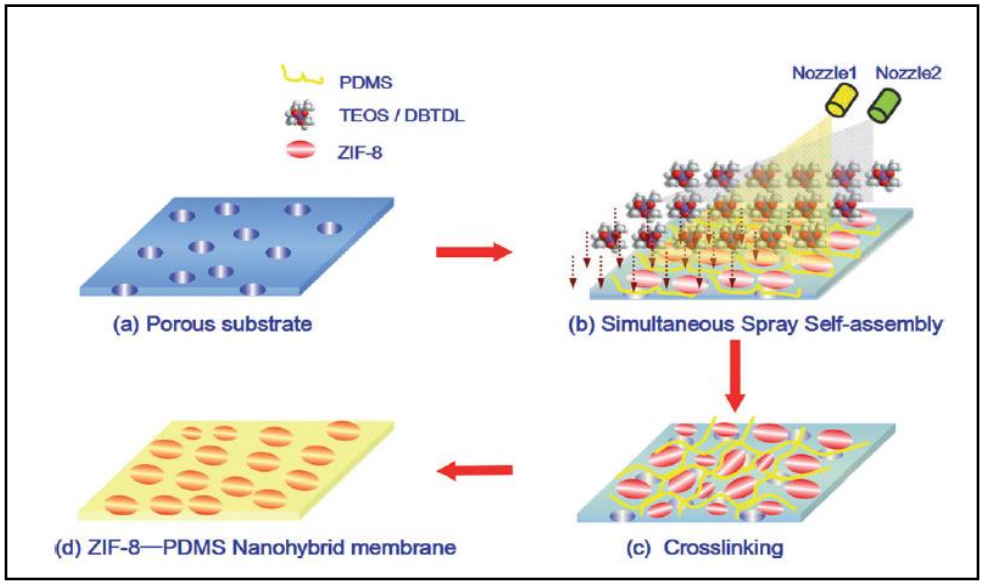

Figure 2-11. Formation of the ZIF-8 PDMS nanohybride composite membrane by simultaneous spray assembly technique[43]

The underlying principle is based on the fact that, upon spraying the MOF/PDMS solution, the particles become evenly distributed on the porous substrate and are further individually separated by the PDMS chains. When the cross-linker/catalyst mixture gets in contact with the porous substrate, cross linking occurs and the ZIF-8 particles are further surrounded individually by PDMS chains, as a result the ZIF-8 in PDMS solution is uniformly dispersed with minimal aggregation irrespective of the filler loadings of up to 40 wt.%. Though this method is efficient for reducing agglomeration of particles, it is regarded not effective due to the large amount of wasted raw materials and not environmentally friendly because of the pollution effects of the organic solvents used. Thus, the coordination driven in-situ self-assembly method seems preferable. Here, the MOF precursors are mixed in the polymer as such, coordination bonds are formed between the metal ions and organic ligand as the membrane is been formed (Fig. 2-12). Zhang and coworkers [42] used this method to prepare MOF hybrid nanofiltration membranes for removal of dye from water. This seems very robust because the concentration of MOF in the final membrane is controlled by the amount of MOF precursors loading which also had a direct relationship with the particle size.

Though the membranes produced showed enhance performance in the nanofiltration experiment with a reduction in static water contact angle (92^o to 59^o) resulting in enhanced flux (up to 270 $L/m^2.h.MPa$) and retention (> 98%), we believe that since there is a possibility that the yield of the MOF particles is most likely less than 100%. This implies that the unreacted precursors could be embedded in the membrane matrix, which might have long term consequences such as fast deterioration of membrane performance and the possibility of breaching of these chemicals, which may lead to reduction of membrane rejection and contamination of the permeate. This also will depend greatly on the compatibility of the precursor moieties and the membrane polymer.

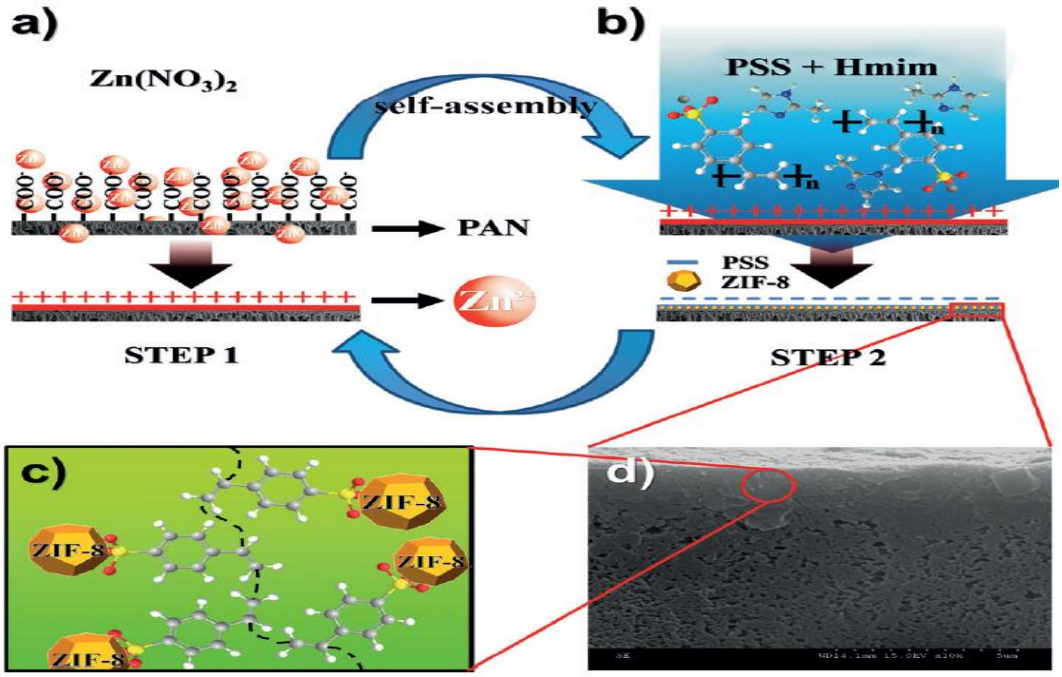

Figure 2-12. Self-assembly preparation of the ZIF-8 hybrid membrane. a) Assembly of Zn2+ on the substrate. b) Assembly of PSS and formation of ZIF-8 particles c) Proposed membrane structure. d) Cross section SEM image of the resulting membrane (2 layers) [42]

MOF composite membranes have also been prepared for ethanol permselective pervaporation [44] using a method known as dip-coating (Fig. 2-13).

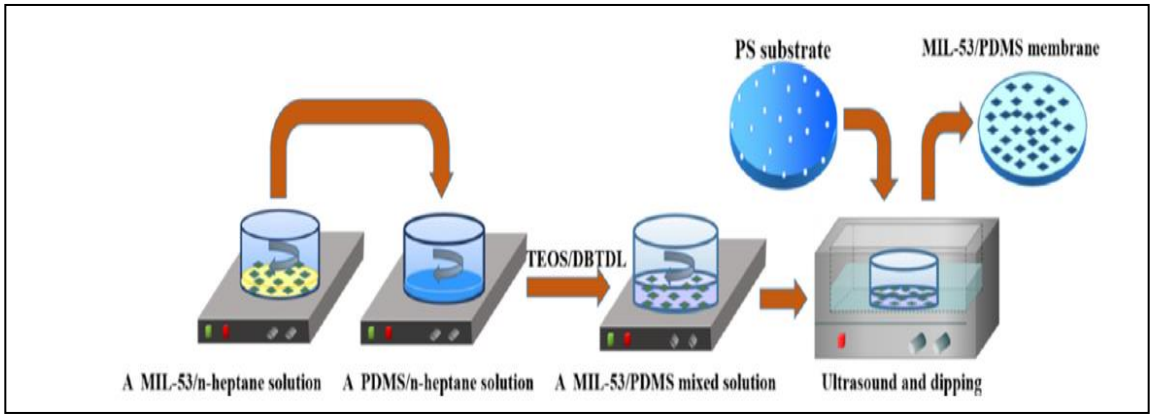

Figure 2-13. Schematic representation of the dip-coating method for preparation for membrane preparation [44]

In this method, the MIL-53 particles were first dispersed and stirred in n-heptane for 1 h before mixing with PDMS solution. A cross-linker and catalyst (TEOS/DBTDL) were added to enhance the particles dispersion under stirring. The mixture was then allowed to degas for 10 min to remove air bubbles at 100 Pa. The MIL-53/PDMS solution was then dip coated with sonication on the surface of PS substrate for 1 min. The substrate was then removed and placed under a hot lamp for 6 h and heat treated in an oven for 12 h at 80 ^{o}C. It must be noted that through this method, particle loading of up 70 wt. % was achieved with a 410.0 nm roughness parameter with the 40 wt. % loading showing the highest flux of 5467 g/m^{2}h. The reduction in flux with the loading increase could be attributed to aggregation of particles at high loadings.

For most MOF composite membranes synthesized on support materials, ceramic substrates have been used. Though not much research has actually been done to investigate the adhesiveness of the prepared membrane on the ceramic surface, most membranes prepared have reported reliable performances. That notwithstanding, to enhance the adhesiveness between the substrate and MOF composite layer, a technique known as pressure driven assembly was investigated [45]. A copper-based MOF ($Cu_3(BTC)_2$) was thoroughly mixed by sonication with PVA-DMF-water solution for 30 min to obtain a homogeneous solution. The ceramic substrate tubes were first pre-treated by immersion in a solution containing 95 wt.% ethanol and 8 g/L silane coupling agent for 2 h after which they were then dried in an oven at 110^{o}C for another 2 h. The MOF/PVA solution was then poured into a vessel where the substrate had been placed (Fig. 2-14). The vessel was then connected to a vacuum pump through a side tube for air suction. The pressure driven assembly was done at a vacuum pressure of -0.08 MPa for 30 min at ambient temperature. The prepared membranes were dried in an oven for 30 min at 40^{o}C.

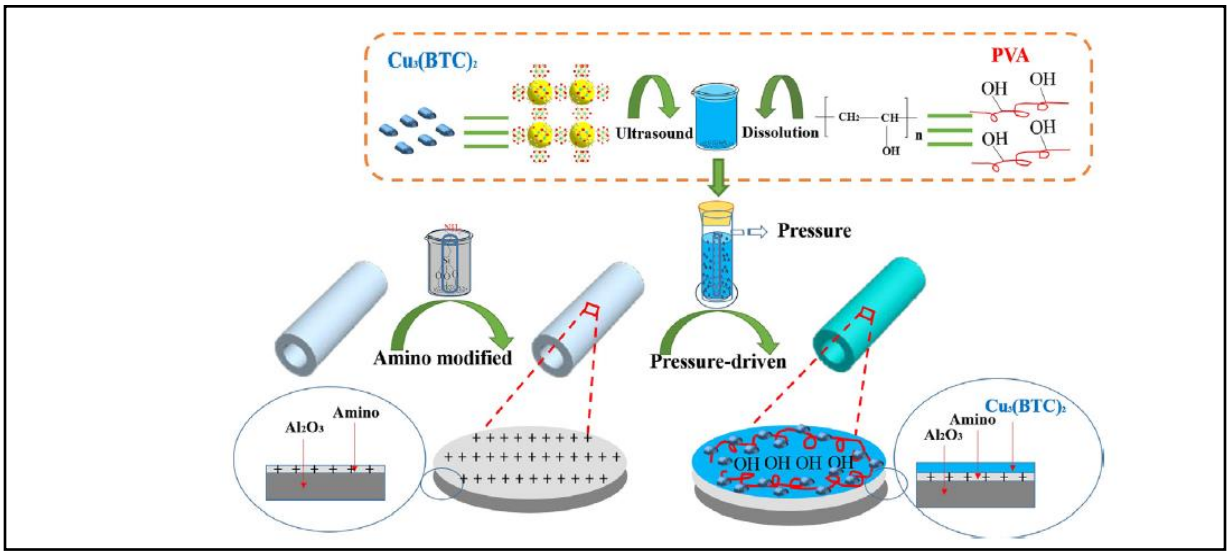

Figure 2-14. Schematic illustration of the pressure driven assembly preparation of MOF/PVA nanohybrid membrane [45]

The prepared membranes were then tested in the separation of a 50 wt. % toluene/ n-heptane mixture with improved separation factors and fluxes compared to the pure PVA membranes. But in this technique, the MOF particles are more susceptible to aggregation as could be seen on the SEM images (Fig. 2-15). As the MOF loading increased to 5 wt.%, more agglomerates could be noticed. We believe that though the pressure driven assembly improves the adhesiveness between the MOF/substrate, the trade-off here is that the MOF particles are allowed to aggregate for an extra time while the pressure driven assembly is ongoing.

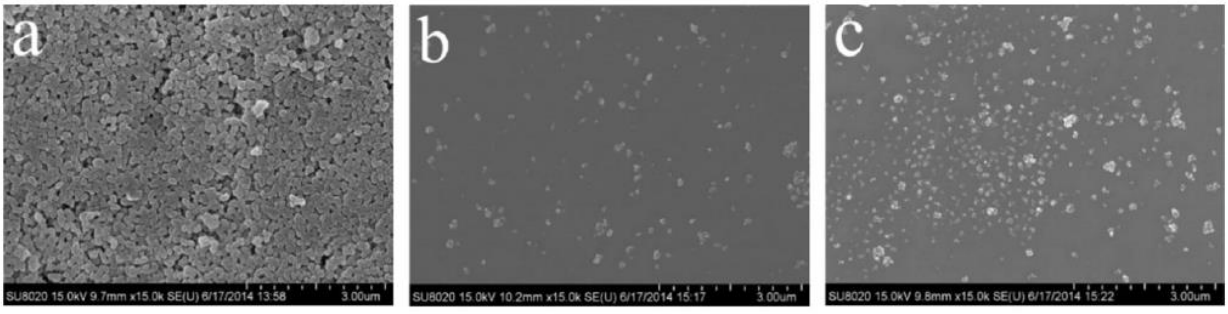

Figure 2-15. SEM images of (a) surface of tubular ceramic substrate (b) surface of 0.75 wt.% MOF/PVA loaded membrane (c) surface of 5 wt.% MOF/PVA loaded membrane [45]

In the same attempt to synthesize MOF composite membranes, a plugging-filling method [46] was used to synthesize a hierarchical ordered stainless steel mesh (HOSSM)-ZIF-8-PMPS nanocomposite membrane for the recovery of furfural by pervaporation. The stainless steel meshes were cut in 18 mm diameter disc and plugged by hand with the ZIF-8 particles (Fig. 2-16), then the voids between the mesh and particles was filled with silicon (hence the name; Plugging-filling).

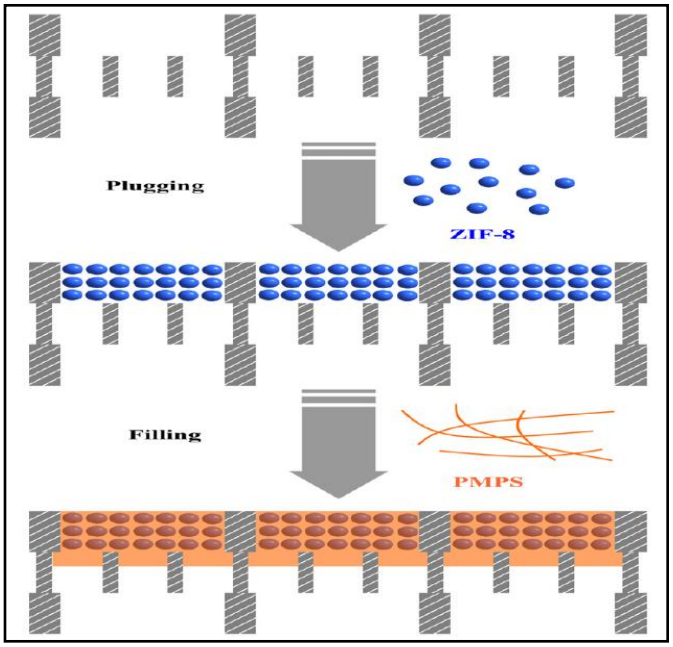

Figure 2-16. Schematic illustration of the preparation procedure of the HOSSM-ZIF-8 PMPS membrane by the plugging filling method [46]

The plugged and filled mesh was then dip-coated into a mixture of a cross-linker (TEOS) and a catalyst (dibutyltin dilaurate) at a dipping and withdrawal speed of 1 mm s^{-1} for 10 s using an automated dip-coater. The prepared membrane is dried at 25^{o}C for 10 min and the dip-coating process is repeated to produce the final membrane which is then dried at 100^{o}C for 12 h and held under vacuum. The MOF loading was > 40 wt.% and the membrane demonstrated enhanced performance in terms of furfural recovery and selectivity from water.

2.6 Electrospinning

Electrospinning from its name entails the spinning of polymer solution into fibers of relatively small diameters through the application of an electric charge force [47,48]. A typical electrospinning setup (Appendix C-1) is made up an electric charge supply, a spinneret or metallic needle, a collector drum usually metallic and a syringe containing the polymer solution usually mounted on syringe pump. When the electric charge comes into contact with the polymer solution through the metallic needle, electrospinning sets off. The induction of electric charges induces some instability in the polymer matrix and the repulsive forces of the charged individual polymer chains produces a force capable of overcoming the surface tension resulting in the flow of the solution. At this stage, a charged conical polymer droplet known as the Taylor cone forms on the tip of the needle. With the collector drum placed at an optimized distance from the needle and grounded, the opposing charges cause the Taylor cone to deform further and spinning the polymer droplet to produce fine threads of nanofibers that are collected on the drum. This Taylor cone spinning and attraction towards the collector drum, causes the polymer to stretch leading to continuous production of fibers from the syringe and deposited on the drum[49,47,50]. This process is capable of producing fibers in the nanoscale (<200 nm in diameter) but could also produce fibers with much greater diameter (> 500 nm in diameter) depending on the purpose end product. Electrospun nanofibers have been used for several applications including, tissue engineering[51], desalination[52], heavy metal adsorption[53], drug delivery[54], wound healing[55]. As such, to obtain the final required product through electrospinning, there are some key factors that should be considered and optimized some of which are discussed next. A successful spinning is most often than not declared when bead-free fibers are produced and the parameters discussed are often optimized to prevent the formation of beads. The electrospinning process parameters could be subdivided into 3 groups; the spinning parameters (applied voltage, flow rate of the solution, distance between drum and needle and

needle diameter), the solution parameters (type of solvent, concentration of the polymer, the conductivity of the solution and solution viscosity) and the environmental parameters (temperature of the surrounding and relative humidity). Some of the key factors as studied in this project are presented.

2.6.1 Solution flow rate

A steady flow of solution through the needle is essential for the formation of bead free nanofibers. As the polymers at the tip of the syringe fiberizes there must be continuous and steady replacement for the fiber production to continue. The rate of replacement of the solution is usually governed by the set speed of the syringe pump. When the flow rate is higher than the rate at which the fibers are produced, excess polymer drips off forming beads as a result of un-fiberized polymer. When the flow rate is too small, the lag in time of appearance of new solution causes the production of discontinued and fragmented fibers which affects the stability of the final product. In some cases, an increase in flow rate results in the formation of larger diameter fibers[56,47] .

2.6.2 Applied voltage

The applied voltage via the spinneret or needle is one of the main contributing factor to electrospinning since the formation of the Taylor cone and its subsequent deformation that leads to nanofiber formation is as a result of the repulsive forces brought about by the applied voltage[48,57]. The applied voltage has to produce strong repulsive forces to overcome the surface tension of the polymer hence different polymers will produce nanofibers at different applied voltages. An increase in the applied voltage leads to a decrease in the size of the Taylor cone which increases the velocity of the polymer jet resulting to an increase in fiber diameter as reported by Deitzel and co-workers[58,59]. Smaller diameter nanofibers have also been reported with an increase in applied voltage due the stretching of the polymer solution and usually bead free [51]. This therefor calls for an optimization process depending on the polymer been used to determine the range of suitable voltage to produce larger or small fiber diameter.

2.6.3 Polymer concentration and solution viscosity

As the applied voltage induces stretching on the charged jet, the surface tension prevents polymer chain entanglement which cause beads to form. When the concentration of the solution is reduced, the viscosity of the solution also drops and chain entanglement can overcome surface tension to produce uniform nanofibers. If the concentration is further reduced or become lower than the critical, surface tension cause polymer chain entanglement and fragments of nanofibers are produced. In a study by Doshi and Reneker [60], they revealed that an optimum viscosity for nanofiber formation by electrospinning is 800-4000 cP. At higher concentration and viscosities, the solution, the flow through the needle tip is affected due to drying of polymer and causes frequent blockages leading to defective nanofibers. In the electrospinning of solutions containing additives like MOFs and other fillers, the concentration/viscosity is of crucial importance because additives always increase the viscosity of the dope solution which could lead to defective nanofibers. To produce defect free composite nanofibers, the polymer concentration and viscosity must be optimized together with the concentration of the fillers.

2.6.4 Needle distance to the collector drum and needle diameter

Similar to the other parameters discussed, the distance of the needle from the drum affects the deposition and evaporation rate of the nanofibers and hence the fiber morphology. When the polymer jet fiberizes at the tip of the needle, it is attracted by the opposite charge on the drum and has to travel to be deposited on the drum. If the drum is very closed to the needle tip, not enough evaporation time is available for the excess solvent to evaporate allowing complete solidification of the fiber, hence, fragmented and unsmooth fibers are collected on the drum. When the drum is too far away from the needle, the attractive force between the opposing charges weakens and the produced fiber can not be stretched out and falls outside of the drum. It is important to allow a suitable distance to obtain uniform nanofibers. The needle diameter has a contribution in the Taylor cone produced as different shapes of the cone affects the

nanofiber morphology. In the electrospinning of polymer solutions with fillers, the size of the particles could block the passage of solution from the needle tip hence a wider tip will be required for smooth passage.

Other factors, like humidity and temperature of the environment have been seen to also affect the nanofiber morphology in that, when all other parameters have been optimized but the spinning occurs in high temperature environment, the solution could dry off easily at the needle tip causing blockage. Elevated temperature environment also enhances rapid solvent evaporation and the produced nanofibers become fragmented and appearance of beads. The role of s suitable solvent in electrospinning can not be underestimated because the polymer must be completely soluble in the solvent and the solvent must have a moderate boiling point. The boiling point determines the volatility of the solvent to avoid drying off too quickly or too slowly. Highly volatile solvents are in most cases avoided because they evaporate faster causing the jet to dry off and block the needle tip. Less volatile solvents will allow for solvent-containing nanofibers to be collected on the drum which at same time dissolves the fiber or produce beads. The most common solvents for electrospinning include tetrahydrofuran (THF)[61], DMF and DMAc [62–64].

2.7 Conclusion

From the review, it is clear that this combination has been presented by other researchers but in the gas field [65]. This was so because of the instability of early MOFs in aqueous systems but further research has produced many water stable MOFs and we believe it is time to dig into the novel research of combining MOFs and polymeric nanofibers for water treatment purposes starting with the removal of some common heavy metal ions. With in-depth studies and further development, this system could stand a chance at improving the future water treatment train. Fabrication of MOF membranes for aqueous and non-aqueous liquids is an emerging front of technology advances and, to our best knowledge, this

research is the first-time fabrication of MOF membranes has been attempted for removal of heavy metal ions from aqueous solution.

At the time of conception of this project, the literature review unveiled a knowledge gap that triggered the objective of section 1.2. With all the potentials posed by MOFs, they have been tested and used basically as standalone material, which will be challenging for practical applications. If standalone MOFs were to be used for industrial water and wastewater treatment purposes, they will be required in substantial quantities thus making the process cost inefficient. To actually increase the viability and potential of this material to be used in the water industry as a cost-effective tool, they must be immobilized unto a substrate that will not impede the functionalities of each other, can seamlessly coordinate to each other without destroying the integrity of the composite. Since nanofiber membranes have undoubtedly shown immersed contributions in the membrane field, it thus ties together to bring these two materials together for a common goal.

Reference

[1] World Water Assessment Programme (WWAP), The United Nations World Water Development Report 2015: Water for a Sustainable World, Facts and Figures, UN Water Rep. (2015) 138. doi:10.1016/S1366-7017(02)00004-1.

[2] H.G. Gorchev, G. Ozolins, WHO guidelines for drinking-water quality., WHO Chron. 38 (2011) 104–108. doi:10.1016/S1462-0758(00)00006-6.

[3] K. Rajeshwar, Advanced Oxidation Processes for Water Treatment, J. Phys. Chem. Lett. 3 (2012) 2112–2113. doi:10.1021/jz200396h.

[4] K.C. Khulbe, C.Y. Feng, T. Matsuura, A.F. Ismail, Progresses in membrane and advanced oxidation processes for water treatment, Membr. Water Treat. 3 (2012). doi:10.12989/mwt.2012.3.3.181.

[5] J. Choi, A. Ide, Y.B. Truong, I.L. Kyratzis, R.A. Caruso, High surface area mesoporous titanium–zirconium oxide nanofibrous web: a heavy metal ion adsorbent, J. Mater. Chem. A. 1 (2013) 5847. doi:10.1039/c3ta00030c.

[6] F. Franco, M. Benítez-Guerrero, I. Gonzalez-Triviño, R. Pérez-Recuerda, C. Assiego, J. Cifuentes-Melchor, J. Pascual-Cosp, Low-cost aluminum and iron oxides supported on dioctahedral and trioctahedral smectites: A comparative study of the effectiveness on the heavy metal adsorption from water, Appl. Clay Sci. 119 (2016) 321–332. doi:10.1016/j.clay.2015.10.035.

[7] D.C. Manatunga, R.M. de Silva, K.M.N. de Silva, R. Ratnaweera, Natural polysaccharides leading to super adsorbent hydroxyapatite nanoparticles for the removal of heavy metals and dyes from aqueous solutions, RSC Adv. 6 (2016) 105618–105630. doi:10.1039/C6RA22662K.

[8] S.P. Mishra, V.K. Singh, Inorganic particulates in removal of toxic heavy metal ions VIII . Removal of zinc, cadmium and mercury ions from aqueous solution by hydrous titanium oxide, J. Radioanal. Nucl. Chem. 241 (1999) 341–346.

[9] S. Kalantari, M. Yousefpour, Z. Taherian, Synthesis of mesoporous silica/iron oxide nanocomposites and application of optimum sample as adsorbent in removal of heavy metals, Rare Met. 36 (2017) 942–950. doi:10.1007/s12598-016-0709-4.

[10] C. MAHAJAN, REMOVAL OF HEAVY METALS FROM WINERY WASTEWATER BY USING NATURAL ADSORBENTS., Int. …. 5 (2014) 69–78. http://search.ebscohost.com/login.aspx?direct=true&profile=ehost&scope=site&authtype=crawler&jrnl=2067533X&AN=95118774&h=guL3767S4V9fiSnoq6DVlXr4MqBmJNF96EbdJhHgWuszFOCbPqo7kKod3UXiNd94ULnSzKIPyFljXggUhyZ32Q%3D%3D&crl=c.

[11] C. Wang, X. Liu, N. Keser Demir, J.P. Chen, K. Li, Applications of water stable metal–organic frameworks, Chem. Soc. Rev. 45 (2016) 5107–5134. doi:10.1039/C6CS00362A.

[12] R. Ricco, K. Konstas, M.J. Styles, J.J. Richardson, R. Babarao, K. Suzuki, P. Scopece, P. Falcaro, Lead(II) uptake by aluminium based magnetic framework composites (MFCs) in water, J. Mater. Chem. A. 3 (2015) 19822–19831. doi:10.1039/C5TA04154F.

[13] I. Erucar, G. Yilmaz, S. Keskin, Recent advances in metal-organic framework-based mixed matrix membranes, in: Chem. - An Asian J., 2013: pp. 1692–1704. doi:10.1002/asia.201300084.

[14] V. V Butova, M.A. Soldatov, A.A. Guda, K.A. Lomachenko, C. Lamberti, Metal-organic frameworks: structure, properties, methods of synthesis and characterization, Russ. Chem. Rev. 85 (2016) 280–307. doi:10.1070/RCR4554.

[15] S. Qiu, M. Xue, G. Zhu, Metal–organic framework membranes: from synthesis to separation

application, Chem. Soc. Rev. 43 (2014) 6116–6140. doi:10.1039/C4CS00159A.

[16] N.A. Khan, S.H. Jhung, Synthesis of metal-organic frameworks (MOFs) with microwave or ultrasound: Rapid reaction, phase-selectivity, and size reduction, Coord. Chem. Rev. 285 (2015) 11–23. doi:10.1016/j.ccr.2014.10.008.

[17] Z.-J. Lin, Z. Yang, T.-F. Liu, Y.-B. Huang, R. Cao, Microwave-assisted synthesis of a series of lanthanide metal-organic frameworks and gas sorption properties., Inorg. Chem. 51 (2012) 1813–20. doi:10.1021/ic202082w.

[18] W. Liang, D.M. D'Alessandro, Microwave-assisted solvothermal synthesis of zirconium oxide based metal-organic frameworks., Chem. Commun. (Camb). 49 (2013) 3706–8. doi:10.1039/c3cc40368h.

[19] Z. Lin, D.S. Wragg, R.E. Morris, Microwave-assisted synthesis of anionic metal–organic frameworks under ionothermal conditions, Chem. Commun. (2006) 2021–2023. doi:10.1039/B600814C.

[20] R. Vakili, S. Xu, N. Al-Janabi, P. Gorgojo, S.M. Holmes, X. Fan, Microwave-assisted synthesis of zirconium-based metal organic frameworks (MOFs): Optimization and gas adsorption, Microporous Mesoporous Mater. 260 (2018) 45–53. doi:10.1016/j.micromeso.2017.10.028.

[21] M. Bechelany, M. Drobek, C. Vallicari, A. Abou Chaaya, A. Julbe, P. Miele, Highly crystalline MOF-based materials grown on electrospun nanofibers, Nanoscale. 7 (2015). doi:10.1039/c4nr06640e.

[22] U. Müller, H. Pütter, M. Hesse, H. Wessel, M. Schubert, Method for electrochemical production of a crystalline porous metal organic skeleton material, WO/2005/049892, 2005.

[23] M. Hartmann, S. Kunz, D. Himsl, O. Tangermann, S. Ernst, A. Wagener, Adsorptive separation

of isobutene and isobutane on Cu3(BTC)2, Langmuir. 24 (2008) 8634–8642. doi:10.1021/la8008656.

[24] G. Nickerl, A. Notzon, M. Heitbaum, I. Senkovska, F. Glorius, S. Kaskel, Selective Adsorption Properties of Cationic Metal–Organic Frameworks Based on Imidazolic Linker, Cryst. Growth Des. 13 (2013) 198–203. doi:10.1021/cg301347t.

[25] L. Xie, D. Liu, H. Huang, Q. Yang, C. Zhong, Efficient capture of nitrobenzene from waste water using metal-organic frameworks, Chem. Eng. J. 246 (2014) 142–149. doi:10.1016/j.cej.2014.02.070.

[26] Z. Hasan, E.J. Choi, S.H. Jhung, Adsorption of naproxen and clofibric acid over a metal–organic framework MIL-101 functionalized with acidic and basic groups, Chem. Eng. J. 219 (2013) 537–544. doi:10.1016/j.cej.2013.01.002.

[27] M. Tong, D. Liu, Q. Yang, S. Devautour-Vinot, G. Maurin, C. Zhong, Influence of framework metal ions on the dye capture behavior of MIL-100 (Fe, Cr) MOF type solids, J. Mater. Chem. A. 1 (2013) 8534. doi:10.1039/c3ta11807j.

[28] X.-X. Huang, L.-G. Qiu, W. Zhang, Y.-P. Yuan, X. Jiang, A.-J. Xie, Y.-H. Shen, J.-F. Zhu, Hierarchically mesostructured MIL-101 metal–organic frameworks: supramolecular template-directed synthesis and accelerated adsorption kinetics for dye removal, CrystEngComm. 14 (2012) 1613–1617. doi:10.1039/C1CE06138K.

[29] B.-J. Yao, W.-L. Jiang, Y. Dong, Z.-X. Liu, Y.-B. Dong, Post-Synthetic Polymerization of UiO-66-NH<inf>2</inf>Nanoparticles and Polyurethane Oligomer toward Stand-Alone Membranes for Dye Removal and Separation, Chem. - A Eur. J. 22 (2016). doi:10.1002/chem.201600817.

[30] Z. Hasan, S.H. Jhung, Removal of hazardous organics from water using metal-organic

frameworks (MOFs): Plausible mechanisms for selective adsorptions, J. Hazard. Mater. 283 (2015) 329–339. doi:10.1016/j.jhazmat.2014.09.046.

[31] H. Furukawa, F. Gándara, Y.-B. Zhang, J. Jiang, W.L. Queen, M.R. Hudson, O.M. Yaghi, Water adsorption in porous metal-organic frameworks and related materials., J. Am. Chem. Soc. 136 (2014) 4369–81. doi:10.1021/ja500330a.

[32] J.J. Low, A.I. Benin, P. Jakubczak, J.F. Abrahamian, S.A. Faheem, R.R. Willis, Virtual high throughput screening confirmed experimentally: Porous coordination polymer hydration, J. Am. Chem. Soc. 131 (2009) 15834–15842. doi:10.1021/ja9061344.

[33] N.U. Qadir, S.A.M. Said, H.M. Bahaidarah, Structural stability of metal organic frameworks in aqueous media - Controlling factors and methods to improve hydrostability and hydrothermal cyclic stability, Microporous Mesoporous Mater. 201 (2015) 61–90. doi:10.1016/j.micromeso.2014.09.034.

[34] T. Loiseau, C. Serre, C. Huguenard, G. Fink, F. Taulelle, M. Henry, T. Bataille, G. Férey, A Rationale for the Large Breathing of the Porous Aluminum Terephthalate (MIL-53) Upon Hydration, Chem. - A Eur. J. 10 (2004) 1373–1382. doi:10.1002/chem.200305413.

[35] J.H. Cavka, S. Jakobsen, U. Olsbye, N. Guillou, C. Lamberti, S. Bordiga, K.P. Lillerud, A new zirconium inorganic building brick forming metal organic frameworks with exceptional stability, J. Am. Chem. Soc. 130 (2008) 13850–13851. doi:10.1021/ja8057953.

[36] H.K. Chae, J. Kim, O.D. Friedrichs, M. O'Keeffe, O.M. Yaghi, Design of frameworks with mixed triangular and octahedral building blocks exemplified by the structure of [Zn4O(TCA)2] having the pyrite topology, Angew. Chemie - Int. Ed. 42 (2003) 3907–3909. doi:10.1002/anie.200351546.

[37] X. Liu, N.K. Demir, Z. Wu, K. Li, Highly Water-Stable Zirconium Metal-Organic Framework UiO-66 Membranes Supported on Alumina Hollow Fibers for Desalination, J. Am. Chem. Soc. 137 (2015) 6999–7002. doi:10.1021/jacs.5b02276.

[38] K. Tan, N. Nijem, P. Canepa, Q. Gong, J. Li, T. Thonhauser, Y.J. Chabal, Stability and hydrolyzation of metal organic frameworks with paddle-wheel SBUs upon hydration, Chem. Mater. 24 (2012) 3153–3167. doi:10.1021/cm301427w.

[39] M. Haouas, C. Volkringer, T. Loiseau, G. Férey, F. Taulelle, The extra-framework sub-lattice of the metal-organic framework MIL-110: A solid-state NMR investigation, Chem. - A Eur. J. 15 (2009) 3139–3146. doi:10.1002/chem.200801856.

[40] J.-Y. Lee, C.Y. Tang, F. Huo, Fabrication of Porous Matrix Membrane (PMM) Using Metal-Organic Framework as Green Template for Water Treatment, Sci. Rep. 4 (2015) 3740. doi:10.1038/srep03740.

[41] J. Duan, Y. Pan, F. Pacheco, E. Litwiller, Z. Lai, I. Pinnau, High-performance polyamide thin-film-nanocomposite reverse osmosis membranes containing hydrophobic zeolitic imidazolate framework-8, J. Memb. Sci. 476 (2015) 303–310. doi:10.1016/j.memsci.2014.11.038.

[42] R. Zhang, S. Ji, N. Wang, L. Wang, G. Zhang, J.-R.J.R. Li, Coordination-driven in situ self-assembly strategy for the preparation of metal-organic framework hybrid membranes, Angew. Chemie - Int. Ed. 53 (2014) 9775–9779. doi:10.1002/anie.201403978.

[43] H. Fan, Q. Shi, H. Yan, S. Ji, J. Dong, G. Zhang, Simultaneous spray self-assembly of highly loaded ZIF-8-PDMS nanohybrid membranes exhibiting exceptionally high biobutanol-permselective pervaporation, Angew. Chemie - Int. Ed. 53 (2014) 5578–5582. doi:10.1002/anie.201309534.

[44] G. Zhang, J. Li, N. Wang, H. Fan, R. Zhang, G. Zhang, S. Ji, Enhanced flux of polydimethylsiloxane membrane for ethanol permselective pervaporation via incorporation of MIL-53 particles, J. Memb. Sci. 492 (2015) 322–330. doi:10.1016/j.memsci.2015.05.070.

[45] Y. Zhang, N. Wang, S. Ji, R. Zhang, C. Zhao, J.R. Li, Metal-organic framework/poly(vinyl alcohol) nanohybrid membrane for the pervaporation of toluene/n-heptane mixtures, J. Memb. Sci. 489 (2015) 144–152. doi:10.1016/j.memsci.2015.04.012.

[46] X. Liu, H. Jin, Y. Li, H. Bux, Z. Hu, Y. Ban, W. Yang, Metal-organic framework ZIF-8 nanocomposite membrane for efficient recovery of furfural via pervaporation and vapor permeation, J. Memb. Sci. 428 (2013) 498–506. doi:10.1016/j.memsci.2012.10.028.

[47] D. Li, Y. Xia, Electrospinning of nanofibers: Reinventing the wheel?, Adv. Mater. 16 (2004) 1151–1170. doi:10.1002/adma.200400719.

[48] S. Agarwal, S. Jiang, Nanofibers and Electrospinning, in: Encycl. Polym. Nanomater., 2015: p. 1323.

[49] W. Teo, Introduction to Electrospinning Parameters and Fiber Control, Introd. to Electrospinning Parameters Fiber Control. (2015) 25–28. http://electrospintech.com/solution.html#.Ve7THhFVikp.

[50] N. Rosman, W.N.W. Salleh, M.A. Mohamed, N.H. Ismail, N. Sazali, J. Jaafar, H. Hasbullah, Electrospun nanofiber-coated membrane: A review, J. Teknol. 78 (2016) 83–88. doi:10.11113/jt.v78.10071.

[51] T.J. Sill, H.A. von Recum, Electrospinning: Applications in drug delivery and tissue engineering, Biomaterials. 29 (2008) 1989–2006. doi:10.1016/j.biomaterials.2008.01.011.

[52] Y.C. Woo, L.D. Tijing, M.J. Park, M. Yao, J.S. Choi, S. Lee, S.H. Kim, K.J. An, H.K. Shon,

Electrospun dual-layer nonwoven membrane for desalination by air gap membrane distillation, Desalination. 403 (2017) 187–198. doi:10.1016/j.desal.2015.09.009.

[53] Y. Tian, M. Wu, R. Liu, Y. Li, D. Wang, J. Tan, R. Wu, Y. Huang, Electrospun membrane of cellulose acetate for heavy metal ion adsorption in water treatment, Carbohydr. Polym. 83 (2011) 743–748. doi:10.1016/j.carbpol.2010.08.054.

[54] X. Hu, S. Liu, G. Zhou, Y. Huang, Z. Xie, X. Jing, Electrospinning of polymeric nanofibers for drug delivery applications, J. Control. Release. 185 (2014) 12–21. doi:10.1016/j.jconrel.2014.04.018.

[55] O.K. Pereao, C. Bode-Aluko, G. Ndayambaje, O. Fatoba, L.F. Petrik, Electrospinning: Polymer Nanofibre Adsorbent Applications for Metal Ion Removal, J. Polym. Environ. 25 (2017) 1175–1189. doi:10.1007/s10924-016-0896-y.

[56] F.E. Ahmed, B.S. Lalia, R. Hashaikeh, A review on electrospinning for membrane fabrication: Challenges and applications, Desalination. 356 (2015) 15–30. doi:10.1016/j.desal.2014.09.033.

[57] R. Dersch, A. Greiner, J.H. Wendorff, Polymer nanofibers by electrospinning, Dekker Encycl. Nanosci. Nanotechnol. 8 (2004) 64–75. doi:10.1016/S1359-0294Ž03.00004-9.

[58] J.. Deitzel, J. Kleinmeyer, D. Harris, N.. Beck Tan, The effect of processing variables on the morphology of electrospun nanofibers and textiles, Polymer (Guildf). 42 (2001) 261–272. doi:10.1016/S0032-3861(00)00250-0.

[59] R. Khajavi, M. Abbasipour, Controlling nanofiber morphology by the electrospinning process, in: Electrospun Nanofibers, 2016: pp. 109–123. doi:10.1016/B978-0-08-100907-9.00005-2.

[60] J. Doshi, D.H. Reneker, Electrospinning process and applications of electrospun fibers, J. Electrostat. 35 (1995) 151–160. doi:10.1016/0304-3886(95)00041-8.

[61] Y.Z. Zhang, Y. Feng, Z.M. Huang, S. Ramakrishna, C.T. Lim, Fabrication of porous electrospun nanofibres, Nanotechnology. 17 (2006) 901–908. doi:10.1088/0957-4484/17/3/047.

[62] J.E. Efome, D. Rana, T. Matsuura, C.Q. Lan, Enhanced performance of PVDF nanocomposite membrane by nanofiber coating: A membrane for sustainable desalination through MD, Water Res. 89 (2016) 39–49. doi:10.1016/j.watres.2015.11.040.

[63] J.E.E. Efome, D. Rana, T. Matsuura, C.Q. Lan, Metal–organic frameworks supported on nanofibers to remove heavy metals, J. Mater. Chem. A. 6 (2018) 4550–4555. doi:10.1039/c7ta10428f.

[64] S. Megelski, J.S. Stephens, D. Bruce Chase, J.F. Rabolt, Micro- and nanostructured surface morphology on electrospun polymer fibers, Macromolecules. 35 (2002) 8456–8466. doi:10.1021/ma020444a.

[65] S.L. James, Metal-organic frameworks, Chem. Soc. Rev. 32 (2003) 276. doi:10.1039/b200393g.

[66] F. Fu, Q. Wang, Removal of heavy metal ions from wastewaters: A review, J. Environ. Manage. 92 (2011) 407–418. doi:10.1016/j.jenvman.2010.11.011.

[67] M. Hua, S. Zhang, B. Pan, W. Zhang, L. Lv, Q. Zhang, Heavy metal removal from water/wastewater by nanosized metal oxides: A review, J. Hazard. Mater. 211–212 (2012) 317–331. doi:10.1016/j.jhazmat.2011.10.016.

[68] S. Wang, Y. Peng, Natural zeolites as effective adsorbents in water and wastewater treatment, Chem. Eng. J. 156 (2010) 11–24. doi:10.1016/j.cej.2009.10.029.

[69] N. Bleiman, Y.G. Mishael, Selenium removal from drinking water by adsorption to chitosan-clay composites and oxides: Batch and columns tests, J. Hazard. Mater. 183 (2010) 590–595. doi:10.1016/j.jhazmat.2010.07.065.

[70] Y. Yurekli, Removal of heavy metals in wastewater by using zeolite nano-particles impregnated polysulfone membranes, J. Hazard. Mater. 309 (2016) 53–64. doi:10.1016/j.jhazmat.2016.01.064.

[71] R.-S. Juang, R.-C. Shiau, Metal removal from aqueous solutions using chitosan-enhanced membrane filtration, J. Memb. Sci. 165 (2000) 159–167. doi:10.1016/S0376-7388(99)00235-5.

[72] Y. Huang, X. Zeng, L. Guo, J. Lan, L. Zhang, D. Cao, Heavy metal ion removal of wastewater by zeolite-imidazolate frameworks, Sep. Purif. Technol. 194 (2018) 462–469. doi:10.1016/j.seppur.2017.11.068.

[73] N. Wang, X.-K. Ouyang, L.-Y. Yang, A.M. Omer, Fabrication of a Magnetic Cellulose Nanocrystal/Metal-Organic Framework Composite for Removal of Pb (II) from Water, ACS Sustain. Chem. Eng. 5 (2017) 10447–10458. doi:10.1021/acssuschemeng.7b02472.

[74] N.D. Rudd, H. Wang, E.M.A. Fuentes-Fernandez, S.J. Teat, F. Chen, G. Hall, Y.J. Chabal, J. Li, Highly Efficient Luminescent Metal-Organic Framework for the Simultaneous Detection and Removal of Heavy Metals from Water, ACS Appl. Mater. Interfaces. 8 (2016) 30294–30303. doi:10.1021/acsami.6b10890.

[75] Y. Peng, H. Huang, Y. Zhang, C. Kang, S. Chen, L. Song, D. Liu, C. Zhong, A versatile MOF-based trap for heavy metal ion capture and dispersion, Nat. Commun. 9 (2018) 187. doi:10.1038/s41467-017-02600-2.

[76] N.N. Yin, K. Wang, L. Wang, Z. Li, Amino-functionalized MOFs combining ceramic membrane ultrafiltration for Pb (II) removal, Chem. Eng. J. 306 (2016) 619–628. doi:10.1016/j.cej.2016.07.064.

[77] J. Liu, C.A. Fernandez, P.F. Martin, P.K. Thallapally, D.M. Strachan, A two-column method for the separation of Kr and Xe from process off-gases, Ind. Eng. Chem. Res. 53 (2014) 12893–

12899. doi:10.1021/ie502156h.

[78] S. Herrmann, L. De Matteis, J.M.J.M. de la Fuente, S.G.S.G. Mitchell, C. Streb, L. De Matteis, J.M. de la Fuente, S.G.S.G. Mitchell, C. Streb, Removal of Multiple Contaminants from Water by Polyoxometalate Supported Ionic Liquid Phases (POM-SILPs), Angew. Chemie - Int. Ed. 56 (2017) 1667–1670. doi:10.1002/anie.201611072.

[79] A.M. Azzam, S.T. El-Wakeel, B.B. Mostafa, M.F. El-Shahat, Removal of Pb, Cd, Cu and Ni from aqueous solution using nano scale zero valent iron particles, J. Environ. Chem. Eng. 4 (2016) 2196–2206. doi:10.1016/j.jece.2016.03.048.

[80] C. Ding, W. Cheng, X. Wang, Z.-Y. Wu, Y. Sun, C. Chen, X. Wang, S.-H. Yu, Competitive sorption of Pb (II), Cu(II) and Ni(II) on carbonaceous nanofibers: A spectroscopic and modeling approach, J. Hazard. Mater. 313 (2016) 253–261. doi:10.1016/j.jhazmat.2016.04.002.

[81] L. Fang, L. Li, Z. Qu, H. Xu, J. Xu, N. Yan, A novel method for the sequential removal and separation of multiple heavy metals from wastewater, J. Hazard. Mater. 342 (2018) 617–624. doi:10.1016/j.jhazmat.2017.08.072.

[82] H. Jeong, W. Jang, J. Yun, H. Byun, Preparation of PVdF/GO nanofiber composite membranes and its heavy metal removal characteristics, Polym. 40 (2016) 489–497. doi:10.7317/pk.2016.40.3.489.

[83] S. Koushkbaghi, P. Jafari, J. Rabiei, M. Irani, M. Aliabadi, Fabrication of PET/PAN/GO/Fe3O4 nanofibrous membrane for the removal of Pb (II) and Cr(VI) ions, Chem. Eng. J. 301 (2016) 42–50. doi:10.1016/j.cej.2016.04.076.

[84] Q.L. Huang, Y. Huang, C.F. Xiao, Y.W. You, C.X. Zhang, Electrospun ultrafine fibrous PTFE-supported ZnO porous membrane with self-cleaning function for vacuum membrane distillation,

J. Memb. Sci. 534 (2017) 73–82. doi:10.1016/j.memsci.2017.04.015.

[85] Y. Wu, F. Li, H. Liu, W. Zhu, M. Teng, Y. Jiang, W. Li, D. Xu, D. He, P. Hannam, G. Li, Electrospun fibrous mats as skeletons to produce free-standing MOF membranes, J. Mater. Chem. 22 (2012) 16971. doi:10.1039/c2jm32570e.

[86] R. Ostermann, J. Cravillon, C. Weidmann, M. Wiebcke, B.M. Smarsly, Metal-organic framework nanofibers via electrospinning, Chem. Commun. 47 (2011). doi:10.1039/c0cc02271c.

[87] J.H. Doh, J.H. Kim, H.J. Kim, R.F. Ali, K. Shin, Y.J. Hong, Enhanced adsorption of aqueous copper(II) ions using dedoped poly-N-phenylglycine nanofibers, Chem. Eng. J. 277 (2015) 352–359. doi:10.1016/j.cej.2015.04.120.

[88] H. Chen, J. Lin, N. Zhang, L. Chen, S. Zhong, Y. Wang, W. Zhang, Q. Ling, Preparation of MgAl-EDTA-LDH based electrospun nanofiber membrane and its adsorption properties of copper(II) from wastewater, J. Hazard. Mater. 345 (2018) 1–9. doi:10.1016/j.jhazmat.2017.11.002.

[89] A.X. Lu, A.M. Ploskonka, T.M. Tovar, G.W. Peterson, J.B. Decoste, Direct Surface Growth of UIO-66-NH<inf>2</inf>on Polyacrylonitrile Nanofibers for Efficient Toxic Chemical Removal, Ind. Eng. Chem. Res. 56 (2017) 14502–14506. doi:10.1021/acs.iecr.7b04202.

[90] S. Egodawatte, K.E. Greenstein, I. Vance, E. Rivera, N.V. Myung, G.F. Parkin, D.M. Cwiertny, S.C. Larsen, Electrospun hematite nanofiber/mesoporous silica core/shell nanomaterials as an efficient adsorbent for heavy metals, RSC Adv. 6 (2016) 90516–90525. doi:10.1039/c6ra19876g.

[91] Z. Cai, J. Kim, M.M. Benjamin, NOM removal by adsorption and membrane filtration using heated aluminum oxide particles, Environ. Sci. Technol. 42 (2008) 619–623. doi:10.1021/es7021285.

[92] M. Bryjak, J. Wolska, I. Soroko, N. Kabay, Adsorption-membrane filtration process in boron

removal from first stage seawater RO permeate, Desalination. 241 (2009) 127–132. doi:10.1016/j.desal.2008.01.062.

[93] M. Abbasi, R.S. Mohammad, A. Salahi, B. Mirza, Modeling of membrane fouling and flux decline in microfiltration of oily wastewater using ceramic membranes, Chem. Eng. Commun. 199 (2012) 78–93. doi:10.1080/00986445.2011.570391.

[94] C. Aydiner, I. Demir, E. Yildiz, Modeling of flux decline in crossflow microfiltration using neural networks: The case of phosphate removal, J. Memb. Sci. 248 (2005) 53–62. doi:10.1016/j.memsci.2004.07.036.

[95] W. Zhang, X. Ruan, Y. Ma, X. Jiang, W. Zheng, Y. Liu, G. He, Modeling and simulation of mitigating membrane fouling under a baffle-filled turbulent flow with permeate boundary, Sep. Purif. Technol. 179 (2017) 13–24. doi:10.1016/j.seppur.2017.01.022.

[96] H. Li, H. Xia, Y. Mei, Modeling organic fouling of reverse osmosis membrane: From adsorption to fouling layer formation, Desalination. 386 (2016) 25–31. doi:10.1016/j.desal.2016.02.037.

[97] E.R. Gomes, A. Santos, S.A. Lima, Numerical Modeling of Straining: The Role of Particle and Pore Size Distributions, Transp. Porous Media. 120 (2017) 535–551. doi:10.1007/s11242-017-0939-4.

[98] J.M. Ochando-Pulido, A. Martínez-Ferez, Fouling modelling on a reverse osmosis membrane in the purification of pretreated olive mill wastewater by adapted crossflow blocking mechanisms, J. Memb. Sci. 544 (2017) 108–118. doi:10.1016/j.memsci.2017.09.018.

[99] W. Li, W. Xing, N. Xu, Modeling of relationship between water permeability and microstructure parameters of ceramic membranes, Desalination. 192 (2006) 340–345. doi:10.1016/j.desal.2005.07.042.

[100] N.K.K. Srivastava, C.B.B. Majumder, Novel biofiltration methods for the treatment of heavy metals from industrial wastewater, J. Hazard. Mater. 151 (2008) 1–8. doi:10.1016/j.jhazmat.2007.09.101.

[101] B.C. J. Jacobe, J.M.L. Lann, H. Pinguad, A generalized approach for dynamic modelling and simulation of biofilters, Chem. Eng. J.,. 65 (1997) 133–143.

[102] Y. Zhao, J.S. Taylor, S. Chellam, Predicting RO/NF water quality by modified solution diffusion model and artificial neural networks, J. Memb. Sci. 263 (2005) 38–46. doi:10.1016/j.memsci.2005.04.004.

[103] M.M. Tomadakis, T.J. Robertson, Viscous permeability of random fiber structures: Comparison of electrical and diffusional estimates with experimental and analytical results, J. Compos. Mater. 39 (2005) 163–188. doi:10.1177/0021998305046438.

[104] Fan Yang, J.. Efome, D. Rana, T. Matsuura, C. Lan, Metal–Organic Frameworks Supported on Nanofiber for Desalination by Direct Contact Membrane Distillation, ACS Appl. Mater. Interfaces. 10 (2018) 11251–11260.

[105] J.E. Efome, M. Baghbanzadeh, D. Rana, T. Matsuura, C.Q. Lan, Effects of superhydrophobic SiO2 nanoparticles on the performance of PVDF flat sheet membranes for vacuum membrane distillation, Desalination. 373 (2015) 47–57. doi:10.1016/j.desal.2015.07.002.

[106] M.A. Barakat, New trends in removing heavy metals from industrial wastewater, Arab. J. Chem. 4 (2011) 361–377. doi:10.1016/j.arabjc.2010.07.019.

[107] M. Ajmal, R.A.K. Rao, R. Ahmad, J. Ahmad, Adsorption studies on Citrus reticulata (fruit peel of orange): Removal and recovery of Ni(II) from electroplating wastewater, J. Hazard. Mater. 79 (2000) 117–131. doi:10.1016/S0304-3894(00)00234-X.

[108] M. Banerjee, R.K. Basu, S.K. Das, Cr(VI) adsorption by a green adsorbent walnut shell: Adsorption studies, regeneration studies, scale-up design and economic feasibility, Process Saf. Environ. Prot. 116 (2018) 693–702. doi:10.1016/j.psep.2018.03.037.

[109] S. Malamis, E. Katsou, A review on zinc and nickel adsorption on natural and modified zeolite, bentonite and vermiculite: Examination of process parameters, kinetics and isotherms, J. Hazard. Mater. 252–253 (2013) 428–461. doi:10.1016/j.jhazmat.2013.03.024.

[110] P.P. Prabhu, B. Prabhu, A Review on Removal of Heavy Metal Ions from Waste Water using Natural/ Modified Bentonite, in: MATEC Web Conf., 2018. doi:10.1051/matecconf/201714402021.

[111] S. Vafakhah, M.E. Bahrololoom, R. Bazarganlari, M. Saeedikhani, Removal of copper ions from electroplating effluent solutions with native corn cob and corn stalk and chemically modified corn stalk, J. Environ. Chem. Eng. 2 (2014) 356–361. doi:10.1016/j.jece.2014.01.005.

[112] C. Li, P. Champagne, Fixed-bed column study for the removal of cadmium (II) and nickel (II) ions from aqueous solutions using peat and mollusk shells, J. Hazard. Mater. 171 (2009) 872–878. doi:10.1016/j.jhazmat.2009.06.084.

[113] J.E. Efome, D. Rana, T. Matsuura, C.Q. Lan, Metal-organic frameworks supported on nanofibers to remove heavy metals, J. Mater. Chem. A. 6 (2018) 4550–4555. doi:10.1039/C7TA10428F.

[114] G. Zheng, H. Ye, Y. Zhang, H. Li, L. Lin, X. Ding, Removal of heavy metal in drinking water resource with cation-exchange resins (Type 110-H) mixed pes membrane adsorbents, J. Hazardous, Toxic, Radioact. Waste. 19 (2015). doi:10.1061/(ASCE)HZ.2153-5515.0000229.

[115] C.W. Abney, J.C. Gilhula, K. Lu, W. Lin, Metal-organic framework templated inorganic sorbents for rapid and effi cient extraction of heavy metals, Adv. Mater. 26 (2014) 7993–7996.

doi:10.1002/adma.201403428.

[116] N. Wang, T. Liu, H. Shen, S. Ji, J.-R. Li, R. Zhang, Ceramic tubular MOF hybrid membrane fabricated through in situ layer-by-layer self-assembly for nanofiltration, AIChE J. 62 (2016). doi:10.1002/aic.15115.

[117] Y. Zhang, N. Wang, S. Ji, R. Zhang, C. Zhao, J.-R. Li, Metal-organic framework/poly(vinyl alcohol) nanohybrid membrane for the pervaporation of toluene/n-heptane mixtures, J. Memb. Sci. 489 (2015). doi:10.1016/j.memsci.2015.04.012.

[118] X. Li, C. Zhang, R. Zhao, X. Lu, X. Xu, X. Jia, C. Wang, L. Li, Efficient adsorption of gold ions from aqueous systems with thioamide-group chelating nanofiber membranes, Chem. Eng. J. 229 (2013) 420–428. doi:10.1016/j.cej.2013.06.022.

[119] Q. Feng, D. Wu, Y. Zhao, A. Wei, Q. Wei, H. Fong, Electrospun AOPAN/RC blend nanofiber membrane for efficient removal of heavy metal ions from water, J. Hazard. Mater. 344 (2018) 819–828. doi:10.1016/j.jhazmat.2017.11.035.

[120] M.A. Barakat, E. Schmidt, Polymer-enhanced ultrafiltration process for heavy metals removal from industrial wastewater, Desalination. 256 (2010) 90–93. doi:10.1016/j.desal.2010.02.008.

[121] Z. Rao, K. Feng, B. Tang, P. Wu, Surface decoration of amino-functionalized metal-organic framework/graphene oxide composite onto polydopamine-coated membrane substrate for highly efficient heavy metal removal, ACS Appl. Mater. Interfaces. 9 (2017). doi:10.1021/acsami.6b15873.

[122] A.Y. Gebreyohannes, L. Giorno, I.F.J. Vankelecom, T. Verbiest, P. Aimar, Effect of operational parameters on the performance of a magnetic responsive biocatalytic membrane reactor, Chem. Eng. J. 308 (2017) 853–862. doi:10.1016/j.cej.2016.09.057.

[123] L. Eykens, I. Hitsov, K. De Sitter, C. Dotremont, L. Pinoy, I. Nopens, B. Van der Bruggen, Influence of membrane thickness and process conditions on direct contact membrane distillation at different salinities, J. Memb. Sci. 498 (2016) 353–364. doi:10.1016/J.MEMSCI.2015.07.037.

[124] S. Mondal, R. Mukherjee, S. De, Process modeling for the removal of phenolic compounds from industrial wastewater using a mixed-matrix membrane, Ind. Eng. Chem. Res. 54 (2015) 514–521. doi:10.1021/ie504358j.

[125] X.B. Ke, Z.F. Zheng, H.W. Liu, H.Y. Zhu, X.P. Gao, L.X. Zhang, N.P. Xu, H. Wang, H.J. Zhao, J. Shi, K.R. Ratinac, High-flux ceramic membranes with a nanomesh of metal oxide nanofibers, J. Phys. Chem. B. 112 (2008) 5000–5006. doi:10.1021/jp709837r.

[126] L.T. Choong, Z. Khan, G.C. Rutledge, Permeability of electrospun fiber mats under hydraulic flow, J. Memb. Sci. 451 (2014) 111–116. doi:10.1016/j.memsci.2013.09.051.

[127] T. Furukawa, K. Kokubo, K. Nakamura, K. Matsumoto, Modeling of the permeate flux decline during MF and UF cross-flow filtration of soy sauce lees, J. Memb. Sci. 322 (2008) 491–502. doi:10.1016/j.memsci.2008.05.068.

[128] D. Zedel, M. Kraume, A. Drews, Modelling and prediction of organic solvent flux and retention of surfactants by organic solvent nanofiltration, J. Memb. Sci. 544 (2017) 323–332. doi:10.1016/j.memsci.2017.09.041.

[129] S. Konishi, K. Saito, S. Furusaki, T. Sugo, Binary metal-ion sorption during permeation through chelating porous membranes, J. Memb. Sci. 111 (1996) 1–6. doi:10.1016/0376-7388(95)00237-5.

[130] Y. Shao, H. Chen, Y. Li, X. Ma, Fabrication of novel porous carbon membrane/sintered metal fibers composite for isopropanol adsorption, Chem. Eng. J. 276 (2015) 51–58.

doi:10.1016/j.cej.2015.04.080.

[131] X. Wang, Y. Li, H. Li, C. Yang, Chitosan membrane adsorber for low concentration copper ion removal, Carbohydr. Polym. 146 (2016) 274–281. doi:10.1016/j.carbpol.2016.03.055.

[132] K. Ohwada, On the pauling electronegativity scales-II, Polyhedron. 3 (1984) 853–859. doi:10.1016/S0277-5387(00)84634-3.

Chapter 3

Metal–organic frameworks supported on nanofibers to remove heavy metals

*Johnson E. Efome, Dipak Rana *, Takeshi Matsuura and Christopher Q. Lan*

Industrial Membrane Research Institute, Department of Chemical and Biological Engineering, University of Ottawa, 161 Louis Pasteur Private, Ottawa, Ontario, K1N 6N5, Canada

This current chapter is a manuscript published in the Journal of material Chemistry A
J. Mater. Chem. A, 2018, 6, 4550-4555

Abstract

Fe (III) and Zr (IV) based metal–organic frameworks (MOFs) were enmeshed in polyacrylonitrile (PAN) and polyvinylidene fluoride (PVDF) electro-spun nanofibers to produce nanofibrous MOF membranes (NMOM). The pristine MOFs showed high adsorption capacity for lead ions and mercury ions from aqueous solution. The Fe (III) based MOFs with PAN based NMOM exhibited a high flux of 348 L m^{-2} h^{-1} with a permeance of 870 L m^{-1} h^{-1} bar^{-1}. At room temperature, the NMOM could treat 395 mL of 100 ppb Pb (II) solution, while maintaining a drinking water standard of < 10 ppb of permeate Pb (II) concentration. Due to the high compatibility between MOF and PVDF nanofibers, MOF was not detected in the permeate even after four cycles of filtration and desorption experiments and more than 90% of the NMOM adsorption capacity was retained. The excellent filtration performance and re-generability of the membrane coupled with the hydro-stability of the MOFs suggests that the NMOMs have potential for water treatment through the process of membrane adsorption.

With the steady rise in global population and the need for continuous industrialization, pollution and contamination have been in the forefront, compromising the essentials of life such as clean water. Water contamination is a growing cause for deteriorating public health as more attention is being focused upon anthropogenic sources of contamination. Developing countries suffer the most with death rates of approximately 6 children per minute as a result of unsafe water and sanitation.[1] Among these contaminants, heavy metals have shown their omnipresence with relatively severe negative health impacts. These heavy metals have been a challenge for the water treatment industry for decades because they cannot be degraded by natural biological mechanisms. As such, solid phase sorbents have been developed for industrial applications to treat contaminated water. Metal oxide and nanoparticles have been developed and used for the adsorptive removal of heavy metals, among others including silver,[2] mercury,[3] arsenic,[4] and copper. The challenges researchers face by using these types of sorbent materials include their low adsorptive capacities, mostly due to low surface area and even the possibility of degradation during the treatment process. Porous mixed-matrix membranes (PMM) have also been developed as filters for heavy metal sequestration. Issues such as large pore size distribution, low rejection, low flux and in some cases, high pressure have always been dominant concerning which have rendered the process cost inefficient.

A new class of material, consisting of a central metal ion or cluster and an organic linker known as metal–organic frameworks (MOFs), is gaining immense attention and has emerged as a superior solution for the porous material industry. These materials use the combined effects of their organic and inorganic moieties to attain extraordinary porosity for a crystal, tunable pore sizes, high surface area to mass ratios (>6000 $m^2 g^{-1}$),[5] even surface area >7000 $m^2 g^{-1}$ (NU-109E and NU-110E reporting up to 7140 $m^2 g^{-1}$),[6] and possess chemical and structural stability.[7,8] These porous materials are very visible in the research of gaseous systems but due to their instability in aqueous medium, a very limited number of MOFs have

been used in water treatment trials. This has triggered further research into developing more chemically, and more importantly, water stable MOFs with the invention of a wide range of water stable MOFs in recent years.[7,9] Among these that have been developed, the common path is through the high valence $Zr^{4+}$and Fe^{3+}metal ions. These contain zirconium metal ion clusters and some iron metal ions and their derivatives. They have either been used as sorbent crystals for adsorption of heavy metals,[10] or as fillers for mixed matrix membranes and as a coated film on ceramic membranes for desalination.[11,12] Some researchers have proposed the use of MOFs as fillers in electrospun nanofibers but in most cases, for gaseous systems.[13] Compared to the conventional method of preparing mixed matrix membranes, electrospinning is a very low cost and simple technique employed in preparing membranes that have relatively high fluxes, porosity and mechanical strength. This process requires very little polymer and little post treatment of membrane, thus making this a more environmentally friendly technique.

The organic moiety of the MOF and the electrospun polymer are usually compatible, making it possible for the MOF crystals to be distributed evenly at high loading rates with less aggregation. MOF–nanofibrous membranes have been used in air pollution controls.[13] Hydrogen storage and in other gaseous related works however there is no available literature in the adsorption or rejection of heavy metals from aqueous solution.

Though MOFs have been incorporated into nanofibers before,[14,15] herein, we report for the first time, a nanofibrous MOF membrane (NMOM) for heavy metal sequestration from an aqueous medium. Two highly water stable MOFs were selected and enmeshed into two polymers, hydrophilic polyacrylonitrile (PAN) and hydrophobic polyvinylidene fluoride (PVDF), for the study involving two heavy metals ions, lead and mercury.

The two MOFs selected for this study were MOF 808, a zirconium based MOF $[Zr_6O_4(OH)_4(COOH)_6(BTC)_2]$ that has an overall diamond-like shape with the Zr_6 cluster in the

secondary building unit (SBU) being coordinated with six benzene tricarboxylate (BTC) with resulting pore dimensions ranging from 4.8 to 18 Å,[16] and BET surface areas of 560 m^2 g^{-1}. The strength of the Zr–O (metal-linker) bond in zirconium-based MOFs has made them very resistant to hydrolysis. Hence, these are suitable for water related applications and particularly for chemical weapon agents hydrolysis.[17] MOF-F300 has iron as a central metal but very little about its structure is known or has been released in the literature. This is due to its poor crystallinity. Some researchers have referred to this as an amorphous structure. It has a BET surface area ranging from 1300–1600 m^2 g^{-1} with a pore aperture of 21 Å. F300 is comparable to Material of Institute Lavoisier (MIL100-Fe) [$Fe_3OF–(H_2O)_2(BTC)_2 \cdot nH_2O$] in that these both have the same central metal ion (Fe), same linkers (BTC), approximately the same pore size, and iron and carbon mass contents.[18]

PAN and PVDF are well known water stable polymers that have been developed and characterized for water related applications. Their hydrothermal, chemical and mechanical properties have placed them among the most suitable polymers for temperature and pressure driven separation processes.

Here, we performed a systematic study of the heavy metal interaction with the MOF alone, with the nanofiber membrane and with the MOF/nanofibrous substrates. It could be deduced that the heavy metals adsorption mechanism involved competitive ion exchange (CIE), electrostatic interactions with the MOF crystals or polymer, and binding to open metal sites on the MOF (pore filling mechanism) (Fig. 3-1).

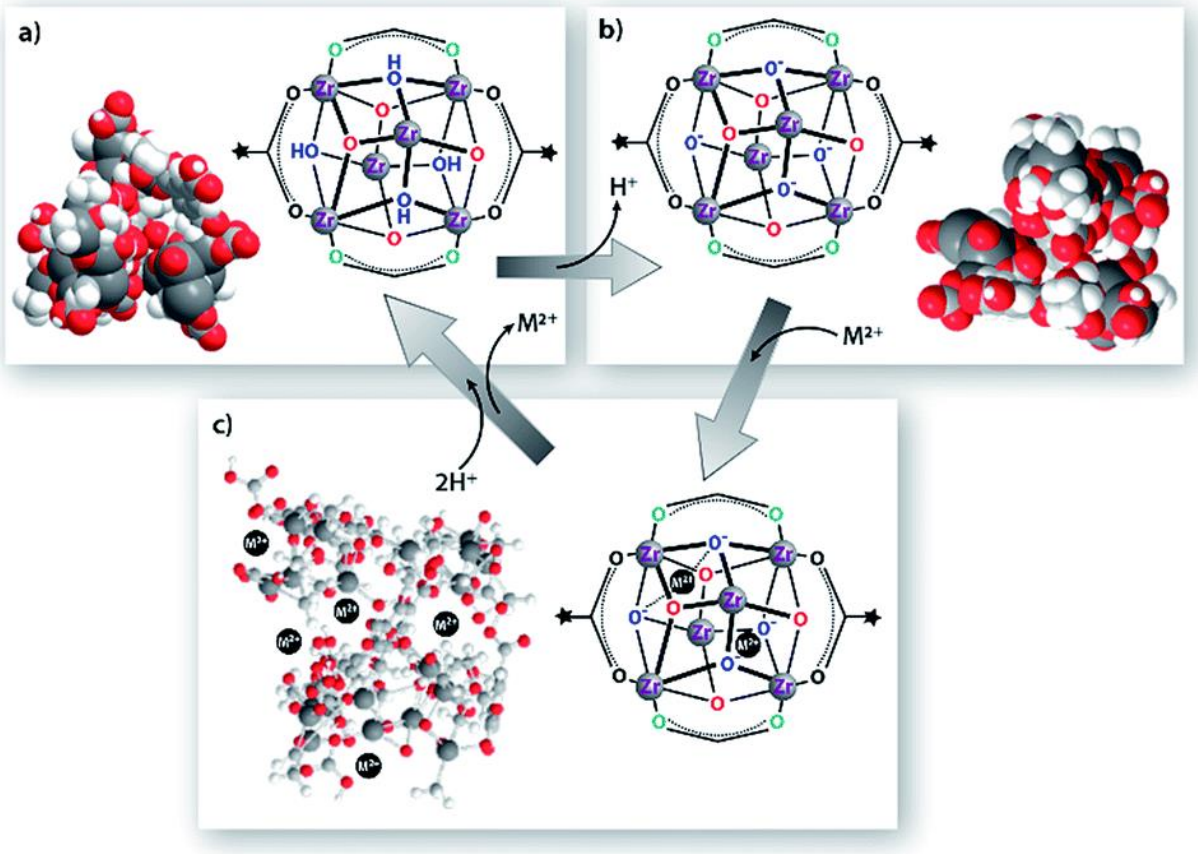

Figure 3-1. MOF 808 demonstration of heavy metal adsorption by electrostatic interaction at the surface and pore space caused by a change in pH. (a) MOF 808, (b) deprotonated MOF 808, and (c) heavy metal ion bound MOF. Color code: Zr = grey, C = ash, O = red, H =white, M^{2+} refers to heavy metal ions, black dots represent adsorbed M^{2+}.

The polymer concentrations, MOF loadings, and electrospinning parameters were all optimized to produce bead free nanofiber mats and to minimize particle aggregation. MOF loadings of up to 20 wt. % were achieved with little aggregation while PAN and PVDF concentrations were 10 wt. % and 20 w/v%, respectively, producing nanofibers with diameters ranging from 100–400 nm (Fig. 3-2). The PXRD spectra of the pristine MOFs, after heavy metal adsorption and when immersed in water, revealed that MOF 808 maintains its crystalline form even after long term exposures, while F300 showed amorphous characteristics before and after adsorption (Fig. A1 and A2 in Appendix A). Transmission

electron microscopy (TEM) images of the MOFs revealed a more rhombic morphology for MOF 808 and a F300 with a rounded edge (Fig. 3-2 and A3–A5 in Appendix A).

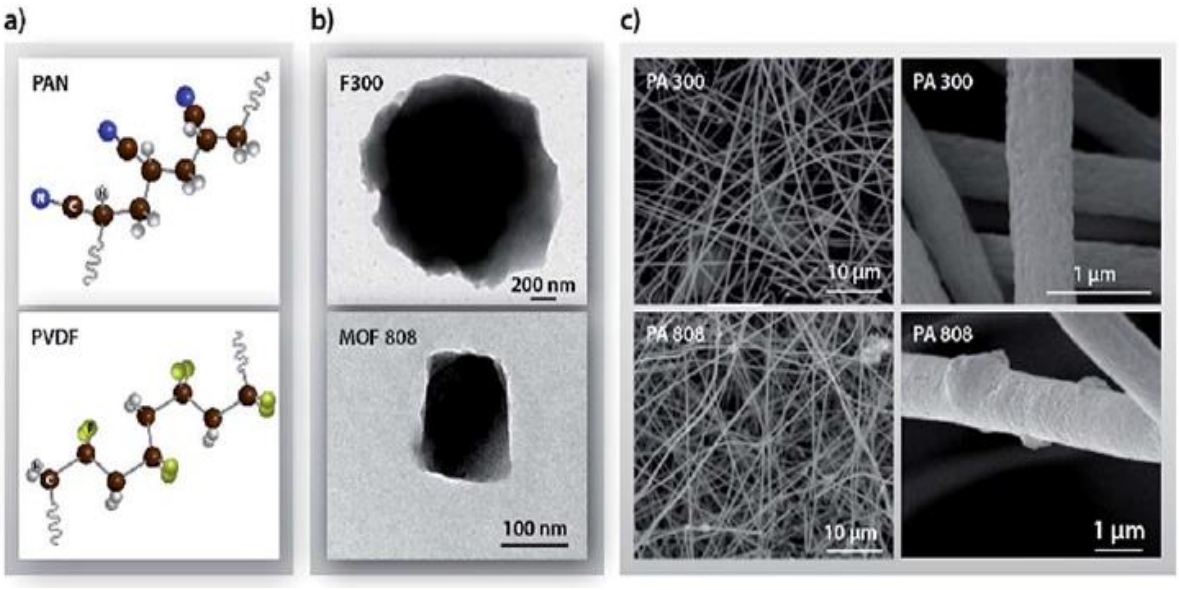

Figure 3-2. Chemical structure of the main polymers: (a) PAN and PVDF; (b) TEM images of the MOFs: F300 and MOF 808; and (c) SEM images of the NMOM with 20 wt. % MOF loading: PA 300 and PA 808.

Thermogravimetric analysis (TGA) curves of the MOFs particles and the NMOM (Fig. A6 in Appendix A) reveal that the composites are much more stable at higher temperatures than the MOFs alone. The neat PVDF nanofibers where very stable at temperatures below 400 °C, while the neat PAN was stable at temperatures below 270 °C, at which temperature, 40% of the weight was lost with a complete degradation taking place beyond 300 °C. The MOF 808 crystals lost 60 wt. % weight at about 330 °C. This massive drop in weight is as a result of the loss of coordinated solvent trapped in the pores. MOF F300 also showed a similar trend, though a lower 25 wt. % loss at 100 °C, due to trapped moisture, with another 40 wt. % loss at approximately 330 °C. The initial weight losses were mainly due to loss of

coordinated solvent and moisture, followed by decomposition of the ligand. Further analysis of the nanofibrous MOF composite revealed that though there was an initial 6–10 wt. % weight loss due to solvent escaping from the MOF, the bulk of the material for both polymers was stable at temperatures up to 300 °C.

Given the porosity of both MOFs and the nanofibers mat, sorption for heavy metals ions (Pb and Hg) were investigated. The MOF powder, as well as pieces of the neat nanofiber mats and pieces of the NMOM were added to specific volumes of 10 ppm heavy metal ion solution for a contact time of 3 h to determine the reaction kinetics. The data was analyzed using the pseudo first and second order and the intra-particle diffusion models. By varying the metal ion concentration (10–900 ppm), the various isotherms were established and fitted using the Langmuir,[19] Freundlich,[20] and Temkin[21] models as denoted respectively by their linearized eqn (3-1)–(3-3).

$$\frac{1}{q_e} = \frac{1}{q_m} + \frac{1}{q_m K_l C_e} \qquad (3-1)$$

$$lnq_e = lnK_f + \frac{1}{n} lnC_e \qquad (3-2)$$

$$q_e = BlnA_T + BlnC_e \qquad (3-3)$$

where q_e is the equilibrium sorption capacity, q_m is the maximum sorption capacity of the sorbent (saturation point), C_e is the concentration of heavy metal ion in solution at equilibrium [mg L^{-1}] and K_l is the Langmuir adsorption constant [L mg^{-1}], K_f = Freundlich isotherm constant [mg g^{-1}(L $mg^{-1})^{1/n}$], n = adsorption intensity, A_T = Temkin isotherm equilibrium binding constant [L g^{-1}], B_T = Temkin isotherm constant [J mol^{-1}], $B = RT/b_T$, constant related to the heat of sorption, T = temperature at 298 K, R = universal gas constant [8.314 J mol^{-1} K^{-1}].

Changes in the pH had a tremendous impact on the adsorption of the heavy metals. A systematic study of the pH variation as demonstrated (Fig. A7 in Appendix A), revealed that for both Hg^{2+} and Pb^{2+}, removal per cents of up to 98% were achieved at a pH > 10. Since heavy metal ions typically precipitate at pH > 5, it is difficult to distinguish the removal mechanism at pH > 5 (either by MOF or precipitation). To understand the prevailing adsorption principle, and be certain that precipitation is negligible, this article only presents data at pH < 5. To further understand MOF–heavy metal interaction, the zeta potential of the MOFs was measured at the varied pH value. As shown in Fig. 3-3, the surface charge for both MOFs became more negative as the pH increased, enhancing electrostatic interactions which accounted for the higher adsorption. At low pH, deprotonation of the COOH group is minimal, but as pH increases, excess OH^- trigger faster deprotonation leading to COO^-. Hence, resulting in a negative surface charge. MOF 808 was deprotonated more than F300, which accounted for its higher negative surface charge (−36 mV) at high pH. The PAN and PVDF showed very little adsorption of the heavy metals due to their low negative surface charge (−10 and −15 mV, respectively). It is thus concluded, from this standpoint, that the mechanism of adsorption between MOF–nanofiber–heavy metals is due to electrostatic attraction of unlike charges.

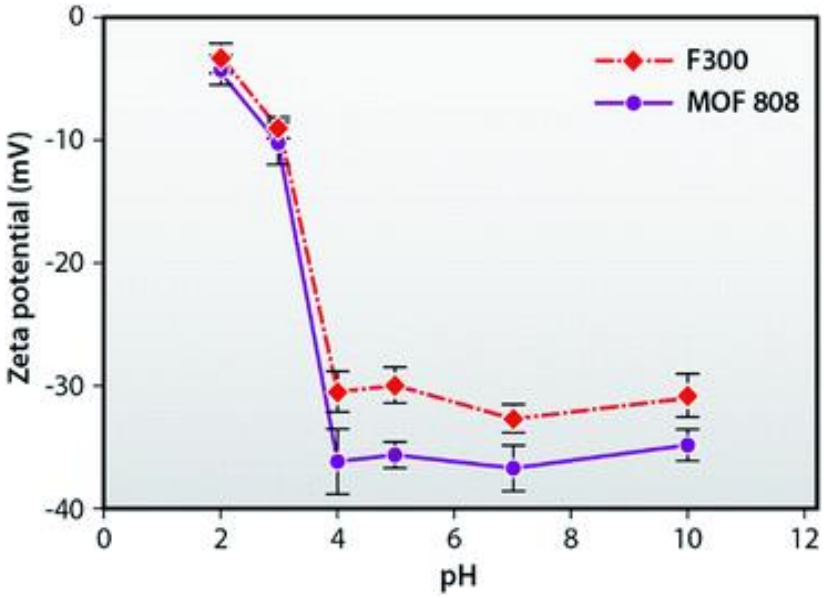

Figure 3-3. Zeta potential vs. pH of the MOFs. The pH of the solution was maintained under buffer conditions for each measurement.

Since the nanofiber mat average pore size (~0.5 μm) by far surpasses the atomic diameter of both Hg and Pb ions (3.0×10^{-4} and 3.6×10^{-4} μm, respectively), rejection due to size exclusion would not play a very significant role in the removal process when compared to electrostatic interactions and confinement of heavy metals ions in the pores of the MOF.

The XPS spectra of the pristine MOF, compared to the MOF after adsorption experiments, (Fig. A8 in Appendix A) revealed that the heavy metal ions were electrostatically attached to the internal functional groups of the MOF since no heavy metal peaks were seen on the spectrum. This was also confirmed from EDX analysis (Fig. A9 in Appendix A) of the NMOM surface after the filtration test. The elemental map could not detect any heavy metal on the surface, implying internal pore adsorption occurred. A plausible mechanism for heavy metal adsorption (Fig. 3-1), is that the negative MOF surface is just a tool for attracting the positively charged cations to itself. Since the pore has a stronger net negative charge due to the sea of COO^- groups surrounding it, the cation will then be 'sucked' into the pores for

'storage' rather than be attached to the external surface of the MOF. This theory was further validated by FTIR absorbance spectra of the MOFs (Fig. A10 in Appendix A), in which any possible Hg–O nor Pb–O bonds were not found. It is therefore worth mentioning that, the positive heavy metal ions were attracted into the pores because, inside the pore cavity, the combined negative charge effect of COO^- was stronger than the floating sporadic COO^- on the MOF surface. Because of this strong electrostatic drag, sorption was effected more in the pores.

Drastic reductions in pH during the sorption experiments were experienced implying ion exchange was occurring simultaneously. The pH of the solution decreased continuously with time indicating that, the heavy metal ions have been exchanged with H^+ ions and have released these to the bulk, thus decreasing the pH. At low pH, the adsorption of heavy metal ion was lower than when compared at higher pH values (Fig. A11 in Appendix A). Using the concept of higher zeta potential at higher pH (Fig. 3-3), there is also less competition for attraction at the pores. At high pH (excess OH^-), positive heavy metal ions bind easily to the MOF of which, at high H^+ concentration (low pH), a competitive adsorption process occurs and protons easily attach to the free COO^-, changing the zeta potential towards positive. Hence, the adsorption reduces.[22] It is for this reason that the pH of the adsorption process was adjusted to be maintained at a specific level. When the pH is not adjusted, as the heavy metal ions are adsorbed and protons are released, a reverse inhibition sets in due to accumulated protons in the system (Fig. A12 in Appendix A). These protons trigger a competitive inhibition mechanism and the adsorption capacity starts reducing because of reduced adsorption sites. This will reduce until protons are exhausted and then heavy metal adsorption kicks in, turning the process into a loop-like mechanism which results in the hill and valley nature of the curve. Determining the maximum adsorption capacity of the adsorbent under these conditions would have been difficult, and therefore there was a need to maintain a constant pH.

The rate of adsorption of heavy metal ions was analyzed using adsorption kinetic models. The kinetic data (Table A1 and Fig. A13 and A14 in Appendix A) demonstrate that the adsorption of both Pb and Hg for both MOFs was fast with equilibrium attained after 1 h. This fast adsorption is attributed to the high negative zeta potential of both MOFs at the studied pH of 4.6 with MOF 808 showing a higher capacity than F300. Further analysis of the data using the pseudo-first, pseudo-second and intra-particle models was performed. It must be noted that, the kinetic experiment of the nanofiber membranes was too slow within the period for generating the data, and thus, this could not be presented in this report. The results showed that both MOFs followed pseudo-second order kinetics ($R^2 > 0.98$).

Fig. 3-4 shows the adsorption behavior of Pb^{2+} and Hg^{2+} ions into the different MOFs and the NMOM. Three isotherm models were used to analyze the adsorption behavior; Langmuir, Freundlich and Temkin as stated by their linear forms [eqn (3-1)–(3-3)] and the results are presented in Fig. A13 and A14 in Appendix A

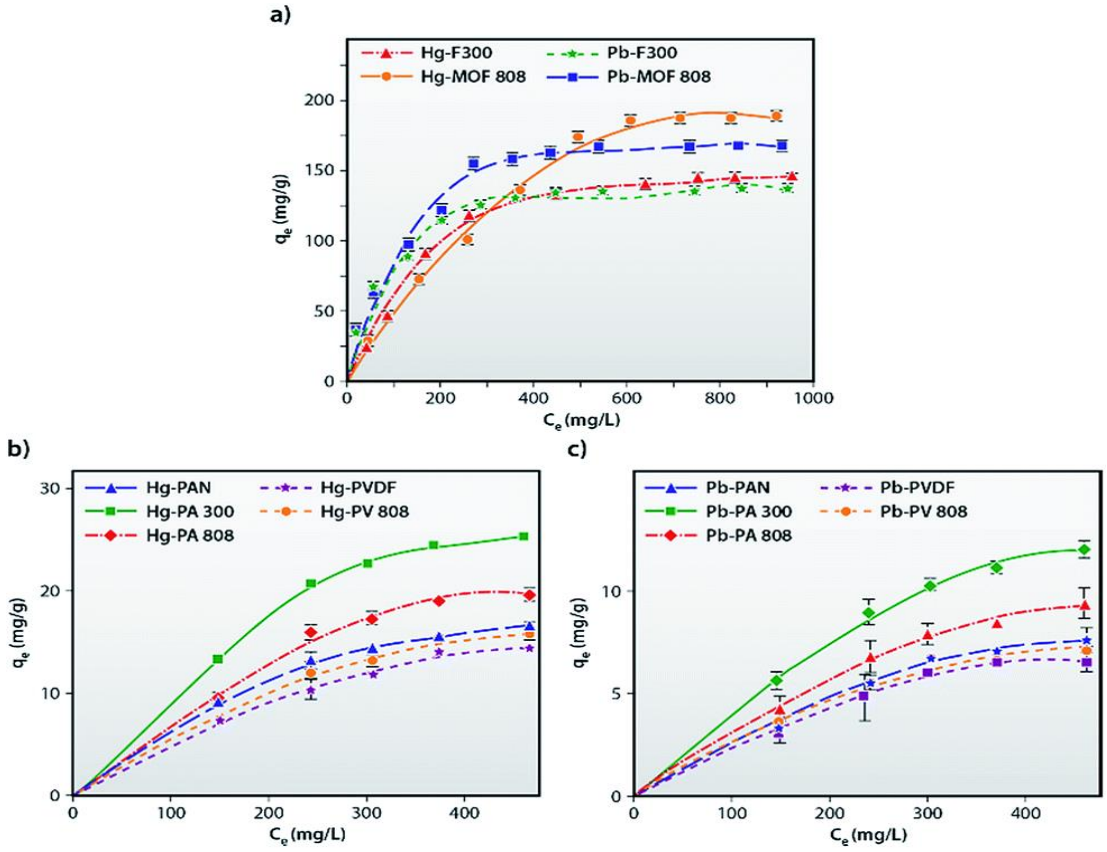

Figure 3-4.(a) Sorption data for the MOF with Pb and Hg ions, (b) sorption data for NMOM and Hg ions, and (c) sorption data for NMOM and Pb ions at a pH of 4.6 ± 0.2.

For all data, the Langmuir model was followed, with the highest R^2 value denoting a homogeneous adsorption, and the maximum adsorption capacities calculated were as follows: 170.74, 276.96, 148.13, and 229.66 mg g^{-1} for the MOF 808 Pb, MOF 808-Hg, F300-Pb, and F300-Hg, respectively (Table 3-1). The adsorption capacity of the nanofiber (NF) and NMOM were also studied and it was revealed that the hydrophilicity and hydrophobicity of the polymers had significant effects. Though PVDF nanofibers have a higher surface area than PAN nanofiber because of the smaller fiber diameter, it is hydrophobic with a contact angle >138°. This posed a greater resistance to the contact between the NF and the solution. Since the MOFs crystals are lying on the surface of NF, this accounted for the low adsorption

performance of the PVDF–NMOM. PAN nanofiber mat showed a much smaller contact angle which facilitates contact with aqueous solution and hence, the higher adsorption capacities were achieved.

Table 3-1. Selected physical and sorption data for the MOFs and NMOM[a]

Sorbent	Composition	z potential [mV]	H_g q_{max} |mg g^{-1}|	Pb q_{max} |mg g^{-1}|	q_{max}^* Hg	q_{max}^* Pb
F300	$[Fe_3OF–(H_2O)_2(BTC)_2nH_2O]$	30	229.66	148.13		
MOF 808	$[Zr_6O_4(OH)_4(CO_2H)_6(BTC)_2]$	36	276.96	170.74		
PAN	$–[C_3H_3N]_n$	10	28.76	15.09		
PA 300	$–[C_3H_3N]_n$ /F300	—	53.09	30.19	265.45	150.95
PA 808	$–[C_3H_3N]_n$ /MOF 808	—	50.88	23.98	254.4	119.9
PVDF	$–[C_2H_2F_2]_n$	18	28.64	13.62		
PV 300	$–[C_2H_2F_2]_n$ /F300	—	—	—		
PV 808	$–[C_2H_2F_2]_n$ /MOF 808	—	42.60	17.19	213	85.95

[a] q_{max}^* represents the normalized adsorption capacity of the MOF with respect to its weight ratio to the polymer. In this case, the weight of the MOF was maintained at 20 wt. %.

Since the NMOM showed improved adsorption capacity compared to the NF and taking into the account the fast kinetics of the heavy metal adsorption process, the NMOMs have high potential for use in water purification systems. It is interesting to note that although MOF 808 showed higher adsorption capacity than F300 as standalone, in the enmeshed form, F300 membranes performed better than MOF 808 membranes. For example, note the Pb adsorption (q^{PA300}_{max} (30.193) > q^{PA808}_{max} (23.977)). This implied that a larger quantity of F300 was available for adsorption in the membrane than MOF 808. It was further

determined (eqn (3-3), Tables A3–A7 in Appendix A) from the adsorption data that for PA 808, only 65.56% of the MOF was available for adsorption while 77.69% for PA 300.

Our results could be attributed to the size of the MOF particles. MOF 808 had smaller particle sizes ranging from 100–700 nm while F300 had a single crystal of up to 900 nm with also large aggregates as measured using SEM/TEM and dynamic light scattering (DLS). It was easier for M808 to be 'engulfed' in the nanofiber than F300. Hence, a lesser region of the particle was exposed to the bulk for adsorption.

These results are in line with what Wu et al. has obtained.[23] Although they worked with a gas phase process, the MOFs accessibility was significantly reduced when enmeshed in the nanofiber mat especially for the PVDF composites. That notwithstanding, Ostermann et al.'s report says that the MOFs are fully accessible even after being enmeshed in nanofiber[14] which was more the case with the PAN composites. The adsorption capacity, source of metal ion, pH, and time to adsorption equilibrium of Pb and Hg with other MOFs and membranes has also been presented in Table A8 in Appendix A for comparison purposes. This data basically indicates that the present MOF–polymer combination is a better sorbent.

As mentioned earlier, due to the hydrophobicity of PVDF nanofiber, the adsorption capacity of PVDF based NMOM was low. Hence the PAN based NMOM was selected for a filtration test of Pb^{2+} ion solution together with the neat PAN nanofiber as the control. A batch system was used to perform the filtration experiment with a feed concentration of ca. 100 ppb at room temperature. The transmembrane pressure was provided from a N_2 cylinder and controlled at 6.0 psig (0.4 barg). It should be noted that a thin PVDF layer (no MOF included) had to be attached to the bottom of the tested PAN based membranes due to the very high flux experienced (>2000 L m^{-2} h^{-1}) by the membrane without PVDF support. It was only in this way that the filtration experiment was possible with measurable fluxes at a reasonable transmembrane pressure. The combined thickness of the membrane was 560 ± 15 μm and the effective

surface area was 3.8×10^{-3} m^2. The breakthrough curves for the passage of heavy metal ion through PA 300 and PA 808 are represented together with the neat PA membrane in Fig. 3-5. The PA 300 membrane could remove Pb^{2+} ions completely from the solution until 395 mL of permeate was collected at a flux of 348 ± 25.8 L m^{-2} h^{-1} and a permeance of 870 L m^{-2} h^{-1} bar^{-1}, while the PA808 membrane could treat 295 mL of contaminated water. This difference in performance aligns with the NMOM adsorption results where F300 performed better than M808.

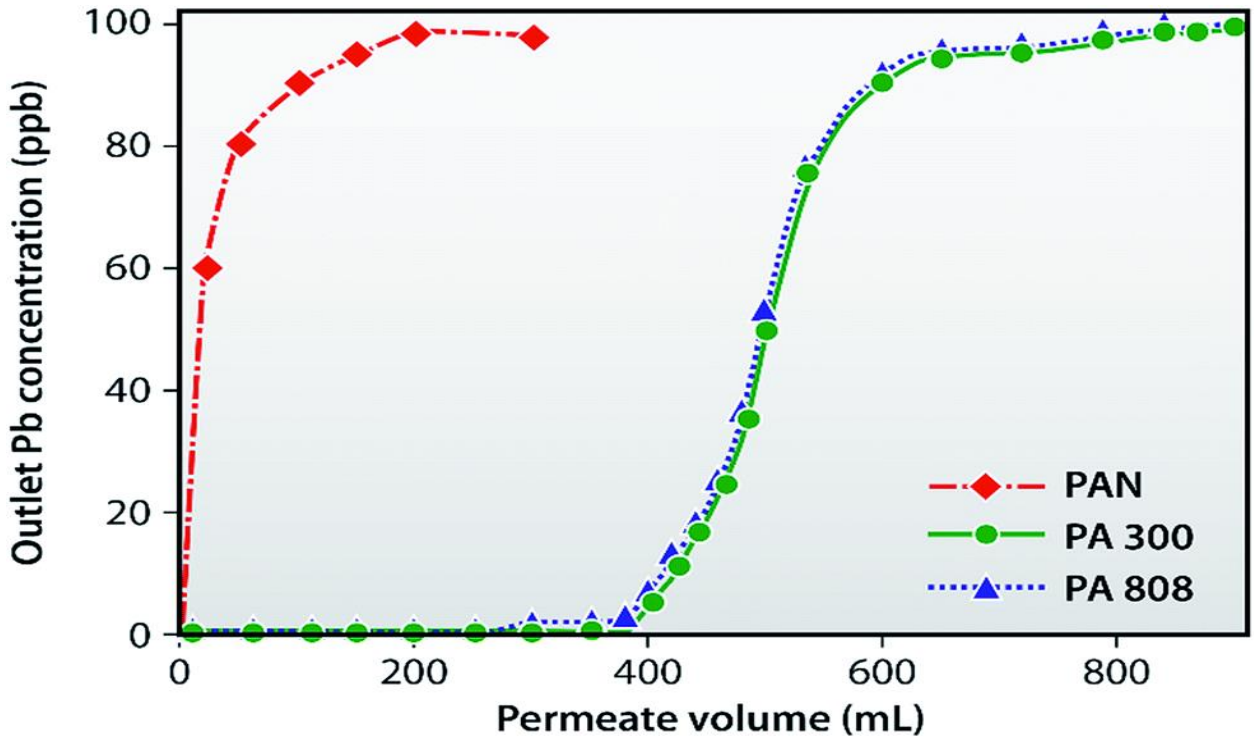

Figure 3-5. Breakthrough curve for the passage of Pb ion through PA 300 and PA 808 at a fixed pressure of 6.0 psig and room temperature. The actual feed concentration was 98.2 ppb.

The adsorption capacity of PA 808 and PA 300 at 10% breakthrough was estimated to be 228.4 and 360 mg Pb g^{-1} membrane, respectively. The collected permeate from both the PA 300 and PA 808 filtration was also tested for MOF leakage. The concentrations of Fe and Zr were measured at the parts per trillion

(ppt) levels and neither Fe nor Zr ions were detected in the blank, feed and permeate solution, which confirms no leakage of MOF from nanofibers membrane into the solution.

For economical operation, the re-use of the membrane is necessary. Four cycles of adsorption and desorption experiments were conducted as shown in Fig. 3-6. The breakthrough curves indicate that after a 4-cycle adsorption–desorption–washing, the capacity of the membrane at 10% breakthrough was still maintained at the same level as the original membrane. Hence, it is evident that the filtration process can be executed for four successful cycles while maintaining the satisfying permeate quality. The adsorption capacity of the membrane could be enhanced to treat higher heavy metal concentrations by stacking the films.

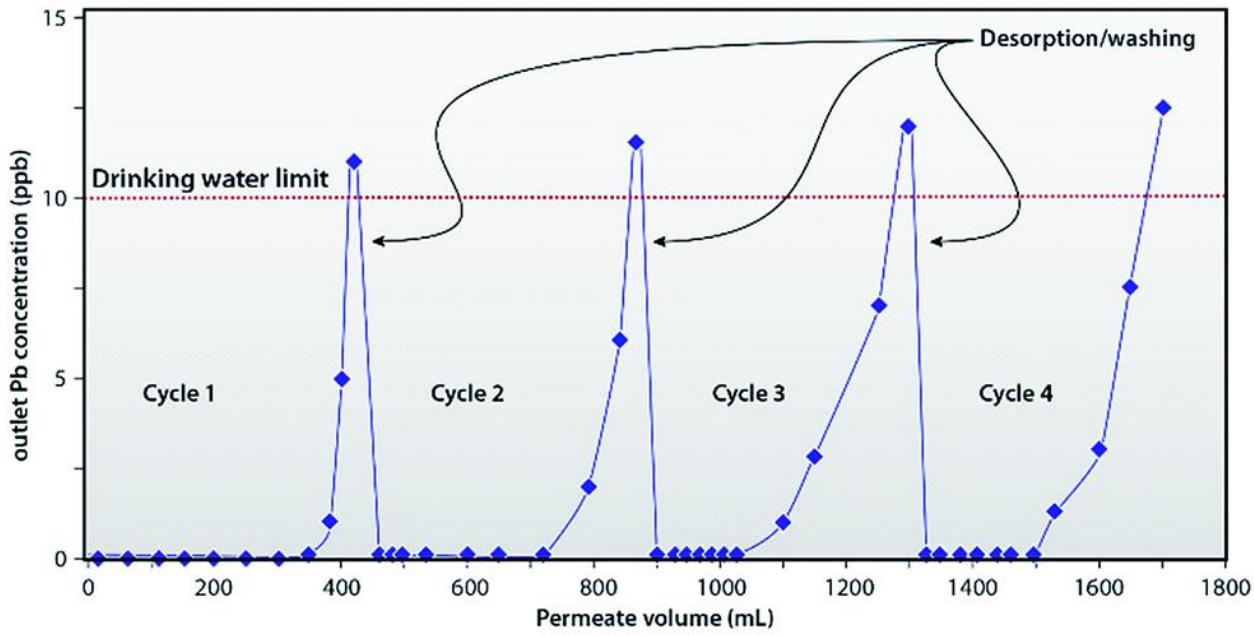

Figure 3-6. Adsorption and desorption filtration data for up to 4 runs for the passage of Pb ions. Desorption was initiated whenever the permeate concentration surpassed the 10-ppb maximum allowable concentration for drinking water. The feed column was re-filled continuously as the runs proceeded. A single run was determined when the permeate concentration exceeded the maximum allowable concentration for drinking water.

In summary, we have developed a novel nanofibrous MOF membrane for efficient water purification. Our membrane filtration module could remove Pb (II) ions from solution with a moderate permeance of

248.57 L m^{-2} h^{-1} bar^{-1} for a membrane thickness of 560 μm. The purity of the permeate met the drinking water standards for the heavy metal studied. The highly negative surface charge of the MOFs facilitated the sequestration of the heavy metals. Since it was proven that not all of the MOF crystals were available for adsorption due to pore blockage and shadowing by the polymer, stacking of membranes could be used to improve the filtration in cases of higher feed concentrations. It is thus evident that, our MOF nanofibrous membrane can be integrated into existing wastewater treatment schemes or be used as a standalone filter for water purification.

3.1 Experimental section

Detailed experimental methods including synthesis MOF 808, batch adsorption–desorption experiments, filtration experiment and instrumentations are presented in the Appendix A-Supporting Information

3.2 Acknowledgements

The authors gratefully acknowledge the financial support from the Natural Sciences and Engineering Council (NSERC) of Canada through Strategic Partnership Grant for Projects (SPTGP) # 463039-2014.

References

1. UNEP, Financing wastewater collection and treatment in relation to the Millennium Development Goals and World Summit on Sustainable Development targets on water and sanitation, Gov. Counc. United Nations Environ. Program 2004, pp. 1–26
2. A. Cao, V. P. Veedu, X. Li, Z. Yao, M. N. Ghasemi-Nejhad and P. M. Ajayan, Nat. Mater., 2005, 4, 540
3. B. Li, Y. Zhang, D. Ma, Z. Shi and S. Ma, Nat. Commun., 2014, 5, 5537
4. J. S. Hu, L. S. Zhong, W. G. Song and L. J. Wan, Adv. Mater., 2008, 20, 2977
5. H.-C. Zhou, J. R. Long and O. M. Yaghi, Chem. Rev., 2012, 112, 673
6. O. K. Farha, I. Eryazici, N. C. Jeong, B. G. Hauser, C. E. Wilmer, A. A. Sarjeant, R. Q. Snurr, S. T. Nguyen, A. Ö. Yazaydın and J. T. Hupp, J. Am. Chem. Soc., 2012, 134(36), 15016–15021
7. H.-C. Zhou and S. Kitagawa, Chem. Soc. Rev., 2014, 43(16), 5415–5418
8. C. Wang, X. Liu, N. K. Demir, J. P. Chen and K. Li, Chem. Soc. Rev., 2016, 45, 5107–5134
9. P. A. Kobielska, A. J. Howarth, O. K. Farha and S. Nayak, Coord. Chem. Rev., 2018, 358, 92–107
10. C. W. Abney, J. C. Gilhula, K. Lu and W. Lin, Adv. Mater., 2014, 26, 7993
11. X. Liu, N. K. Demir, Z. Wu and K. Li, J. Am. Chem. Soc., 2015, 137, 6999
12. N. Yin, K. Wang, L. Wang and Z. Li, Chem. Eng. J., 2016, 306, 619
13. Y. Zhang, S. Yuan, X. Feng, H. Li, J. Zhou and B. Wang, J. Am. Chem. Soc., 2016, 138, 5785
14. R. Ostermann, J. Cravillon, C. Weidmann, M. Wiebcke and B. M. Smarsly, Chem. Commun., 2011, 47, 442
15. M. Bechelany, M. Drobek, C. Vallicari, A. Abou Chaaya, A. Julbe and P. Miele, Nanoscale, 2015, 7, 5794

16. H. Furukawa, F. Gándara, Y.-B. Zhang, J. Jiang, W. L. Queen, M. R. Hudson and O. M. Yaghi, J. Am. Chem. Soc., 2014, 136, 4369
17. S. S. Mondal and H. J. Holdt, Angew. Chem., Int. Ed., 2016, 55, 42
18. A. Dhakshinamoorthy, M. Alvaro, P. Horcajada, E. Gibson, M. Vishnuvarthan, A. Vimont, J.-M. Grenèche, C. Serre, M. Daturi and H. Garcia, ACS Catal., 2012, 2, 2060
19. Langmuir, J. Am. Chem. Soc., 1918, 40, 1361
20. H. Freundlich, Trans. Faraday Soc., 1931, 28, 195
21. M. I. Temkin, Zh. Fiz. Khim., 1941, 15, 296
22. D. Chen, W. Shen, S. Wu, C. Chen, X. Luo and L. Guo, Nanoscale, 2016, 8, 7172
23. Y. Wu, F. Li, H. Liu, W. Zhu, M. Teng, Y. Jiang, W. Li, D. Xu, D. He, P. Hannam and G. Li, J. Mater. Chem., 2012, 22, 16971

Chapter 4

Insight Studies on Metal-Organic Framework Nanofibrous Membrane Adsorption and Activation for Heavy Metal Ions Removal from Aqueous Solution

Johnson E. Efome, Dipak Rana, Takeshi Matsuura and Christopher Q. Lan*

Industrial Membrane Research Institute, Department of Chemical and Biological Engineering, University of Ottawa, 161 Louis Pasteur Private, Ottawa, Ontario, K1N 6N5, Canada

This current chapter is a manuscript published in the ACS journal
Applied Materials & Interfaces, 2018,* 10 *(22), 18619–18629

Abstract

Electrospun nanofiber composite membranes containing water-stable metal-organic frameworks (MOFs) particles (Zr-based MOF-808) supported on polyacrylonitrile (PAN) nanofiber synthesized via co-electrospinning have been prepared. MOF particles were dispersed in the organic polymer, and their subsequent presence was inferred by scanning electron microscopy. Membrane performance in heavy metal ion adsorption in batch filtration was evaluated on the basis of Cd^{2+} and Zn^{2+} ions sequestration. The adsorption capacities of the pristine MOF and the MOF composite membrane revealed that MOF particles in the membrane could be accessed for adsorption in the hydrophilic PAN membranes. The maximum adsorption capacities were 225.05 and 287.06 mg g^{-1} for Cd^{2+} and Zn^{2+}, respectively. Conventional thermal activation of pristine MOF and composite membrane revealed a crystal downsizing, while "hydractivation" (activation through water), produced an expanded MOF with enhanced adsorption potentials. The PAN/MOF-808 "hydractivated" composite membrane could treat 580 mL of Cd, whereas the conventional vacuum-activated composite treated 464 mL. The high separation performance and reusability of the membranes and the outstanding water stability of the MOFs suggested the developed membrane as a potential candidate for water treatment.

4.1 Introduction

Adsorption has been regarded as an easy and facile technique for removal of contaminants from contaminated streams.(1) This process is made feasible because of the porous nature of the adsorbents and the pore geometry of the materials. The underlying adsorption mechanism has always been up for debate, but research has shown that the surface to mass ratio of the adsorbent is a key factor in retaining contaminants. Metal-organic frameworks (MOFs), a new generation of materials comprising of metal ions/clusters linked by organic moieties, have been proven to possess the highest achievable surface to mass ratio of any material with tunable pore geometry and chemical stability.(2) It is for such reasons that MOFs have been present in a diverse range of applications including and more prevalent in gas storage/capture,(3,4) metal ion sensing,(5−7) separation, drug delivery,(8,9) catalysis,(10,11) sensors,(12,13) and even in aqueous medium sequestration of heavy metal ions.(14−17) Heavy metals are known for their indigestive behavior as they easily accumulate in the human body causing serious illnesses ranging from liver damage to kidney failure. It is for this reason that the World Health Organization has set specific guidelines regarding the water quality components, including heavy metals ions.(18)

The direct use of MOFs for heavy metal removal has been limited to laboratory scale experiments because the particles would be required in large amounts for practical applications. As such, immobilization of the particles on a substrate will broaden its application. MOFs have been grown in situ on ceramic membranes for desalination,(19,20) used as pore forming additives for ultrafiltration membranes,(21) incorporated into nanofibers for gas adsorption,(22−24) fabricated into hollow tubes to trap both air and liquid contaminants,(25) and used as fillers for mixed matrix membranes.(26,27)

MOFs as fillers in electrospun nanofibers have shown that almost all of the particles are still available for adsorption as compared to MOFs in flat sheet membranes and coatings on ceramics, with the exceptions of thin-film coatings.(28) Electrospinning is a facile technique to fabricate nanofibers through

polymer fiberization resulting in a highly porous, nonwoven interconnected mesh.(29) Furthermore, it is noted that metal oxides and their nanocomposites have been electrospun into fibers for metal ion removal purposes.(30−34) Since the polymers used are usually organic, it makes compatibility with MOF particles easy, thereby allowing for nanofibers to act as a potential substrate for nanofibrous MOF membranes (NMOMs).(35,36) With the omnipresence of membrane technology in the water and wastewater industry, a straightforward practical approach is imperative to help mitigate the water scarcity crisis through treatment of used or contaminated water. With the advantages provided by porosity and surface area by both nanofiber and MOF particles, including a relatively economical fabrication technique and high chemical and thermal resistances, MOF crystals were integrated as fillers in nanofiber membranes through co-electrospinning to produce nanofibrous MOF membranes (NMOMs) for rapid and efficient removal of cadmium and zinc ions under room temperature.

The process of activation of mesoporous crystals has been extensively studied in gas separation, but nothing has been reported in the literature for the treatment of aqueous solutions. After MOF synthesis, solvent is usually entrapped in the void spaces of the crystals, which, in most cases, must be removed through a suitable activation route. Activated crystals gain more void spaces for foreign material capture due to enhanced porosity, but not all activated crystals have seen this benefit. Engel et al.(37) prepared soft MOF and used different activation routes and noticed a drop in CO_2 adsorption of the activated sample caused by structure shrinkage. The common activation route is conventional heating under atmospheric conditions where the prepared MOF crystals are heated above the boiling point of the solvent used.(38,39) For solvents with high boiling points, a vacuum is employed to reduce the boiling temperature, or the high boiling point solvent is exchanged with a low boiling point solvent, and, as such, the evaporation process is done at reduced temperatures. This mitigates any possible crystal structure distortion that could result from high heating.(40) Similarly, other activation methods like supercritical

CO_2 drying,(41) freeze drying,(42) multiple-coordination exchanges,(43) and photothermal activation(44) are known to enhance MOF performance.

Herein, we present a Zr-based MOF-808 [$Zr_6O_4(OH)_4(COOH)_6(BTC)_2$] and its composite polyacrylonitrile (PAN) membrane fabricated via electrospinning based upon our previous research.(45) To enhance contact between the aqueous phase and substrate, PAN nanofibers were selected because of their intrinsic hydrophilicity. The composite membrane containing 20 wt. % MOF particles was subjected to a systematic study on the removal efficiencies for Cd and Zn ions from aqueous media using standalone MOF crystals and NMOM. Various activation routes, including hydractivation (Scheme 4-1), were tested to show the potentials of this simplistic method. Kinetic and isotherm analysis of the MOFs and NMOM were made at room temperature and pH 4.6, followed by a batch filtration experiment to determine the flux.

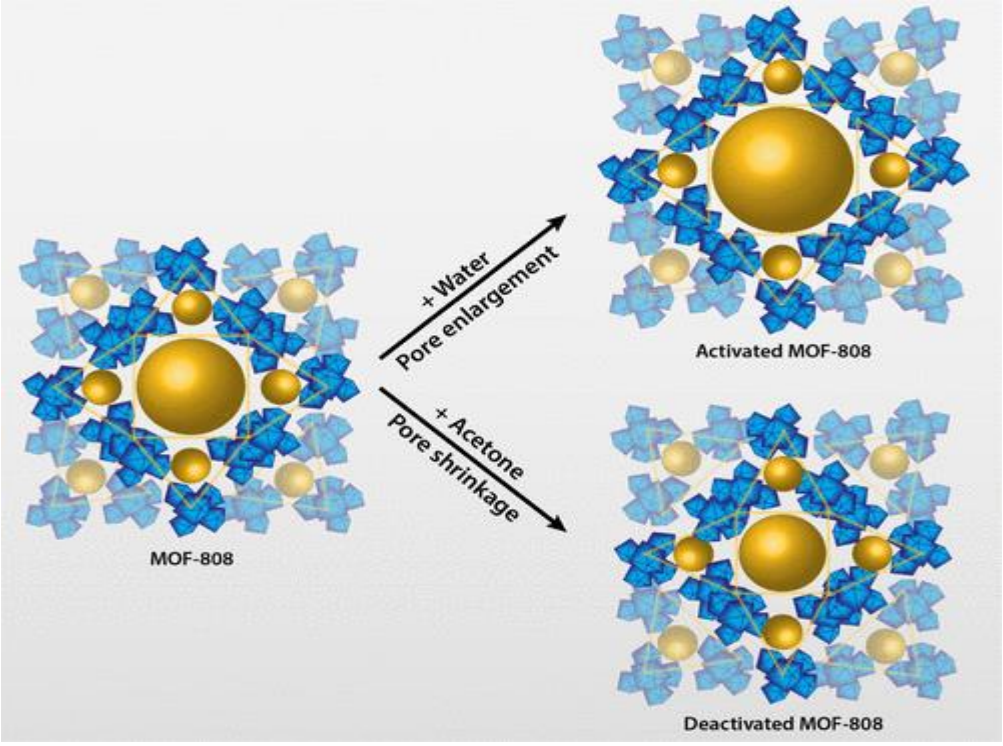

Scheme 4-1. Hydractivation of 1 Showing Pore Expansion Route with Water after Vacuum Drying and Hydractivation of Pore Shrinkage Route with Acetone after Vacuum Drying

4.2 Materials and Methods

4.2.1 Materials

All chemicals were of analytical grade >99% purity. Dimethylformamide (DMF) and acetone from Sigma-Aldrich Inc., formic acid from Alfa Aesar, and $ZrCl_4$ from Strem Chemical Inc. were all used as received without further purification.

The crystals were synthesized following a facile microwave procedure,(1) typically with a reaction involving 0.699 g of $ZrCl_4$ and H_3BTC (0.210 g) dissolved in a mixture of DMF/formic acid (45/45 mL) in a 200 mL boiling flask. The flask was irradiated at 400 W for 30 min in a microwave oven. The resulting suspension was centrifuged, followed by washing with DMF (10 mL × 3), then dried at 70 °C for 12 h. Solvent exchange with acetone and water was also done by washing (10 mL × 3), followed by vacuum drying at 100 °C.

4.2.2 Preparation of Spinning Dope for Nanofibrous Membranes and NMOM

PAN solution: 0.5 g of PAN (M_w = 150 kDa) was added to 5 g of DMF, and the mixture was placed in a shaker (180 rpm) for 24 h at 50 °C to form a homogenous 10 wt. % solution.

Poly (vinylidene difluoride) (PVDF) solution: 1.0 g of PVDF pellets was added to 5 mL of DMF, and the mixture stirred overnight to form a 20 w/v homogeneous solution.

Preparation of MOF/polymer dope solution: 0.1 g of MOF was first primed in 3 g of DMF and then 0.5 g of PAN was mixed to the remainder of 2 g solvent, separately. Then, both were combined to form a suspension with 20 wt. % MOF loading with respect to polymer weight.

4.2.3 Preparation of Nanofibrous Membrane without MOF Loading

A 10 mL syringe was filled with the 10 wt. % PAN/DMF solution that is electrospun on an aluminum foil at a syringe feed rate of 0.15 mm min^{-1} and a voltage of 15 kV. The distance between the end of the

syringe needle to the rotating drum wrapped with an aluminum foil and rotating at 140 rpm, was 15 cm. The temperature and humidity were maintained at 25 °C and 40%, respectively. The collected unwoven fibers were dried at room temperature and used for further characterization. The 20 w/v PVDF/DMF solution was electrospun at a voltage of 18 kV.

4.2.4 Preparation of Nanofibrous Membrane with MOF Loading

The spinning condition is the same as that of PAN/DMF solution without MOF except for the syringe feed rate of 0.11 mm min^{-1}. The nanofibrous PAN/MOF-808 membrane was placed on top of nanofibrous PVDF membrane to prepare the multilayer membrane for filtration experiments.

4.2.5 Batch Adsorption–Desorption Experiments

Cadmium and zinc ion solutions were prepared by dissolving cadmium chloride and zinc chloride in distilled water with further dilution to the desired concentrations. The heavy metal concentrations were measured using flame atomic absorption spectroscopy (FAAS). The amount of heavy metal adsorbed was obtained from the difference in concentrations between before and after adsorption by eqtn. 4-1.

The amount of heavy metal ions adsorbed per unit mass of adsorbent, q (mg g^{-1}), is given by 4-1 below

$$q = \frac{(Co - Ce)\,V}{m} \qquad (4\text{-}1)$$

where m (g) is the mass of adsorbent, V (L) is the volume of the solution, C_0 and C_e are the heavy metal ion concentration before and after adsorption (mg L^{-1}), respectively.

Adsorption kinetics experiments were performed to determine the rate of adsorption and the time for the MOF to reach the adsorption equilibrium. MOF-808 (1, 20 mg) on nanofibrous membrane was loaded in 30 mL of solution with initial cadmium or zinc ion concentration of 20 ppm. The solution was agitated

slowly at room temperature for 3 h, and solution samples were collected at predetermined time intervals for analysis.

The adsorption isotherms of the MOF were established using the same mass of the MOF-808 and nanofibrous membrane as above but with various initial concentrations of the heavy metal ions.

Since heavy metals precipitate at pH > 5, all experiments were conducted below pH 5, i.e., pH was adjusted to 4.6 ± 0.2 using 0.1 M HCl or 0.1 M NaOH.

Desorption solution of 2 wt. % nitric acid was used to alter the pH and the surface charge to ease desorption of bound heavy metal ions. After the adsorption process, the membrane was immersed into 30 mL of desorption solution and kept under mild agitation for 1 h at room temperature.

For the adsorption isotherm and kinetic study, the following equations were used. Isotherm equations (Langmuir, Freundlich, and Temkin)

$$\frac{1}{q_e} = \frac{1}{q_m} + \frac{1}{q_m K_l C_e} \qquad (4-2)$$

$$lnq_e = lnK_f + \frac{1}{n} lnC_e \qquad (4-3)$$

$$q_e = BlnA_T + BlnC_e \qquad (4-4)$$

where $B = \frac{RT}{b_T}$

Kinetic equations (pseudo-first order, pseudo-second order, and intraparticle)

$$\log(q_e - q_t) = logq_e - \frac{k_1}{2.303} t \qquad (4-5)$$

$$\frac{t}{q_t} = \frac{1}{k_2 q_e^2} + \frac{1}{q_e} t \qquad (4-6)$$

$$q_t = k_{id} t^{1/2} \qquad (4-7)$$

where q_e is the equilibrium sorption capacity (mg g^{-1}), q_m is the maximum sorption capacity of the sorbent (saturation point) (mg g^{-1}), C_e is the concentration of heavy metal ion in solution at equilibrium (mg L^{-1}), K_l is the Langmuir adsorption constant (L mg^{-1}), K_f is the Freundlich isotherm constant (mg g^{-1}(L $mg^{-1})^{1/n}$), n is the adsorption intensity, A_T is the Temkin isotherm equilibrium binding constant (L g^{-1}), b_T is the Temkin isotherm constant (J mol^{-1}), B is the constant related to the heat of sorption, T is the temperature at 298 (K), R is the universal gas constant (8.314 J mol^{-1} K^{-1}), t is time (min), k_1 (min^{-1}) and k_2 (mg g^{-1} min^{-1}) are the first- and second-order rate constants, respectively, k_{id} is the intraparticle diffusion rate constant (mg g^{-1} min^{-1}), and q_t is the amount of heavy metal ion (mg g^{-1}) adsorbed at time t.

4.2.6 Batch Adsorption Experiment for Selectivity Testing

Since single-component ion systems are usually not common, the efficiency of the composite membrane is worth testing in multi-ion systems to determine the selectivity of the adsorbent. Some of the most common ions present in water were selected for this test including both divalent (Ca^{2+} and Mg^{2+}) and monovalent (Na^{+}) cations. A cocktail of the solution contained the co-existing ions in abundance relative to the heavy metal ion Cd^{2+}. A cocktail solution of 30 mL was mixed with 50–60 mg of the composite membranes (1a–c) for 2 h and then tested for the adsorbed Cd^{2+}.

4.2.7 Filtration Experiment

A dead-end cell with 300 mL capacity (re-fillable) was used for the filtration experiments. The filtration system was automated using LabVIEW, where fluxes, temperatures, mass flow rate, pressure, permeability (thickness normalized flux), and permeance (pressure normalized flux), were monitored real time, as shown in Figure B1 (see the Appendix B). A circular membrane (multilayer) coupon with an effective area of 3.8×10^{-3} m^2 was placed at the bottom of the feed chamber, and an O-ring was applied to seal the setup and to prevent the leak. Solution containing 30 ppb of cadmium or zinc ion was driven

through the membrane at room temperature and at a pressure of 0.4 bar supplied from a nitrogen cylinder. The permeate was collected at specific time intervals and analyzed to determine the membrane performance. For reuse tests, the cell was filled with desorption solution (2 wt. % nitric acid) and flushed at a flux of 250 L m^{-2} h^{-1}. The regenerated membrane was then washed with deionized (DI) water to remove residual desorption solution. The cycle was repeated four times consecutively to determine membrane reusability. The term "recovery" is defined as the amount of permeate collected before the permeate concentration reached 3 ppm at the *n*th cycle/the amount of permeate collected before the permeate concentration reached 3 ppm in the first cycle.

4.2.8 Characterization of MOF and Nanofibrous Membranes

Powered X-ray diffraction (PXRD) analysis was carried out at room temperature on a Rigaku Ultima IV powder diffractometer in Bragg–Brentano geometry using Cu Kα radiation (λ = 1.5418 A). A step width of 0.02° and scan speed of 2° min^{-1} covered 2θ range of 2–32°. The simulated PXRD patterns were calculated over a range of 2θ between 2 and 32° in 0.02° step width using the Mercury software (CSD 3.8, build RC2, Cambridge Crystallographic Data Centre, Cambridge, U.K., 2016). Transmission electron microscopy (TEM) was carried out to investigate MOF crystal shape and size using a FEI Tecnai F20 apparatus equipped with an Oxford Aztec 80 mm SDD detector. A suspension of the samples prepared in deionized water was dropped on copper grids and analyzed at 300 kV. In the case of nanofibrous membranes, short single fibers were harvested for TEM–energy-dispersive spectrometry (EDS) analysis as follows. A piece of the PAN and PAN/MOF-808 nanofibrous membranes was crushed in liquid N_2 for 5 min. The powder was then suspended in ethanol and sonicated for 10 min. Two drops of the supernatant were dropped on the TEM grid for analysis.

Scanning electron microscopy (SEM) images were taken using a Tescan, Vega-II XMU equipped with a 250X EDS, Oxford Inca Energy apparatus. Samples were affixed onto the holder by means of a

conductive adhesive and then gold-coated under vacuum using Anatech Hummer VII equipment. Images were taken at suitable resolutions.

Thermogravimetric analysis (TGA, TA Instruments, model Q5000 IR TGA) was used to analyze the thermal stability of the MOF with conventional vacuum drying, exchanged with acetone, then vacuum dried and exchanged with water and again vacuum dried (see Table 4-1), with a heating rate of 10 °C min^{-1} under nitrogen atmosphere.

Table 4-1.Different Phases of 1 and the Details of the Post-treatment Methods

material code	details
1	as-synthesized MOF-808 with oven drying at 70 °C
1A	MOF-808 with conventional vacuum drying at 100 °C
1B	MOF-808 exchanged with acetone then vacuum dried at 100 °C
1C	MOF-808 exchanged with water then vacuum dried at 100 °C
1a	PAN/MOF-808 nanofiber membrane conventional vacuum dried at 100 °C
1b	PAN/MOF-808 nanofiber membrane exchanged with acetone, then vacuum dried at 100 °C
1c	PAN/MOF-808 nanofiber membrane exchanged with water, then vacuum dried at 100 °C

The surface area and pore volume of the synthesized and activated MOF samples were determined by the Brunauer–Emmett–Teller (BET) method using nitrogen at 77 K with Micromeritics 3FLEX volumetric equipment. Before the nitrogen adsorption measurements, the samples were degassed under a purge flow of nitrogen at a flow rate of 40 cm^3 min^{-1} and 90 °C for 1 h. The data in the relative pressure (P/P_0) range 0.05–0.2 were used to calculate the specific surface area using the BET formula.

The glass transition temperature (T_g) of ENMs was measured using a TA Instruments differential scanning calorimeter (DSC) Q2000 V24.11 Build 124. A ∼5 mg nanofibrous membrane sample was put into a Tzero Aluminum Hermetic pan, annealed at 150 °C for 10 min, then quenched to 25 °C, and then maintained isothermal at 25 °C for 10 min. T_g measurements were done by heating the samples to 150 °C at a rate of 5 °C min^{-1}.

The mechanical properties of the nanofibrous membranes were determined according to the standard method ASTM D 882 using an ElectroPuls Instron E3000 machine at 25 °C at a constant crosshead speed of 5 mm min^{-1}. Membrane samples of thickness 60–90 μm, 10 mm width, and 20 mm length were used. The samples were carefully selected to avoid the inhomogeneous edges, and the selected tensile stress–strain curves were obtained for the samples with final rupture of at least 2 mm from the edge of the clamps.

4.3 Results and Discussion

4.3.1 Synthesis of MOF-808

MOF-808 [$Zr_6O_4(OH)_4(COOH)_6(BTC)_2$] was synthesized according to a protocol reported elsewhere.(46) The reaction for the synthesis of MOF-808 controlled by the concentration of $ZrCl_4$ and the high irradiation power provided by the microwave oven lead to fast nucleation with the production of white crystal. The as-synthesized crystals were oven dried at 70 °C for 12 h to serve as initial sorbent

referred to as 1 (see Table 4-1). Figure 4-1 displays the octahedral crystals with an average diameter of 200 nm, agreeing well with an earlier report.(47) The BET plot of the MOF-808 materials is shown in Figure B2. The BET surface area, pore volume, and average pore width are presented in Table B1. The surface morphology of the nanofibrous membranes with MOF loading of 20 wt. % is shown in Figure 4-2 as PAN with MOF-808. The fiber diameter of the PAN with MOF-808 was significantly larger than the PAN without MOF loading, resulting from the presence of the MOF particles, which also contributed to increasing the surface roughness. The fabricated nanofibers were all nonwoven with interconnected pore geometry with pore sizes ranging from 0.5 to 1 μm. The elemental mapping spectrum by TEM–EDS of PAN/MOF-808 nanofibrous membrane shows the presence of zirconium (Figure 4-3). The DSC thermogram and tensile stress–strain curves of PAN and PAN/MOF-808 are displayed in Figure 4-4. The T_g of the PAN membrane is around 79 °C. However, the T_g of the PAN/MOF-808 is slightly increased. It is noted that T_g shifted by 3 °C toward higher temperature due to the restricted PAN chain movement induced by the close interaction between MOF-808 and PAN polymers (Figure 4-4a). The tensile mechanical properties, namely, Young's modulus, yield stress, elongation at break, and stress at break of PAN/MOF-808 membrane are superior to the PAN membrane (Figure 4-4b and Table B2). This is also due to the strong interaction between PAN and MOF-808 materials. The powder X-ray diffraction (PXRD) spectrum of the composite membranes is shown in Figure 4-5. It could be seen that the MOF maintains its crystallinity even in the composite with its characteristic peaks indicated. The characteristic peak of PAN polymer is also maintained at $2\theta = 16.9°$. This profile clearly indicates that the various activation routes did not affect the crystalline properties of the materials for the conditions applied. The good compatibility between MOF and PAN, accounted for by their individual organic moieties, prevents the appearance of free-standing MOF particles. This enhances the stability of the MOF-containing nanofibrous membranes, preventing MOF leakage into the permeate during application. The cross-sectional image (Figure B3) of the filtration membrane shows the multilayered membrane structure with

PVDF nanofibers as the support layer and PAN/MOF-808 nanofibrous membrane as the top layer. The multilayer membrane did not show any signs of compaction after the filtration experiment, indicative of membrane stability.

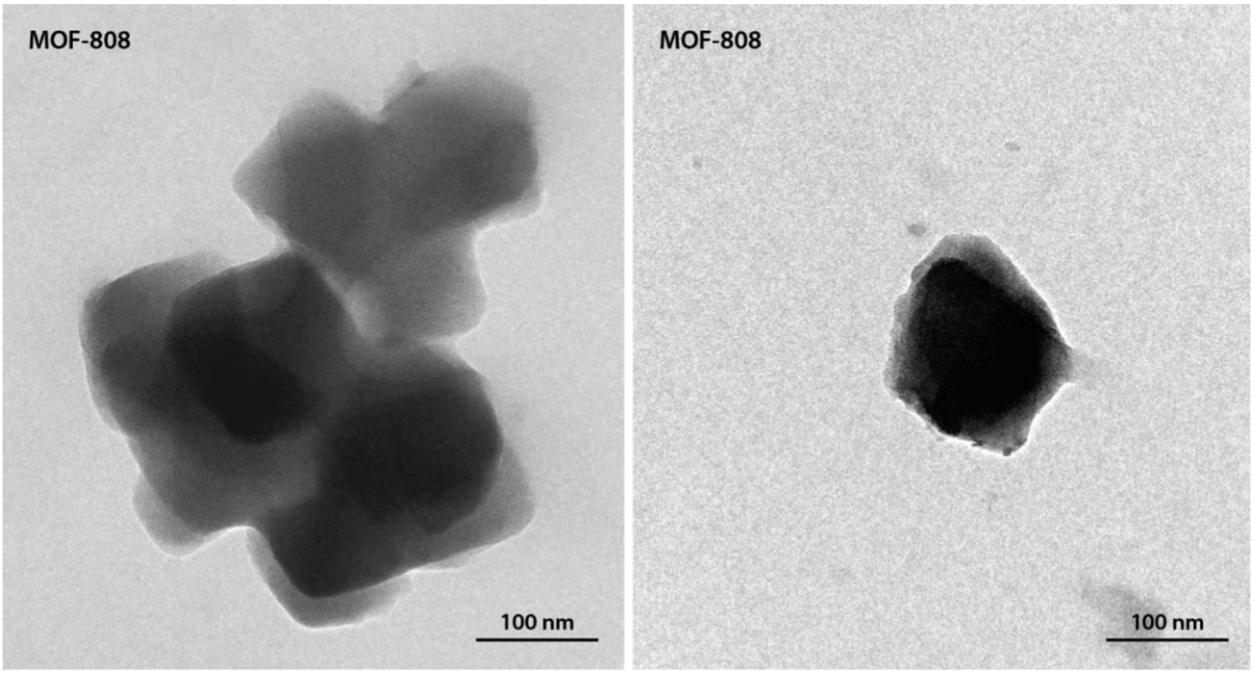

Figure 4-1. Transmission electron microscopy images of MOF808 showing an octahedral-like shape.

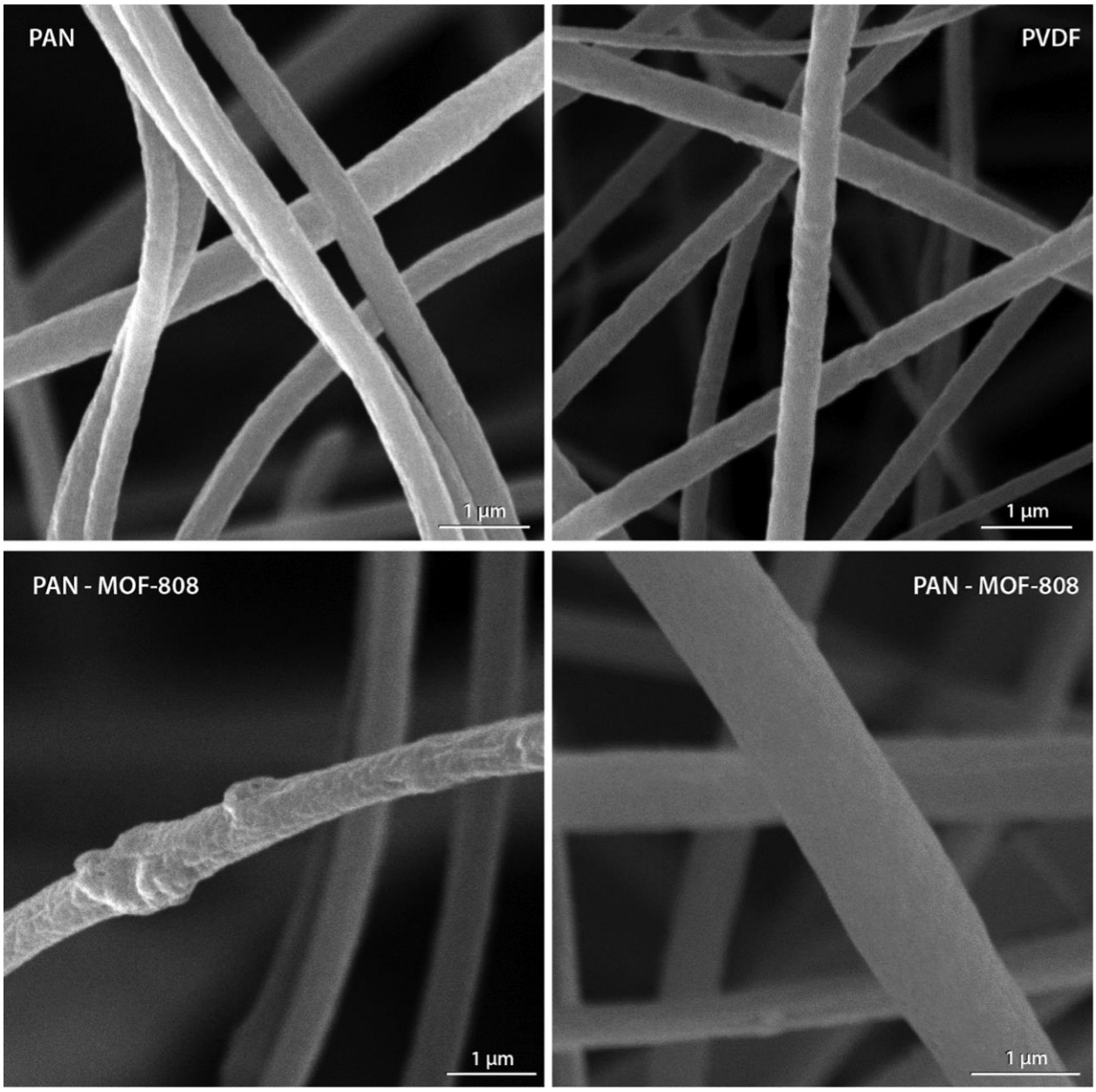

Figure 4-2. Scanning electron microscopic images of the nanofibrous membranes PAN, PVDF, and PAN/MOF-808 at two different locations.

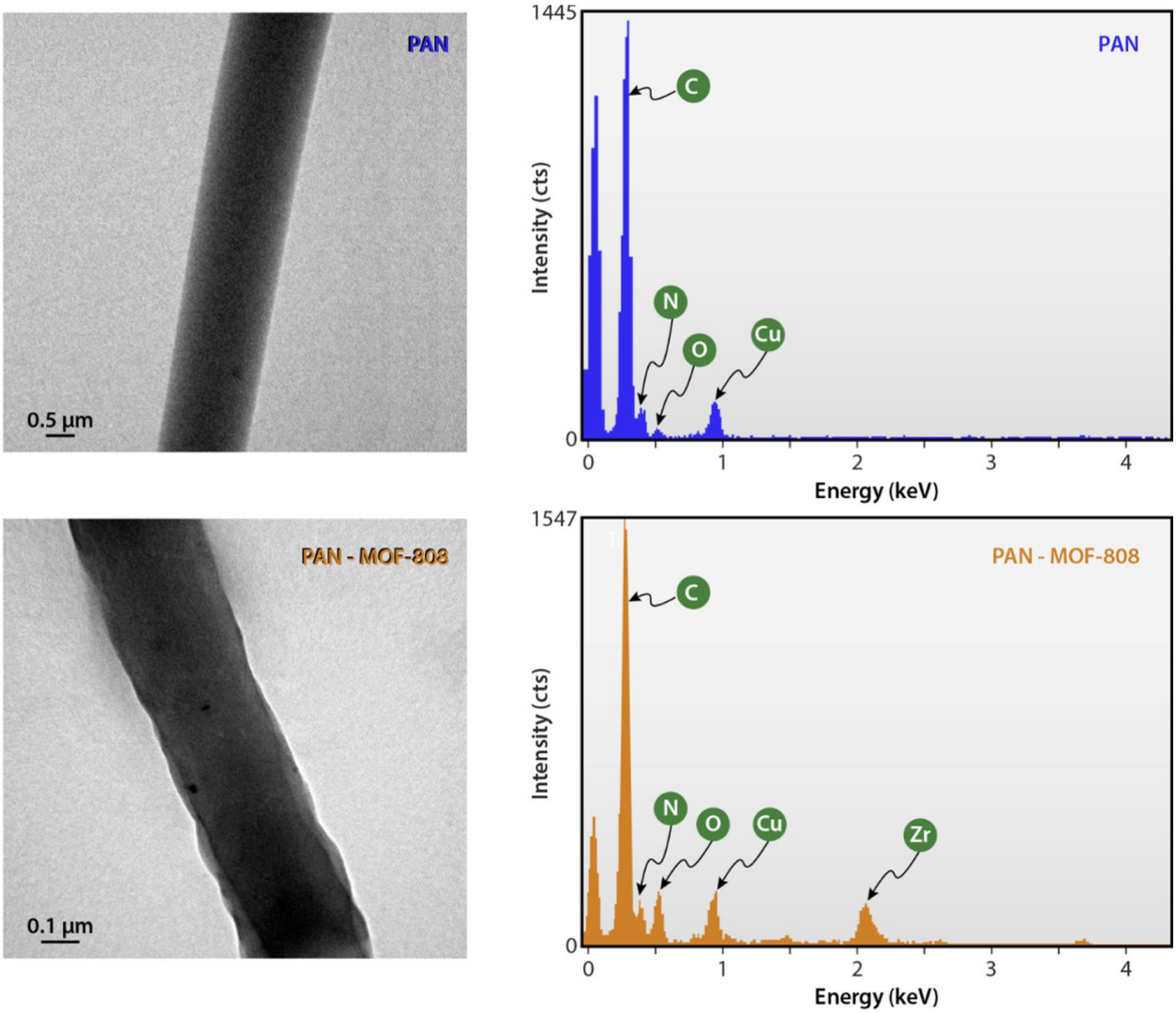

Figure 4-3. Transmission electron microscopy images and energy-dispersive spectrum of the PAN and PAN/MOF-808 nanofibrous membranes.

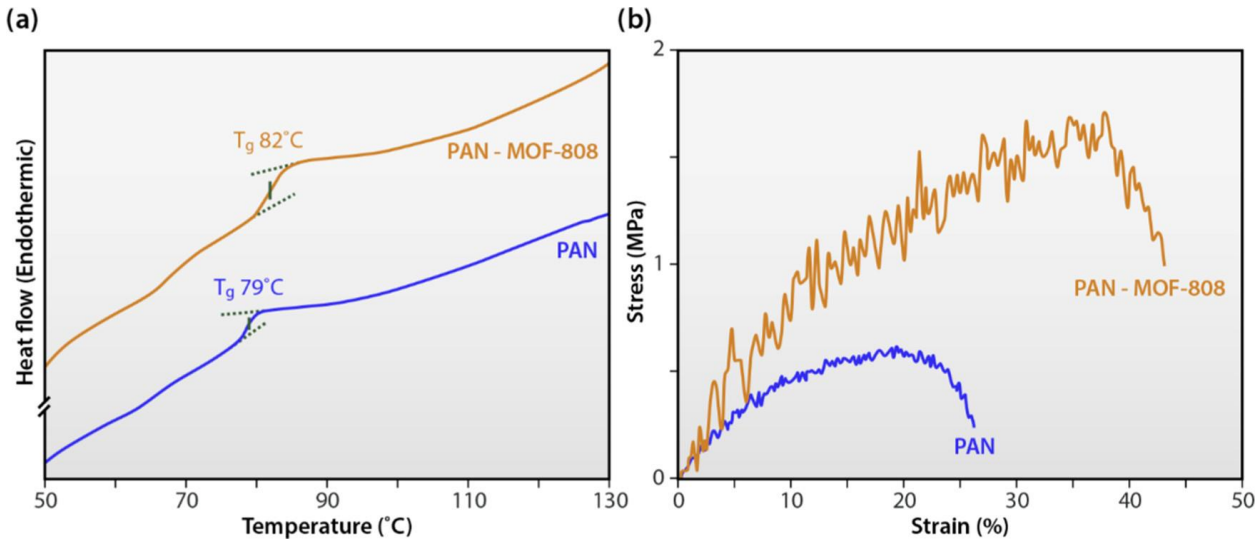

Figure 4-4. (a) DSC thermogram and (b) tensile stress−strain curve of the PAN and PAN/MOF-808 nanofibrous membranes.

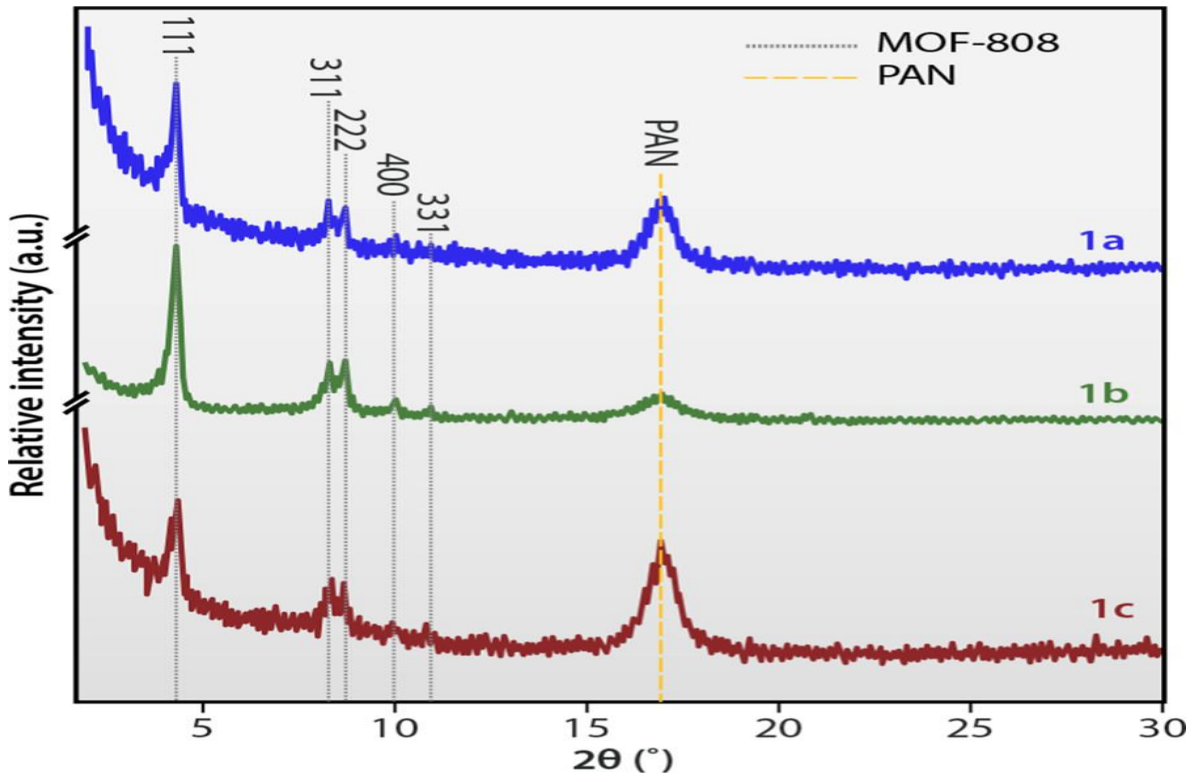

Figure 4-5. PXRD spectrum of the PAN/MOF-808 nanofibrous membranes.

4.3.2 Heavy Metal Uptake and Release

The kinetic data obtained was fitted using three models (pseudo-first and second order(48) and the intraparticle models(49)), whereas the isotherm data was fitted using the Langmuir,(50) Freundlich,(51) and Temkin(52) models. The equations used in the kinetic and isotherm analyses are demonstrated in their linear form in (4-2) -(4-7).

As displayed in Figure B4 and Table B3, the kinetic experimental data fit the pseudo-second order model with R^2 greater than 0.99 for both Zn and Cd. This is indicative of a physical sorption process with no covalent bonding involved (an easy to reverse process). The relatively high k_2 value corresponds to the fast adsorption as the saturation was attained after 10 min. The Langmuir adsorption isotherm model fits the experimental data of 1 better than Freundlich and Temkin (Table B4) models depicting a homogenous, monolayer adsorption process. The maximum adsorption capacities of 1 were 225.055 and 287.064 mg g^{-1} for Cd and Zn, respectively. This is attributed to the higher surface charge of 1 (ζ potential = −36 mV) measured at pH 4.5 and its high surface area of 939 m^2 g^{-1}. It implies the electrostatic drag on the small Zn ion (ionic radius 1.35 Å) compared to the larger Cd ion (ionic radius 1.55 Å) made way for more Zn ions to be entrapped, and hence, the higher adsorption capacity.

4.3.3 Heavy Metal Uptake in the Presence of Co-ions

The selectivity of the composite membrane for the heavy metal ion was maintained, but the removal efficiency was reduced by almost 20% for all membranes, as shown in Figure 4-6. This is mainly due to the competitive effect of adsorption sites with the co-existing ions. The selectivity for Cd^{2+} could be attributed to the high electronegativity of the ion (Pauling electronegativity scale, χ for Na^{+}(0.93), Mg^{2+}(1.31), Ca^{2+}(1.00), and Cd^{2+}(1.69)),(53) making it easier to be attracted by the MOF carboxylic group (COO^{-}) compared to the other ions.

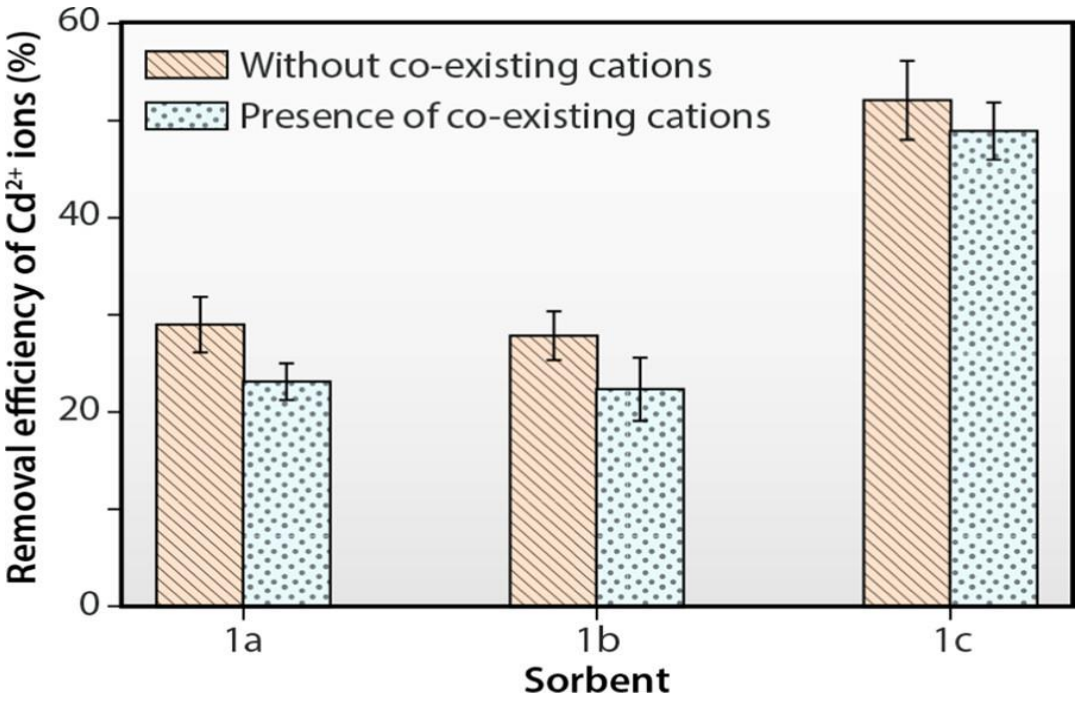

Figure 4-6. Solution for co-existing ion test comprised precisely of 48.3 ppm Ca2+, 49.7 ppm Mg2+, 45.1 ppm Na+, and 1.1 ppm Cd2+ ions.

4.3.4 Activation and Percent Removal

With an attempt to enhance the adsorption capacity of 1, three different routes were employed. These activation routes included conventional vacuum drying at 100 °C, solvent exchange with acetone and solvent exchange with water, followed by vacuum drying at 100 °C, all denoted as 1A, 1B, and 1C, respectively. These were then blended in PAN in nanofibrous membranes, which were coded as 1a, 1b, and 1c, respectively (as presented in Table 4-1 for clarity). Since MOF-808 has been reported with a surface area greater than 2000 $m^2 g^{-1}$,(47) it is evident that 1 (surface area, 939 $m^2 g^{-1}$) had some solvent trapped in its pores without being removed by the heat treatment at 70 °C, which was also confirmed by thermogravimetric analysis (TGA) thermos-grams (Figure 4-7). TGA revealed that the drying process and temperature affected the amount of solvent removed. At higher temperature under vacuum, the MOF crystals showed a lesser amount of solvent contained, with the oven drying performing worst. 1B

performed best with an initial weight loss of <5% contributed by the solvent removal. This is due to the low boiling point of acetone, which makes evaporation and escaping from the MOF pores easier.

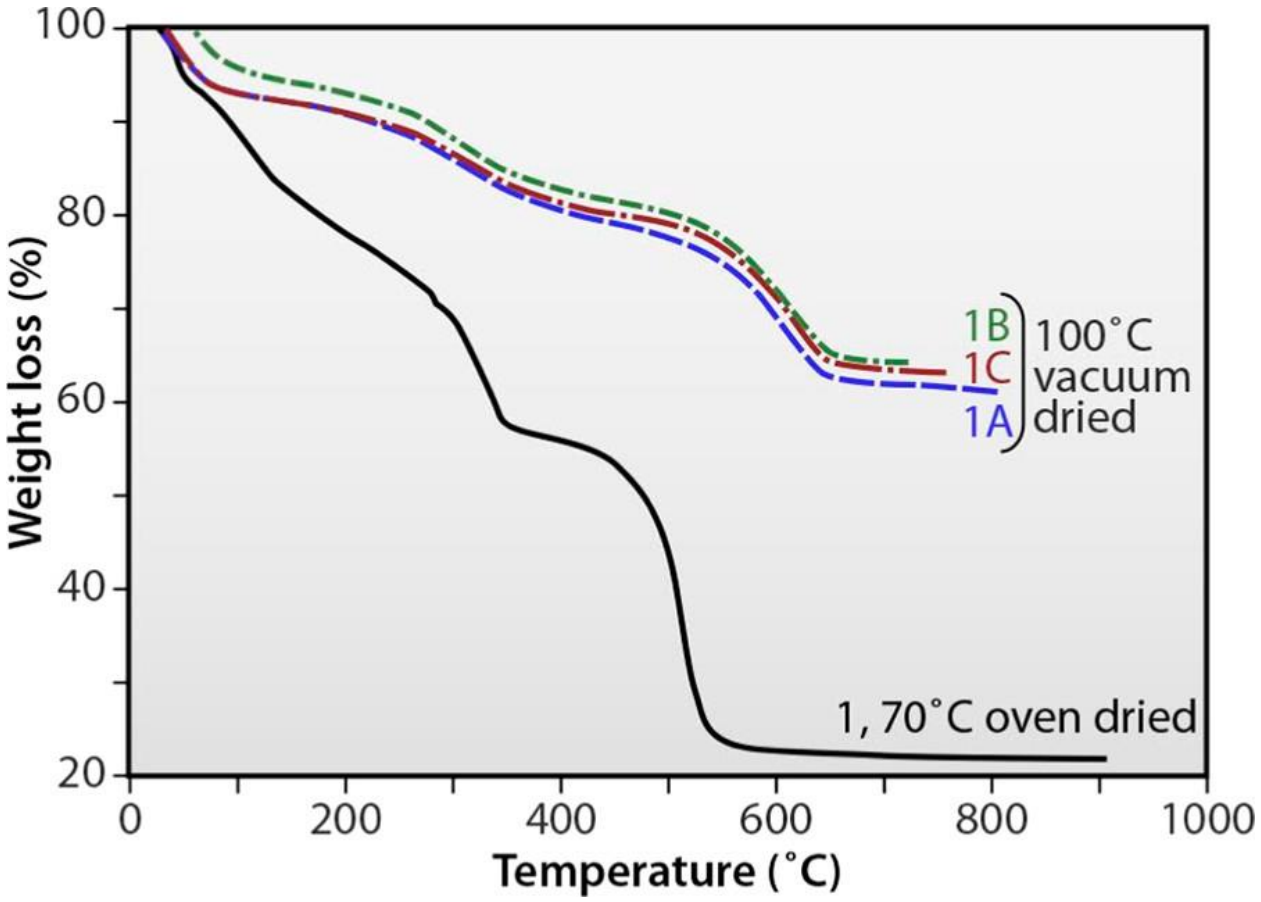

Figure 4-7. Thermogravimetric analysis plot of all samples.

Investigations were further carried out on the effect of freeing the pores from the heavy metal ion adsorption. The sorption experiment entailed the soaking of a specific amount of sorbent in 30 mL of 1 ppm heavy metal ion solution at constant pH and room temperature for 2 h. Under mild agitation, solution samples were collected and analyzed by flame atomic absorption spectroscopy. The results showed a 28% decrease from 1 to 1A, in the removal of both heavy metals (see Figure 4-8). Attempting to investigate this phenomenon further, BET analysis was performed. The results (Table B1) show that, upon removing DMF, the pore volume dropped from 0.162 to 0.124 $cm^3 g^{-1}$, indicative of pore shrinkage of at least 20%

of its original volume. It is noted that the pore volume increased from 0.124 to 0.204 $cm^3\ g^{-1}$, indicative of pore expansion for 1C. However, in the case of 1B, pore volume decreased from 0.124 to 0.105 $cm^3\ g^{-1}$ resulting from pore shrinkage (Scheme 4-1). Ma et al.(54) observed that the Langmuir surface areas are 86.9 $m^2\ g^{-1}$ for freeze-benzene dried and 343.9 $m^2\ g^{-1}$ for supercritical carbon dioxide activated, which were about a 5- and 21-fold enhancement, respectively, over that for the regular vacuum-dried MOF, namely, $[Zn_{22}(BTC)_{12}\text{-}(H_2O)_{22}(NO_3)_8]\cdot x$ guest, in where H_3BTC = 1,3,5-benzenetricarboxylate acid. Framework collapse can often be attributed to the high surface tension and capillary forces imposed on the structure by the liquid- to gas-phase transformation of trapped solvent molecules, especially when the solvent has a high boiling point and/or high surface tension.(55)

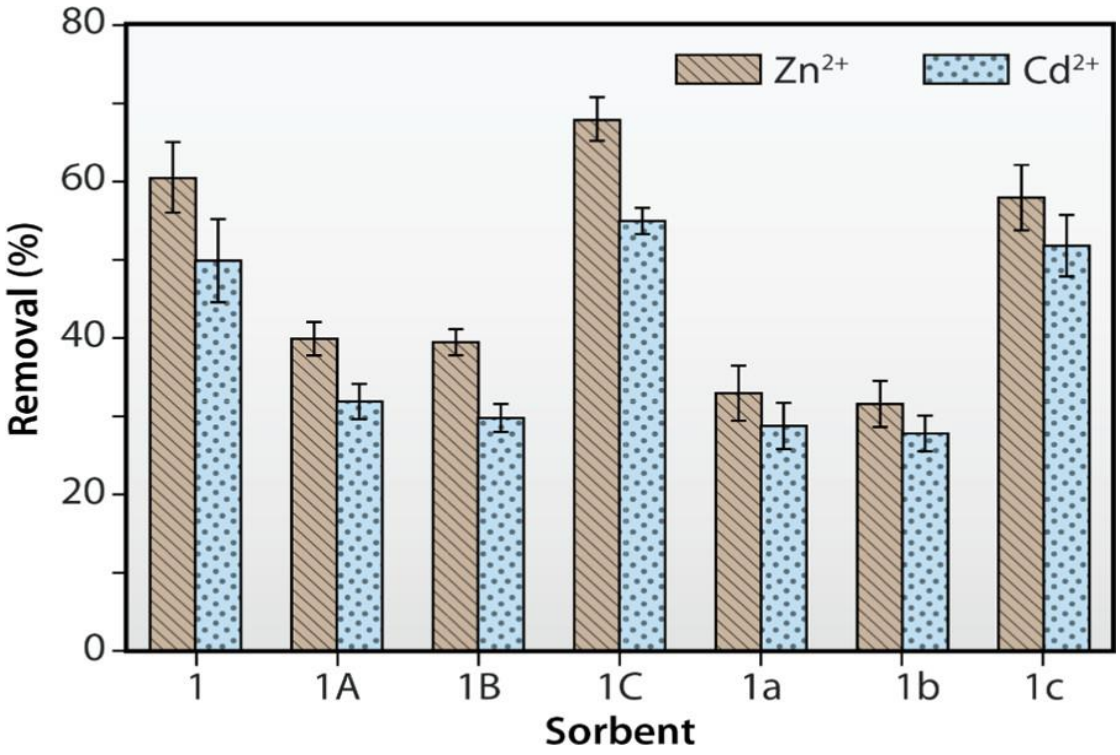

Figure 4-8. Activated samples and their sorption experimental results.

It is expected that upon removal of guest solvent, the pore volume should increase, but as also reported elsewhere, this activation route does not usually result in a more porous material as pore downsizing occurs.(37)

It is thus speculated that, though the pores are required to be as void as possible, some of the solvent is required to maintain the pore integrity and prevent it from shrinking. 1A and 1B vacuum dried at 100 °C did not show any significant difference from each other in the removal performance for both heavy metals, but the TGA plot showed that vacuum drying at 100 °C was better in terms of removing guest molecules from the pores. Hence, all samples including the membranes were vacuum dried at 100 °C.

In Figure 4-8, 1C shows a 10% increase in heavy metal removal from 1, which is corroborated by the 19% increase of specific pore volume compared to 1 (0.162–0.202 $cm^3\ g^{-1}$). For the pore geometry to change by either contraction or expansion, some form of structural change will be noticed in the lattice,

which prompted a PXRD analysis (Figure 4-9). Ma et al.(56) studied a Zn-based MOF (UMCM-9) by

exchanging DMF with CH_2Cl_2 and *n*-hexane and experienced an increased surface area with *n*-hexane exchange, compared to CH_2Cl_2 due to the low surface tension of *n*-hexane.

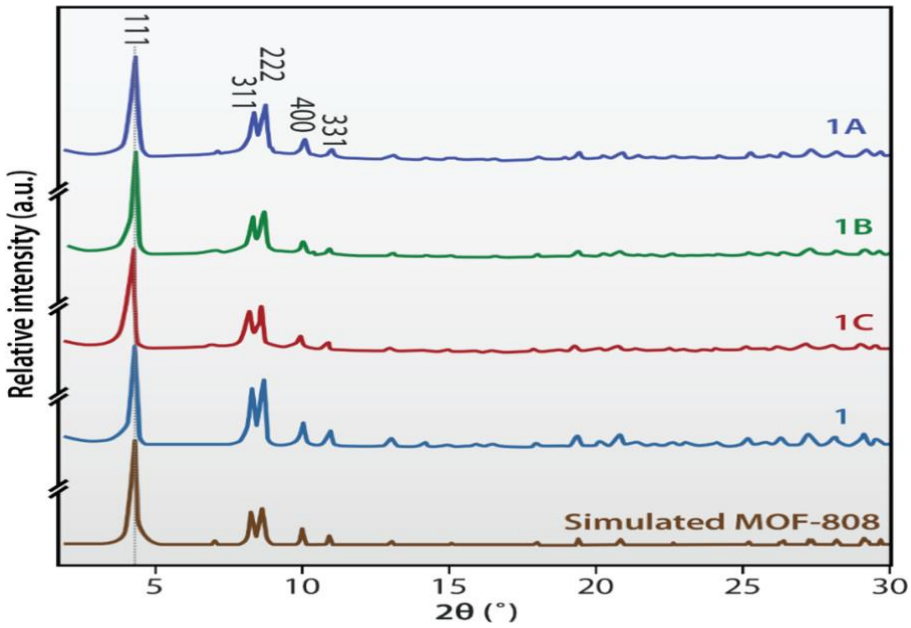

Figure 4-9. Comparison of the simulated MOF-808 to the experimental samples with respective code definitions on Table 4-1.

Figure 4-9 shows the PXRD spectra for all MOF samples together with the simulated MOF-808. It is obvious that the insertion of guest molecules into the pores causes a shift of the diffraction peaks pattern. A shift to the lower 2θ direction is associated with an expansion of the lattice according to Bragg's law, whereas a higher 2θ shift demonstrates contraction.(57,58) Table B5 summarizes all peak shifts observed for all MOFs. In particular, sample 1C shows a (111) peak shift from 4.36° of 1 to 3.91°, a (311) peak shift from 8.36° to 8.01°, and a (222) peak shift from 8.726° to 8.51°. It is thus evident that, upon water occupying the pore space, the lattice was stretched out causing a distortion of MOF structure resulting in pore enlargement. However, after vacuum drying, the pore did not regain its original size, which caused an increase in the adsorption capacity. It is safe to say that the volatility of acetone in 1B might have prevented its ability to cause an expansion change. The ability of water to activate 1 (hydractivation) implies that hydractivation could offer a simple technique for activation of water-stable porous materials prepared from polar solvents like DMF.

A specific weight of the nanofibrous membranes was also soaked in 30 mL of 1 ppm heavy metal ion solution, and the solution samples were collected after 2 h with mild agitation and analyzed by the FAAS and then the sorption capacities normalized with the wt. % of the MOF (reported values were obtained by dividing the experimental value by the MOF fraction). The results are also shown in Figure 4-7. When the MOF particles were entrapped in the nanofibers, their adsorption capacity decreased only slightly, i.e., the normalized % removal of sample 1a and 1b decreased by 16% from 1A and 1B, whereas 1c experienced a 15% drop from 1C. From these results, we can deduce that the PAN macromolecules surrounding the MOF particles contributed an extra resistance for metal ions to reach the pores. As well, the reduced effective surface charge of the particle also caused the reduction of the electrostatic drag. The lattice expansion brought about by hydractivation in the standalone MOF was still present when the MOF was in the nanofiber, but the presence of macromolecules around the particle could have limited the lattice expansion. This could not, however, be confirmed since the MOF could not be retrieved from the nanofiber for further analysis to investigate the structural change.

4.3.5 Filtration

The efficiency of contaminated water treatment using the prepared membranes in terms of practical applicability was tested using a dead-end filtration setup. Since the PAN NMOM alone could not retain the water, a thin layer of hydrophobic PVDF (~30 μm thick) nanofibrous was attached to the bottom of the PAN NMOM to prevent direct water penetration and increase residence time (Figure B2). A 400 ± 32 μm thick bilayer membrane (PAN NMOM + PVDF) was therefore used for the filtration. It is worth noting that the thin PVDF base layer was designed to have a liquid entry pressure of water (LEP_w) equal to 0.4 bar. The membrane adsorption was conducted in a batch mode at room temperature using the feed solution containing 30 ppb Cd^{2+} ion that is 10 times the allowed concentration of 3 ppb for drinking water.(15)

Both 1a and 1c membranes showed a water flux of 348 ± 55 L m^{-2} h^{-1} at the operating pressure of 0.4 bar with the ability of 1c to treat 580 mL of contaminated water before the permeate reached the allowable limit of 3 ppb, whereas 1a could treat 464 mL. This difference in performance correlates with the sorption performance earlier demonstrated. Hydractivated 1c showed that the pore volume increased, which prevented an early breakthrough of the heavy metal ions compared to 1a, which is indicative of an increase in the number of adsorption sites per pore volume.

Multiple cycles of filtration experiments to test membrane reusability are important for practical applications. A cycle of filtration was considered from the initial start of the experiment until when the permeate concentration reached the maximum allowable Cd^{2+} ion concentration for drinking water. After the cycle, the membrane was washed with 500 mL desorption solution and rinsed with DI water. As shown in the embedded figure in Figure 4-10, the bilayer composite membrane maintained its flux and removal capacity after four cycles of adsorption and subsequent washing (for the definition of recovery see Appendix B). The collected permeate was also tested for MOF leakage by inductively coupled plasma-mass spectrometry in the parts per trillion levels. Neither did the permeate of the first filtration cycle nor did the permeate from the fourth cycle show any MOF particles. This is indicative of the strong compatibility between MOF and polymer, which is necessary for long-term operation and applications of the composite membrane. The absorption capacity of MOF-808 is better than the values reported in Table B6. It should be noted that MOFs particles are wrapped by PAN materials reducing the access of heavy metal ions to the pore of the MOFs in the PAN/MOF-808 nanofibrous membrane.

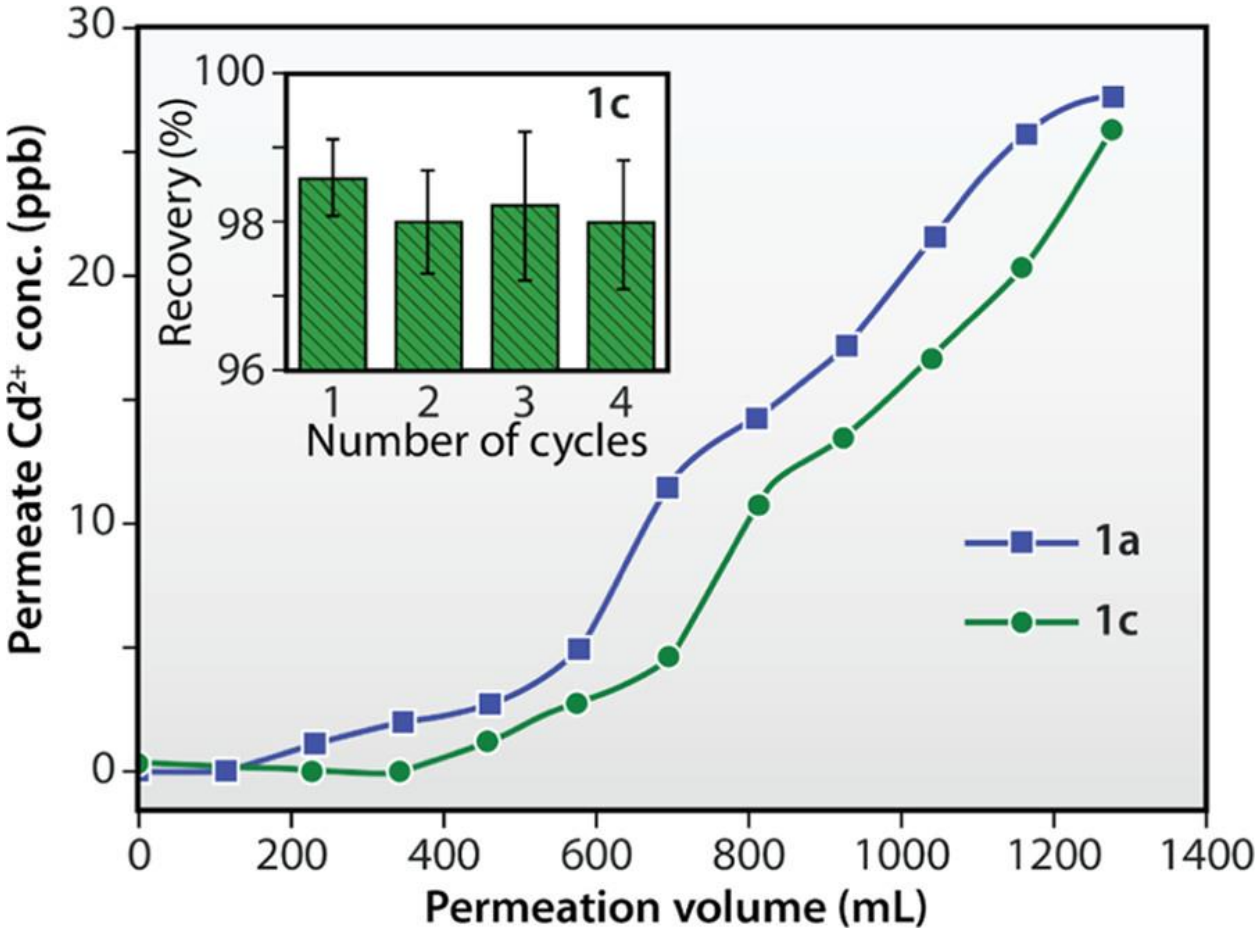

Figure 4-10. Breakthrough filtration result for Cd2+ ion using PAN/ MOF-808 nanofibrous membrane activated by conventional vacuum drying (1a) and hydractivated membrane (1c).

4.4 Conclusions

In summary, we have reported a nanofibrous MOF membrane prepared by co-electrospinning of Zr-based MOF-808 and hydrophilic PAN. The MOF loading of up to 20 wt.% could be achieved and tested for Cd and Zn ion removal from aqueous solution. Systematic studies on kinetics, isotherm, and filtration were performed to determine the practical applicability of the nanofibrous MOF membranes. With the good adsorption capacities of the MOF and the ability of the MOF to be accessible in the entrapped state, PAN/MOF-808 membranes could treat a reasonable amount of Cd solution at a flux of 348 L m^2h^{-1}. We have established a facile activation technique for porous water-stable material (hydractivation), which

could be optimized further for specific materials. This MOF composite membrane represents a new generation of fast and efficient wastewater treatment membranes, which can be optimized further in terms of MOF concentration, permeance, and permeability. This membrane can be employed to develop robust membrane modules to produce point-of-use water of high quality or be integrated into pre-existing treatment systems as an innovation in the wastewater treatment industry.

Acknowledgments

The authors gratefully acknowledge the financial support from the Natural Sciences and Engineering Council (NSERC) of Canada through Strategic Partnership Grant for Projects (SPTGP) # 463039-2014.

REFERENCES

1. Wankat, P. C. Separation Process Engineering: Includes Mass Transfer Analysis, 4th ed.; Prentice Hall: Upper Saddle River, NJ, 2016.
2. Zhou, H.-C.; Long, J. R.; Yaghi, O. M. Introduction to Metal-Organic Frameworks. Chem. Rev. 2012, 112, 673−674.
3. Yang, X.; Xu, Q. Bimetallic Metal−Organic Frameworks for Gas Storage and Separation. Cryst. Growth Des. 2017, 17, 1450−1455.
4. Li, B.; Wen, H.-M.; Zhou, W.; Chen, B. Porous Metal−Organic Frameworks for Gas Storage and Separation: What, How, and Why? J. Phys. Chem. Lett. 2014, 5, 3468−3479.
5. Rudd, N. D.; Wang, H.; Fuentes-Fernandez, E. M. A.; Teat, S. J.; Chen, F.; Hall, G.; Chabel, Y. J.; Li, J. Highly Efficient Luminescent Metal-Organic Framework for the Simultaneous Detection and Removal of Heavy Metals from Water. ACS Appl. Mater. Interfaces 2016, 8, 30294−30303.
6. Xue, H.; Chen, Q.; Jiang, F.; Yuan, D.; Lv, G.; Liang, L.; Liu, L.; Hong, M. A Regenerative Metal-Organic Framework for Reversible Uptake of Cd (II): From Effective Adsorption to: In Situ Detection. Chem. Sci. 2016, 7, 5983−5988.
7. Samanta, P.; Desai, A. V.; Sharma, S.; Chandra, P.; Ghosh, S. K. Selective Recognition of Hg^{2+} Ion in Water by a Functionalized Metal-Organic Framework (MOF) based Chemodosimeter. Inorg. Chem. 2018, 57, 2360−2364.
8. Wu, M.-X.; Yang, Y.-W. Metal-Organic Framework (MOF)-Based Drug/Cargo Delivery and Cancer Therapy. Adv. Mater. 2017, 29, No. 1606134.
9. Horcajada, P.; Chalati, T.; Serre, C.; Gillet, B.; Sebrie, C.; Baati, T.; Eubank, J. F.; Heurtaux, D.; Clayette, P.; Kreuz, C.; Cheang, J.-S.; Hwang, Y. K.; Marsaud, V.; Bories, P.-N.; Cynober, L.;

Gil, S.; Ferey, G.; Couvreur, P.; Gref, R. Porous Metal-Organic-Framework Nano-scale Carriers as a Potential Platform for Drug Delivery and Imaging. Nat. Mater. 2010, 9, 172−178.

10. Zhu, L.; Liu, X.-Q.; Jiang, H.-L.; Sun, L.-B. Metal-Organic Frameworks for Heterogeneous Basic Catalysis. Chem. Rev. 2017, 117, 8129−8176.
11. Farha, O. K.; Hupp, J. T. Rational Design, Synthesis, Purification, and Activation of Metal−Organic Framework Materials. Acc. Chem. Res. 2010, 43, 1166−1175.
12. Lustig, W. P.; Mukherjee, S.; Rudd, N. D.; Desai, A. V.; Li, J.; Ghosh, S. K. Metal-Organic Frameworks: Functional Luminescent and Photonic Materials for Sensing Applications. Chem. Soc. Rev. 2017, 46, 3242−3285.
13. Yi, F.-Y.; Chen, D.; Wu, M.-K.; Han, L.; Jiang, H.-L. Chemical Sensors Based on Metal−Organic Frameworks. ChemPlusChem 2016, 81, 675−690.
14. Rudd, N. D.; Wang, H.; Fuentes-Fernandez, E. M. A.; Teat, S. J.; Chen, F.; Hall, G.; Chabal, Y. J.; Li, J. Highly Efficient Luminescent Metal−Organic Framework for the Simultaneous Detection and Removal of Heavy Metals from Water. ACS Appl. Mater. Interfaces 2016, 8, 30294−30303.
15. Shariful, M. I.; Bin Sharif, S.; Lee, J. J. L.; Habiba, U.; Ang, B. C.; Amalina, M. A. Adsorption of Divalent Heavy Metal Ion by Mesoporous-High Surface Area Chitosan/Poly (Ethylene Oxide) Nanofibrous Membrane. Carbohydr. Polym. 2017, 157, 57−64.
16. Abney, C. W.; Gilhula, J. C.; Lu, K.; Lin, W. Metal-Organic Framework Templated Inorganic Sorbents for Rapid and Effi cient Extraction of Heavy Metals. Adv. Mater. 2014, 26, 7993−7996.
17. Herrmann, S.; De Matteis, L.; de la Fuente, J. M.; Mitchell, S. G.; Streb, C. Removal of Multiple Contaminants from Water by Polyoxometalate Supported Ionic Liquid Phases (POM-SILPs). Angew. Chem., Int. Ed. 2017, 56, 1667−1670.

18. Gorchev, H. G.; Ozolins, G. WHO Guidelines for Drinking-Water Quality. WHO Chron. 1984, 38, 104−108.
19. Liu, X.; Demir, N. K.; Wu, Z.; Li, K. Highly Water-Stable Zirconium Metal−Organic Framework UiO-66 Membranes Supported on Alumina Hollow Fibers for Desalination. J. Am. Chem. Soc. 2015, 137, 6999−7002.
20. Wang, N.; Liu, T.; Shen, H.; Ji, S.; Li, J.-R.; Zhang, R. Ceramic Tubular MOF Hybrid Membrane Fabricated Through In Situ Layer-by-Layer Self-Assembly for Nanofiltration. AIChE J. 2016, 62, 538− 546.
21. Lee, J.-Y.; Tang, C. Y.; Huo, F. Mesoporous Silica Gel-Based Mixed Matrix Membranes for Improving Mass Transfer in Forward Osmosis: Effect of Pore Size of Filler. Sci. Rep. 2015, 4, No. 3740.
22. Zhang, Y.; Yuan, S.; Feng, X.; Li, H.; Zhou, J.; Wang, B. Preparation of Nanofibrous Metal-Organic Framework Filters for Efficient Air Pollution Control. J. Am. Chem. Soc. 2016, 138, 5785− 5788.
23. Lange, L. E.; Ochanda, F. O.; Obendorf, S. K.; Hinestroza, J. P. CuBTC Metal-Organic Frameworks Enmeshed in Polyacrylonitrile Fibrous Membrane Remove Methyl Parathion from Solutions. Fibers Polym. 2014, 15, 200−207.
24. Ostermann, R.; Cravillon, J.; Weidmann, C.; Wiebcke, M.; Smarsly, B. M. Metal-Organic Framework Nanofibers via Electro-spinning. Chem. Commun. 2011, 47, 442−444.
25. Chen, Y.; Chen, F.; Zhang, S.; Cai, Y.; Cao, S.; Li, S.; Zhao, W.; Yuan, S.; Feng, X.; Cao, A.; Ma, X.; Wang, B. Facile Fabrication of Multifunctional Metal-Organic Framework Hollow Tubes to Trap Pollutants. J. Am. Chem. Soc. 2017, 139, 16482−16485.

26. Zhu, L.; Yu, H.; Zhang, H.; Shen, J.; Xue, L.; Gao, C.; van der Bruggen, B. Mixed Matrix Membranes Containing MIL-53(Al) for Potential Application in Organic Solvent Nanofiltration. RSC Adv. 2015, 5, 73068−73076.
27. Xie, Z.; Xu, W.; Cui, X.; Wang, Y. Recent Progress in Metal− Organic Frameworks and Their Derived Nanostructures for Energy and Environmental Applications. ChemSusChem 2017, 10, 1645−1663.
28. Wu, Y.; Li, F.; Liu, H.; Zhu, W.; Teng, M.; Jiang, Y.; Li, W.; Xu, D.; He, D.; Hannam, P.; Li, G. Electrospun Fibrous Mats as Skeletons to Produce Free-Standing MOF Membranes. J. Mater. Chem. 2012, 22, 16971−16978.
29. Bhardwaj, N.; Kundu, S. C. Electrospinning: A Fascinating Fiber Fabrication Technique. Biotechnol. Adv. 2010, 28, 325−347.
30. Almasian, A.; Najafi, F.; Maleknia, L.; Giahi, M. Mesoporous MgO/PPG Hybrid Nanofibers: Synthesis, Optimization, Character- ization and Heavy Metal Removal Property. New J. Chem. 2018, 42, 2013−2029.
31. Dichiara, A. B.; Webber, M. R.; Gorman, W. R.; Rogers, R. E. Removal of Copper Ions from Aqueous Solutions via Adsorption on Carbon Nanocomposites. ACS Appl. Mater. Interfaces 2015, 7, 15674− 15680.
32. You, W.; Hong, M.; Zhang, H.; Wu, Q.; Zhuang, Z.; Yu, Y. Functionalized Calcium Silicate Nanofibers with Hierarchical Structure Derived from Oyster Shells and Their Application in Heavy Metal Ions Removal. Phys. Chem. Chem. Phys. 2016, 18, 15564−15573.
33. Sharma, D. K.; Li, F.; Wu, Y. Electrospinning of Nafion and Polyvinyl Alcohol into Nanofiber Membranes: A Facile Approach to Fabricate Functional Adsorbent for Heavy Metals. Colloids Surf., A 2014, 457, 236−243.

34. Mehdinia, A.; Shegefti, S.; Shemirani, F. Removal of Lead (II), Copper (II) and Zinc (II) Ions from Aqueous Solutions using Magnetic Amine-Functionalized Mesoporous Silica Nanocomposites. J. Braz. Chem. Soc. 2015, 26, 2249−2257.
35. Shooto, N. D.; Dikio, C. W.; Wankasi, D.; Sikhwivhilu, L. M.; Mtunzi, F. M.; Dikio, E. D. Novel PVA/MOF Nanofibres: Fabrication, Evaluation and Adsorption of Lead Ions from Aqueous Solution. Nanoscale Res. Lett. 2016, 11, 414.
36. Li, Z.; Zhou, G.; Dai, H.; Yang, M.; Fu, Y.; Ying, Y.; Li, Y. Biomineralization-Mimetic Preparation of Hybrid Membranes with Ultra-High Loading of Pristine Metal-Organic Frameworks Grown on Silk Nanofibers for Hazard Collection in Water. J. Mater. Chem. A 2018, 6, 3402−3413.
37. Engel, E. R.; Jouaiti, A.; Bezuidenhout, C. X.; Hosseini, M. W.; Barbour, L. J. Activation-Dependent Breathing in a Flexible Metal-Organic Framework and the Effects of Repeated Sorption/Desorption Cycling. Angew. Chem., Int. Ed. 2017, 56, 8874−8878.
38. Furukawa, H.; Go, Y. B.; Ko, N.; Park, Y. K.; Uribe-Romo, F. J.; Kim, J.; O'Keeffe, M.; Yaghi, O. M. Isoreticular Expansion of Metal− Organic Frameworks with Triangular and Square Building Units and the Lowest Calculated Density for Porous Crystals. Inorg. Chem. 2011, 50, 9147−9152.
39. Park, K. S.; Ni, Z.; Côte,́A. P.; Choi, J. Y.; Huang, R.; Uribe-Romo, F. J.; Chae, H. K.; O'Keeffe, M.; Yaghi, O. M. Exceptional Chemical and Thermal Stability of Zeolitic Imidazolate Frameworks. Proc. Natl. Acad. Sci. U.S.A. 2006, 103, 10186−10191.
40. Böhme, U.; Barth, B.; Paula, C.; Kuhnt, A.; Schwieger, W.; Mundstock, A.; Caro, J.; Hartmann, M. Ethene/Ethane and Propene/ Propane Separation via the Olefin and Paraffin Selective Metal−Organic Framework Adsorbents CPO-27 and ZIF-8. Langmuir 2013, 29, 8592−8600.

41. Mondloch, J. E.; Karagiaridi, O.; Farha, O. K.; Hupp, J. T. Activation of Metal−Organic Framework Materials. CrystEngComm 2013, 15, 9258−9264.
42. Nelson, A. P.; Farha, O. K.; Mulfort, K. L.; Hupp, J. T. Supercritical Processing as a Route to High Internal Surface Areas and Permanent Microporosity in Metal−Organic Framework Materials. J. Am. Chem. Soc. 2009, 131, 458−460.
43. Bae, J.; Choi, J. S.; Hwang, S.; Yun, W. S.; Song, D.; Lee, J.-D.; Jeong, N. C. Multiple Coordination Exchanges for Room-Temperature Activation of Open-Metal Sites in Metal−Organic Frameworks. ACS Appl. Mater. Interfaces 2017, 9, 24743−24752.
44. Espín, J.; Garzoń-Tovar, L.; Carne-́Sanchez,́ A.; Imaz, I.; Maspoch, D. Photothermal Activation of Metal−Organic Frameworks Using a UV−Vis Light Source. ACS Appl. Mater. Interfaces 2018, 10, 9555−9562.
45. Efome, J. E.; Rana, D.; Matsuura, T.; Lan, C. Q. Metal-Organic Frameworks Supported on Nanofibers to Remove Heavy Metals. J. Mater. Chem. A 2018, 6, 4550−4555.
46. Li, Z.-Q.; Yang, J.-C.; Sui, K.-W.; Yin, N. Facile Synthesis of Metal-Organic Framework MOF-808 for Arsenic Removal. Mater. Lett. 2015, 160, 412−414.
47. Furukawa, H.; Gandara,́ F.; Zhang, Y.-B.; Jiang, J.; Queen, W. L.; Hudson, M. R.; Yaghi, O. M. Water Adsorption in Porous Metal- Organic Frameworks and Related Materials. J. Am. Chem. Soc. 2014,136, 4369−4381.
48. Lagergren, S. About the Theory of so-called Adsorption of Soluble Substances. K. Sven. Vetenskapsakad. Handl. 1898, 24, 1−39.
49. Weber, J. C.; Morris, W. J. In Advances in Water Pollution Research: Removal of Biologically Resistant Pollutant from Waste Water by Adsorption, International Conference on Water Pollution and Treatment; Pergamon: Oxford, U.K., 1962; Vol. 2, pp 231−266.

50. Langmuir, I. The Adsorption of Gases on Plane Surfaces of Glass, Mica and Platinum. J. Am. Chem. Soc. 1918, 40, 1361−1403.
51. Freundlich, H. Of the Adsorption of Gases. Section 11. Kinetics and Energetics of Gas Adsorption. Trans. Faraday Soc. 1932, 28, 195− 201.
52. Temkin, M. I. Adsorption Equilibrium and the Kinetics of Processes on Nonhomogeneous Surfaces and in the Interaction Between Adsorbed Molecules. Zh. Fiz. Khim. 1941, 15, 296−332.
53. Ohwada, K. On the Pauling Electronegativity Scales - I. Polyhedron 1983, 2, 423−424.
54. Ma, H.; Wang, S.; Liu, H.; Meng, F.; Zheng, W.; Gao, W. Tuning the Sorption Properties via Activation Treatments of a Metastable Zn-1,3,5-Benzenetricarboxylate Framework with Dodeca-hedral and Cubic Cages. CrystEngComm 2015, 17, 1001−1004.
55. Mondloch, J. E.; Katz, M. J.; Planas, N.; Semrouni, D.; Gagliardi, L.; Hupp, J. T.; Farha, O. K. Are Zr_6-based MOFs Water Stable? Linker Hydrolysis vs. Capillary-Force-Driven Channel Collapse. Chem. Commun. 2014, 50, 8944−8946.
56. Ma, J.; Kalenak, A. P.; Wong-Foy, A. G.; Matzger, A. J. Rapid Guest Exchange and Ultra-Low Surface Tension Solvents Optimize Metal−Organic Framework Activation. Angew. Chem., Int. Ed. 2017, 56, 14618−14621.
57. Kang, F.; Peng, M.; Lei, D. Y.; Zhang, Q. Recoverable and Unrecoverable Bi^{3+}-Related Photoemissions Induced by Thermal Expansion and Contraction in $LuVO_4$:Bi^{3+} and $ScVO_4$:Bi^{3+} Com-pounds. Chem. Mater. 2016, 28, 7807−7815.
58. Wang, Y.; Panzik, J. E.; Kiefer, B.; Lee, K. K. M. Crystal Structure of Graphite under Room-Temperature Compression and Decompression. Sci. Rep. 2012, 2, No. 520.

Chapter 5

Experiment and modeling for flux and permeate concentration of heavy metal ion in adsorptive membrane filtration using a metal-organic framework incorporated nanofibrous membrane

Johnson E. Efome, Dipak Rana, Takeshi Matsuura and Christopher Q. Lan*

Industrial Membrane Research Institute, Department of Chemical and Biological Engineering, University of Ottawa, 161 Louis Pasteur Private, Ottawa, Ontario, K1N 6N5, Canada

This current chapter is a manuscript published with the Chemical Engineering Journal
Chem. Eng. J. 352(2018)737-744

Abstract

Removal of heavy metal (Lead) ions by membrane adsorption/filtration was studied using nanofibrous membranes in which the adsorbent MOF808 was embedded. S-shaped breakthrough curves were obtained experimentally when the heavy metal concentration in the permeate was plotted vs the filtration period. Simple model equations that enable to reproduce the S-shaped breakthrough curve were derived. It was found that the model equations could simulate the experimental data reasonably well. Attempts were further made to correlate the parameters involved in the model equations to the properties of mixed matrix nanofibrous membranes, such as the pore size and pore size distribution, membrane thickness, fiber diameter, the adsorption rate constant, the Langmuir adsorption constant and the maximum adsorption capacity. The model equation parameters were also correlated to the operating conditions such as the heavy metal concentration in the feed and the transmembrane pressure difference. It is believed that the model equations, despite its simplicity, can provide deeper insight into the membrane adsorption/filtration phenomena and also contribute to the process design.

5.1 Introduction

With the continual increase in water pollution and emergence of new pollutants, the growing need for efficient and effective removal systems has surged in the last decade resulting in processes like chemical precipitation combined with other methods[66]. These adsorbents are expected to pose fast kinetic rates for fast adsorption of pollutants and also to be regenerated easily[67]. Several materials have been engineered for this purpose ranging from naturally occurring substances[68–71] to highly complex 3D metal-organic frameworks[70,72–76]. In most of these materials the rate of removal of heavy metal ions ranges from very slow to extremely fast thus broadening the scope of choice for application depending on the process and the contaminant to be removed. Specific materials like partially fluorinated Cu and Zn MOFs were used for removal of radioactive material from aqueous solution with significant results[77]. Adsorbents for adsorption of multi-ions were also tested for removal of more than five ions simultaneously with significant re-usability and high adsorption capacity[78–81]. These intrinsic properties of the adsorbent turn to enhance the economic viability of the existing process.

In cases where the particles cannot be used as standalone materials, they are immobilized onto a substrate which also contributes to improve the dispersion and at times adsorption increases due to improved surface coverage. Substrate materials have mostly been either flat sheet membranes or nanofibers made from water stable polymers like PAN, PVDF, PES and PTFE [62,70,82–90] among others. These polymers have shown significant chemical and thermal stabilities suitable for aqueous applications. Non-polymeric materials like ceramics have also been developed and used as substrate[76].

For applicability purposes, these composite membranes can either function as membranes for adsorption or filtration or a combination of the two mechanisms as presented in adsorptive-filtration membrane processes[91,92]. Depending on the pore size distribution and the size of the pollutant to be treated, the composite membrane will adopt membrane adsorption when the size of pollutant is smaller than the

membrane pore hence size exclusion is insignificant. Here, the adsorbent particles immobilized on the substrate play the dominant role which in most cases depends on the extent of exposure and contact between the pollutants and the adsorbent. If the particles are completely embedded or enmeshed into the polymer matrix or nanofiber, then exposure and contact could be reduced leading to low adsorption capacity and vice versa. The performance of these particles outside of the substrate and when immobilized has been debated by some researchers saying that the performances are comparable in the immobilized and free-standing state. It should be however noted that this particular report is more prevalent for nanofiber membranes than flat sheet membranes[85]. The composite membranes are usually used as filters to remove heavy metal ions and their performances are evaluated in terms of the membrane flux and the heavy metal concentration in the permeate. Obviously, the performance is affected by many parameters, which include the properties of the composite membranes such as the pore size, pore size distribution, porosity, thickness, fiber diameter (in the case of nanofibrous membranes), amount of the adsorbent embedded and its adsorption capacity. Other parameters are the process parameters such as the heavy metal ion concentration and the transmembrane pressure difference. Therefore, some mathematical models are required to describe the effects of the parameters on the membrane performance quantitatively, especially for process design purposes. Most of the models developed in membrane processes, however, focus on prediction of flux and fouling [93–98] with little attention on the permeate quality. The transport models developed for the nonporous membranes are not applicable for the highly porous nanofibrous membranes. Particularly, no model has been developed for the adsorbent embedded nanofibrous membranes, although the applicability of such composite membranes for membrane adsorption was shown by our previous work[63].

The objective of this work is to present a model to describe the breakthrough curve (time dependent permeate concentration) obtained from the membrane adsorption/filtration experiments as accurately as

possible. Although the model is very simple, it includes all the above-mentioned parameters that can potentially affect the membrane adsorption performance. It should also be emphasized that those parameters were determined quantitatively in our previous work, in which no detailed filtration experiments were conducted. Thus, we believe that the analysis of the experimental data by the proposed model will not only provide the in-depth understanding of the phenomena but also contribute to the process design of membrane adsorption, although we should admit that further refinement of the model is required.

5.2 Modeling approach

The model consists of two parts. In the first, Carman-Kozeny (C-K) equation is employed to estimate the flux of the nanofibrous membrane. The C-K equation has been used in several mathematical models in predicting the flux of porous membranes[94,99] with high compatibility between model and experimental data. The model calculation is made under the condition that the heavy metal concentration is in the ppb range so that the permeate flux is nearly equal to that of pure water. In the second part, an attempt is made to reproduce the breakthrough curve of the permeate concentration based on the mass balance including the rate of heavy metal in- and out flux and the heavy metal adsorption rate. This easy to implement but reliable mass balance approach has shown its presence in modeling designs from RO to UF [100–102].

5.2.1 Carman-Kozeny equation for flux calculation

The membrane flux, J (kg/m^2 h) is calculated according to the Darcy's law by eq. (5-1)

$$J = \frac{3600\rho K}{\mu\delta}\Delta P \qquad (5\text{-}1)$$

where ρ is the density of water (kg/m^3), μ is the viscosity of water (Pa s), δ is the membrane thickness (m), ΔP is the transmembrane pressure difference (Pa) and 3600 is for the conversion of seconds to hour.

K is the permeability coefficient (m^2) which can be calculated by the following Carman-Kozeny equation (eq. 5-2)

$$K = \frac{d_f^2 \varepsilon^3}{16\, k_{CK}(1-\varepsilon)^2} \quad (5\text{-}2)$$

where Ɛ is the membrane porosity (-), d_f is the fiber diameter (m). k_{CK} is the Carman-Kozeny constant, a parameter dependent on the structure of the membrane material. For this study, a k_{CK} value of 4.5 is used based on the work of Tomadakis and Roberston [103], where they provided k_{CK} for different fiber alignments ranging from randomly oriented fibers to fully aligned fibers.

5.2.2 Breakthrough curve of the heavy metal ion concentration in the permeate

From mass balance, the rate of heavy metal ion outlet from the membrane is the rate of heavy metal ion inlet into the membrane minus the rate of heavy metal adsorption as given by eq. (5-3).

$$JAc_p = JAc_f - w\frac{dq_t}{dt} \quad (5\text{-}3)$$

Where *J* is water flux (L/m^2 h, is used here instead of kg/m^2 h), *A* is effective membrane area (m^2), c_p and c_f are permeate and feed heavy metal ion concentration (mg/L), respectively, *w* is the mass of the adsorbent embedded membrane (g), q_t is the amount of the heavy metal ion adsorbed by the unit mass of the membrane (mg/g) at time *t* (h).

Using the first order kinetics,

$$\frac{dq_t}{dt} = k_1(q_{max} - q_t) \quad (5\text{-}4)$$

Where q_{max} is the maximum adsorption capacity of the membrane (mg/g) and k_1 is the pseudo-first order kinetic constant (h^{-1}).

Integrating

$$q_t = q_{max}(1 - e^{-k_1 t}) \quad (5\text{-}5)$$

From eq. (5-4) and (5-5)

$$\frac{dq_t}{dt} = k_1 q_{max} e^{-k_1 t} \quad (5\text{-}6)$$

From eq. (5-3) and (5-6)

$$JAc_p = JAc_f - wk_1 q_{max} e^{-k_1 t} \quad (5\text{-}7)$$

There are two cases:

$$JAc_f < wk_1 q_{max} e^{-k_1 t} \quad (5\text{-}8)$$

In this case, the rate of the heavy metal ion influx is less than the rate of adsorption. Then, c_p is zero.

$$JAc_f \geq wk_1 q_{max} e^{-k_1 t} \quad (5\text{-}9)$$

In this case the rate of heavy metal ion influx is more than the rate of adsorption and the heavy metal ion appears in the permeate making eq. (5-7) relevant.

Rearranging eq. (5-7)

$$\ln\left(1 - \frac{c_p}{c_f}\right) = \ln\left(\frac{wk_1 q_{max}}{JAc_f}\right) - k_1 t \quad (5\text{-}10)$$

According to eq. (5-10), k_1 and $\ln\left(\frac{wk_1 q_{max}}{JAc_f}\right)$ can be obtained from the slope and the intercept with the y axis of the linear plot, $y = \ln\left(1 - \frac{c_p}{c_f}\right)$ vs t, respectively.

When membrane adsorption is overlapped by the membrane rejection R (defined as (1 - cp/c_f) when there is no adsorption), eqtns. (5-7) and (5-10) becomes

$$JAc_p = JA(1-R)c_f - wk_1q_{max}e^{-k_1t} \tag{5-11}$$

and

$$\ln\left(1-\frac{c_p}{c_f}\right) = \ln\left(\frac{wk_1q_{max}}{JA(1-R)c_f}\right) - k_1t \tag{5-12}$$

respectively.

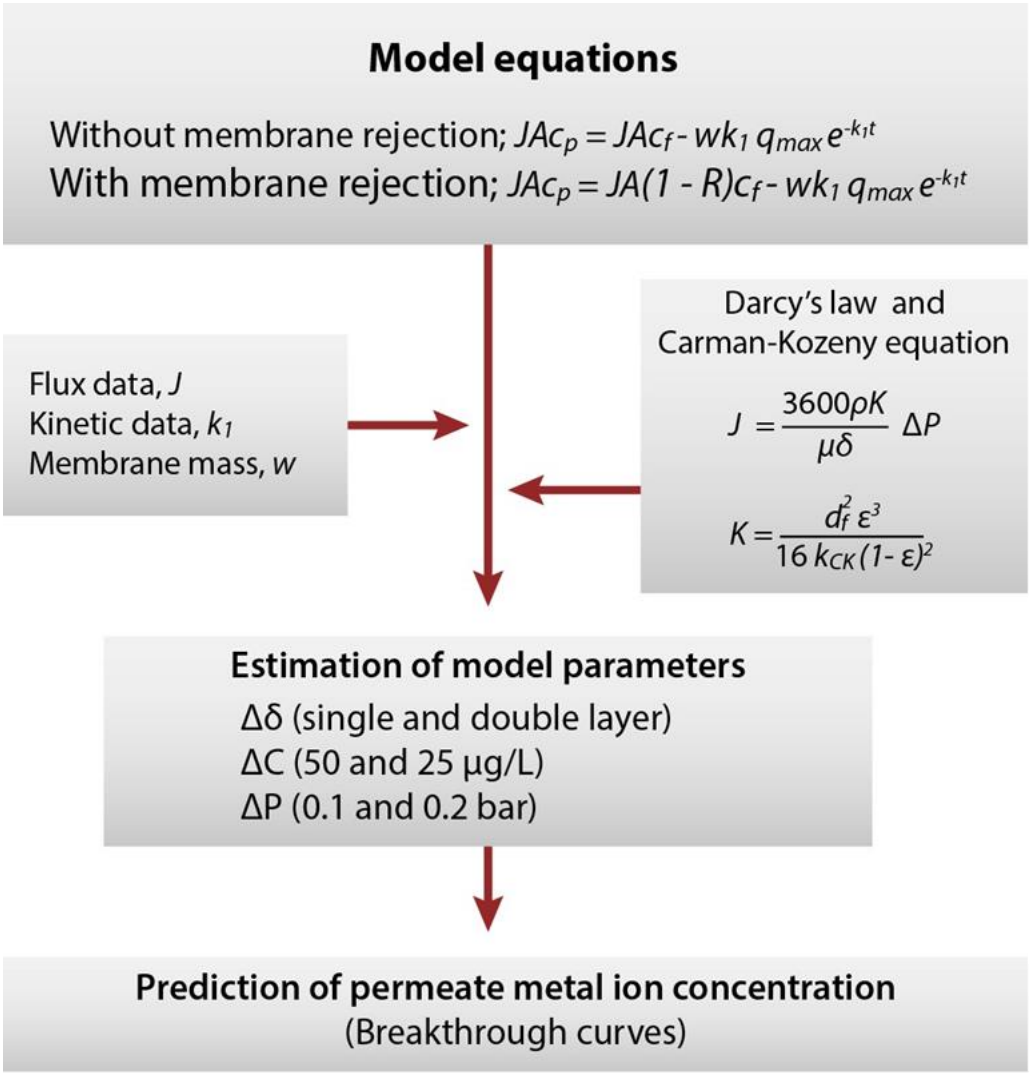

Scheme 5-1. Block diagram demonstrating modeling route. The model equations provide the backbone on which the C-K and Darcy's equations were applied, and the effect of other changes were reflected in the generated breakthrough curves.

5.3 Experimental

It should be noted that the membrane used for the membrane adsorption/filtration was comprised of the following two layers; the top PAN nanofibrous membrane with the embedded MOF808 and the bottom PVDF nanofibrous membrane. The top PAN/MOF808 membrane controls the heavy metal adsorption due to the presence of adsorbent MOF808 and the bottom PVDF membrane controls the flux due to its

hydrophobic property. These composite nanofibrous membranes were prepared following our previous protocol [63].

The pore and fiber characteristics of the PVDF nanofiber membrane were obtained by analysing the SEM images using the ImageJ software. The PVDF membrane porosity was obtained by gravimetric method using butanol [104,105].

The weight of the PAN/MOF808 layer was obtained by weighing several sheets of PAN/MOF808 membrane that were electrospun without the bottom PVDF layer. The first order adsorption rate constant of the MOF particle, k_1 = 1.38 1/h, and the Langmuir adsorption constant, K_L = 0.001 L/mg, and the maximum adsorption capacity, q_{max} = 23.98 mg/g, of the PAN/MOF808 layer were obtained by batch adsorption experiments in our previous work[63].

The filtration experiments were carried out using a continuous filtration setup with a 7 L reservoir which was connected to a feed pump. A feed flow rate of 1.5 LPM was maintained. With such a large feed volume compared to the flux, the feed volume as well as the heavy metal concentration in the feed can be assumed to be constant. The exit valve of the module was used in adjusting the TMP. A specified volume of permeate was collected at predetermined time intervals to calculate the flux. The permeate sample was further subjected to the flame atomic adsorption spectrometry to measure the heavy metal (lead) ion concentration. It must be emphasized that for all the experimental runs (1-6), different membrane coupons were used per run.

5.4 Results and discussion

5.4.1 Membrane flux

As mentioned in the experimental section, PAN808/PVDF multilayer membranes were used for the filtration experiments, since the hydrophilic PAN808 membrane alone showed practically no resistance

against the permeant (water) flow. A PVDF layer was necessary to be placed under the PAN808 layer to make the flux measurable at the applied transmembrane pressure difference (1 and 2 x 10^4 Pa). Therefore, the water flux is solely controlled by the PVDF bottom layer and the membrane properties of the PVDF membrane can be used for the estimation of the membrane flux by eqtns. (5-1) and (5-2).

Table 5-1. Properties of PVDF membrane and water

Parameter	Description	Value
Membrane properties		
ε	PVDF membrane porosity	0.612
d_f	average diameter of PVDF nanofiber	2.027 x10^{-7} m
k_{CK}	Carman-Kozeny constant	4.5
δ	PVDF membrane thickness	3.0 x 10^{-5} m
Properties of water		
ρ	density	0.997 x 10^3 kg/m^3
μ	viscosity	8.9 x 10^{-4} Pa s

The membrane flux was calculated using the membrane properties as well as the properties of water, both summarized in Table 5-1, under the transmembrane pressure difference of 10^4 Pa (0.1 bar). The result was 1091 kg/m^2 h. On the other hand, the experimentally obtained membrane flux was 348.9 kg/m^2 h. The approximately 3 times higher theoretical value is probably due to the high porosity value of 0.612.

The porosity is highly likely reduced under the pressure to a value of 0.597 (decrease of 2.5 %) due to compaction, by which the theoretical flux agrees with the experimentally observed flux.

5.4.2 Permeate concentration

An attempt was made to interpret the breakthrough curve of the heavy metal ion concentration in the permeate by the model equations. First, the effect of the feed heavy metal ion concentration was studied by using 50 and 25 x10^{-3} mg/L in the feed. The thickness and the mass of the membranes are reported in Table 5-2 together with the transmembrane pressure difference and the feed heavy metal concentration of Run 1and 2. The membrane flux was 348.9 kg/m^2 h, as reported in section 5.4.1.

Table 5-2.The thickness of the PAN808 membrane, experimental conditions and some experimental results for Run 1 and 2.

Run	Membrane thickness[a] (m) x 10^6	Transmembrane pressure difference (Pa) x 10^{-4}	Feed concentration (mg/L) x 10^3	Flux (kg/m^2 h)	Rejection by membrane (%)
1	560	1	50	348.9	10.1
2	560	1	25	348.9	1.8

[a] This is the thickness of the of PAN808 membrane where adsorption takes place. The membrane area, *A*, was 0.0038 m^2 and the mass of the membrane, *w*, was averaged 100 mg.

Table 5-3. Results of regression analysis for Run 1 and 2

Run	k_1 (1/h)	Intercept with t axis (min)	Intercept with y axis and $\left(\ln\left(\frac{wk_1q_{max}}{JA(1-R)c_f}\right)\right)$ (-)	Coefficient of determination, R^2
1	1.342	103.8	2.323 (3.980)	0.826
2	2.256	128.2	4.819 (5.115)	0.968

Figure 5-1 shows the experimental permeate concentration versus time for Run 1 and 2. Both of them are the typical S-shaped breakthrough curves with Run 1 and 2 leveling off at 45.4 and 24.6 x 10^{-3} mg/L, corresponding to the rejection of 10.1 and 1.8 %, respectively. These rejections are also reported in Table 5-2. Although the values are low, the rejection of the heavy metal ion was unexpected since the size of the heavy metal ion is much smaller than the nanofiber membrane pore size. One of the plausible explanations is that the adsorption rate has become very slow at the last stage of the filtration experiment, exhibiting very slow approach of the breakthrough curve to the targeted value, which is the concentration in the feed.

$\ln\left(1-\frac{c_p}{c_f}\right)$ versus t plot shown in Fig. 5-2 is almost linear. The data were therefore subjected to the linear regression analysis, according to eq. (5-12) without including the first few data where c_p is equal to zero and the last one that is considered as the leveled off value. The results of the regression analysis are shown in Table 5-3.

The coefficient of determination, R^2, is given in the last column of the Table 3, which indicates that fitting of Run 1 was poor relative to the excellent fitting of Run 2.

k_1 values for Run 1 and 2 are 1.342 and 2.256 1/h, respectively. These values are in the same order of magnitude as 1.38 1/h obtained for stand-alone MOF808 in our previous work [63], suggesting that the adsorption is controlled by the heavy metal transport in MOF.

Regarding the intercept with t-axis, the data coincide with the times when the heavy metal ion starts to appear in the permeate (see Fig. 5-1). This lag time is longer for Run 2 due to the lower feed heavy metal ion concentration.

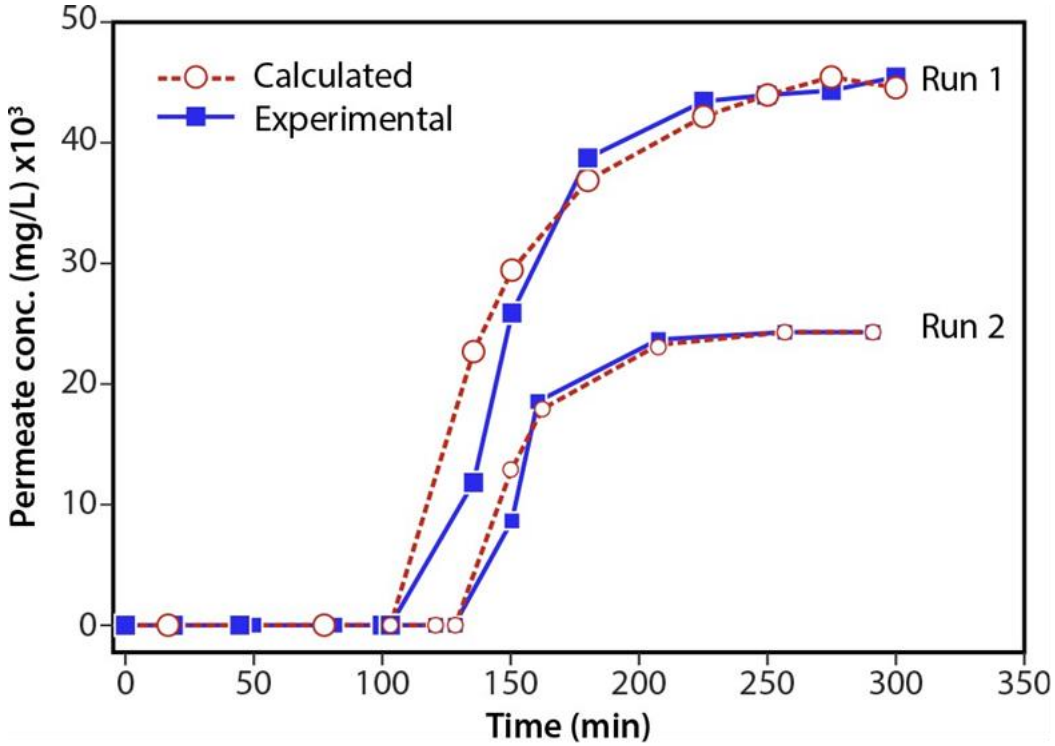

Figure 5-1. Effect of feed concentration on the amount of permeate produced for Run 1 and 2.

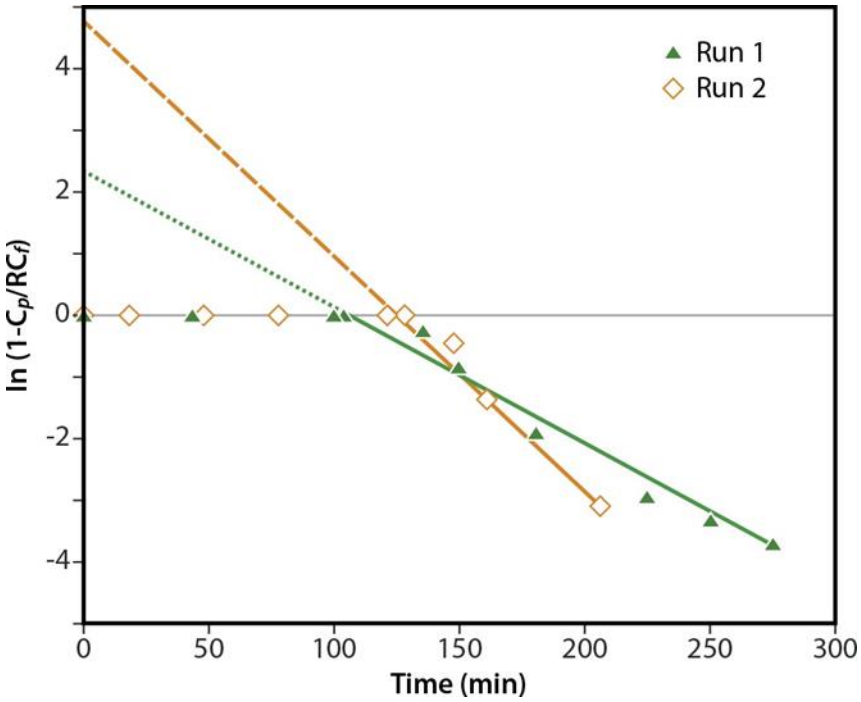

Figure 5-2. Plot for Runs 1 and 2 to obtain the regression data.

Regarding the intercept with y-axis, it should be equal to $\ln\left(\frac{wk_1q_{max}}{JA(1-R)c_f}\right)$ as shown in eq. (5-12). In order to test if the intercepts obtained from the regression analysis indeed satisfy the theoretical requirement, $\ln\left(\frac{wk_1q_{max}}{JA(1-R)c_f}\right)$ was calculated for Run 1 and 2, using q_{max} = 23.98 mg/g for PAN 808 membrane, a value obtained by our previous work [63]. w, k_1, J, A, R and c_f are shown in Tables 5-2 and 5-3. The results are also included in Table 5-3 in the fourth column in the parenthesis. The agreement is very good for Run 2 but for Run 1, the theoretical value was larger than the one obtained by the regression analysis, indicating that the total adsorption capacity in the membrane, wq_{max} was not fully utilized in the filtration experiment for Run 1.

It should be noted that some ambiguity remains in the interpretation of q_{max}. According to the definition of pseudo-first order adsorption q_e, which is the amount of heavy metal ion adsorbed at equilibrium with the equilibrium concentration, should be used in eq. (5-4) instead of q_{max}.

As well, according to the Langmuir adsorption equilibrium

$$q_e = \frac{q_{max}K_Lc_e}{1 + K_Lc_e}$$

Which will be nearly equal to $q_{max}K_Lc_e$, when c_e is as low as or lower than the feed concentration of 0.05 mg/L used in this work. Since q_{max} is 23.98 mg/g and K_L is 0.001 L/mg (see experimental section) $q_{max}K_Lc_e$ is equal to or less than 0.0012mg/g.

Then, using q_e instead of q_{max}, theoretical $\ln\left(\frac{wk_1q_{max}}{JA(1-R)c_f}\right)$ becomes less than -5.923, which is unreasonable especially with its negative sign. Therefore, q_{max} will be used instead of q_e from now on for the calculation of the theoretical $\ln\left(\frac{wk_1q_{max}}{JA(1-R)c_f}\right)$.

In Table 5-3 both y-axis intercept and the theoretical $\ln\left(\frac{wk_1q_{max}}{JA(1-R)c_f}\right)$ increase from Run 1 to 2 due to the smaller c_f of the latter.

The simulation of the breakthrough curve is also presented in Fig. 1 together with the experimental data for Run 1 and 2.

Table 5-4.The thickness of the PAN808 membrane, experimental conditions and some experimental results for Run 3 and 4.

Run	Membrane thickness[a] (m) x 10^6	Transmembrane pressure difference (Pa) x 10^{-4}	Feed concentration (mg/L) x 10^3	Flux (kg/m^2 h)	Rejection by membrane (%)
3	530	1	41.7	348.9	0
4	1060	1	41.7	348.9	0

Table 5-5.Results of regression analysis for Run 3 and 4

Run	k_1 (1/h)	Intercept with t axis (min)	Intercept with y axis and $\left(\ln\left(\frac{wk_1q_{max}}{JA(1-R)c_f}\right)\right)$ (-)	Coefficient of determination, R^2
3	1.482	56.48	1.395 (2.56)	0.987
4	1.740	83.75	2.429 (3.41)	0.943

In the next group of experiments (Run 3 and 4), the thickness of the membrane was changed. In Run 3 a single layer of the PAN808 membrane with a thickness of 530 x 10^{-6} m was used while in Run 4 the membrane thickness was doubled by placing one PAN808 membrane on top of the other PAN808 membrane. The membrane property, experimental conditions and some of the experimental results are shown in Table 5-4. Note that the membrane flux has not changed from Run 3 to 4 despite doubling of the PAN808 membrane thickness, since PAN808 membrane has shown practically no resistance for the permeate flow. The results of the regression analysis are shown in Table 5-5.

The coefficients of determination are very high for both Run 3 and 4, indicating the excellent linear fitting.

The k_1 values for Run 3 and 4 were 1.482 and 1.740 1/h, which were again close to the k_1 observed earlier for the stand-alone MOF808 particle.

The lag time (intercept on t-axis) of Run 4 was longer than Run 3 as expected.

The theoretical $\ln\left(\frac{wk_1q_{max}}{JA(1-R)c_f}\right)$ increased from Run 3 to 4, since the mass of PAN808 membrane, *w*, was doubled when the thickness was doubled. The y-axis intercept of linear regression was smaller than the theoretical value, again due to the underutilization of the adsorption capacity.

Table 5-6.The thickness of the PAN808 membrane, experimental conditions and some experimental results for Run 5 and 6.

Experiment	Membrane thickness[a] (m) x 10^6	Transmembrane pressure difference (Pa) x 10^{-4}	Feed concentration (mg/L) x 10^3	Flux (kg/m^2 h)	Rejection by membrane (%)
5	560	1	41.7	348.9±26	0
6	560	2	41.7	693.6±42	0

Table 5-7.Results of regression analysis for Run 5 and 6

Run	k_1 (1/h)	Intercept with t axis (min)	Intercept with y axis and $(\ln\left(\frac{wk_1q_{max}}{JA(1-R)c_f}\right))$ (-)	Coefficient of determination, R^2
5	1.08	79.55	1.432 (3.849)	0.994
	4.464	159.5	11.90 (5.268)	1.0
6	0.798	46.14	0.6137 (2.854)	0.915
	1.89	132.5	4.146 (3.716)	0.978

In the next experiments (Run 5 and 6) the transmembrane pressure difference was changed from 1 to $2x10^4$ Pa. The flux was doubled as shown in Table 5-6. The breakthrough curve of the heavy metal concentration in the permeate is shown in Fig. 5-3. Interestingly, an inflection point appeared for both run 5 and 6 at 180 min, indicating some change in the membrane properties. Therefore, in the model analysis, the linear regression was carried out in the two separate parts of the breakthrough curve, i.e. before and after 180 min, and the results shown in Table 5-7.

It should be noted that in the second regression of Run 5, only the data at 180 and 210 min were used because the curve quickly leveled off after 210 min. Therefore, the slope and intercept obtained are less reliable despite the high coefficient of determination of 1.0.

In Table 5-7, k_1 values are again in the reasonable range, except for the second part of Run 5. The increase of k_1 from the first to the second regression reflects the sudden increase the slope at 180 min.

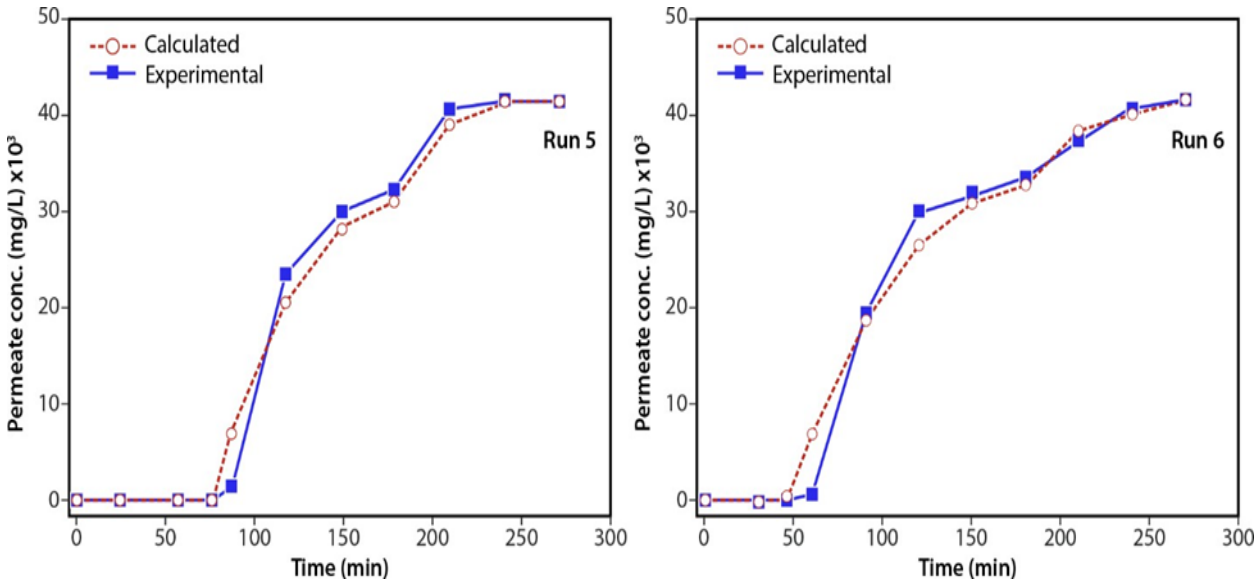

Figure 5-3. Effect of TMP pressure depicted by Run 5(0.1 bar) and Run 6 (0.2 bar)

As for the lag time, it increases from the first to the second regression, reflecting the shape of the breakthrough curve. The lag time decreases with an increase in the transmembrane pressure difference, which is reasonable since the rate of heavy metal entry surpasses the rate of adsorption sooner when the flux is doubled.

Regarding the y axis intercept, it increased significantly from the first to the second regression due to the increase in k_1, but as already mentioned the value for the second regression part is less reliable. Both y axis intercept and the theoretical ln $\left(\frac{wk_1q_{max}}{JA(1-R)c_f}\right)$ value decreased with an increase in the transmembrane pressure difference due to the doubling of the flux. The simulation of the breakthrough curve is also presented in Fig. 5-3 together with the experimental data for Run 5 and 6.

5.5 Conclusions

The following conclusions can be drawn from this work.

The Darcy's law and Carman-Kozeny equations, when applied for the nanofibrous membrane, reveals slight membrane compaction under the pressure.

The newly developed model reproduces the S-shaped breakthrough curve of the heavy metal concentration in the permeate reasonably well, when the slope and the intercept obtained from the linear regression analysis are used.

The slope agrees with the adsorption rate constant obtained from the independent adsorption experiment reasonably well.

The intercept can be related to the parameters such as the mass of the membrane, membrane thickness, adsorption rate constant, maximum adsorption capacity of the membrane, transmembrane pressure difference, and heavy metal ion concentration in the feed.

Currently, however, the precise prediction of the membrane performance is not yet possible, since

a) The degree of the membrane compaction under the pressure can not be predicted.
b) The adsorption rate constant varies considerably from membrane to membrane.
c) The maximum adsorption capacity is not fully utilized. The degree of utilization should be affected by the pore size and pore size distribution, fiber diameter of PAN808 layer and also the distribution of MOF particles in the nanofiber. Therefore, it is necessary to correlate the utilization of the maximum adsorption capacity to the above-mentioned parameters to enable the precise prediction of the membrane adsorption performance for the MOF embedded nanofibrous membrane.

5.6 Acknowledgement

The authors would like to thank the support of NSERC strategic grant # 128655.

Nomenclature

J	water flux [m^3/m^2 s]	Greek letters	
A	effective membrane area [m^2]	δ	membrane thickness [m]
w	amount of MOF [g]	ε	porosity [-]
q_{max}	maximum adsorption capacity [mol/g]	μ	dynamic viscosity [kg/m s]
q_t	time adsorption capacity [mol/g]		
c_f	feed concentration [mol/ m^3]		
c_p	permeate concentration [mol/m^3]		
k_1	first order kinetic constant [1/s]		
t	time [s]		
R	rejection [%]		
V	Volume of feed [m^3]		
K_{CK}	Carman-Kozeny constant [-]		
K	permeability coefficient [m/s]		
d_f	average fiber diameter		

References

[1] World Water Assessment Programme (WWAP), The United Nations World Water Development Report 2015: Water for a Sustainable World, Facts and Figures, UN Water Rep. (2015) 138. doi:10.1016/S1366-7017(02)00004-1.

[2] H.G. Gorchev, G. Ozolins, WHO guidelines for drinking-water quality., WHO Chron. 38 (2011) 104–108. doi:10.1016/S1462-0758(00)00006-6.

[3] K. Rajeshwar, Advanced Oxidation Processes for Water Treatment, J. Phys. Chem. Lett. 3 (2012) 2112–2113. doi:10.1021/jz200396h.

[4] K.C. Khulbe, C.Y. Feng, T. Matsuura, A.F. Ismail, Progresses in membrane and advanced oxidation processes for water treatment, Membr. Water Treat. 3 (2012). doi:10.12989/mwt.2012.3.3.181.

[5] J. Choi, A. Ide, Y.B. Truong, I.L. Kyratzis, R.A. Caruso, High surface area mesoporous titanium–zirconium oxide nanofibrous web: a heavy metal ion adsorbent, J. Mater. Chem. A. 1 (2013) 5847. doi:10.1039/c3ta00030c.

[6] F. Franco, M. Benítez-Guerrero, I. Gonzalez-Triviño, R. Pérez-Recuerda, C. Assiego, J. Cifuentes-Melchor, J. Pascual-Cosp, Low-cost aluminum and iron oxides supported on dioctahedral and trioctahedral smectites: A comparative study of the effectiveness on the heavy metal adsorption from water, Appl. Clay Sci. 119 (2016) 321–332. doi:10.1016/j.clay.2015.10.035.

[7] D.C. Manatunga, R.M. de Silva, K.M.N. de Silva, R. Ratnaweera, Natural polysaccharides leading to super adsorbent hydroxyapatite nanoparticles for the removal of heavy metals and dyes from aqueous solutions, RSC Adv. 6 (2016) 105618–105630. doi:10.1039/C6RA22662K.

[8] S.P. Mishra, V.K. Singh, Inorganic particulates in removal of toxic heavy metal ions VIII . Removal of zinc, cadmium and mercury ions from aqueous solution by hydrous titanium oxide, J. Radioanal. Nucl. Chem. 241 (1999) 341–346.

[9] S. Kalantari, M. Yousefpour, Z. Taherian, Synthesis of mesoporous silica/iron oxide nanocomposites and application of optimum sample as adsorbent in removal of heavy metals, Rare Met. 36 (2017) 942–950. doi:10.1007/s12598-016-0709-4.

[10] C. MAHAJAN, REMOVAL OF HEAVY METALS FROM WINERY WASTEWATER BY USING NATURAL ADSORBENTS., Int. …. 5 (2014) 69–78. http://search.ebscohost.com/login.aspx?direct=true&profile=ehost&scope=site&authtype=crawler&jrnl=2067533X&AN=95118774&h=guL3767S4V9fiSnoq6DVlXr4MqBmJNF96EbdJhHgWuszFOCbPqo7kKod3UXiNd94ULnSzKIPyFljXggUhyZ32Q%3D%3D&crl=c.

[11] C. Wang, X. Liu, N. Keser Demir, J.P. Chen, K. Li, Applications of water stable metal–organic frameworks, Chem. Soc. Rev. 45 (2016) 5107–5134. doi:10.1039/C6CS00362A.

[12] R. Ricco, K. Konstas, M.J. Styles, J.J. Richardson, R. Babarao, K. Suzuki, P. Scopece, P. Falcaro, Lead(II) uptake by aluminium based magnetic framework composites (MFCs) in water, J. Mater. Chem. A. 3 (2015) 19822–19831. doi:10.1039/C5TA04154F.

[13] I. Erucar, G. Yilmaz, S. Keskin, Recent advances in metal-organic framework-based mixed matrix membranes, in: Chem. - An Asian J., 2013: pp. 1692–1704. doi:10.1002/asia.201300084.

[14] V. V Butova, M.A. Soldatov, A.A. Guda, K.A. Lomachenko, C. Lamberti, Metal-organic frameworks: structure, properties, methods of synthesis and characterization, Russ. Chem. Rev. 85 (2016) 280–307. doi:10.1070/RCR4554.

[15] S. Qiu, M. Xue, G. Zhu, Metal–organic framework membranes: from synthesis to separation

application, Chem. Soc. Rev. 43 (2014) 6116–6140. doi:10.1039/C4CS00159A.

[16] N.A. Khan, S.H. Jhung, Synthesis of metal-organic frameworks (MOFs) with microwave or ultrasound: Rapid reaction, phase-selectivity, and size reduction, Coord. Chem. Rev. 285 (2015) 11–23. doi:10.1016/j.ccr.2014.10.008.

[17] Z.-J. Lin, Z. Yang, T.-F. Liu, Y.-B. Huang, R. Cao, Microwave-assisted synthesis of a series of lanthanide metal-organic frameworks and gas sorption properties., Inorg. Chem. 51 (2012) 1813–20. doi:10.1021/ic202082w.

[18] W. Liang, D.M. D'Alessandro, Microwave-assisted solvothermal synthesis of zirconium oxide based metal-organic frameworks., Chem. Commun. (Camb). 49 (2013) 3706–8. doi:10.1039/c3cc40368h.

[19] Z. Lin, D.S. Wragg, R.E. Morris, Microwave-assisted synthesis of anionic metal–organic frameworks under ionothermal conditions, Chem. Commun. (2006) 2021–2023. doi:10.1039/B600814C.

[20] R. Vakili, S. Xu, N. Al-Janabi, P. Gorgojo, S.M. Holmes, X. Fan, Microwave-assisted synthesis of zirconium-based metal organic frameworks (MOFs): Optimization and gas adsorption, Microporous Mesoporous Mater. 260 (2018) 45–53. doi:10.1016/j.micromeso.2017.10.028.

[21] M. Bechelany, M. Drobek, C. Vallicari, A. Abou Chaaya, A. Julbe, P. Miele, Highly crystalline MOF-based materials grown on electrospun nanofibers, Nanoscale. 7 (2015). doi:10.1039/c4nr06640e.

[22] U. Müller, H. Pütter, M. Hesse, H. Wessel, M. Schubert, Method for electrochemical production of a crystalline porous metal organic skeleton material, WO/2005/049892, 2005.

[23] M. Hartmann, S. Kunz, D. Himsl, O. Tangermann, S. Ernst, A. Wagener, Adsorptive separation

of isobutene and isobutane on Cu3(BTC)2, Langmuir. 24 (2008) 8634–8642. doi:10.1021/la8008656.

[24] G. Nickerl, A. Notzon, M. Heitbaum, I. Senkovska, F. Glorius, S. Kaskel, Selective Adsorption Properties of Cationic Metal–Organic Frameworks Based on Imidazolic Linker, Cryst. Growth Des. 13 (2013) 198–203. doi:10.1021/cg301347t.

[25] L. Xie, D. Liu, H. Huang, Q. Yang, C. Zhong, Efficient capture of nitrobenzene from waste water using metal-organic frameworks, Chem. Eng. J. 246 (2014) 142–149. doi:10.1016/j.cej.2014.02.070.

[26] Z. Hasan, E.J. Choi, S.H. Jhung, Adsorption of naproxen and clofibric acid over a metal–organic framework MIL-101 functionalized with acidic and basic groups, Chem. Eng. J. 219 (2013) 537–544. doi:10.1016/j.cej.2013.01.002.

[27] M. Tong, D. Liu, Q. Yang, S. Devautour-Vinot, G. Maurin, C. Zhong, Influence of framework metal ions on the dye capture behavior of MIL-100 (Fe, Cr) MOF type solids, J. Mater. Chem. A. 1 (2013) 8534. doi:10.1039/c3ta11807j.

[28] X.-X. Huang, L.-G. Qiu, W. Zhang, Y.-P. Yuan, X. Jiang, A.-J. Xie, Y.-H. Shen, J.-F. Zhu, Hierarchically mesostructured MIL-101 metal–organic frameworks: supramolecular template-directed synthesis and accelerated adsorption kinetics for dye removal, CrystEngComm. 14 (2012) 1613–1617. doi:10.1039/C1CE06138K.

[29] B.-J. Yao, W.-L. Jiang, Y. Dong, Z.-X. Liu, Y.-B. Dong, Post-Synthetic Polymerization of UiO-66-NH<inf>2</inf>Nanoparticles and Polyurethane Oligomer toward Stand-Alone Membranes for Dye Removal and Separation, Chem. - A Eur. J. 22 (2016). doi:10.1002/chem.201600817.

[30] Z. Hasan, S.H. Jhung, Removal of hazardous organics from water using metal-organic

frameworks (MOFs): Plausible mechanisms for selective adsorptions, J. Hazard. Mater. 283 (2015) 329–339. doi:10.1016/j.jhazmat.2014.09.046.

[31] H. Furukawa, F. Gándara, Y.-B. Zhang, J. Jiang, W.L. Queen, M.R. Hudson, O.M. Yaghi, Water adsorption in porous metal-organic frameworks and related materials., J. Am. Chem. Soc. 136 (2014) 4369–81. doi:10.1021/ja500330a.

[32] J.J. Low, A.I. Benin, P. Jakubczak, J.F. Abrahamian, S.A. Faheem, R.R. Willis, Virtual high throughput screening confirmed experimentally: Porous coordination polymer hydration, J. Am. Chem. Soc. 131 (2009) 15834–15842. doi:10.1021/ja9061344.

[33] N.U. Qadir, S.A.M. Said, H.M. Bahaidarah, Structural stability of metal organic frameworks in aqueous media - Controlling factors and methods to improve hydrostability and hydrothermal cyclic stability, Microporous Mesoporous Mater. 201 (2015) 61–90. doi:10.1016/j.micromeso.2014.09.034.

[34] T. Loiseau, C. Serre, C. Huguenard, G. Fink, F. Taulelle, M. Henry, T. Bataille, G. Férey, A Rationale for the Large Breathing of the Porous Aluminum Terephthalate (MIL-53) Upon Hydration, Chem. - A Eur. J. 10 (2004) 1373–1382. doi:10.1002/chem.200305413.

[35] J.H. Cavka, S. Jakobsen, U. Olsbye, N. Guillou, C. Lamberti, S. Bordiga, K.P. Lillerud, A new zirconium inorganic building brick forming metal organic frameworks with exceptional stability, J. Am. Chem. Soc. 130 (2008) 13850–13851. doi:10.1021/ja8057953.

[36] H.K. Chae, J. Kim, O.D. Friedrichs, M. O'Keeffe, O.M. Yaghi, Design of frameworks with mixed triangular and octahedral building blocks exemplified by the structure of [Zn4O(TCA)2] having the pyrite topology, Angew. Chemie - Int. Ed. 42 (2003) 3907–3909. doi:10.1002/anie.200351546.

[37] X. Liu, N.K. Demir, Z. Wu, K. Li, Highly Water-Stable Zirconium Metal-Organic Framework UiO-66 Membranes Supported on Alumina Hollow Fibers for Desalination, J. Am. Chem. Soc. 137 (2015) 6999–7002. doi:10.1021/jacs.5b02276.

[38] K. Tan, N. Nijem, P. Canepa, Q. Gong, J. Li, T. Thonhauser, Y.J. Chabal, Stability and hydrolyzation of metal organic frameworks with paddle-wheel SBUs upon hydration, Chem. Mater. 24 (2012) 3153–3167. doi:10.1021/cm301427w.

[39] M. Haouas, C. Volkringer, T. Loiseau, G. Férey, F. Taulelle, The extra-framework sub-lattice of the metal-organic framework MIL-110: A solid-state NMR investigation, Chem. - A Eur. J. 15 (2009) 3139–3146. doi:10.1002/chem.200801856.

[40] J.-Y. Lee, C.Y. Tang, F. Huo, Fabrication of Porous Matrix Membrane (PMM) Using Metal-Organic Framework as Green Template for Water Treatment, Sci. Rep. 4 (2015) 3740. doi:10.1038/srep03740.

[41] J. Duan, Y. Pan, F. Pacheco, E. Litwiller, Z. Lai, I. Pinnau, High-performance polyamide thin-film-nanocomposite reverse osmosis membranes containing hydrophobic zeolitic imidazolate framework-8, J. Memb. Sci. 476 (2015) 303–310. doi:10.1016/j.memsci.2014.11.038.

[42] R. Zhang, S. Ji, N. Wang, L. Wang, G. Zhang, J.-R.J.R. Li, Coordination-driven in situ self-assembly strategy for the preparation of metal-organic framework hybrid membranes, Angew. Chemie - Int. Ed. 53 (2014) 9775–9779. doi:10.1002/anie.201403978.

[43] H. Fan, Q. Shi, H. Yan, S. Ji, J. Dong, G. Zhang, Simultaneous spray self-assembly of highly loaded ZIF-8-PDMS nanohybrid membranes exhibiting exceptionally high biobutanol-permselective pervaporation, Angew. Chemie - Int. Ed. 53 (2014) 5578–5582. doi:10.1002/anie.201309534.

[44] G. Zhang, J. Li, N. Wang, H. Fan, R. Zhang, G. Zhang, S. Ji, Enhanced flux of polydimethylsiloxane membrane for ethanol permselective pervaporation via incorporation of MIL-53 particles, J. Memb. Sci. 492 (2015) 322–330. doi:10.1016/j.memsci.2015.05.070.

[45] Y. Zhang, N. Wang, S. Ji, R. Zhang, C. Zhao, J.R. Li, Metal-organic framework/poly(vinyl alcohol) nanohybrid membrane for the pervaporation of toluene/n-heptane mixtures, J. Memb. Sci. 489 (2015) 144–152. doi:10.1016/j.memsci.2015.04.012.

[46] X. Liu, H. Jin, Y. Li, H. Bux, Z. Hu, Y. Ban, W. Yang, Metal-organic framework ZIF-8 nanocomposite membrane for efficient recovery of furfural via pervaporation and vapor permeation, J. Memb. Sci. 428 (2013) 498–506. doi:10.1016/j.memsci.2012.10.028.

[47] D. Li, Y. Xia, Electrospinning of nanofibers: Reinventing the wheel?, Adv. Mater. 16 (2004) 1151–1170. doi:10.1002/adma.200400719.

[48] S. Agarwal, S. Jiang, Nanofibers and Electrospinning, in: Encycl. Polym. Nanomater., 2015: p. 1323.

[49] W. Teo, Introduction to Electrospinning Parameters and Fiber Control, Introd. to Electrospinning Parameters Fiber Control. (2015) 25–28. http://electrospintech.com/solution.html#.Ve7THhFVikp.

[50] N. Rosman, W.N.W. Salleh, M.A. Mohamed, N.H. Ismail, N. Sazali, J. Jaafar, H. Hasbullah, Electrospun nanofiber-coated membrane: A review, J. Teknol. 78 (2016) 83–88. doi:10.11113/jt.v78.10071.

[51] T.J. Sill, H.A. von Recum, Electrospinning: Applications in drug delivery and tissue engineering, Biomaterials. 29 (2008) 1989–2006. doi:10.1016/j.biomaterials.2008.01.011.

[52] Y.C. Woo, L.D. Tijing, M.J. Park, M. Yao, J.S. Choi, S. Lee, S.H. Kim, K.J. An, H.K. Shon,

Electrospun dual-layer nonwoven membrane for desalination by air gap membrane distillation, Desalination. 403 (2017) 187–198. doi:10.1016/j.desal.2015.09.009.

[53] Y. Tian, M. Wu, R. Liu, Y. Li, D. Wang, J. Tan, R. Wu, Y. Huang, Electrospun membrane of cellulose acetate for heavy metal ion adsorption in water treatment, Carbohydr. Polym. 83 (2011) 743–748. doi:10.1016/j.carbpol.2010.08.054.

[54] X. Hu, S. Liu, G. Zhou, Y. Huang, Z. Xie, X. Jing, Electrospinning of polymeric nanofibers for drug delivery applications, J. Control. Release. 185 (2014) 12–21. doi:10.1016/j.jconrel.2014.04.018.

[55] O.K. Pereao, C. Bode-Aluko, G. Ndayambaje, O. Fatoba, L.F. Petrik, Electrospinning: Polymer Nanofibre Adsorbent Applications for Metal Ion Removal, J. Polym. Environ. 25 (2017) 1175–1189. doi:10.1007/s10924-016-0896-y.

[56] F.E. Ahmed, B.S. Lalia, R. Hashaikeh, A review on electrospinning for membrane fabrication: Challenges and applications, Desalination. 356 (2015) 15–30. doi:10.1016/j.desal.2014.09.033.

[57] R. Dersch, A. Greiner, J.H. Wendorff, Polymer nanofibers by electrospinning, Dekker Encycl. Nanosci. Nanotechnol. 8 (2004) 64–75. doi:10.1016/S1359-0294Ž03.00004-9.

[58] J.. Deitzel, J. Kleinmeyer, D. Harris, N.. Beck Tan, The effect of processing variables on the morphology of electrospun nanofibers and textiles, Polymer (Guildf). 42 (2001) 261–272. doi:10.1016/S0032-3861(00)00250-0.

[59] R. Khajavi, M. Abbasipour, Controlling nanofiber morphology by the electrospinning process, in: Electrospun Nanofibers, 2016: pp. 109–123. doi:10.1016/B978-0-08-100907-9.00005-2.

[60] J. Doshi, D.H. Reneker, Electrospinning process and applications of electrospun fibers, J. Electrostat. 35 (1995) 151–160. doi:10.1016/0304-3886(95)00041-8.

[61] Y.Z. Zhang, Y. Feng, Z.M. Huang, S. Ramakrishna, C.T. Lim, Fabrication of porous electrospun nanofibres, Nanotechnology. 17 (2006) 901–908. doi:10.1088/0957-4484/17/3/047.

[62] J.E. Efome, D. Rana, T. Matsuura, C.Q. Lan, Enhanced performance of PVDF nanocomposite membrane by nanofiber coating: A membrane for sustainable desalination through MD, Water Res. 89 (2016) 39–49. doi:10.1016/j.watres.2015.11.040.

[63] J.E.E. Efome, D. Rana, T. Matsuura, C.Q. Lan, Metal–organic frameworks supported on nanofibers to remove heavy metals, J. Mater. Chem. A. 6 (2018) 4550–4555. doi:10.1039/c7ta10428f.

[64] S. Megelski, J.S. Stephens, D. Bruce Chase, J.F. Rabolt, Micro- and nanostructured surface morphology on electrospun polymer fibers, Macromolecules. 35 (2002) 8456–8466. doi:10.1021/ma020444a.

[65] S.L. James, Metal-organic frameworks, Chem. Soc. Rev. 32 (2003) 276. doi:10.1039/b200393g.

[66] F. Fu, Q. Wang, Removal of heavy metal ions from wastewaters: A review, J. Environ. Manage. 92 (2011) 407–418. doi:10.1016/j.jenvman.2010.11.011.

[67] M. Hua, S. Zhang, B. Pan, W. Zhang, L. Lv, Q. Zhang, Heavy metal removal from water/wastewater by nanosized metal oxides: A review, J. Hazard. Mater. 211–212 (2012) 317–331. doi:10.1016/j.jhazmat.2011.10.016.

[68] S. Wang, Y. Peng, Natural zeolites as effective adsorbents in water and wastewater treatment, Chem. Eng. J. 156 (2010) 11–24. doi:10.1016/j.cej.2009.10.029.

[69] N. Bleiman, Y.G. Mishael, Selenium removal from drinking water by adsorption to chitosan-clay composites and oxides: Batch and columns tests, J. Hazard. Mater. 183 (2010) 590–595. doi:10.1016/j.jhazmat.2010.07.065.

[70] Y. Yurekli, Removal of heavy metals in wastewater by using zeolite nano-particles impregnated polysulfone membranes, J. Hazard. Mater. 309 (2016) 53–64. doi:10.1016/j.jhazmat.2016.01.064.

[71] R.-S. Juang, R.-C. Shiau, Metal removal from aqueous solutions using chitosan-enhanced membrane filtration, J. Memb. Sci. 165 (2000) 159–167. doi:10.1016/S0376-7388(99)00235-5.

[72] Y. Huang, X. Zeng, L. Guo, J. Lan, L. Zhang, D. Cao, Heavy metal ion removal of wastewater by zeolite-imidazolate frameworks, Sep. Purif. Technol. 194 (2018) 462–469. doi:10.1016/j.seppur.2017.11.068.

[73] N. Wang, X.-K. Ouyang, L.-Y. Yang, A.M. Omer, Fabrication of a Magnetic Cellulose Nanocrystal/Metal-Organic Framework Composite for Removal of Pb (II) from Water, ACS Sustain. Chem. Eng. 5 (2017) 10447–10458. doi:10.1021/acssuschemeng.7b02472.

[74] N.D. Rudd, H. Wang, E.M.A. Fuentes-Fernandez, S.J. Teat, F. Chen, G. Hall, Y.J. Chabal, J. Li, Highly Efficient Luminescent Metal-Organic Framework for the Simultaneous Detection and Removal of Heavy Metals from Water, ACS Appl. Mater. Interfaces. 8 (2016) 30294–30303. doi:10.1021/acsami.6b10890.

[75] Y. Peng, H. Huang, Y. Zhang, C. Kang, S. Chen, L. Song, D. Liu, C. Zhong, A versatile MOF-based trap for heavy metal ion capture and dispersion, Nat. Commun. 9 (2018) 187. doi:10.1038/s41467-017-02600-2.

[76] N.N. Yin, K. Wang, L. Wang, Z. Li, Amino-functionalized MOFs combining ceramic membrane ultrafiltration for Pb (II) removal, Chem. Eng. J. 306 (2016) 619–628. doi:10.1016/j.cej.2016.07.064.

[77] J. Liu, C.A. Fernandez, P.F. Martin, P.K. Thallapally, D.M. Strachan, A two-column method for the separation of Kr and Xe from process off-gases, Ind. Eng. Chem. Res. 53 (2014) 12893–

12899. doi:10.1021/ie502156h.

[78] S. Herrmann, L. De Matteis, J.M.J.M. de la Fuente, S.G.S.G. Mitchell, C. Streb, L. De Matteis, J.M. de la Fuente, S.G.S.G. Mitchell, C. Streb, Removal of Multiple Contaminants from Water by Polyoxometalate Supported Ionic Liquid Phases (POM-SILPs), Angew. Chemie - Int. Ed. 56 (2017) 1667–1670. doi:10.1002/anie.201611072.

[79] A.M. Azzam, S.T. El-Wakeel, B.B. Mostafa, M.F. El-Shahat, Removal of Pb, Cd, Cu and Ni from aqueous solution using nano scale zero valent iron particles, J. Environ. Chem. Eng. 4 (2016) 2196–2206. doi:10.1016/j.jece.2016.03.048.

[80] C. Ding, W. Cheng, X. Wang, Z.-Y. Wu, Y. Sun, C. Chen, X. Wang, S.-H. Yu, Competitive sorption of Pb (II), Cu(II) and Ni(II) on carbonaceous nanofibers: A spectroscopic and modeling approach, J. Hazard. Mater. 313 (2016) 253–261. doi:10.1016/j.jhazmat.2016.04.002.

[81] L. Fang, L. Li, Z. Qu, H. Xu, J. Xu, N. Yan, A novel method for the sequential removal and separation of multiple heavy metals from wastewater, J. Hazard. Mater. 342 (2018) 617–624. doi:10.1016/j.jhazmat.2017.08.072.

[82] H. Jeong, W. Jang, J. Yun, H. Byun, Preparation of PVdF/GO nanofiber composite membranes and its heavy metal removal characteristics, Polym. 40 (2016) 489–497. doi:10.7317/pk.2016.40.3.489.

[83] S. Koushkbaghi, P. Jafari, J. Rabiei, M. Irani, M. Aliabadi, Fabrication of PET/PAN/GO/Fe3O4 nanofibrous membrane for the removal of Pb (II) and Cr(VI) ions, Chem. Eng. J. 301 (2016) 42–50. doi:10.1016/j.cej.2016.04.076.

[84] Q.L. Huang, Y. Huang, C.F. Xiao, Y.W. You, C.X. Zhang, Electrospun ultrafine fibrous PTFE-supported ZnO porous membrane with self-cleaning function for vacuum membrane distillation,

J. Memb. Sci. 534 (2017) 73–82. doi:10.1016/j.memsci.2017.04.015.

[85] Y. Wu, F. Li, H. Liu, W. Zhu, M. Teng, Y. Jiang, W. Li, D. Xu, D. He, P. Hannam, G. Li, Electrospun fibrous mats as skeletons to produce free-standing MOF membranes, J. Mater. Chem. 22 (2012) 16971. doi:10.1039/c2jm32570e.

[86] R. Ostermann, J. Cravillon, C. Weidmann, M. Wiebcke, B.M. Smarsly, Metal-organic framework nanofibers via electrospinning, Chem. Commun. 47 (2011). doi:10.1039/c0cc02271c.

[87] J.H. Doh, J.H. Kim, H.J. Kim, R.F. Ali, K. Shin, Y.J. Hong, Enhanced adsorption of aqueous copper(II) ions using dedoped poly-N-phenylglycine nanofibers, Chem. Eng. J. 277 (2015) 352–359. doi:10.1016/j.cej.2015.04.120.

[88] H. Chen, J. Lin, N. Zhang, L. Chen, S. Zhong, Y. Wang, W. Zhang, Q. Ling, Preparation of MgAl-EDTA-LDH based electrospun nanofiber membrane and its adsorption properties of copper(II) from wastewater, J. Hazard. Mater. 345 (2018) 1–9. doi:10.1016/j.jhazmat.2017.11.002.

[89] A.X. Lu, A.M. Ploskonka, T.M. Tovar, G.W. Peterson, J.B. Decoste, Direct Surface Growth of UIO-66-NH<inf>2</inf>on Polyacrylonitrile Nanofibers for Efficient Toxic Chemical Removal, Ind. Eng. Chem. Res. 56 (2017) 14502–14506. doi:10.1021/acs.iecr.7b04202.

[90] S. Egodawatte, K.E. Greenstein, I. Vance, E. Rivera, N.V. Myung, G.F. Parkin, D.M. Cwiertny, S.C. Larsen, Electrospun hematite nanofiber/mesoporous silica core/shell nanomaterials as an efficient adsorbent for heavy metals, RSC Adv. 6 (2016) 90516–90525. doi:10.1039/c6ra19876g.

[91] Z. Cai, J. Kim, M.M. Benjamin, NOM removal by adsorption and membrane filtration using heated aluminum oxide particles, Environ. Sci. Technol. 42 (2008) 619–623. doi:10.1021/es7021285.

[92] M. Bryjak, J. Wolska, I. Soroko, N. Kabay, Adsorption-membrane filtration process in boron

removal from first stage seawater RO permeate, Desalination. 241 (2009) 127–132. doi:10.1016/j.desal.2008.01.062.

[93] M. Abbasi, R.S. Mohammad, A. Salahi, B. Mirza, Modeling of membrane fouling and flux decline in microfiltration of oily wastewater using ceramic membranes, Chem. Eng. Commun. 199 (2012) 78–93. doi:10.1080/00986445.2011.570391.

[94] C. Aydiner, I. Demir, E. Yildiz, Modeling of flux decline in crossflow microfiltration using neural networks: The case of phosphate removal, J. Memb. Sci. 248 (2005) 53–62. doi:10.1016/j.memsci.2004.07.036.

[95] W. Zhang, X. Ruan, Y. Ma, X. Jiang, W. Zheng, Y. Liu, G. He, Modeling and simulation of mitigating membrane fouling under a baffle-filled turbulent flow with permeate boundary, Sep. Purif. Technol. 179 (2017) 13–24. doi:10.1016/j.seppur.2017.01.022.

[96] H. Li, H. Xia, Y. Mei, Modeling organic fouling of reverse osmosis membrane: From adsorption to fouling layer formation, Desalination. 386 (2016) 25–31. doi:10.1016/j.desal.2016.02.037.

[97] E.R. Gomes, A. Santos, S.A. Lima, Numerical Modeling of Straining: The Role of Particle and Pore Size Distributions, Transp. Porous Media. 120 (2017) 535–551. doi:10.1007/s11242-017-0939-4.

[98] J.M. Ochando-Pulido, A. Martínez-Ferez, Fouling modelling on a reverse osmosis membrane in the purification of pretreated olive mill wastewater by adapted crossflow blocking mechanisms, J. Memb. Sci. 544 (2017) 108–118. doi:10.1016/j.memsci.2017.09.018.

[99] W. Li, W. Xing, N. Xu, Modeling of relationship between water permeability and microstructure parameters of ceramic membranes, Desalination. 192 (2006) 340–345. doi:10.1016/j.desal.2005.07.042.

[100] N.K.K. Srivastava, C.B.B. Majumder, Novel biofiltration methods for the treatment of heavy metals from industrial wastewater, J. Hazard. Mater. 151 (2008) 1–8. doi:10.1016/j.jhazmat.2007.09.101.

[101] B.C. J. Jacobe, J.M.L. Lann, H. Pinguad, A generalized approach for dynamic modelling and simulation of biofilters, Chem. Eng. J.,. 65 (1997) 133–143.

[102] Y. Zhao, J.S. Taylor, S. Chellam, Predicting RO/NF water quality by modified solution diffusion model and artificial neural networks, J. Memb. Sci. 263 (2005) 38–46. doi:10.1016/j.memsci.2005.04.004.

[103] M.M. Tomadakis, T.J. Robertson, Viscous permeability of random fiber structures: Comparison of electrical and diffusional estimates with experimental and analytical results, J. Compos. Mater. 39 (2005) 163–188. doi:10.1177/0021998305046438.

[104] Fan Yang, J.. Efome, D. Rana, T. Matsuura, C. Lan, Metal–Organic Frameworks Supported on Nanofiber for Desalination by Direct Contact Membrane Distillation, ACS Appl. Mater. Interfaces. 10 (2018) 11251–11260.

[105] J.E. Efome, M. Baghbanzadeh, D. Rana, T. Matsuura, C.Q. Lan, Effects of superhydrophobic SiO2 nanoparticles on the performance of PVDF flat sheet membranes for vacuum membrane distillation, Desalination. 373 (2015) 47–57. doi:10.1016/j.desal.2015.07.002.

[106] M.A. Barakat, New trends in removing heavy metals from industrial wastewater, Arab. J. Chem. 4 (2011) 361–377. doi:10.1016/j.arabjc.2010.07.019.

[107] M. Ajmal, R.A.K. Rao, R. Ahmad, J. Ahmad, Adsorption studies on Citrus reticulata (fruit peel of orange): Removal and recovery of Ni(II) from electroplating wastewater, J. Hazard. Mater. 79 (2000) 117–131. doi:10.1016/S0304-3894(00)00234-X.

[108] M. Banerjee, R.K. Basu, S.K. Das, Cr(VI) adsorption by a green adsorbent walnut shell: Adsorption studies, regeneration studies, scale-up design and economic feasibility, Process Saf. Environ. Prot. 116 (2018) 693–702. doi:10.1016/j.psep.2018.03.037.

[109] S. Malamis, E. Katsou, A review on zinc and nickel adsorption on natural and modified zeolite, bentonite and vermiculite: Examination of process parameters, kinetics and isotherms, J. Hazard. Mater. 252–253 (2013) 428–461. doi:10.1016/j.jhazmat.2013.03.024.

[110] P.P. Prabhu, B. Prabhu, A Review on Removal of Heavy Metal Ions from Waste Water using Natural/ Modified Bentonite, in: MATEC Web Conf., 2018. doi:10.1051/matecconf/201714402021.

[111] S. Vafakhah, M.E. Bahrololoom, R. Bazarganlari, M. Saeedikhani, Removal of copper ions from electroplating effluent solutions with native corn cob and corn stalk and chemically modified corn stalk, J. Environ. Chem. Eng. 2 (2014) 356–361. doi:10.1016/j.jece.2014.01.005.

[112] C. Li, P. Champagne, Fixed-bed column study for the removal of cadmium (II) and nickel (II) ions from aqueous solutions using peat and mollusk shells, J. Hazard. Mater. 171 (2009) 872–878. doi:10.1016/j.jhazmat.2009.06.084.

[113] J.E. Efome, D. Rana, T. Matsuura, C.Q. Lan, Metal-organic frameworks supported on nanofibers to remove heavy metals, J. Mater. Chem. A. 6 (2018) 4550–4555. doi:10.1039/C7TA10428F.

[114] G. Zheng, H. Ye, Y. Zhang, H. Li, L. Lin, X. Ding, Removal of heavy metal in drinking water resource with cation-exchange resins (Type 110-H) mixed pes membrane adsorbents, J. Hazardous, Toxic, Radioact. Waste. 19 (2015). doi:10.1061/(ASCE)HZ.2153-5515.0000229.

[115] C.W. Abney, J.C. Gilhula, K. Lu, W. Lin, Metal-organic framework templated inorganic sorbents for rapid and effi cient extraction of heavy metals, Adv. Mater. 26 (2014) 7993–7996.

doi:10.1002/adma.201403428.

[116] N. Wang, T. Liu, H. Shen, S. Ji, J.-R. Li, R. Zhang, Ceramic tubular MOF hybrid membrane fabricated through in situ layer-by-layer self-assembly for nanofiltration, AIChE J. 62 (2016). doi:10.1002/aic.15115.

[117] Y. Zhang, N. Wang, S. Ji, R. Zhang, C. Zhao, J.-R. Li, Metal-organic framework/poly(vinyl alcohol) nanohybrid membrane for the pervaporation of toluene/n-heptane mixtures, J. Memb. Sci. 489 (2015). doi:10.1016/j.memsci.2015.04.012.

[118] X. Li, C. Zhang, R. Zhao, X. Lu, X. Xu, X. Jia, C. Wang, L. Li, Efficient adsorption of gold ions from aqueous systems with thioamide-group chelating nanofiber membranes, Chem. Eng. J. 229 (2013) 420–428. doi:10.1016/j.cej.2013.06.022.

[119] Q. Feng, D. Wu, Y. Zhao, A. Wei, Q. Wei, H. Fong, Electrospun AOPAN/RC blend nanofiber membrane for efficient removal of heavy metal ions from water, J. Hazard. Mater. 344 (2018) 819–828. doi:10.1016/j.jhazmat.2017.11.035.

[120] M.A. Barakat, E. Schmidt, Polymer-enhanced ultrafiltration process for heavy metals removal from industrial wastewater, Desalination. 256 (2010) 90–93. doi:10.1016/j.desal.2010.02.008.

[121] Z. Rao, K. Feng, B. Tang, P. Wu, Surface decoration of amino-functionalized metal-organic framework/graphene oxide composite onto polydopamine-coated membrane substrate for highly efficient heavy metal removal, ACS Appl. Mater. Interfaces. 9 (2017). doi:10.1021/acsami.6b15873.

[122] A.Y. Gebreyohannes, L. Giorno, I.F.J. Vankelecom, T. Verbiest, P. Aimar, Effect of operational parameters on the performance of a magnetic responsive biocatalytic membrane reactor, Chem. Eng. J. 308 (2017) 853–862. doi:10.1016/j.cej.2016.09.057.

[123] L. Eykens, I. Hitsov, K. De Sitter, C. Dotremont, L. Pinoy, I. Nopens, B. Van der Bruggen, Influence of membrane thickness and process conditions on direct contact membrane distillation at different salinities, J. Memb. Sci. 498 (2016) 353–364. doi:10.1016/J.MEMSCI.2015.07.037.

[124] S. Mondal, R. Mukherjee, S. De, Process modeling for the removal of phenolic compounds from industrial wastewater using a mixed-matrix membrane, Ind. Eng. Chem. Res. 54 (2015) 514–521. doi:10.1021/ie504358j.

[125] X.B. Ke, Z.F. Zheng, H.W. Liu, H.Y. Zhu, X.P. Gao, L.X. Zhang, N.P. Xu, H. Wang, H.J. Zhao, J. Shi, K.R. Ratinac, High-flux ceramic membranes with a nanomesh of metal oxide nanofibers, J. Phys. Chem. B. 112 (2008) 5000–5006. doi:10.1021/jp709837r.

[126] L.T. Choong, Z. Khan, G.C. Rutledge, Permeability of electrospun fiber mats under hydraulic flow, J. Memb. Sci. 451 (2014) 111–116. doi:10.1016/j.memsci.2013.09.051.

[127] T. Furukawa, K. Kokubo, K. Nakamura, K. Matsumoto, Modeling of the permeate flux decline during MF and UF cross-flow filtration of soy sauce lees, J. Memb. Sci. 322 (2008) 491–502. doi:10.1016/j.memsci.2008.05.068.

[128] D. Zedel, M. Kraume, A. Drews, Modelling and prediction of organic solvent flux and retention of surfactants by organic solvent nanofiltration, J. Memb. Sci. 544 (2017) 323–332. doi:10.1016/j.memsci.2017.09.041.

[129] S. Konishi, K. Saito, S. Furusaki, T. Sugo, Binary metal-ion sorption during permeation through chelating porous membranes, J. Memb. Sci. 111 (1996) 1–6. doi:10.1016/0376-7388(95)00237-5.

[130] Y. Shao, H. Chen, Y. Li, X. Ma, Fabrication of novel porous carbon membrane/sintered metal fibers composite for isopropanol adsorption, Chem. Eng. J. 276 (2015) 51–58.

doi:10.1016/j.cej.2015.04.080.

[131] X. Wang, Y. Li, H. Li, C. Yang, Chitosan membrane adsorber for low concentration copper ion removal, Carbohydr. Polym. 146 (2016) 274–281. doi:10.1016/j.carbpol.2016.03.055.

[132] K. Ohwada, On the pauling electronegativity scales-II, Polyhedron. 3 (1984) 853–859. doi:10.1016/S0277-5387(00)84634-3.

Chapter 6

Effects of operating parameters and co-existing ions on the efficiency of lead removal by Nano-fibrous MOF membrane filtration process

Johnson E. Efome, Dipak Rana, Takeshi Matsuura, Christopher Q. Lan*

Industrial Membrane Research Institute, Department of Chemical and Biochemical Engineering, University of Ottawa. 161 Louis Pasteur Ottawa ON Canada, K1N 6N5

This current chapter is a manuscript to be submitted to the Chemical Engineering Journal

Abstract:

The purification process of wastewater containing heavy metal ions like lead using nano-fibrous MOF808 embedded polyacrylonitrile (PAN) membrane has been studied and presented. A continuous flow cell was used for the filtration process at room temperature. The process parameters that were evaluated included feed concentration, transmembrane pressure (TMP), membrane thickness and the effect of co-existing cations in the solution. The concentration of the heavy metal ions in the permeate was determined using flame atomic absorption spectroscopy (FAAS). Experimental results indicate a substantial variation in the feed volume that the membrane can treat before the permeate lead concentration reaches the allowable limit of 10 ppb, depending on the process parameter. An increase in the membrane thickness showed the most significant improvement (25%) with 515 L h^{-1} of the treated feed volume after doubling the membrane layer. An increase in TMP could reduce the treated feed volume by 27% while a decrease in feed concentration led to a 12% increase in the treated feed volume. In the presence of other common background cations in the solution, the removal efficiency of lead ions by the adsorption onto MOF808 dropped by 18% in the presence of up to three other cations but was minimal in the presence of a single cation indicative of good selectivity.

6.1 Introduction

Heavy metal ions even at relatively low concentrations pose serious long-term health hazards to both the environment and public due to their non-biodegradability causing them to accumulate in the systems. With the rising water and air pollution resulting from population increase, it becomes paramount to develop and apply removal techniques to mitigate the effects of heavy metal accumulation. Various physical and chemical treatment processes have been used for treating wastewater and contaminated water. They may be as simple as pH changes[106] or they use a wide range of adsorbents from natural substances [68,107–112] to 3D complex materials[74–76,113–115]. The removal process involving most of these materials is usually governed by their surface area, electrostatic interaction and the level of exposure and contact with the contaminant in the feed. As such, the quantity of the material as a ratio of the contaminant in feed could be very large. Immobilization on substrates is a method that has been widely used to enhance adsorbent performance through increasing the effective surface area and reducing particle agglomeration. Substrates, although mostly polymeric, have ranged from flat sheet membranes[114], ceramic membranes[116,117] and nanofibrous membranes[118,119] and the performance of the materials has been debated compared to the non-immobilized state.

Practical applicability of these composite membranes has been tested in systems like ultrafiltration[120], nanofiltration [121]and others to determine their viability in removing heavy metal ions from wastewater and contaminated water. In these filtration processes, there are governing parameters that determine the performance of the process and they must be carefully evaluated and optimized to harness the maximum potential of the process. In the heavy metal removal processes, the quantity of the contaminant in feed that can be treated by the system is the point of centricity through which most of the systems are evaluated. To improve the efficiency of the treatment process, the underlying mechanism(s) and

principles must be understood, studied and optimized. In a typical filtration process, a porous membrane with or without fillers is used for a batch or continuous process to produce a permeate of better quality than the feed.

There are two mechanisms of contaminant removal by filtration using the adsorbent embedded membrane. When the membrane pores are smaller than contaminant species, separation based on size exclusion becomes the prevailing mechanism and usually there could be a cake formation causing a reduction in flux with time. On the other hand, when the membrane pores are larger than the contaminant, removal is controlled by the adsorption affinity of either the membrane surface or the adsorbents immobilized on the membrane. These two mechanisms may work separately or simultaneously.

As such, the rate of the contaminant removal is controlled by the factors which may include the filtration transmembrane pressure (TMP), the temperature of the process, the available surface area for adsorption, and the adsorption rate between adsorbent and adsorbate. These factors have been studied for various systems to optimize the filtration process to produce quality permeate[109,122–124].

We illustrate the effects of some main filtration parameters like TMP, feed contaminant concentration and membrane thickness on the volume of feed the system is capable of treating. The study is based on the filtration of lead (Pb^{2+} ions) from the aqueous medium. The removal efficiency of Pb^{2+} in preference to the other background cations commonly present in water was also studied. The membrane used in this study was developed in our previous work and comprised of a zirconium MOF (MOF 808) enmeshed in polyacrylonitrile nanofibers.

6.2 Experimental section

The MOF808 embedded nanofibrous membrane was fabricated based on our previous work [113].

$ZrCl_4$, DMF, PAN powder and H_3BTC were purchased from Sigma Aldrich, Formic acid from Alfar Aesar, PVDF was donated by Arkema Inc (Philadelphia). Typically, the MOF was prepared as follows: 0.699 g of $ZrCl_4$ and H_3BTC (0.210g) were dissolved in a mixture of DMF/Formic acid (45/45mL) in a 200-mL boiling flask. The flask was then transferred into a microwave and irradiated at 400 W for 30 min. The resulting suspension was filtered by centrifugation, washed with DMF three times (10 x 3) and dried at 100 ^oC for 12 h. The dried MOF (0.125g) was primed in 3 g of DMF then 0.5 g of PAN was added with the remainder of 2 g solvent to form a suspension with 20 wt. % MOF loading. The solution was placed in shaker for 24 h at 50^oC, degassed and electrospun on aluminium foil at 15-20 kV, 0.11-0.15 mm/min syringe feed rate, at room temperature and 40% humidity. The collected membranes were room dried to remove excess solvent then activated by washing in acetone then water followed by vacuum drying at 100^oC.

The filtration set up were also reported in our earlier communication (ref). It should be noted that the membrane used for the filtration experiment was comprised of the following two layers; the top PAN nanofibrous membrane with the embedded MOF808 and the bottom PVDF nanofibrous membrane. The top PAN/MOF808 membrane controls the heavy metal adsorption due to the presence of adsorbent MOF808 and the bottom PVDF membrane controls the flux due to its hydrophobic property. As such, the thickness of the membrane referred to here represents solely that of the PAN/MOF808 layer. The PVDF layer thickness was unchanged to maintain the constant permeation rate. The filtration experiments were carried out using a continuous filtration setup with a 7 L reservoir which was connected to a feed pump. A feed flow rate of 1.5 LPM was maintained. A specified volume of permeate was collected at predetermined time intervals and the permeate sample was subjected to the flame atomic

adsorption spectrophotometry (Thermo Scientific iCE 3000) to measure the heavy metal (lead) ion concentration. The conditions for the single lead ion filtration are summarized in Table 6-1.

The filtration protocol is the same in the presence of the co-existing ions, where the mixture of Na^{+}, Mg^{2+}, and Ca^{2+} (47.9, 49.3, 50.5 ppm respectively) was added to the feed solution. A single PAN/MOF808 membrane was used at 0.1 bar TMP.

The adsorption experiments were carried out following the protocol described thoroughly in the earlier report[113]. Briefly, lead nitrate solutions with 1 ppm of lead ion concentration was prepared without and with the addition of the coexisting ions, either individually or simultaneously. 20 mg of MOF808 was added to 30 mL of the prepared solution and after 3 h, the lead ion concentration was measured. The removal efficiency of lead ions was defined by equation 6-1.

$$\text{Removal efficiency} = 1 - \left\{\frac{Pb\ conc_{after\ adsorption}}{Pb\ conc_{initial}}\right\} \quad (6\text{-}1)$$

The membrane mechanical properties were obtained using the standard method ASTM D 882 with an Electropuls Intron E3000 equipment at room temperature and crosshead speed of 5 mm/min. The thickness and length of the membrane samples were 560 µm and 20-mm respectively with a width of 10-mm. Inhomogeneous samples were rejected and only stress-strain results from samples with breakage at least 2-mm from the edges were selected.

Table 6-1.Process operating parameters summary

Parameter	Value
Membrane thickness (single layer)	560±32 µm
Effective membrane area	$3.8x10^{-3}$ m^2
TMP	0.1 and 0.2 bar
Initial Pb^{2+} conc. (in lead nitrate)	50 ppb

6.3 Results and discussion

6.3.1 Effect of transmembrane pressure (TMP)

The effect of the applied TMP was investigated at a constant feed concentration of ~50 ppb using a single layer of PAN/MOF808 on the PVDF base layer at room temperature. Figure 6-1 shows typical breakthrough curves of the membrane filtration. During the initial lag period the lead ion concentration in the permeate is maintained nearly equal to zero due to the strong adsorption capacity of the PAN/MOF808 layer. After the lag period, the lead concentration starts to increase since the adsorption site is largely saturated with the lead ions. The figure shows that the lag period decreases with an increase in TMP. This is because the membrane flux increases with an increase in TMP according to the Darcy's equation[125,126] and the amount of lead ions that can be treated by the PAN/MOF808 layer is supplied to the membrane within a shorter period. At 0.1 bar, the membrane could treat 577.5 L (normalized per m^2 of membrane) of feed before the permeate lead concentration reached the maximum allowable concentration (MAC) of 10 ppb. This volume is called hereafter the "concentration effect volume". Upon

doubling the TMP to 0.2 bar, the concentration effect volume was reduced to 421 L (27% reduction). The decrease in contact time between the aqueous feed and MOF particles at the higher TMP may also account for the appearance of heavy metal ions earlier in the breakthrough curve as reported elsewhere [91]. This increase in pressure will not be sufficient to cause any mechanical deformations on the membrane since the membrane showed relatively high Young's modulus and stress at break values (Fig. 6-2)

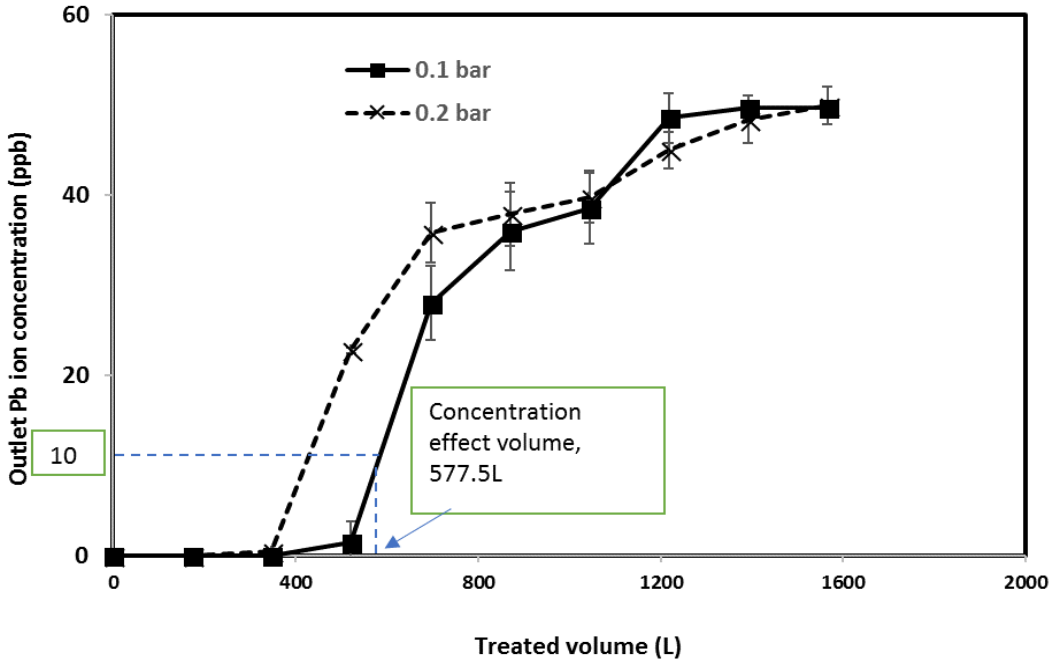

Figure 6-1. Effects of changes in TMP on the breakthrough curve

An increase in TMP also has the tendency to cause the membrane to suffer from compaction [127,128] which leads to a reduction in porosity. However, in the presence of the PAN/MOF808 layer on top of the flux controlling PVDF layer, the effect of compaction of PVDF layer on the permeate flux was minimized.

It is desirable to increase the flux to treat a large amount of contaminated water within a shorter period. Increasing the TMP is one way of increasing the flux and another way is to reduce the thickness of the flux controlling PVDF layer. In both ways, however, the concentration effect volume decreases, which results in the shorter interval between membrane regenerations. Hence, optimization of membrane thickness and operating pressure is necessary to find out the balance between these two opposing requirements.

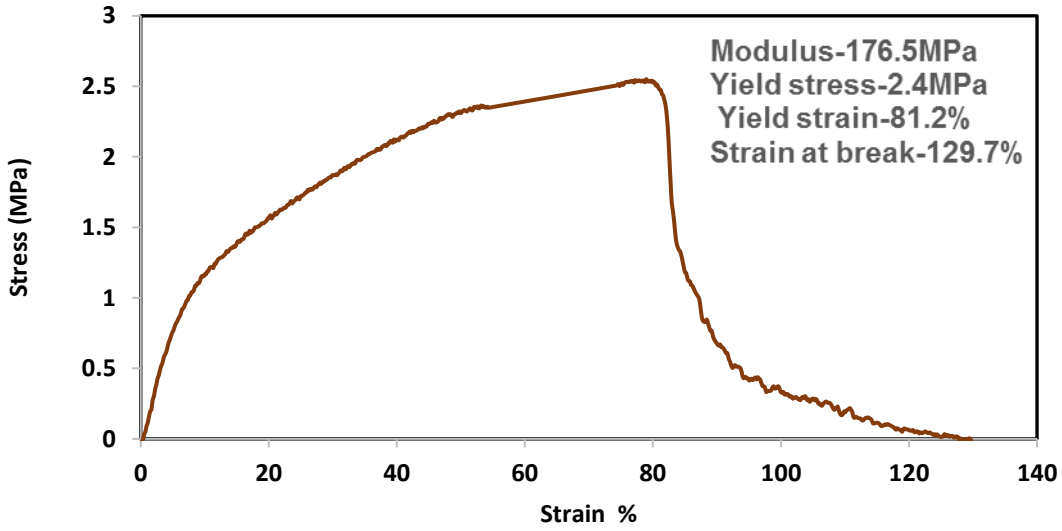

Figure 6-2. Mechanical property test of the filtration membrane.

6.3.2 Effect of feed concentration

In treatment centers, seasonal changes and the location of the treatment facility may affect the feed concentration of the wastewater or water to be treated. It is therefore important to understand the functionality of the membrane at varied feed concentrations in order to meet the treatment requirements. With the initial feed concentration of 50 ppb, Fig 6-3 shows that when the concentration is reduced by half, the membrane can treat more of the feed.

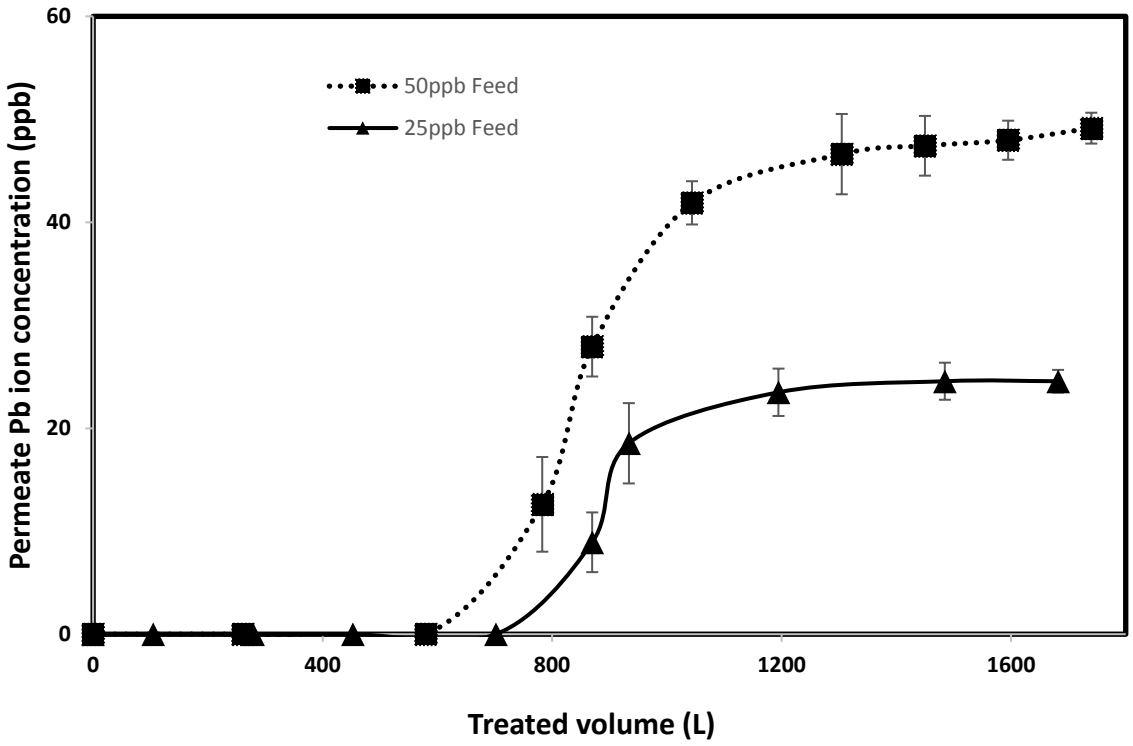

Figure 6-3. Effects of initial lead ion concentration in feed on the permeate lead ion concentration.

From the figure, at 50 ppb feed solution, the concentration effect volume of the single layered membrane was 641.1 L while it was 827.2 L when the concentration was reduced by 50%, representing about 29% increase. When the concentration reduces, the amount of heavy metal ions that come to contact with the PAN/MOF808 membrane also reduces, which delays the saturation of the adsorbent. The membrane was expected to treat more feed at half the original feed concentration but with just a 29% increase, it is most likely that some parts of the membrane might not be in full contact with the feed solution. This will imply that the adsorbent MOF particles were not completely used for adsorption.

6.3.3 Effect of membrane thickness

It must be noted that the change in membrane thickness investigated refers to the change in the PAN/MOF808 layer which, was varied from single to doubled layer with the PVDF layer thickness kept constant at all times. Increasing the membrane thickness is usually associated to increase in mass resistance which should reduce the flux at constant operating pressure [129–131]. However, as already mentioned, the flux does not change even when the PAN/MOF808 layer thickness is changed, since the PVDF layer is flux controlling. The effect of doubling the PAN/MOF808 layer thickness on the breakthrough curve is illustrated in Fig. 6-4.

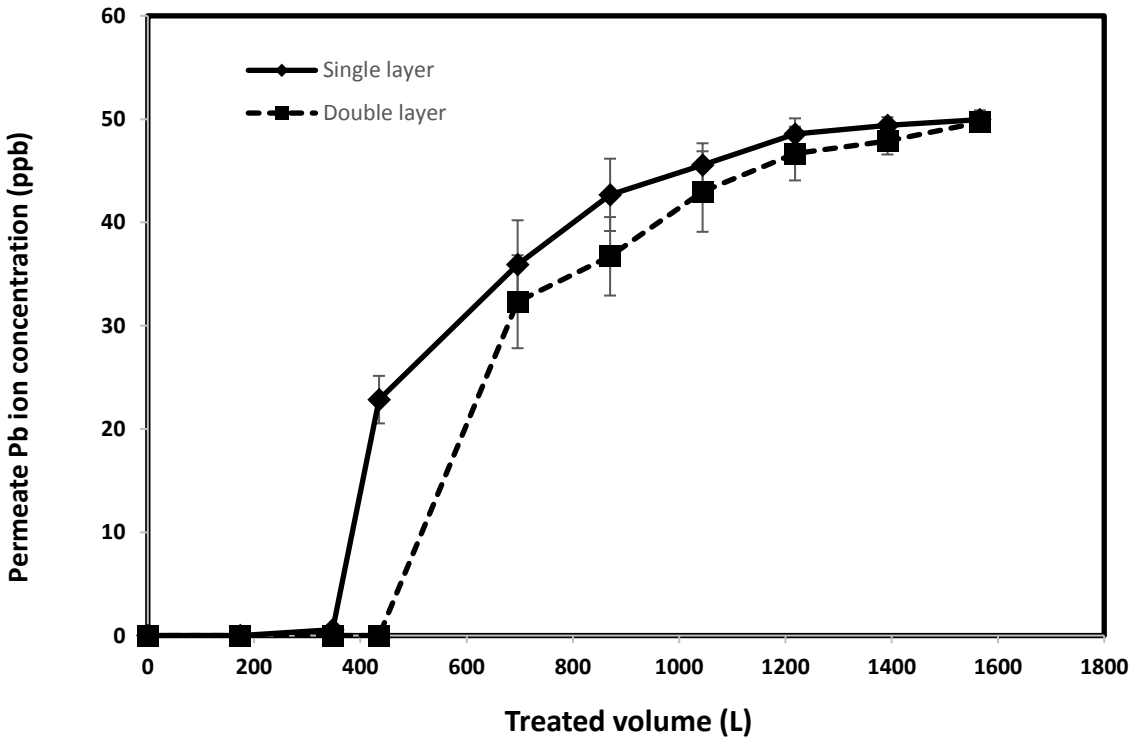

Figure 6-4. Effects of membrane thickness on the permeate lead ion concentration.

For a single layer membrane, 348.8 L of treated solution can be produced compared to 515.7 L for a double layer membrane corresponding to a 25% increase. Since it is estimated that every PAN layer contains approximately 20 wt.% MOF, doubling the PAN layer should correspond to a close to double the MOF quantity available for adsorption. With only a 25% increase, it is an indication that not all of the MOF particles were available for adsorption, a phenomenon earlier reported [113]. Not limiting to the availability of the MOF for adsorption, particle agglomeration in the nanofiber membrane could be another contributing factor in reducing the available adsorption sites for adsorption.

6.3.4 Effect of co-existing cations

The presence of other cations like Na^{+}, Mg^{2+}, K^{+}, Ca^{2+} in wastewater is inevitable and therefore their effect on the removal efficiency of the MOF808 for Pb^{++} ions was assessed and its PAN/MOF808 membrane also investigated for filtration using a feed containing background ions. As presented in Fig. 6-5, MOF808 retained its lead removal capabilities in the presence of other metal ions tested at varied concentrations of the background ions. The removal efficiency of the standalone MOF was decreased by 18% in the presence of all Na^{+}, Mg^{2+}, Ca^{2+} ions (presented in Fig. 6-5 as cocktail) but for a single ion, the efficiency was reduced by 20% in the presence of 50 ppm Mg^{2+} ions. The preferential adsorption of Pb^{2+} could be due to the higher electronegativity of Pb^{2+} ion than any of the co-existing ions (Pauling electronegativity χ Na^{+}(0.93), Mg^{2+}(1.31), Ca^{2+}(1.00), Pb^{2+}(1.8)[132]), which makes the electrostatic interaction between Pb^{2+} and the COO^{-} group in MOF the strongest.

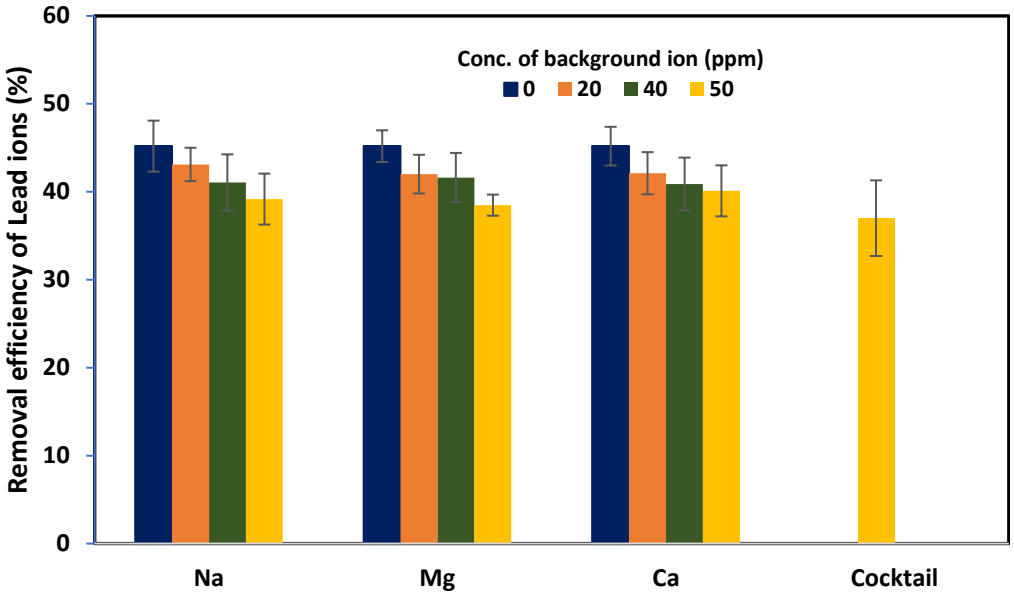

Figure 6-5. Effects of co-existing ions on the removal efficiency of lead ions by MOF808 particles. The cocktail solution comprised of all three background ions at approx. 50 ppm each.

As for the filtration experiment, the concentration effect volume was 485.6 L in the presence of all three co-existing ions. This represents 24% less compared to the concentration effect volume (641.1 L, see section 6.3.2) in the absence of co-existing ions. Co-existing ions compete with Pb^{++} ions for active sites on the MOF and though the affinity for Pb^{++} ions seem to be higher, the other ions are also bound to the active sites due to electrostatic drag that exists, thus reducing the capacity of the MOF in terms of Pb^{++} ion adsorption. This effect shows that the presence of co-existing ions can not be completely undermined and should be studied in detail to mitigate their effects and enhance the efficiency of the MOF material.

6.4 Conclusion

PAN/MOF808 nanofiber mat was prepared by co-electrospinning of MOF808 and PAN polymer and then used as adsorption filters for removal of Pb (II) ions to study the effect of the various process parameters. The volume of the feed treated before the lead ion concentration reached the maximum allowable limit in drinking water (10 ppb) was determined at different TMPs, membrane thicknesses, initial feed concentrations and in the presence and absence of co-existing ions. It was found that the lead adsorption capacity of MOF808 was reduced only moderately in the presence of other background ions. This slight reduction could be due to the preference of the MOF808 to lead ions or also because the active sites are different a phenomenon that could be studied in greater details.

It was also found that, reducing the initial feed concentration and lowing the TMP had the greatest impact in increasing of the treatable feed volume. Our work therefore provides a fundamental backbone in understanding and developing nanofibrous MOF membranes (NMOM) systems for processing of contaminated water. Ongoing work in our research will include the testing of the NMOM system for other complex contaminant solutions like nuclear processed water or processed water from the mining industry and for developing an in-depth understanding of the background ion effects.

Acknowledgement

This work was supported financially through the Natural Science and Engineering Council (NSERC) of Canada on a Strategic Partnership Grant (SPTGP) # 463039-2014.

Reference

[1] World Water Assessment Programme (WWAP), The United Nations World Water Development Report 2015: Water for a Sustainable World, Facts and Figures, UN Water Rep. (2015) 138. doi:10.1016/S1366-7017(02)00004-1.

[2] H.G. Gorchev, G. Ozolins, WHO guidelines for drinking-water quality., WHO Chron. 38 (2011) 104–108. doi:10.1016/S1462-0758(00)00006-6.

[3] K. Rajeshwar, Advanced Oxidation Processes for Water Treatment, J. Phys. Chem. Lett. 3 (2012) 2112–2113. doi:10.1021/jz200396h.

[4] K.C. Khulbe, C.Y. Feng, T. Matsuura, A.F. Ismail, Progresses in membrane and advanced oxidation processes for water treatment, Membr. Water Treat. 3 (2012). doi:10.12989/mwt.2012.3.3.181.

[5] J. Choi, A. Ide, Y.B. Truong, I.L. Kyratzis, R.A. Caruso, High surface area mesoporous titanium–zirconium oxide nanofibrous web: a heavy metal ion adsorbent, J. Mater. Chem. A. 1 (2013) 5847. doi:10.1039/c3ta00030c.

[6] F. Franco, M. Benítez-Guerrero, I. Gonzalez-Triviño, R. Pérez-Recuerda, C. Assiego, J. Cifuentes-Melchor, J. Pascual-Cosp, Low-cost aluminum and iron oxides supported on dioctahedral and trioctahedral smectites: A comparative study of the effectiveness on the heavy metal adsorption from water, Appl. Clay Sci. 119 (2016) 321–332. doi:10.1016/j.clay.2015.10.035.

[7] D.C. Manatunga, R.M. de Silva, K.M.N. de Silva, R. Ratnaweera, Natural polysaccharides leading to super adsorbent hydroxyapatite nanoparticles for the removal of heavy metals and dyes from aqueous solutions, RSC Adv. 6 (2016) 105618–105630. doi:10.1039/C6RA22662K.

[8] S.P. Mishra, V.K. Singh, Inorganic particulates in removal of toxic heavy metal ions VIII . Removal of zinc, cadmium and mercury ions from aqueous solution by hydrous titanium oxide, J. Radioanal. Nucl. Chem. 241 (1999) 341–346.

[9] S. Kalantari, M. Yousefpour, Z. Taherian, Synthesis of mesoporous silica/iron oxide nanocomposites and application of optimum sample as adsorbent in removal of heavy metals, Rare Met. 36 (2017) 942–950. doi:10.1007/s12598-016-0709-4.

[10] C. MAHAJAN, REMOVAL OF HEAVY METALS FROM WINERY WASTEWATER BY USING NATURAL ADSORBENTS., Int. …. 5 (2014) 69–78. http://search.ebscohost.com/login.aspx?direct=true&profile=ehost&scope=site&authtype=crawler&jrnl=2067533X&AN=95118774&h=guL3767S4V9fiSnoq6DVlXr4MqBmJNF96EbdJhHgWuszFOCbPqo7kKod3UXiNd94ULnSzKIPyFljXggUhyZ32Q%3D%3D&crl=c.

[11] C. Wang, X. Liu, N. Keser Demir, J.P. Chen, K. Li, Applications of water stable metal–organic frameworks, Chem. Soc. Rev. 45 (2016) 5107–5134. doi:10.1039/C6CS00362A.

[12] R. Ricco, K. Konstas, M.J. Styles, J.J. Richardson, R. Babarao, K. Suzuki, P. Scopece, P. Falcaro, Lead(II) uptake by aluminium based magnetic framework composites (MFCs) in water, J. Mater. Chem. A. 3 (2015) 19822–19831. doi:10.1039/C5TA04154F.

[13] I. Erucar, G. Yilmaz, S. Keskin, Recent advances in metal-organic framework-based mixed matrix membranes, in: Chem. - An Asian J., 2013: pp. 1692–1704. doi:10.1002/asia.201300084.

[14] V. V Butova, M.A. Soldatov, A.A. Guda, K.A. Lomachenko, C. Lamberti, Metal-organic frameworks: structure, properties, methods of synthesis and characterization, Russ. Chem. Rev. 85 (2016) 280–307. doi:10.1070/RCR4554.

[15] S. Qiu, M. Xue, G. Zhu, Metal–organic framework membranes: from synthesis to separation

application, Chem. Soc. Rev. 43 (2014) 6116–6140. doi:10.1039/C4CS00159A.

[16] N.A. Khan, S.H. Jhung, Synthesis of metal-organic frameworks (MOFs) with microwave or ultrasound: Rapid reaction, phase-selectivity, and size reduction, Coord. Chem. Rev. 285 (2015) 11–23. doi:10.1016/j.ccr.2014.10.008.

[17] Z.-J. Lin, Z. Yang, T.-F. Liu, Y.-B. Huang, R. Cao, Microwave-assisted synthesis of a series of lanthanide metal-organic frameworks and gas sorption properties., Inorg. Chem. 51 (2012) 1813–20. doi:10.1021/ic202082w.

[18] W. Liang, D.M. D'Alessandro, Microwave-assisted solvothermal synthesis of zirconium oxide based metal-organic frameworks., Chem. Commun. (Camb). 49 (2013) 3706–8. doi:10.1039/c3cc40368h.

[19] Z. Lin, D.S. Wragg, R.E. Morris, Microwave-assisted synthesis of anionic metal–organic frameworks under ionothermal conditions, Chem. Commun. (2006) 2021–2023. doi:10.1039/B600814C.

[20] R. Vakili, S. Xu, N. Al-Janabi, P. Gorgojo, S.M. Holmes, X. Fan, Microwave-assisted synthesis of zirconium-based metal organic frameworks (MOFs): Optimization and gas adsorption, Microporous Mesoporous Mater. 260 (2018) 45–53. doi:10.1016/j.micromeso.2017.10.028.

[21] M. Bechelany, M. Drobek, C. Vallicari, A. Abou Chaaya, A. Julbe, P. Miele, Highly crystalline MOF-based materials grown on electrospun nanofibers, Nanoscale. 7 (2015). doi:10.1039/c4nr06640e.

[22] U. Müller, H. Pütter, M. Hesse, H. Wessel, M. Schubert, Method for electrochemical production of a crystalline porous metal organic skeleton material, WO/2005/049892, 2005.

[23] M. Hartmann, S. Kunz, D. Himsl, O. Tangermann, S. Ernst, A. Wagener, Adsorptive separation

of isobutene and isobutane on Cu3(BTC)2, Langmuir. 24 (2008) 8634–8642. doi:10.1021/la8008656.

[24] G. Nickerl, A. Notzon, M. Heitbaum, I. Senkovska, F. Glorius, S. Kaskel, Selective Adsorption Properties of Cationic Metal–Organic Frameworks Based on Imidazolic Linker, Cryst. Growth Des. 13 (2013) 198–203. doi:10.1021/cg301347t.

[25] L. Xie, D. Liu, H. Huang, Q. Yang, C. Zhong, Efficient capture of nitrobenzene from waste water using metal-organic frameworks, Chem. Eng. J. 246 (2014) 142–149. doi:10.1016/j.cej.2014.02.070.

[26] Z. Hasan, E.J. Choi, S.H. Jhung, Adsorption of naproxen and clofibric acid over a metal–organic framework MIL-101 functionalized with acidic and basic groups, Chem. Eng. J. 219 (2013) 537–544. doi:10.1016/j.cej.2013.01.002.

[27] M. Tong, D. Liu, Q. Yang, S. Devautour-Vinot, G. Maurin, C. Zhong, Influence of framework metal ions on the dye capture behavior of MIL-100 (Fe, Cr) MOF type solids, J. Mater. Chem. A. 1 (2013) 8534. doi:10.1039/c3ta11807j.

[28] X.-X. Huang, L.-G. Qiu, W. Zhang, Y.-P. Yuan, X. Jiang, A.-J. Xie, Y.-H. Shen, J.-F. Zhu, Hierarchically mesostructured MIL-101 metal–organic frameworks: supramolecular template-directed synthesis and accelerated adsorption kinetics for dye removal, CrystEngComm. 14 (2012) 1613–1617. doi:10.1039/C1CE06138K.

[29] B.-J. Yao, W.-L. Jiang, Y. Dong, Z.-X. Liu, Y.-B. Dong, Post-Synthetic Polymerization of UiO-66-NH<inf>2</inf>Nanoparticles and Polyurethane Oligomer toward Stand-Alone Membranes for Dye Removal and Separation, Chem. - A Eur. J. 22 (2016). doi:10.1002/chem.201600817.

[30] Z. Hasan, S.H. Jhung, Removal of hazardous organics from water using metal-organic

frameworks (MOFs): Plausible mechanisms for selective adsorptions, J. Hazard. Mater. 283 (2015) 329–339. doi:10.1016/j.jhazmat.2014.09.046.

[31] H. Furukawa, F. Gándara, Y.-B. Zhang, J. Jiang, W.L. Queen, M.R. Hudson, O.M. Yaghi, Water adsorption in porous metal-organic frameworks and related materials., J. Am. Chem. Soc. 136 (2014) 4369–81. doi:10.1021/ja500330a.

[32] J.J. Low, A.I. Benin, P. Jakubczak, J.F. Abrahamian, S.A. Faheem, R.R. Willis, Virtual high throughput screening confirmed experimentally: Porous coordination polymer hydration, J. Am. Chem. Soc. 131 (2009) 15834–15842. doi:10.1021/ja9061344.

[33] N.U. Qadir, S.A.M. Said, H.M. Bahaidarah, Structural stability of metal organic frameworks in aqueous media - Controlling factors and methods to improve hydrostability and hydrothermal cyclic stability, Microporous Mesoporous Mater. 201 (2015) 61–90. doi:10.1016/j.micromeso.2014.09.034.

[34] T. Loiseau, C. Serre, C. Huguenard, G. Fink, F. Taulelle, M. Henry, T. Bataille, G. Férey, A Rationale for the Large Breathing of the Porous Aluminum Terephthalate (MIL-53) Upon Hydration, Chem. - A Eur. J. 10 (2004) 1373–1382. doi:10.1002/chem.200305413.

[35] J.H. Cavka, S. Jakobsen, U. Olsbye, N. Guillou, C. Lamberti, S. Bordiga, K.P. Lillerud, A new zirconium inorganic building brick forming metal organic frameworks with exceptional stability, J. Am. Chem. Soc. 130 (2008) 13850–13851. doi:10.1021/ja8057953.

[36] H.K. Chae, J. Kim, O.D. Friedrichs, M. O'Keeffe, O.M. Yaghi, Design of frameworks with mixed triangular and octahedral building blocks exemplified by the structure of [Zn4O(TCA)2] having the pyrite topology, Angew. Chemie - Int. Ed. 42 (2003) 3907–3909. doi:10.1002/anie.200351546.

[37] X. Liu, N.K. Demir, Z. Wu, K. Li, Highly Water-Stable Zirconium Metal-Organic Framework UiO-66 Membranes Supported on Alumina Hollow Fibers for Desalination, J. Am. Chem. Soc. 137 (2015) 6999–7002. doi:10.1021/jacs.5b02276.

[38] K. Tan, N. Nijem, P. Canepa, Q. Gong, J. Li, T. Thonhauser, Y.J. Chabal, Stability and hydrolyzation of metal organic frameworks with paddle-wheel SBUs upon hydration, Chem. Mater. 24 (2012) 3153–3167. doi:10.1021/cm301427w.

[39] M. Haouas, C. Volkringer, T. Loiseau, G. Férey, F. Taulelle, The extra-framework sub-lattice of the metal-organic framework MIL-110: A solid-state NMR investigation, Chem. - A Eur. J. 15 (2009) 3139–3146. doi:10.1002/chem.200801856.

[40] J.-Y. Lee, C.Y. Tang, F. Huo, Fabrication of Porous Matrix Membrane (PMM) Using Metal-Organic Framework as Green Template for Water Treatment, Sci. Rep. 4 (2015) 3740. doi:10.1038/srep03740.

[41] J. Duan, Y. Pan, F. Pacheco, E. Litwiller, Z. Lai, I. Pinnau, High-performance polyamide thin-film-nanocomposite reverse osmosis membranes containing hydrophobic zeolitic imidazolate framework-8, J. Memb. Sci. 476 (2015) 303–310. doi:10.1016/j.memsci.2014.11.038.

[42] R. Zhang, S. Ji, N. Wang, L. Wang, G. Zhang, J.-R.J.R. Li, Coordination-driven in situ self-assembly strategy for the preparation of metal-organic framework hybrid membranes, Angew. Chemie - Int. Ed. 53 (2014) 9775–9779. doi:10.1002/anie.201403978.

[43] H. Fan, Q. Shi, H. Yan, S. Ji, J. Dong, G. Zhang, Simultaneous spray self-assembly of highly loaded ZIF-8-PDMS nanohybrid membranes exhibiting exceptionally high biobutanol-permselective pervaporation, Angew. Chemie - Int. Ed. 53 (2014) 5578–5582. doi:10.1002/anie.201309534.

[44] G. Zhang, J. Li, N. Wang, H. Fan, R. Zhang, G. Zhang, S. Ji, Enhanced flux of polydimethylsiloxane membrane for ethanol permselective pervaporation via incorporation of MIL-53 particles, J. Memb. Sci. 492 (2015) 322–330. doi:10.1016/j.memsci.2015.05.070.

[45] Y. Zhang, N. Wang, S. Ji, R. Zhang, C. Zhao, J.R. Li, Metal-organic framework/poly(vinyl alcohol) nanohybrid membrane for the pervaporation of toluene/n-heptane mixtures, J. Memb. Sci. 489 (2015) 144–152. doi:10.1016/j.memsci.2015.04.012.

[46] X. Liu, H. Jin, Y. Li, H. Bux, Z. Hu, Y. Ban, W. Yang, Metal-organic framework ZIF-8 nanocomposite membrane for efficient recovery of furfural via pervaporation and vapor permeation, J. Memb. Sci. 428 (2013) 498–506. doi:10.1016/j.memsci.2012.10.028.

[47] D. Li, Y. Xia, Electrospinning of nanofibers: Reinventing the wheel?, Adv. Mater. 16 (2004) 1151–1170. doi:10.1002/adma.200400719.

[48] S. Agarwal, S. Jiang, Nanofibers and Electrospinning, in: Encycl. Polym. Nanomater., 2015: p. 1323.

[49] W. Teo, Introduction to Electrospinning Parameters and Fiber Control, Introd. to Electrospinning Parameters Fiber Control. (2015) 25–28. http://electrospintech.com/solution.html#.Ve7THhFVikp.

[50] N. Rosman, W.N.W. Salleh, M.A. Mohamed, N.H. Ismail, N. Sazali, J. Jaafar, H. Hasbullah, Electrospun nanofiber-coated membrane: A review, J. Teknol. 78 (2016) 83–88. doi:10.11113/jt.v78.10071.

[51] T.J. Sill, H.A. von Recum, Electrospinning: Applications in drug delivery and tissue engineering, Biomaterials. 29 (2008) 1989–2006. doi:10.1016/j.biomaterials.2008.01.011.

[52] Y.C. Woo, L.D. Tijing, M.J. Park, M. Yao, J.S. Choi, S. Lee, S.H. Kim, K.J. An, H.K. Shon,

Electrospun dual-layer nonwoven membrane for desalination by air gap membrane distillation, Desalination. 403 (2017) 187–198. doi:10.1016/j.desal.2015.09.009.

[53] Y. Tian, M. Wu, R. Liu, Y. Li, D. Wang, J. Tan, R. Wu, Y. Huang, Electrospun membrane of cellulose acetate for heavy metal ion adsorption in water treatment, Carbohydr. Polym. 83 (2011) 743–748. doi:10.1016/j.carbpol.2010.08.054.

[54] X. Hu, S. Liu, G. Zhou, Y. Huang, Z. Xie, X. Jing, Electrospinning of polymeric nanofibers for drug delivery applications, J. Control. Release. 185 (2014) 12–21. doi:10.1016/j.jconrel.2014.04.018.

[55] O.K. Pereao, C. Bode-Aluko, G. Ndayambaje, O. Fatoba, L.F. Petrik, Electrospinning: Polymer Nanofibre Adsorbent Applications for Metal Ion Removal, J. Polym. Environ. 25 (2017) 1175–1189. doi:10.1007/s10924-016-0896-y.

[56] F.E. Ahmed, B.S. Lalia, R. Hashaikeh, A review on electrospinning for membrane fabrication: Challenges and applications, Desalination. 356 (2015) 15–30. doi:10.1016/j.desal.2014.09.033.

[57] R. Dersch, A. Greiner, J.H. Wendorff, Polymer nanofibers by electrospinning, Dekker Encycl. Nanosci. Nanotechnol. 8 (2004) 64–75. doi:10.1016/S1359-0294Ž03.00004-9.

[58] J.. Deitzel, J. Kleinmeyer, D. Harris, N.. Beck Tan, The effect of processing variables on the morphology of electrospun nanofibers and textiles, Polymer (Guildf). 42 (2001) 261–272. doi:10.1016/S0032-3861(00)00250-0.

[59] R. Khajavi, M. Abbasipour, Controlling nanofiber morphology by the electrospinning process, in: Electrospun Nanofibers, 2016: pp. 109–123. doi:10.1016/B978-0-08-100907-9.00005-2.

[60] J. Doshi, D.H. Reneker, Electrospinning process and applications of electrospun fibers, J. Electrostat. 35 (1995) 151–160. doi:10.1016/0304-3886(95)00041-8.

[61] Y.Z. Zhang, Y. Feng, Z.M. Huang, S. Ramakrishna, C.T. Lim, Fabrication of porous electrospun nanofibres, Nanotechnology. 17 (2006) 901–908. doi:10.1088/0957-4484/17/3/047.

[62] J.E. Efome, D. Rana, T. Matsuura, C.Q. Lan, Enhanced performance of PVDF nanocomposite membrane by nanofiber coating: A membrane for sustainable desalination through MD, Water Res. 89 (2016) 39–49. doi:10.1016/j.watres.2015.11.040.

[63] J.E.. Efome, D. Rana, T. Matsuura, C.Q. Lan, Metal–organic frameworks supported on nanofibers to remove heavy metals, J. Mater. Chem. A. 6 (2018) 4550–4555. doi:10.1039/c7ta10428f.

[64] S. Megelski, J.S. Stephens, D. Bruce Chase, J.F. Rabolt, Micro- and nanostructured surface morphology on electrospun polymer fibers, Macromolecules. 35 (2002) 8456–8466. doi:10.1021/ma020444a.

[65] S.L. James, Metal-organic frameworks, Chem. Soc. Rev. 32 (2003) 276. doi:10.1039/b200393g.

[66] F. Fu, Q. Wang, Removal of heavy metal ions from wastewaters: A review, J. Environ. Manage. 92 (2011) 407–418. doi:10.1016/j.jenvman.2010.11.011.

[67] M. Hua, S. Zhang, B. Pan, W. Zhang, L. Lv, Q. Zhang, Heavy metal removal from water/wastewater by nanosized metal oxides: A review, J. Hazard. Mater. 211–212 (2012) 317–331. doi:10.1016/j.jhazmat.2011.10.016.

[68] S. Wang, Y. Peng, Natural zeolites as effective adsorbents in water and wastewater treatment, Chem. Eng. J. 156 (2010) 11–24. doi:10.1016/j.cej.2009.10.029.

[69] N. Bleiman, Y.G. Mishael, Selenium removal from drinking water by adsorption to chitosan-clay composites and oxides: Batch and columns tests, J. Hazard. Mater. 183 (2010) 590–595. doi:10.1016/j.jhazmat.2010.07.065.

[70] Y. Yurekli, Removal of heavy metals in wastewater by using zeolite nano-particles impregnated

polysulfone membranes, J. Hazard. Mater. 309 (2016) 53–64. doi:10.1016/j.jhazmat.2016.01.064.

[71] R.-S. Juang, R.-C. Shiau, Metal removal from aqueous solutions using chitosan-enhanced membrane filtration, J. Memb. Sci. 165 (2000) 159–167. doi:10.1016/S0376-7388(99)00235-5.

[72] Y. Huang, X. Zeng, L. Guo, J. Lan, L. Zhang, D. Cao, Heavy metal ion removal of wastewater by zeolite-imidazolate frameworks, Sep. Purif. Technol. 194 (2018) 462–469. doi:10.1016/j.seppur.2017.11.068.

[73] N. Wang, X.-K. Ouyang, L.-Y. Yang, A.M. Omer, Fabrication of a Magnetic Cellulose Nanocrystal/Metal-Organic Framework Composite for Removal of Pb (II) from Water, ACS Sustain. Chem. Eng. 5 (2017) 10447–10458. doi:10.1021/acssuschemeng.7b02472.

[74] N.D. Rudd, H. Wang, E.M.A. Fuentes-Fernandez, S.J. Teat, F. Chen, G. Hall, Y.J. Chabal, J. Li, Highly Efficient Luminescent Metal-Organic Framework for the Simultaneous Detection and Removal of Heavy Metals from Water, ACS Appl. Mater. Interfaces. 8 (2016) 30294–30303. doi:10.1021/acsami.6b10890.

[75] Y. Peng, H. Huang, Y. Zhang, C. Kang, S. Chen, L. Song, D. Liu, C. Zhong, A versatile MOF-based trap for heavy metal ion capture and dispersion, Nat. Commun. 9 (2018) 187. doi:10.1038/s41467-017-02600-2.

[76] N.N. Yin, K. Wang, L. Wang, Z. Li, Amino-functionalized MOFs combining ceramic membrane ultrafiltration for Pb (II) removal, Chem. Eng. J. 306 (2016) 619–628. doi:10.1016/j.cej.2016.07.064.

[77] J. Liu, C.A. Fernandez, P.F. Martin, P.K. Thallapally, D.M. Strachan, A two-column method for the separation of Kr and Xe from process off-gases, Ind. Eng. Chem. Res. 53 (2014) 12893–12899. doi:10.1021/ie502156h.

[78] S. Herrmann, L. De Matteis, J.M.J.M. de la Fuente, S.G.S.G. Mitchell, C. Streb, L. De Matteis, J.M. de la Fuente, S.G.S.G. Mitchell, C. Streb, Removal of Multiple Contaminants from Water by Polyoxometalate Supported Ionic Liquid Phases (POM-SILPs), Angew. Chemie - Int. Ed. 56 (2017) 1667–1670. doi:10.1002/anie.201611072.

[79] A.M. Azzam, S.T. El-Wakeel, B.B. Mostafa, M.F. El-Shahat, Removal of Pb, Cd, Cu and Ni from aqueous solution using nano scale zero valent iron particles, J. Environ. Chem. Eng. 4 (2016) 2196–2206. doi:10.1016/j.jece.2016.03.048.

[80] C. Ding, W. Cheng, X. Wang, Z.-Y. Wu, Y. Sun, C. Chen, X. Wang, S.-H. Yu, Competitive sorption of Pb (II), Cu(II) and Ni(II) on carbonaceous nanofibers: A spectroscopic and modeling approach, J. Hazard. Mater. 313 (2016) 253–261. doi:10.1016/j.jhazmat.2016.04.002.

[81] L. Fang, L. Li, Z. Qu, H. Xu, J. Xu, N. Yan, A novel method for the sequential removal and separation of multiple heavy metals from wastewater, J. Hazard. Mater. 342 (2018) 617–624. doi:10.1016/j.jhazmat.2017.08.072.

[82] H. Jeong, W. Jang, J. Yun, H. Byun, Preparation of PVdF/GO nanofiber composite membranes and its heavy metal removal characteristics, Polym. 40 (2016) 489–497. doi:10.7317/pk.2016.40.3.489.

[83] S. Koushkbaghi, P. Jafari, J. Rabiei, M. Irani, M. Aliabadi, Fabrication of PET/PAN/GO/Fe3O4 nanofibrous membrane for the removal of Pb (II) and Cr(VI) ions, Chem. Eng. J. 301 (2016) 42–50. doi:10.1016/j.cej.2016.04.076.

[84] Q.L. Huang, Y. Huang, C.F. Xiao, Y.W. You, C.X. Zhang, Electrospun ultrafine fibrous PTFE-supported ZnO porous membrane with self-cleaning function for vacuum membrane distillation, J. Memb. Sci. 534 (2017) 73–82. doi:10.1016/j.memsci.2017.04.015.

[85] Y. Wu, F. Li, H. Liu, W. Zhu, M. Teng, Y. Jiang, W. Li, D. Xu, D. He, P. Hannam, G. Li, Electrospun fibrous mats as skeletons to produce free-standing MOF membranes, J. Mater. Chem. 22 (2012) 16971. doi:10.1039/c2jm32570e.

[86] R. Ostermann, J. Cravillon, C. Weidmann, M. Wiebcke, B.M. Smarsly, Metal-organic framework nanofibers via electrospinning, Chem. Commun. 47 (2011). doi:10.1039/c0cc02271c.

[87] J.H. Doh, J.H. Kim, H.J. Kim, R.F. Ali, K. Shin, Y.J. Hong, Enhanced adsorption of aqueous copper(II) ions using dedoped poly-N-phenylglycine nanofibers, Chem. Eng. J. 277 (2015) 352–359. doi:10.1016/j.cej.2015.04.120.

[88] H. Chen, J. Lin, N. Zhang, L. Chen, S. Zhong, Y. Wang, W. Zhang, Q. Ling, Preparation of MgAl-EDTA-LDH based electrospun nanofiber membrane and its adsorption properties of copper(II) from wastewater, J. Hazard. Mater. 345 (2018) 1–9. doi:10.1016/j.jhazmat.2017.11.002.

[89] A.X. Lu, A.M. Ploskonka, T.M. Tovar, G.W. Peterson, J.B. Decoste, Direct Surface Growth of UIO-66-NH<inf>2</inf>on Polyacrylonitrile Nanofibers for Efficient Toxic Chemical Removal, Ind. Eng. Chem. Res. 56 (2017) 14502–14506. doi:10.1021/acs.iecr.7b04202.

[90] S. Egodawatte, K.E. Greenstein, I. Vance, E. Rivera, N.V. Myung, G.F. Parkin, D.M. Cwiertny, S.C. Larsen, Electrospun hematite nanofiber/mesoporous silica core/shell nanomaterials as an efficient adsorbent for heavy metals, RSC Adv. 6 (2016) 90516–90525. doi:10.1039/c6ra19876g.

[91] Z. Cai, J. Kim, M.M. Benjamin, NOM removal by adsorption and membrane filtration using heated aluminum oxide particles, Environ. Sci. Technol. 42 (2008) 619–623. doi:10.1021/es7021285.

[92] M. Bryjak, J. Wolska, I. Soroko, N. Kabay, Adsorption-membrane filtration process in boron removal from first stage seawater RO permeate, Desalination. 241 (2009) 127–132.

doi:10.1016/j.desal.2008.01.062.

[93] M. Abbasi, R.S. Mohammad, A. Salahi, B. Mirza, Modeling of membrane fouling and flux decline in microfiltration of oily wastewater using ceramic membranes, Chem. Eng. Commun. 199 (2012) 78–93. doi:10.1080/00986445.2011.570391.

[94] C. Aydiner, I. Demir, E. Yildiz, Modeling of flux decline in crossflow microfiltration using neural networks: The case of phosphate removal, J. Memb. Sci. 248 (2005) 53–62. doi:10.1016/j.memsci.2004.07.036.

[95] W. Zhang, X. Ruan, Y. Ma, X. Jiang, W. Zheng, Y. Liu, G. He, Modeling and simulation of mitigating membrane fouling under a baffle-filled turbulent flow with permeate boundary, Sep. Purif. Technol. 179 (2017) 13–24. doi:10.1016/j.seppur.2017.01.022.

[96] H. Li, H. Xia, Y. Mei, Modeling organic fouling of reverse osmosis membrane: From adsorption to fouling layer formation, Desalination. 386 (2016) 25–31. doi:10.1016/j.desal.2016.02.037.

[97] E.R. Gomes, A. Santos, S.A. Lima, Numerical Modeling of Straining: The Role of Particle and Pore Size Distributions, Transp. Porous Media. 120 (2017) 535–551. doi:10.1007/s11242-017-0939-4.

[98] J.M. Ochando-Pulido, A. Martínez-Ferez, Fouling modelling on a reverse osmosis membrane in the purification of pretreated olive mill wastewater by adapted crossflow blocking mechanisms, J. Memb. Sci. 544 (2017) 108–118. doi:10.1016/j.memsci.2017.09.018.

[99] W. Li, W. Xing, N. Xu, Modeling of relationship between water permeability and microstructure parameters of ceramic membranes, Desalination. 192 (2006) 340–345. doi:10.1016/j.desal.2005.07.042.

[100] N.K.K. Srivastava, C.B.B. Majumder, Novel biofiltration methods for the treatment of heavy

metals from industrial wastewater, J. Hazard. Mater. 151 (2008) 1–8. doi:10.1016/j.jhazmat.2007.09.101.

[101] B.C. J. Jacobe, J.M.L. Lann, H. Pinguad, A generalized approach for dynamic modelling and simulation of biofilters, Chem. Eng. J.,. 65 (1997) 133–143.

[102] Y. Zhao, J.S. Taylor, S. Chellam, Predicting RO/NF water quality by modified solution diffusion model and artificial neural networks, J. Memb. Sci. 263 (2005) 38–46. doi:10.1016/j.memsci.2005.04.004.

[103] M.M. Tomadakis, T.J. Robertson, Viscous permeability of random fiber structures: Comparison of electrical and diffusional estimates with experimental and analytical results, J. Compos. Mater. 39 (2005) 163–188. doi:10.1177/0021998305046438.

[104] Fan Yang, J.. Efome, D. Rana, T. Matsuura, C. Lan, Metal–Organic Frameworks Supported on Nanofiber for Desalination by Direct Contact Membrane Distillation, ACS Appl. Mater. Interfaces. 10 (2018) 11251–11260.

[105] J.E. Efome, M. Baghbanzadeh, D. Rana, T. Matsuura, C.Q. Lan, Effects of superhydrophobic SiO2 nanoparticles on the performance of PVDF flat sheet membranes for vacuum membrane distillation, Desalination. 373 (2015) 47–57. doi:10.1016/j.desal.2015.07.002.

[106] M.A. Barakat, New trends in removing heavy metals from industrial wastewater, Arab. J. Chem. 4 (2011) 361–377. doi:10.1016/j.arabjc.2010.07.019.

[107] M. Ajmal, R.A.K. Rao, R. Ahmad, J. Ahmad, Adsorption studies on Citrus reticulata (fruit peel of orange): Removal and recovery of Ni(II) from electroplating wastewater, J. Hazard. Mater. 79 (2000) 117–131. doi:10.1016/S0304-3894(00)00234-X.

[108] M. Banerjee, R.K. Basu, S.K. Das, Cr(VI) adsorption by a green adsorbent walnut shell:

Adsorption studies, regeneration studies, scale-up design and economic feasibility, Process Saf. Environ. Prot. 116 (2018) 693–702. doi:10.1016/j.psep.2018.03.037.

[109] S. Malamis, E. Katsou, A review on zinc and nickel adsorption on natural and modified zeolite, bentonite and vermiculite: Examination of process parameters, kinetics and isotherms, J. Hazard. Mater. 252–253 (2013) 428–461. doi:10.1016/j.jhazmat.2013.03.024.

[110] P.P. Prabhu, B. Prabhu, A Review on Removal of Heavy Metal Ions from Waste Water using Natural/ Modified Bentonite, in: MATEC Web Conf., 2018. doi:10.1051/matecconf/201714402021.

[111] S. Vafakhah, M.E. Bahrololoom, R. Bazarganlari, M. Saeedikhani, Removal of copper ions from electroplating effluent solutions with native corn cob and corn stalk and chemically modified corn stalk, J. Environ. Chem. Eng. 2 (2014) 356–361. doi:10.1016/j.jece.2014.01.005.

[112] C. Li, P. Champagne, Fixed-bed column study for the removal of cadmium (II) and nickel (II) ions from aqueous solutions using peat and mollusk shells, J. Hazard. Mater. 171 (2009) 872–878. doi:10.1016/j.jhazmat.2009.06.084.

[113] J.E. Efome, D. Rana, T. Matsuura, C.Q. Lan, Metal-organic frameworks supported on nanofibers to remove heavy metals, J. Mater. Chem. A. 6 (2018) 4550–4555. doi:10.1039/C7TA10428F.

[114] G. Zheng, H. Ye, Y. Zhang, H. Li, L. Lin, X. Ding, Removal of heavy metal in drinking water resource with cation-exchange resins (Type 110-H) mixed pes membrane adsorbents, J. Hazardous, Toxic, Radioact. Waste. 19 (2015). doi:10.1061/(ASCE)HZ.2153-5515.0000229.

[115] C.W. Abney, J.C. Gilhula, K. Lu, W. Lin, Metal-organic framework templated inorganic sorbents for rapid and effi cient extraction of heavy metals, Adv. Mater. 26 (2014) 7993–7996. doi:10.1002/adma.201403428.

[116] N. Wang, T. Liu, H. Shen, S. Ji, J.-R. Li, R. Zhang, Ceramic tubular MOF hybrid membrane fabricated through in situ layer-by-layer self-assembly for nanofiltration, AIChE J. 62 (2016). doi:10.1002/aic.15115.

[117] Y. Zhang, N. Wang, S. Ji, R. Zhang, C. Zhao, J.-R. Li, Metal-organic framework/poly(vinyl alcohol) nanohybrid membrane for the pervaporation of toluene/n-heptane mixtures, J. Memb. Sci. 489 (2015). doi:10.1016/j.memsci.2015.04.012.

[118] X. Li, C. Zhang, R. Zhao, X. Lu, X. Xu, X. Jia, C. Wang, L. Li, Efficient adsorption of gold ions from aqueous systems with thioamide-group chelating nanofiber membranes, Chem. Eng. J. 229 (2013) 420–428. doi:10.1016/j.cej.2013.06.022.

[119] Q. Feng, D. Wu, Y. Zhao, A. Wei, Q. Wei, H. Fong, Electrospun AOPAN/RC blend nanofiber membrane for efficient removal of heavy metal ions from water, J. Hazard. Mater. 344 (2018) 819–828. doi:10.1016/j.jhazmat.2017.11.035.

[120] M.A. Barakat, E. Schmidt, Polymer-enhanced ultrafiltration process for heavy metals removal from industrial wastewater, Desalination. 256 (2010) 90–93. doi:10.1016/j.desal.2010.02.008.

[121] Z. Rao, K. Feng, B. Tang, P. Wu, Surface decoration of amino-functionalized metal-organic framework/graphene oxide composite onto polydopamine-coated membrane substrate for highly efficient heavy metal removal, ACS Appl. Mater. Interfaces. 9 (2017). doi:10.1021/acsami.6b15873.

[122] A.Y. Gebreyohannes, L. Giorno, I.F.J. Vankelecom, T. Verbiest, P. Aimar, Effect of operational parameters on the performance of a magnetic responsive biocatalytic membrane reactor, Chem. Eng. J. 308 (2017) 853–862. doi:10.1016/j.cej.2016.09.057.

[123] L. Eykens, I. Hitsov, K. De Sitter, C. Dotremont, L. Pinoy, I. Nopens, B. Van der Bruggen,

Influence of membrane thickness and process conditions on direct contact membrane distillation at different salinities, J. Memb. Sci. 498 (2016) 353–364. doi:10.1016/J.MEMSCI.2015.07.037.

[124] S. Mondal, R. Mukherjee, S. De, Process modeling for the removal of phenolic compounds from industrial wastewater using a mixed-matrix membrane, Ind. Eng. Chem. Res. 54 (2015) 514–521. doi:10.1021/ie504358j.

[125] X.B. Ke, Z.F. Zheng, H.W. Liu, H.Y. Zhu, X.P. Gao, L.X. Zhang, N.P. Xu, H. Wang, H.J. Zhao, J. Shi, K.R. Ratinac, High-flux ceramic membranes with a nanomesh of metal oxide nanofibers, J. Phys. Chem. B. 112 (2008) 5000–5006. doi:10.1021/jp709837r.

[126] L.T. Choong, Z. Khan, G.C. Rutledge, Permeability of electrospun fiber mats under hydraulic flow, J. Memb. Sci. 451 (2014) 111–116. doi:10.1016/j.memsci.2013.09.051.

[127] T. Furukawa, K. Kokubo, K. Nakamura, K. Matsumoto, Modeling of the permeate flux decline during MF and UF cross-flow filtration of soy sauce lees, J. Memb. Sci. 322 (2008) 491–502. doi:10.1016/j.memsci.2008.05.068.

[128] D. Zedel, M. Kraume, A. Drews, Modelling and prediction of organic solvent flux and retention of surfactants by organic solvent nanofiltration, J. Memb. Sci. 544 (2017) 323–332. doi:10.1016/j.memsci.2017.09.041.

[129] S. Konishi, K. Saito, S. Furusaki, T. Sugo, Binary metal-ion sorption during permeation through chelating porous membranes, J. Memb. Sci. 111 (1996) 1–6. doi:10.1016/0376-7388(95)00237-5.

[130] Y. Shao, H. Chen, Y. Li, X. Ma, Fabrication of novel porous carbon membrane/sintered metal fibers composite for isopropanol adsorption, Chem. Eng. J. 276 (2015) 51–58. doi:10.1016/j.cej.2015.04.080.

[131] X. Wang, Y. Li, H. Li, C. Yang, Chitosan membrane adsorber for low concentration copper ion removal, Carbohydr. Polym. 146 (2016) 274–281. doi:10.1016/j.carbpol.2016.03.055.

[132] K. Ohwada, On the pauling electronegativity scales-II, Polyhedron. 3 (1984) 853–859. doi:10.1016/S0277-5387(00)84634-3.

Chapter 7

Conclusions and Recommendations

The potentials of membrane technology have been exploited and investigated upon through the development of nanofibrous membranes embedded with metal-organic frameworks (MOFs) and the experiments on the adsorptive removal of heavy metal ion from aqueous solution. The combined high surface area and active sites of the MOF and nanofibers make them good candidates for adsorption of heavy metal ions. The adsorption capacity of the standalone MOFs was tested for removing lead, mercury, zinc and cadmium. The proof of concept was established using two water stable MOFs; i.e. a zirconium MOF808 and a commercial iron-based MOF F300 were enmeshed in the nanofiber of two different polymers (PAN and PVDF) through co-electrospinning. The adsorption capacities of the MOFs for the different heavy metals analyzed were; MOF 808 (Pb-170.74 mg g^{-1}, Zn-287 mg g^{-1}, Cd-225.05 mg g^{-1}, Hg-276.96 mg g^{-1}) and F300 (Pb-148.13 mg g^{-1}, Hg-229.66 mg g^{-1}) while the adsorption capacities of the MOF 808 and F300 containing PA membranes were; PA808 (Pb-23.98 mg g^{-1}, Hg-50.88 mg g^{-1}), PA300 (Pb-30.19 mg g^{-1}, Hg-53.09 mg g^{-1}).

MOFs were enmeshed into nanofibers following the electrospinning technique reported by many membrane experts. The application of these membranes though, is what makes this work interesting. Gas phase separation has so far been dominating the use of MOFs enmeshed nanofibers. This work, on the other hand, focuses on the liquid phase separation and shows that it is possible to remove heavy metal ions. The removal efficiency of these membranes was, at least, as good as other adsorption membranes.

Since it was established during the proof of concept that MOF activation is important in enhancing the adsorption capacity of the MOF and its corresponding membranes, an activation study was attempted

using conventional drying, acetone and water washing. These activation techniques were employed by other researchers mostly for porous materials to enhance their performance. This work is unique, since these techniques were employed for the performance enhancement of the MOF-nanofiber membranes. In as much as deactivation occurred with conventional vacuum drying, washing with water brought about 'hydractivation' with a slight increase in removal capacity of the tested MOF 808 alongside the PAN/MOF808 nanofibrous membrane. After 'hydractivation', the removal efficiency of the MOF for cadmium ions was improved by 30% averaging with its PAN membrane. This improvement is worth studying more in details since 'hydractivation' is much easier than the supercritical CO_2 drying process recommended by some MOF researchers. Further emphasis was then laid on the practical application of the PAN/MOF808 membrane in the removal of lead ions by studying some governing process parameters that affect the efficiency of treatment processes. For the practical applications of the novel MOF-nanofiber membranes, it is indispensable to know the effect of process parameters on the membrane performance. It must be noted that these parametric studies have not been conducted for the membranes made of similar materials at this moment, hence comparison could not be done. Among the parameters studied, reducing the feed concentration of metal ion and the reducing the transmembrane pressure produced significant results in the volume of feed the membrane could treat per unit surface area. Therefore, this is an indication that the developed composite membrane could be suitable for secondary and tertiary stages of waste water treatment. A mathematical model has also been proposed to enable the prediction of the performance of the membrane based on the process parameters analyzed. This model shows significant agreements with experimental data but the model could be improved as stated in the recommendations below.

7.1 Recommendations

From the data gathered during this project, the developed membrane system and performance results, this project could be stretched to include the following studies;

It is proven and presented in chapter 3 that the full potential of the metal-organic framework particles is not completely utilized partly due to agglomeration. It is possible that upon complete utilization of the MOFs active sites, adsorption capacity could be greatly improved. Further investigations into possible dispersion techniques that could be coupled with electrospinning to produce completely dispersed MOFs in the nanofibers.

The feed test solutions used for this project are the synthetic solutions made by dissolving the corresponding salts, to simulate real life water treatment systems, it is recommended to run all experiments using real waste water feed collected at the effluent of the treatment center.

All experiments are conducted at room temperature for this project. For a country like Canada with extreme temperature conditions, it is reasonable to investigate the performance of the MOF membrane under varied temperature conditions. Though it is known clearly that adsorption is an exothermic process favoured by lower temperatures, the assumption of enhanced capacity at lower temperatures is too general, and therefore further investigation is proposed.

The method of quantification of the heavy metals employed in this project is by flame atomic absorption spectrometry. Since any slight changes in heavy metal ion in treated water has lasting consequences on the human health, it is important to validate the results obtained by using another method and if possible more advanced method such as Inductive coupled plasma-mass spectrometry (ICP-MS).

A more fine-tuned process parameter analysis could be beneficial in developing a complete understanding of the effects of the process parameters and to create a balance in parameters like membrane thickness effect and flux.

The mathematical model developed during this work could safely predict the permeate quality with respect to the considered parameters. This model could be developed further to account for other factors like nanoparticle agglomeration, membrane pore size, batch systems and also co-existing ion effects, which will increase the sophistication of the model but make it more application for real life treatment processes.

Appendix A: Supporting Information (SI) for

Chapter 3: Metal-organic frameworks supported on nanofibers to remove heavy metals

Johnson E. Efome, Dipak Rana, Takeshi Matsuura, Christopher Q. Lan*

Industrial Membrane Research Institute, Department of Chemical and Biochemical Engineering, University of Ottawa, 161 Louis Pasteur Ottawa, ON K1N 6N5, Canada

Experimental section

All chemicals were of analytical grade, commercially available from Sigma Aldrich, Alfa Aesar and Strem chemical, and used as received without further purification.

Synthesis of MOF 808

The crystals were synthesized by facile microwave procedure1, with a modified route from Furukawa et al.[2]. Typically, 0.699 g of ZrCl4 and H_3BTC (0.210 g) were dissolved in a mixture of N, N-dimethyl formamide (DMF)/Formic acid (45/45 mL) in a 200 mL boiling flask. The flask was then transferred into a microwave and irradiated at 400 W for 30 min. The resulting suspension was filtered by centrifugation, washed with DMF three times (10 mL x 3) and dried at 70 ^{o}C for 12 h. Solvent exchange in acetone and water followed by vacuum drying at 50 ^{o}C was also done as an activation route.

MOF F300

This was a commercially purchased MOF from Sigma Aldrich Co., St. Louis, MO, produced by BASF, Germany and marketed under the name Basolite F300 (CAS # 1195763-37-1, Mw = 262.96 Da) and also known as Fe-BTC, Iron 1,3,5-Benzenetricarboxylate (BTC). The manufacturer reported it has a BET (Brunauer, Emmett and Teller) surface area of 1300-1600 m^2/g, and bulk density of 0.16-0.35 g/cm^3.

Preparation of electrospinning solution:

PAN solution: 0.5 g of PAN (average Mw = 150 kDa, and density of 1.184 g/cm^3 from Sigma Aldrich Co., St. Louis, MO) was added to 5 g of DMF and the solution was placed in a shaker (180 rpm) for 24 h at 50 ^{o}C to form a homogenous 10 wt.% solution.

PVDF solution: 1.0 g of PVDF (Mw = 410 kDa; melt viscosity 18.5 ± 2.5 kPoise; melting temperature, Tm 160.1^{o}C, Kynar® 740 Pellet from Arkema Inc., Philadelphia, PA) pellets was added to 5 mL of DMF and the mixture stirred overnight (under same temperature and rpm as above) to form a 20 w/v homogeneous solution.

Preparation of MOF/polymer dope solution: 0.125 g of MOF was primed in 3 g of DMF. Then 0.5 g of PAN was added with the remainder of 2 g solvent to form a suspension with 20 wt. % MOF loading. For PVDF, since the viscosity was optimized, MOF loading was kept at a maximum of 16 wt. %.

Preparation of nanofiber membranes and NMOM: Neat membranes

The 10 wt.% PAN/DMF solution was filled into a 10-mL syringe and electrospun at a syringe feed rate of 0.15mm/min. A voltage of 15 kV was applied to a spinneret of 0.6 mm ID separated from a 140-rpm rotating drum 15 cm apart. The temperature and humidity were maintained at 25 ^{o}C and 40%, respectively. The nonwoven fibers were collected on aluminum foil and dried at room temperature for 24 h. The 20 w/v PVDF/DMF solution was electrospun at a voltage of 18 kV, syringe feed rate of 0.1 mm/min, and a spinneret collector drum distance of 15 cm.

MOF/PAN nanofibers

The dope solution was electrospun on aluminum foil at 15-17 kV depending upon dope viscosity, 0.15 mm/min syringe feed rate and under the same temperature and humidity as above.

MOF/PVDF nanofibers

Fibers were also collected on aluminum foil under an applied voltage of 18-20 kV based on dope viscosity, 0.10-0.12 mm/min syringe feed rate and 15 cm drum-spinneret distance.

Batch adsorption-desorption experiments

The synthetic lead and mercury solution were made by dissolving lead (II) nitrate and mercury (II) chloride, respectively (From Strem chemicals), in distilled water and were further diluted to the required concentrations. All sample concentrations were measured using flame atomic absorption spectroscopy (FAAS). To determine the amount of heavy metal adsorbed to MOFs, the difference in concentrations between before and after adsorption was computed. To reuse membranes after each cycle, the adsorbates, heavy metals, were desorbed from NMOM. Desorption experiment were carried out using 2 wt. % nitric acid solution. Since heavy metals precipitation turns to occur at pH >5, all experiments were conducted below pH 5 i.e., pH 4.6 ± 0.2 adjusted using 0.1 M HCl or 0.1 M NaOH. Adsorption kinetics experiments were performed to determine adsorption rate and the time for the MOF to reach the adsorption equilibrium. Twenty milligrams (20 mg) of M808 and 10 mg of F300 were used in separate experiments with 30 mL of 20 ppm lead, and 50 ppm of mercury initial concentration. The samples, collected at predetermined time intervals, were agitated slowly at room temperature for a total contact time of 3 h.

The adsorption isotherms of the MOF were established by using the same masses of the MOFs as above but with different initial heavy metal concentrations; Lead (10-1000 ppm), mercury (50-1000 ppm). From the results of kinetics experiments, 2 h was sufficient for equilibrium to be attained. The membrane isotherms were established by weighing specific mass of the membrane (with and without MOF) ranging between 50-70 mg and using the same concentrations and volumes of the heavy metal solutions. The pH was maintained at 4.6±0.2 by using nitric acid/sodium hydroxide and the temperature was kept at room temperature. The bound heavy metal was desorbed by soaking the membrane in 30 mL of diluted nitric acid, to decrease the pH and change the surface charge, under mild agitation for 1 h at room temperature.

The amount of adsorbate adsorbed per unit mass of adsorbent q_e (mg/g) and the distribution coefficient (mass-weighted coefficient representing the sorbent's affinity for a sorbate: K_d) are given by equations (A-1) and (A-2), respectively.

$$q_e = \frac{(Co - Ce)\,V}{m} \qquad \text{(A-1)}$$

$$K_d = \frac{Co - Ce}{Ce} * \frac{V}{m} \qquad \text{(A-2)}$$

where m (g) is the mass of adsorbent, V (L) is the volume of the solution, Co and Ce are the initial and equilibrium concentrations (mg/L). K_d values were determined using a 2-ppm solution of the heavy metal ion with the same volume and mass of sorbent as in the kinetics analysis.

To calculate the percent of MOF available for adsorption, when enmeshed and not enmeshed:

$$q_{max}^{NMOM} = q_{max}^{NFM} * (\%NFM) + q_{max}^{MOF} * (\%MOF) \qquad \text{(A-3)}$$

where the superscript NFM is the nanofiber mat, NMOM is the nanofiber MOF membrane, MOF is the metal-organic framework. q_{max} is the maximum adsorption capacities of the respective sorbent.

Filtration experiment

Filtration experiments were conducted using a dead-end cell of 300 mL volume capacity and an effective membrane area of 3.8×10^{-3} m^2. The test membrane of about 250 µm thickness was sized in a circular shape and an O-ring was used to compress and seal the setup to prevent leaks. Solution containing 100

ppb of lead was forced through the membrane by an externally applied pressure (using a nitrogen cylinder) of 0.4 bar at room temperature to obtain an almost similar flux of 348±25.8 L/m^2h. The permeate was collected at specific time intervals and analyzed to determine the membrane performance. Upon saturation of the membrane, for re-use tests, the cell was filled with desorption solution (dilute nitric acid solution) and flushed at a flux of 278 L/m^2h. The regenerated membrane was then washed with deionized water to remove residual desorption solution. The cycle was repeated four times to determine membrane reusability.

Instrumentations

X-ray diffraction analysis of powder was carried out at room temperature on RigakuUltima IV powder diffractometer in Bragg-Brentano geometry, using Cu Kα radiation (λ = 1.5418 A). The 2Θ range of 2° to 32° was covered with 0.02° step width and 2°/min scan speed.

ATR-FTIR analyses of the pristine MOF crystals, heavy metal treated MOFs and the nanofibrous MOF membranes were carried out using Agilent tech- Cary 630 (Agilent, Canada) spectrometer carrying a diamond sampling accessory. The samples were pressed on a diamond prism and the infrared spectra were collected at 4 cm^{-1} resolution, 64 scans within a wave number range of 500-3000 cm^{-1} at room temperature.

Transmission electron microscopy (TEM) was carried out to investigate MOF crystal shape and size using a FEI Tecnai F20 apparatus equipped with an Oxford Aztec 80 mm SDD detector. A suspension of the samples prepared in deionized water was dropped on copper grids and analyzed at 300 kV.

Scanning electron microscopy (SEM) images were taken using a Tescan, Vega-II XMU equipped with a 250X EDS, Oxford Inca Energy apparatus. Samples were affixed onto the holder by means of a

conductive adhesive, then gold coated under vacuum using an Anatech Hummer VII equipment. Images were taken at suitable resolutions.

Zeta potential and hydrodynamic diameter were recorded using a Zetasizer nano ZS, Malvern instrument. The zeta potential was measured as a function of pH using buffer solutions of different pH. Measurements were carried out using disposable 0.5 mL folded capillary cuvettes and 1 cm length cuvettes for zeta potential and dynamic light scattering measurements, respectively.

The surface elemental composition was determined by X- ray Photoelectron Spectroscopy (XPS, Kratos Axis HS, Manchester, UK). The samples were excited using monochromatized Al Ka X-radiation and a 180o hemisphere analyzer and a three-channel detector was employed. The samples were analyzed for specific elements at a time in a pressurized chamber ($1.33x10^{-4}$ to $1.33x10^{-5}$ Pa) using an X-ray gun operated at 15 kV and 20 mA. The maximum X-ray penetration depth at $\theta=0^{o}$ (sample was perpendicular to the detector) was 6.3 nm.

The surface characteristics of the synthesized materials were determined by Brunauer–Emmett–Teller (BET) using nitrogen at 77 K with a Micromeritics 3FLEX volumetric apparatus. Before the nitrogen adsorption measurements, the samples were degassed under a purge flow of nitrogen of 40 cm^3/min at 90°C for 1 h. The data in the relative pressure ($P/P0$) range 0.05–0.2 were used to calculate the specific surface area with the BET equation.

Characterization:

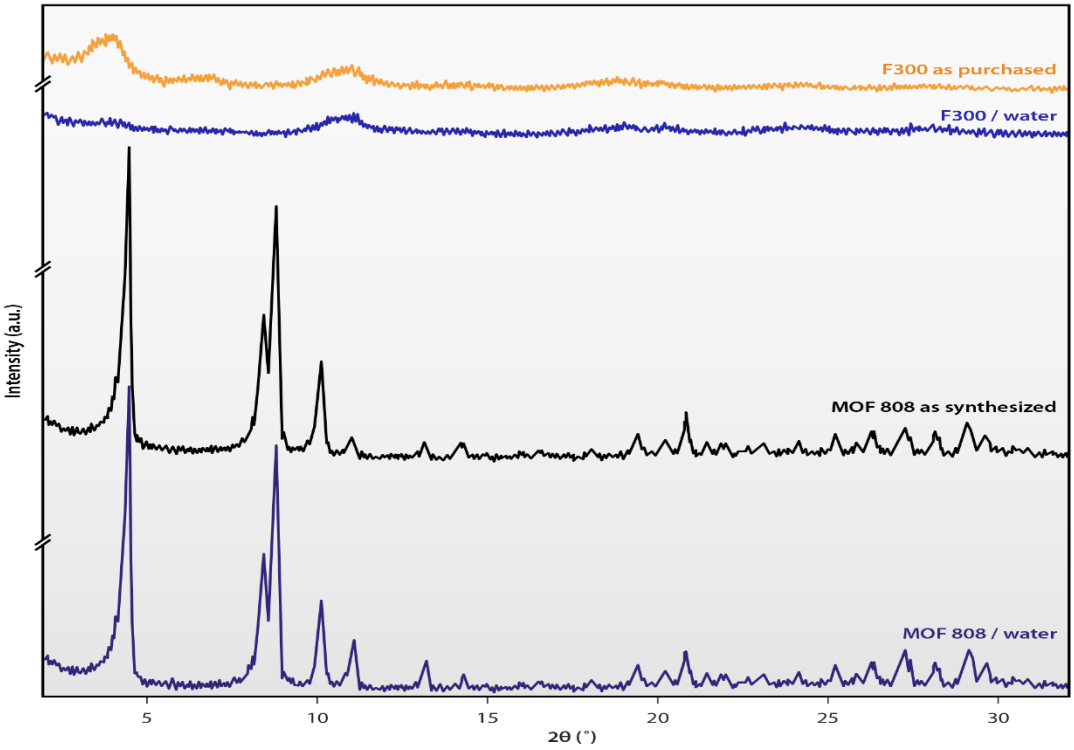

Figure A- 1. PXRD analysis of the MOF crystals and when immersed in water for 48 h.

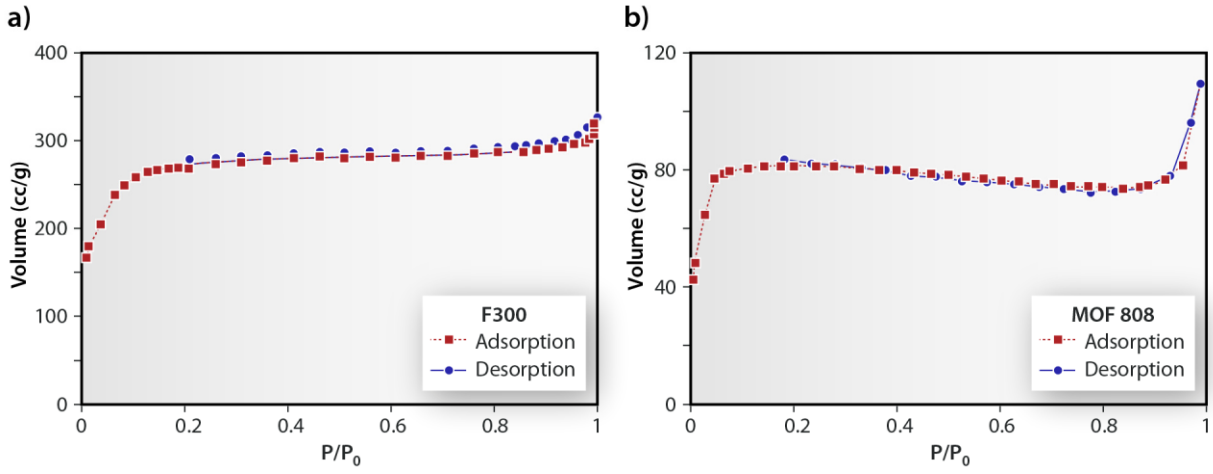

Figure A- 2. N_2 isotherm plot for M808 and F300

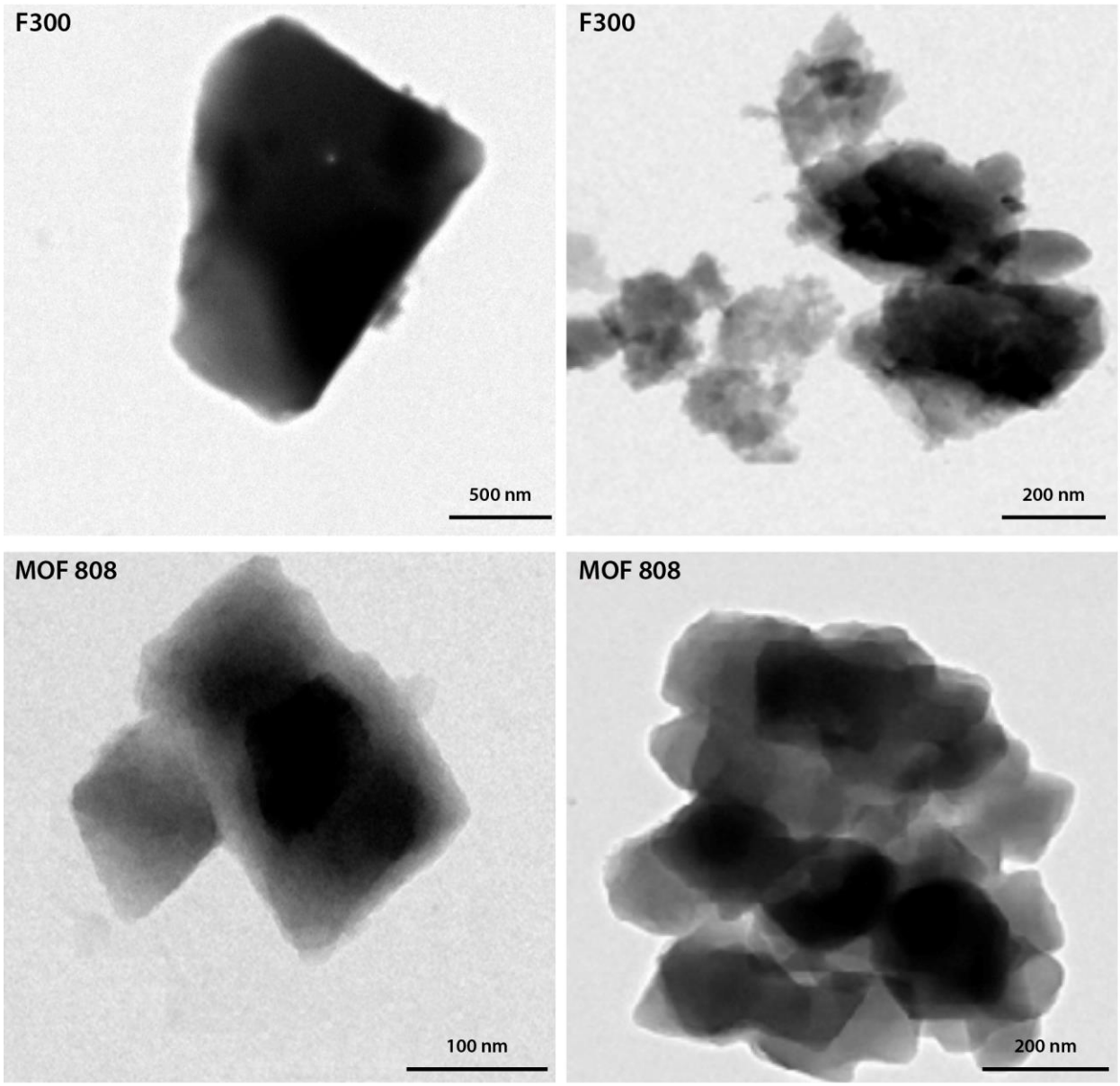

Figure A- 3. TEM images of M808 and F300

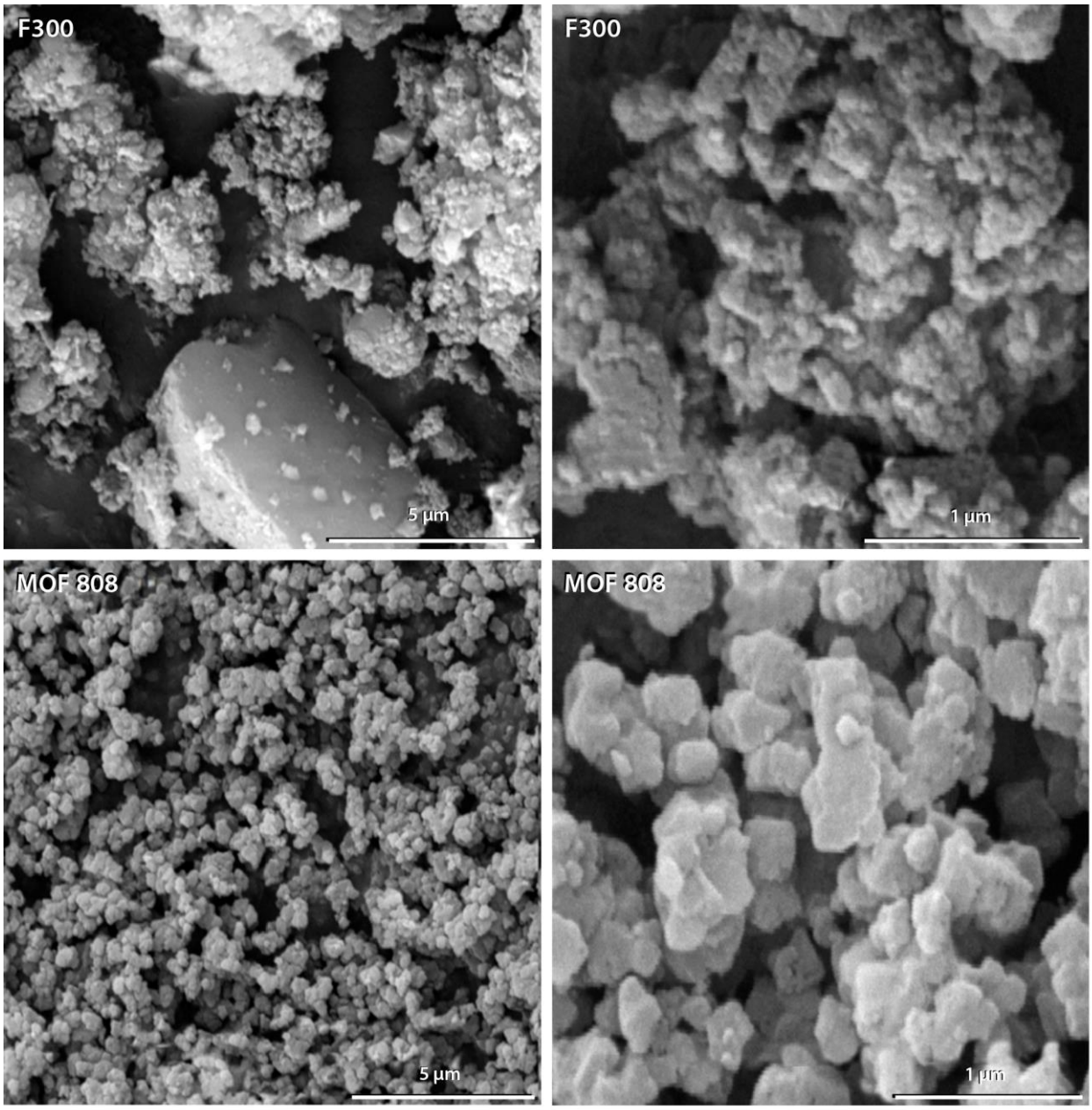

Figure A- 4. SEM images of the MOF crystals, M808 and F300

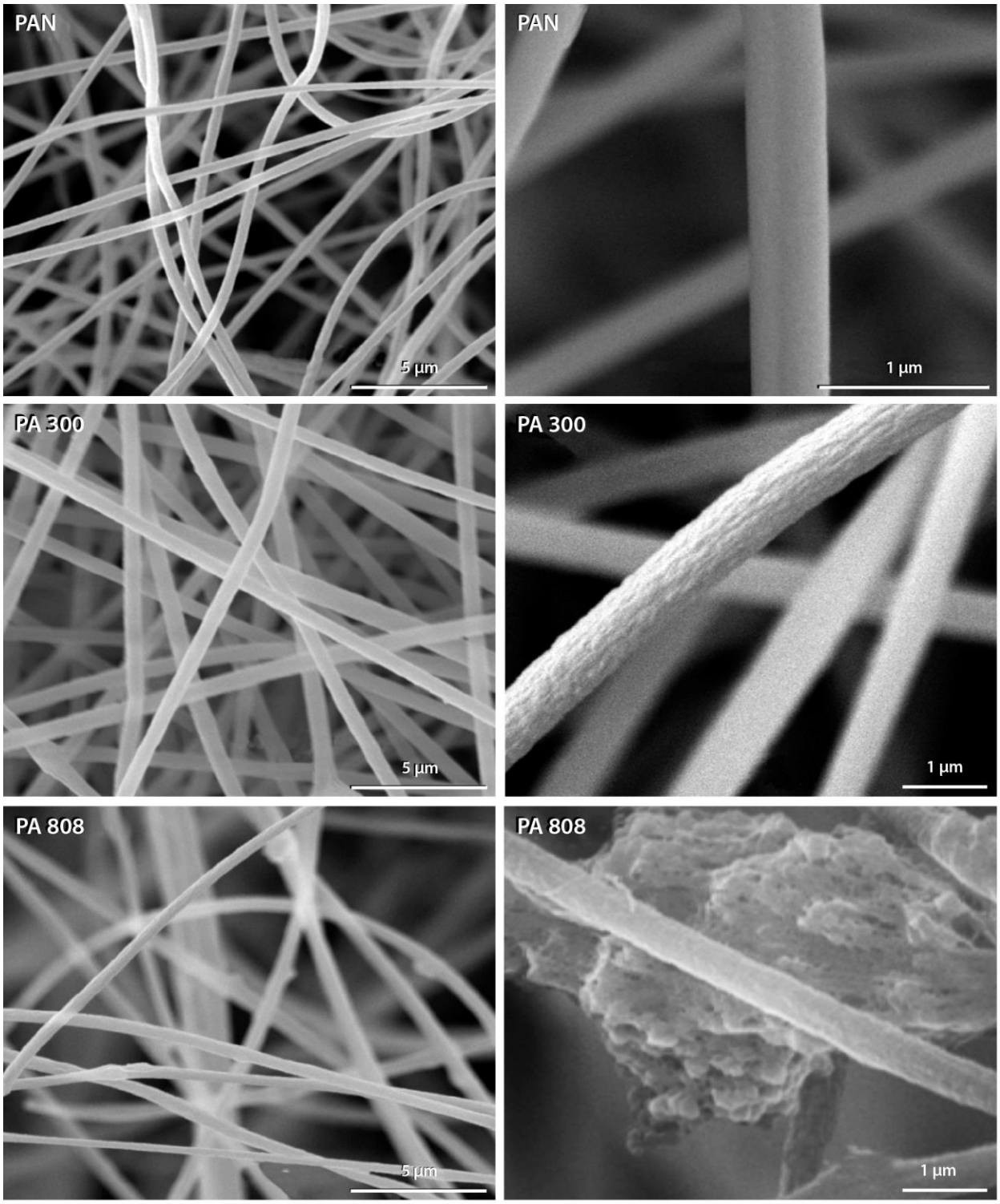

Figure A- 5A. SEM images of PAN nanofibers. PAN without MOF (PAN), PAN with F300 (PA300) and PAN with MOF 808 (PA808).

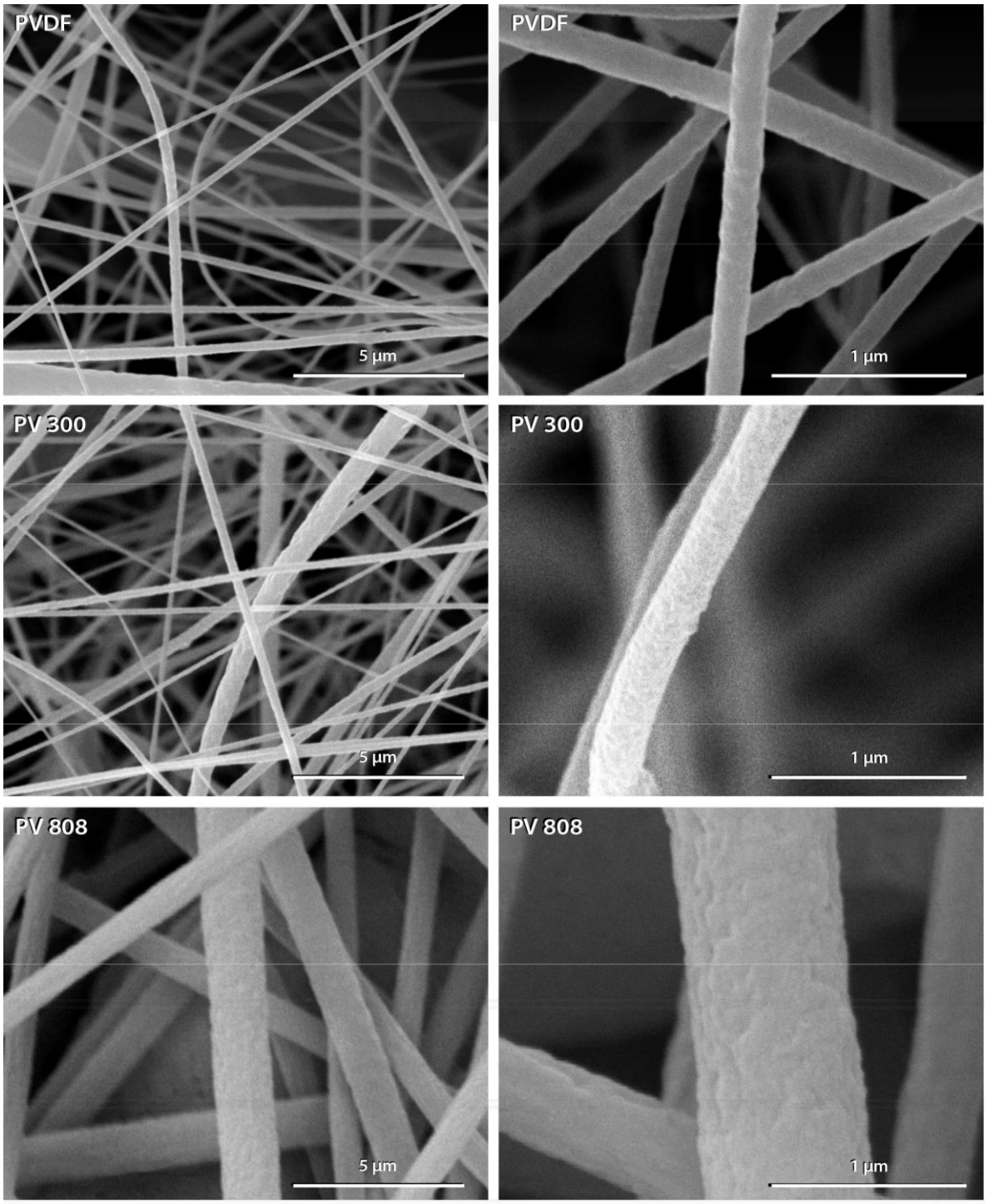

Figure S5B. SEM images of PVDF-MOF nanofibers. PV300 refers to PVDF with F300 incorporated and PV808 refers to PVDF with M808 incorporated.

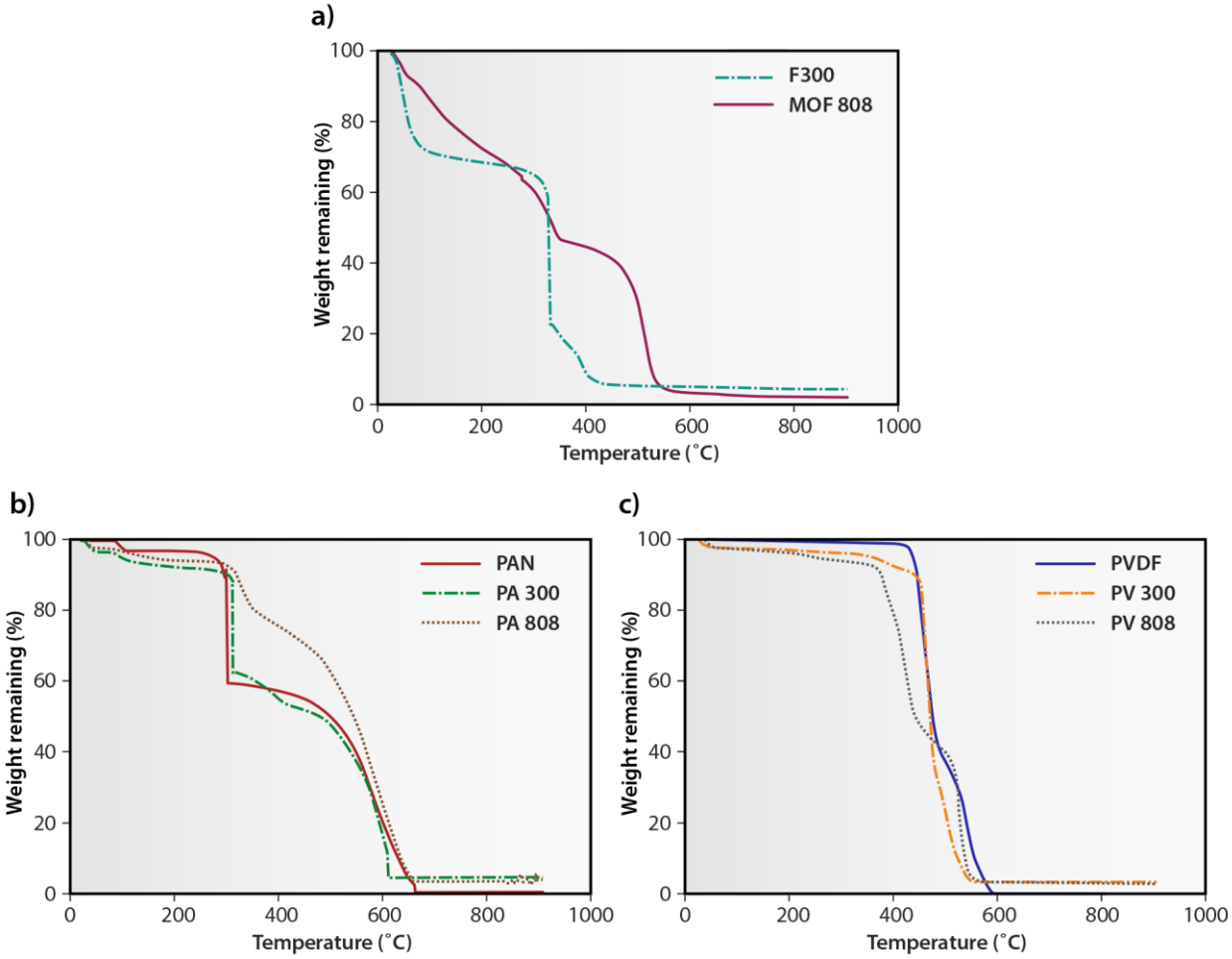

Figure A- 6. Thermogravimetric analysis (TGA) curves for the MOF crystals (M808 and F300) and the NMOM. PV is PVDF and PA is PAN and the number denotes the MOF particle incorporated e.g. PA300 is PAN with F300 incorporated while PV808 is PVDF with MOF 808 incorporated.

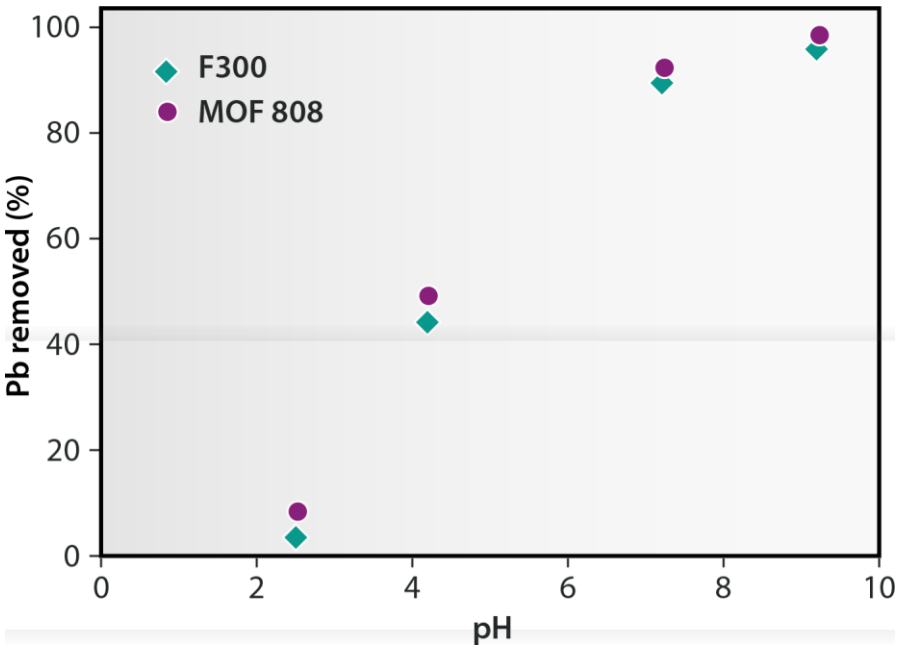

Figure A- 7. The change in pH against the amount of Pb ion removed.

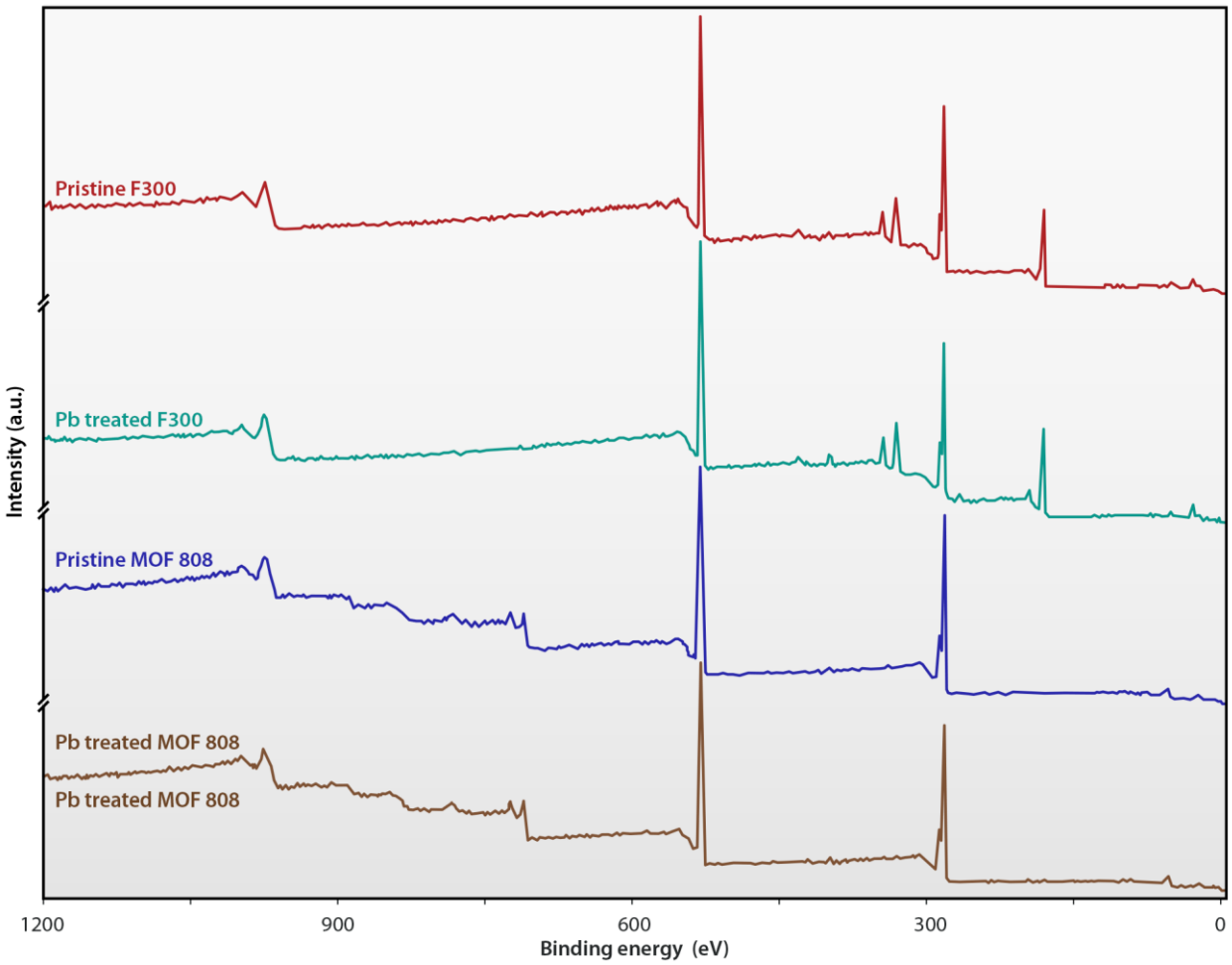

Figure A- 8. X-ray photoelectron spectra (XPS) of the pristine MOFs and the MOF after treatment with heavy metal ion. The similarity of the spectra reveals that the heavy metal ions were not present at surface but inside of the MOF (internal pores).

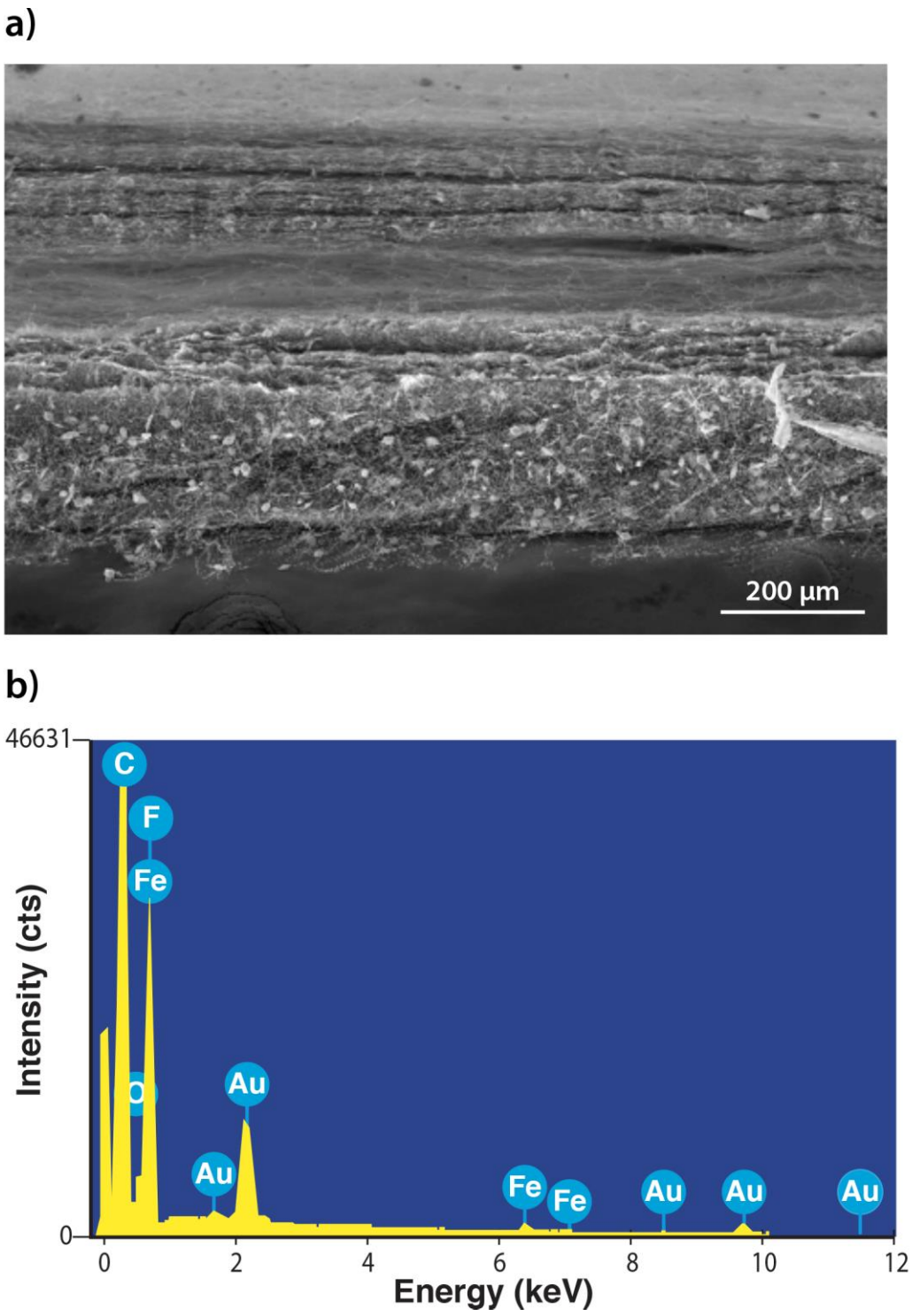

Figure A- 9A. Elemental EDX mapping of the cross-sectional view of PA300 after filtration experiments.

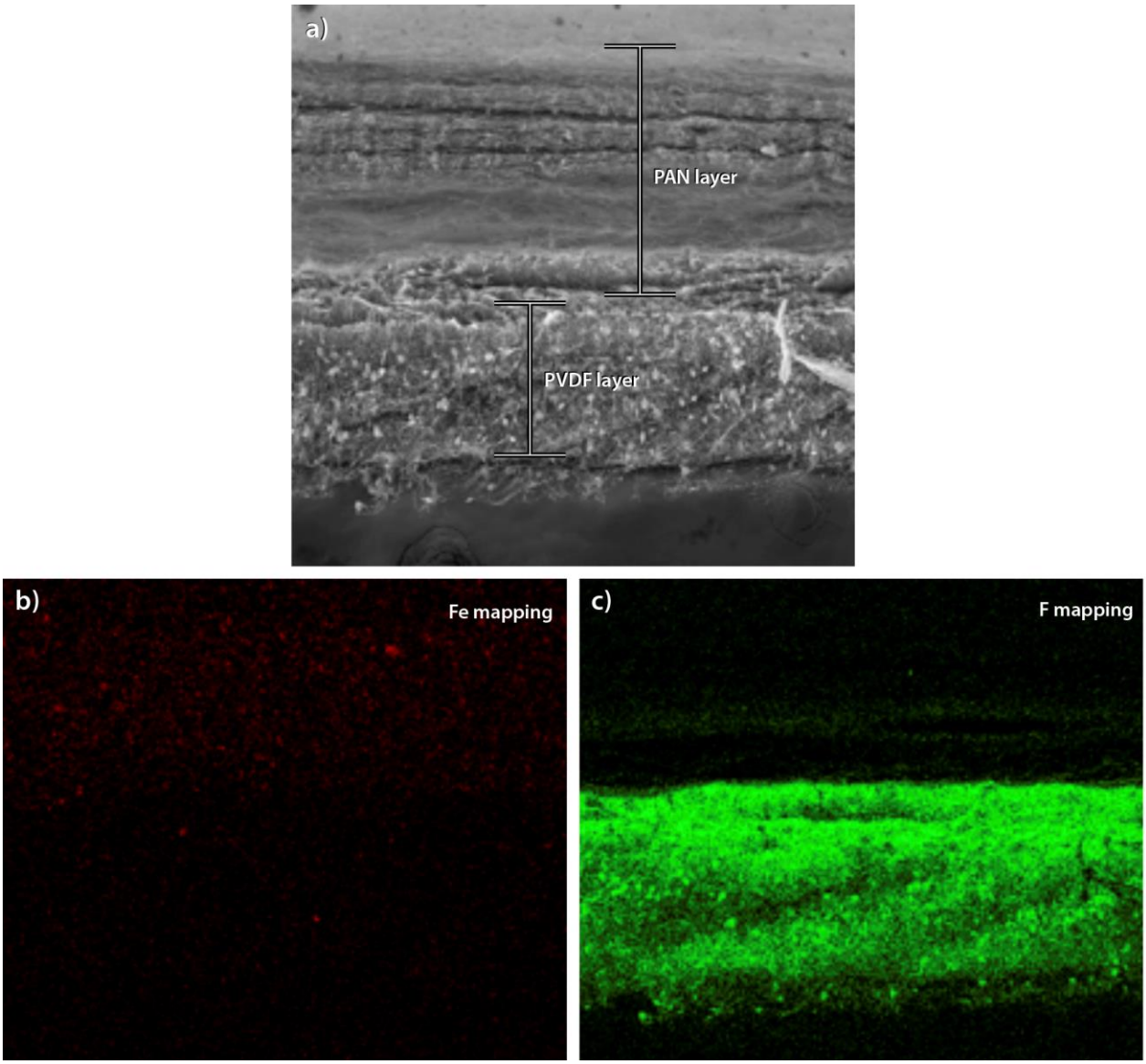

Figure A-9B. EDX elemental mapping of the lower PVDF layer and top PAN300 layer. The green color represents the Fluoride ion of the PVDF and red for Fe ions of the F300.

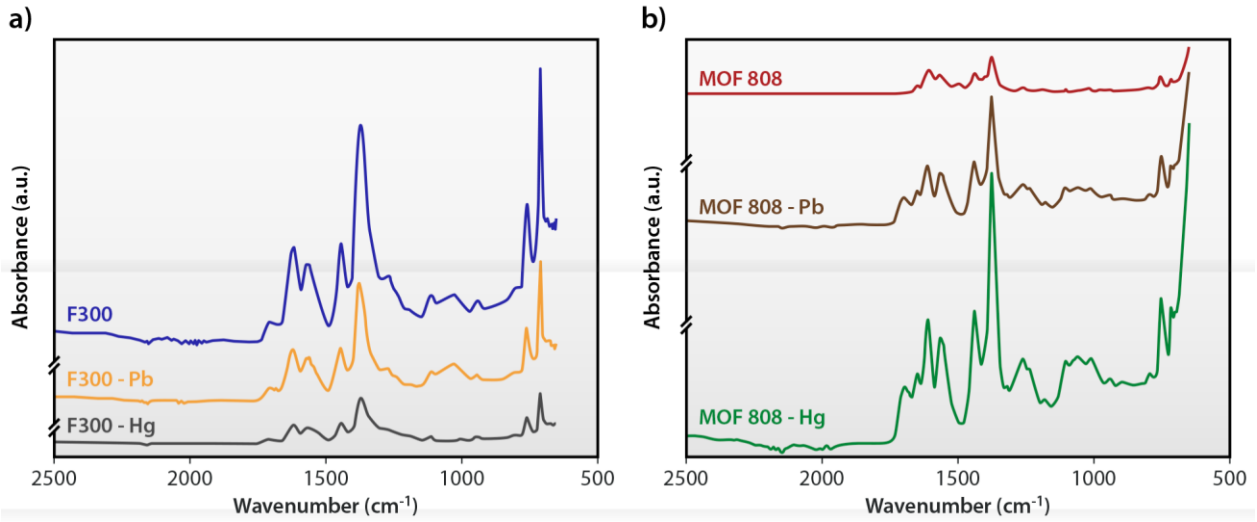

Figure A- 10. FTIR spectra of MOF crystal before and after heavy metal adsorption.

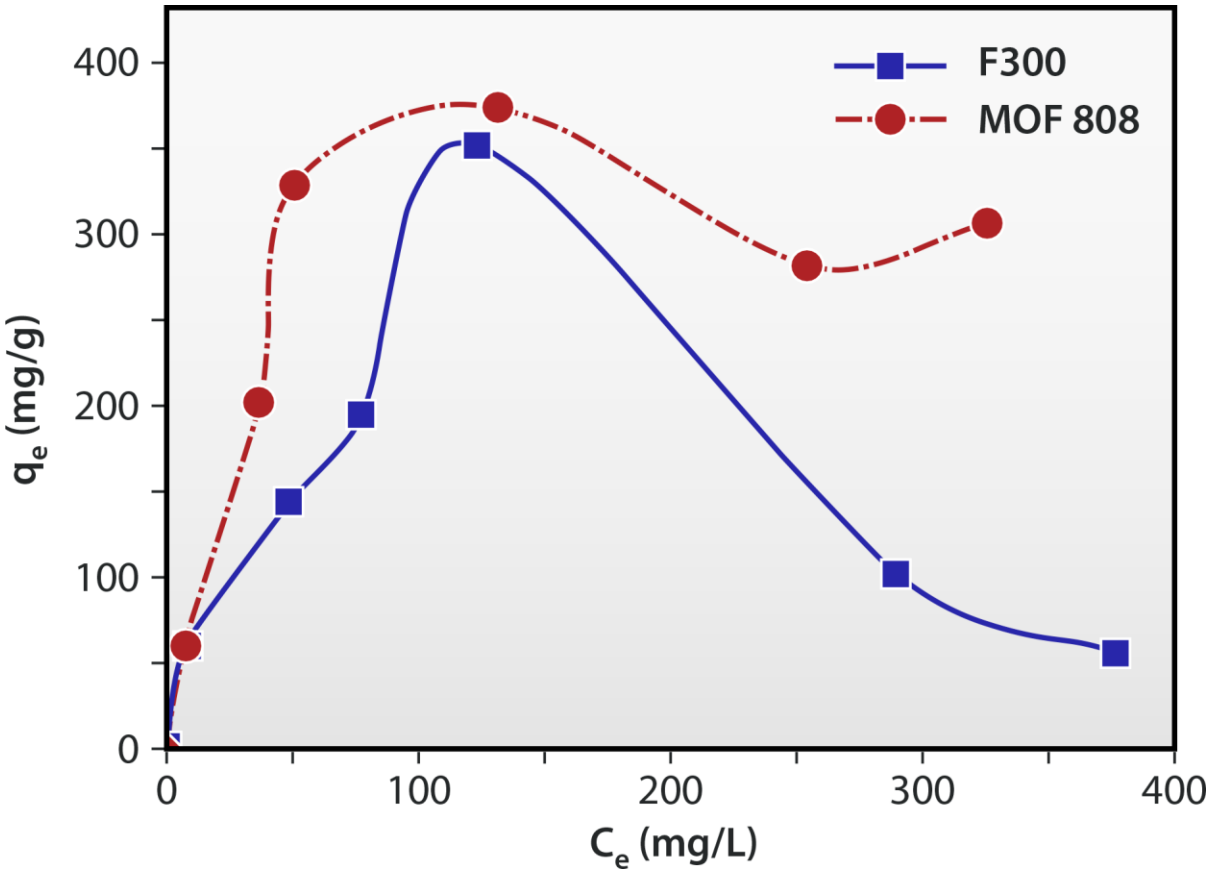

Figure A- 11. Sorption data for Pb and the two MOFs when the pH of the system is not adjusted. The shape of the curve is accounted for by the competitive binding of protons and Pb ions.

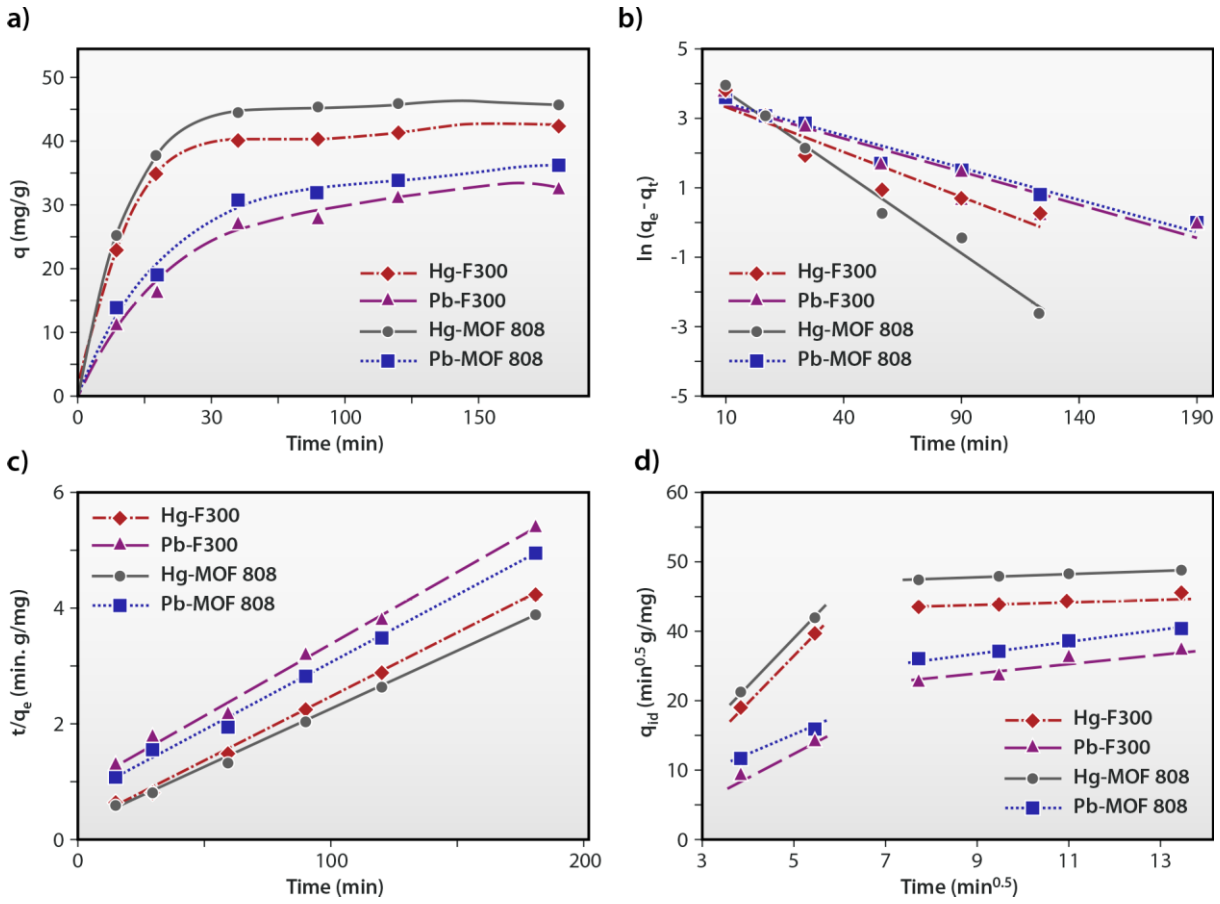

Figure A- 12. (A) Sorption kinetic data of the MOFs with Pb and Hg ions, (B) Analysis using pseudo-first order, (C) Pseudo-second order model4, and (D) Morris-Webber5 intra-particle model showing that the sorption is a multistage process and that intra-particle diffusion is not the dominant mechanism.

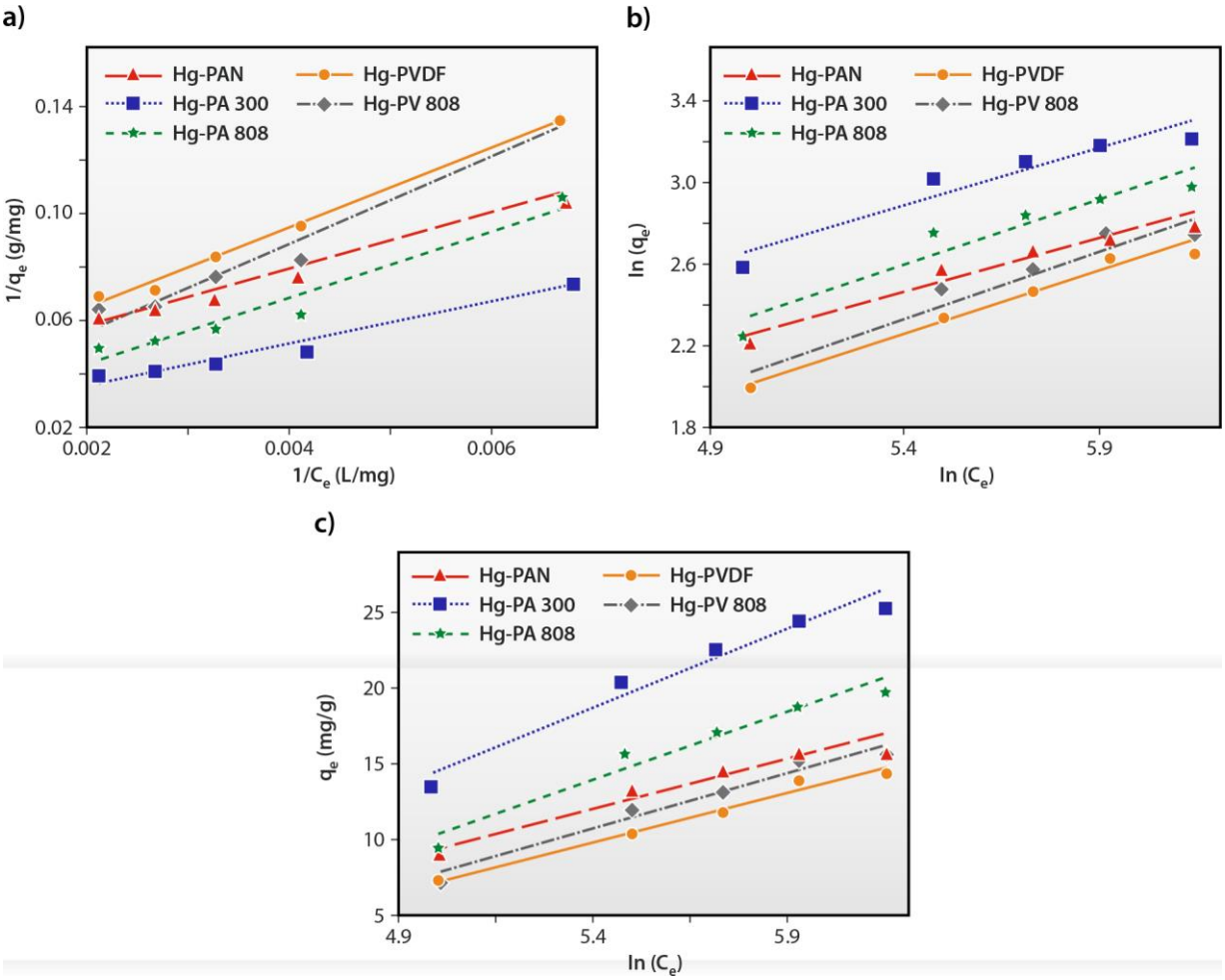

Figure A- 13. Linearized sorption data for Hg as fitted by (A) Langmuir, (B) Freundlich, and (C) Temkin Isotherms.

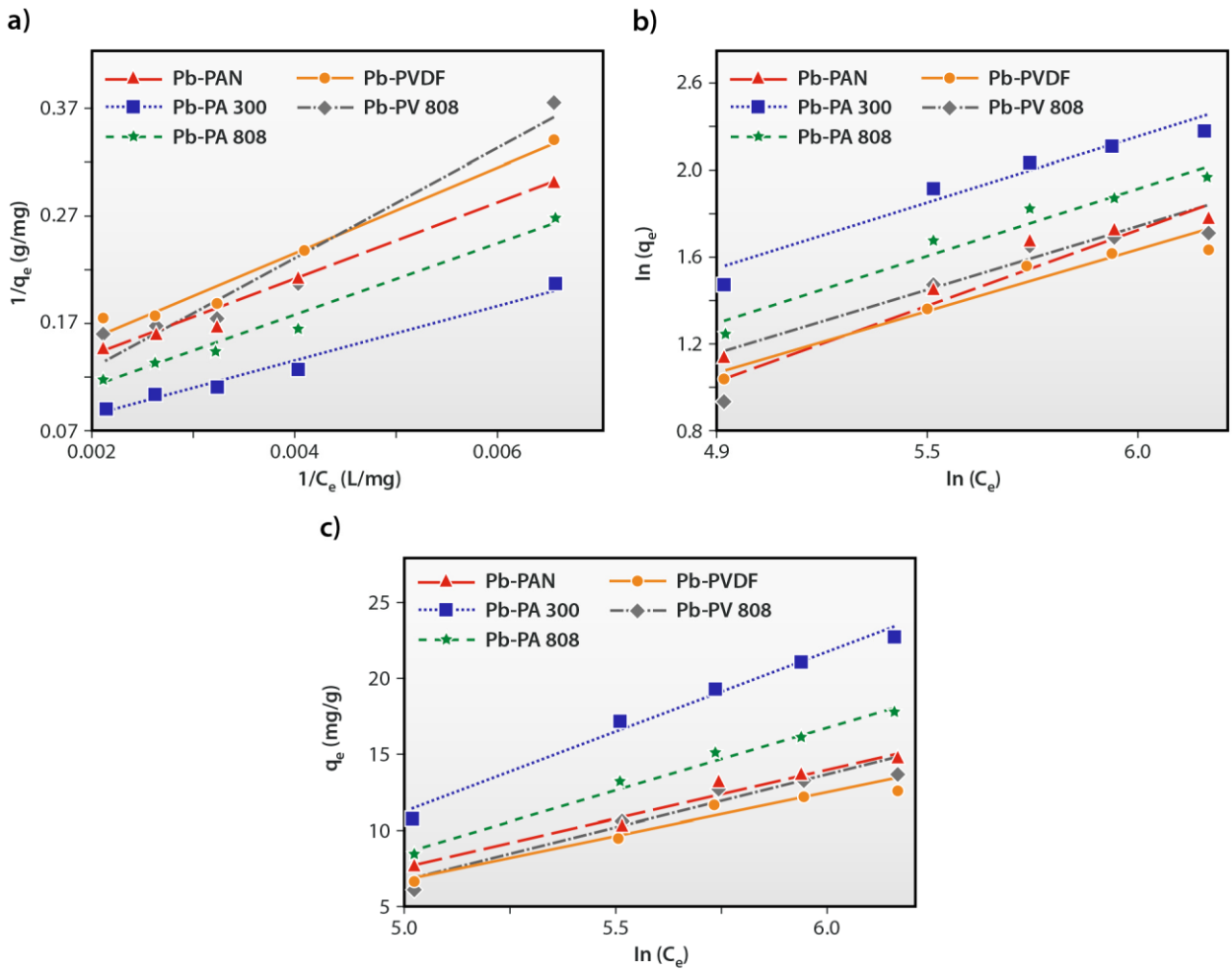

Figure A- 14. Linearized sorption models for Pb: (A) Langmuir Isotherm, (B) Freundlich Isotherm, and (C) Temkin Isotherm models.

Table A- 1 Kinetic model parameters for all three models with the two MOFs.

		First order			Second order			Intra-particle	
Adsorbate	Sorbent	k_1	q_e	R^2	k_2	q_e	R^2	k_{id}	R2
Pb (II)	F300	0.025	32.237	0.971	0.880	40.013	0.994	2.610	0.942
	M808	0.023	32.256	0.969	0.723	43.130	0.994	2.843	0.934
Hg (II)	F300	0.028	25.908	0.894	0.234	45.436	0.998	3.071	0.798
	M808	0.052	42.423	0.987	0.196	49.328	0.997	3.386	0.795

k_1 [1/min], k_2 [mg/g min], k_{id} [mg/g min], and q_e [mg/g].

Table A- 2. Langmuir model parameters for sorption of Pb (II).

Sorbent	q_{max} (mg/g)	K_l (L/mg)	R^2	K_d (mL/g)
F300	148.133	0.014	0.995	2.7×10^4
M808	170.740	0.014	0.970	1.3×10^4
PAN	15.097	0.002	0.983	8.1×10^3
PA808	23.977	0.001	0.980	1.1×10^4
PA300	30.193	0.001	0.976	1.4×10^4
PVDF	13.621	0.002	0.975	6.0×10^3
PV300	NA□	NA	NA	NA
PV808	17.191	0.0001	0.945	9.3×10^3

□NA means Not Available

Table A- 3. Freundlich model parameters for sorption of Pb (II).

Sorbent	*k*	*n*	R^2
F300	12.181(mg/g (L/mg)$^{1/n}$	2.555	0.933
M808	10.471	2.231	0.961
PAN	0.130	1.541	0.956
PA300	0.159	1.442	0.947
PA808	0.056	1.274	0.890
PVDF	0.122	1.566	0.934
PV300	NA	NA	NA
PV808	0.056	1.274	0.890

Table A- 4. Temkin model parameters for Pb (II) sorption.

Sorbent	*B*	A_T (L/g)	b_T (J/mol)	R^2
F300	30.512	0.027	81.201	0.970
M808	40.874	0.027	60.614	0.956
PAN	3.085	0.019	802.981	0.968
PA300	5.056	0.018	490.032	0.984
PA808	3.966	0.017	624.689	0.989
PVDF	2.669	0.020	928.215	0.952
PV300	NA	NA	NA	NA
PV808	3.302	0.016	750.349	0.927

Table A- 5. Langmuir model parameters for sorption of Hg (II).

Sorbent	q_{max} (mg/g)	K_l (L/mg)	K_d (mL/g)	R_L	R^2
F300	229.659	0.003	3.1 x 104	0.373	0.992
M808	276.960	0.002	3.9 x 104	0.374	0.995
PAN	28.767	0.003	9.4 x 103	0.478	0.987
PA808	53.088	0.002	2.3 x 104	0.481	0.951
PA300	50.889	0.003	3.1 x 104	0.470	0.965
PVDF	28.640	0.002	5.2 x 103	0.484	0.994
PV300	NA	NA	NA	NA	NA
PV808	42.603	0.001	8.3 x 103	0.485	0.971

Table A- 6. Freundlich model parameters for sorption of Hg (II).

Sorbent	$k\ (mgg^{-1}(L/mg)^{1/n})$	n	R^2
F300	4.261	1.841	0.905
M808	2.490	1.519	0.978
PAN	0.693	1.908	0.958
PA300	0.868	1.780	0.917
PA808	0.400	1.540	0.904
PVDF	0.352	1.632	0.978
PV300	NA	NA	NA
PV808	0.269	1.483	0.936

Table A- 7. Temkin model parameters for Hg (II) sorption.

Sorbent	B	A_T (L/g)	b_T (J/mol)	R^2
F300	40.357	0.049	61.391	0.968
M808	60.858	0.027	40.711	0.961
PAN	6.533	0.028	379.249	0.984
PA300	10.544	0.026	234.977	0.951
PA808	9.100	0.021	272.269	0.947
PVDF	6.496	0.021	381.389	0.981
PV300	NA	NA	NA	NA
PV808	7.475	0.019	331.461	0.966

Table A- 8. The adsorption capacity, source of metal ion, pH, and time to adsorption equilibrium of Pb and Hg.

Metal ion	Sorbent	Adsorption capacity [mg/g]	Metal ion source	pH	Time to adsorption equilibrium [min]	Reference
Pb	Melamine-Zr-MOFs	122	$Pb(NO_3)_2$	5	120	6
	$Fe_3O_4@Cu_3(BTC)_2$	215.05	$Pb(NO_3)_2$	6	120	7
	PVA nanofiber/La-TBC	184	$Pb(NO_3)_2$	-	10	8
	PVA/Co-MOF	49.64		5.03	30	9
	Cu-terepthalate MOF	80	$Pb(NO_3)_2$	7	120	10
	HKUST-1-MW@$H_3PW_{12}O_{40}$	98		7	10	11
	UiO-66-NHC(S)NHMe	232	¶NA	-	240	12
	TMU-5	251	NA	10	15	13
	MOF 800	170.74	$Pb(NO_3)_2$	5	50	This study
	PA808	119.9	$Pb(NO_3)_2$	5	90	This study
	PV808	85.95	$Pb(NO_3)_2$	5	90	This study
	F300	148.13	$Pb(NO_3)_2$	5	50	This study
	PA300	150.95	$Pb(NO_3)_2$	5	90	This study
Hg	Pt NP@UiO-66-NH_2	206.25	$HgCl_2$	5	30	14
	ZIF-90-SH	22	$HgCl_2$	-	1440	15
	MIL-101-Thymine	52	$HgCl_2$	6	200	16
	AMOF-1	78	NA	-	1440	16
	$Fe_3O_4@SiO_2$@HKUST-1	264	$HgCl_2$	3	10	18
	Zn(hip)(L)(DMF)(H_2O)	333	$Hg(NO_3)_2$	5	60	19
	SH@SiO_2/$Cu(BTC)_2$	210	NA	5.5	60	20
	MOF-74-Zn	63	$Hg(NO_3)_2$	6	90	21
	MOF 800	276.96	$HgCl_2$	5	50	This study
	PA808	254.4	$HgCl_2$	5	90	This study
	PV808	213	$HgCl_2$	5	90	This study
	F300	229.66	$HgCl_2$	5	50	This study

NA means Not Available

References

1. Li, Z.-Q., Yang, J.-C., Sui, K.-W. & Yin, N. Facile synthesis of metal-organic framework MOF-808 for arsenic removal. *Mater. Lett.* 2015, 160, 412–414.
2. Furukawa, H. Gándara, F., Zhang, Y.-B., Jiang, J., Queen, W. L., Hudson, M. R. & Yaghi, O.
3. M. Water adsorption in porous metal-organic frameworks and related materials. *J. Am. Chem. Soc.* 2014, 136, 4369–4381.
4. Fryxell, G. E. Lin, Y., Fiskum, S., Birnbaum, J. C., Wu, H., Kemner, K. & Kelly, S. Actinide sequestration using self-assembled monolayers on mesoporous supports. *Environ. Sci. Technol.* 2005, 39, 1324–1331.
5. Lagergren, S. About the theory of so-called adsorption of soluble substances. *K. Sven. vetenskapsakademiens* 1898, 24, 1–39.
6. Weber, W.J; Morris, J. C. Advances in water pollution research: removal of biologically resistant pollutant from waste water by adsorption. in *International Conference on Water Pollution Symposium* 231–266 (Vol. 2. Pergamon, Oxford, 1962).
7. N. Yin, K. Wang, Y. Xia, Z. Li, Novel melamine modified metal-organic frameworks for remarkably high removal of heavy metal Pb (II). *Desalination* 2012, 430, 120–127.
8. Q. Yang, Q. Zhao, S. S. Ren, Q. Lu, Guo, Z. Chen, Fabrication of core-shell Fe3O4@MIL-100(Fe) magnetic microspheres for the removal of Cr (VI) in aqueous solution. *J. Solid State Chem.* 2016, 244, 25–30.

9. N. D. Shooto, C. W. Dikio, D. Wankasi, L. M. Sikhwivhilu, F. M. Mtunzi, E. D. Dikio, Novel PVA/MOF Nanofibres: Fabrication, Evaluation and Adsorption of Lead Ions from Aqueous Solution. *Nanoscale Res. Lett.* 2016, 11, 414 (13 pp).
10. N. D. Shooyo, D. Wankasi, L. M. Sikhwivhilu, E. D. Dikio, Modified Electro-spun Polyvinyl Alcohol Nanofibers Used as Super Adsorbing Material for Lead Ions in Aqueous Solution. *J. Residuals Sci. Tech.* 2016, 13, 233–242.
11. N. Yin, K. Wang, L. Wang, Z. Li, Amino-functionalized MOFs combining ceramic membrane ultrafiltration for Pb (II) removal. *Chem. Eng. J.* 2016, 306, 619–628.
12. F. Zou, R. Yu, R. Li, W. Li, Microwave-Assisted Synthesis of HKUST-1 and Functionalized HKUST-1-@H3PW12O40: Selective Adsorption of Heavy Metal Ions in Water Analyzed with Synchrotron Radiation. *ChemPhysChem* 2013, 14, 2825–2832.
13. F. Ke, J. Jiang, Y. Li, J. Liang, X. Wan, S. Ko, Highly selective removal of Hg2+ and Pb2+ by thiol-functionalized Fe3O4@metal-organic framework core-shell magnetic microspheres. *Appl. Surf. Sci.* 2017, 413, 266–274.
14. H. Saleem, U. Rafique, R. P. Davies, Investigations on post-synthetically modified UiO-66- NH2 for the adsorptive removal of heavy metal ions from aqueous solution. *Microporous Mesoporous Mater.* 2016, 221, 238–244.
15. L. Wang, X. Zhao, J. Zhang, Z. Xiong, Selective adsorption of Pb (II) over the zinc-based MOFs in aqueous solution-kinetics, isotherms, and the ion exchange mechanism. *Environ. Sci. Pollut. Res.* 2017, 24, 14198–14206.
16. H. Li, H. Liu, J. Zhang, Y. Cheng, C. Zhang, X. Fei, Y. Xian, Platinum Nanoparticle Encapsulated Metal−Organic Frameworks for Colorimetric Measurement and Facile Removal of Mercury (II). *ACS Appl. Mater. Interfaces* 2017, 9, 40716–40725.

17. X. Luo, T. Shen, L. Ding, W. Zhong, J. Luo, S. Luo, Novel thymine-functionalized MIL-101 prepared by post-synthesis and enhanced removal of Hg (2+) from water. *J. Hazard. Mater.* 2016, 306, 313–322.
18. Q.-R. Fang, D.-Q. Yuan, J. Sculley, J.-R. Li, Z.-B. Han, H.-C. Zhou, Functional Mesoporous Metal−Organic Frameworks for the Capture of Heavy Metal Ions and Size-Selective Catalysis. *Inorg. Chem.* 2010, 49, 11637–11642.
19. L. Liang, Q. Chen, F. Jiang, D. Yuan, J. Qian, G. Lv, H. Xue, L. Liu, H.-L. Jiang, M. Hong, *In situ* large-scale construction of sulfur-functionalized metal–organic framework and its efficient removal of Hg (II) from water. *J. Mater. Chem. A* 2016, 4, 15370–15374.
20. F. Luo, J. L. Chen, L. L. Dang, W. N. Zhou, H. L. Lin, J. Q. Li, S. J. Liu, M. B. Luo, High-performance Hg2+ removal from ultra-low-concentration aqueous solution using both acylamide- and hydroxyl-functionalized metal–organic framework. *J. Mater. Chem. A* 2015, 3, 9616–9620.
21. Y. Y. Xiong, J. Q. Li, L. L. Gong, X. F. Feng, L. N. Meng, L. Zhang, P. P. Meng, M. B. Luo,
22. F. Luo, Using MOF-74 for Hg2+ removal from ultra-low concentration aqueous solution. *J. Solid State Chem.* 2016, 246, 16–22.
23. S. Bhattacharjee, Y.-R. Lee, W.-S. Ahn, Post-synthesis functionalization of a zeolitic imidazolate structure ZIF-90: a study on removal of Hg (II) from water and epoxidation of alkenes. *CrystEngComm* 2015, 17, 2575–2582.

Appendix B. Supporting Information (SI) for

Chapter 4

Insight Studies on Metal-Organic Framework Nanofibrous Membrane Adsorption and Activation for Heavy Metal Ions Removal from Aqueous Solution

Johnson E. Efome, Dipak Rana*, Takeshi Matsuura, Christopher Q. Lan

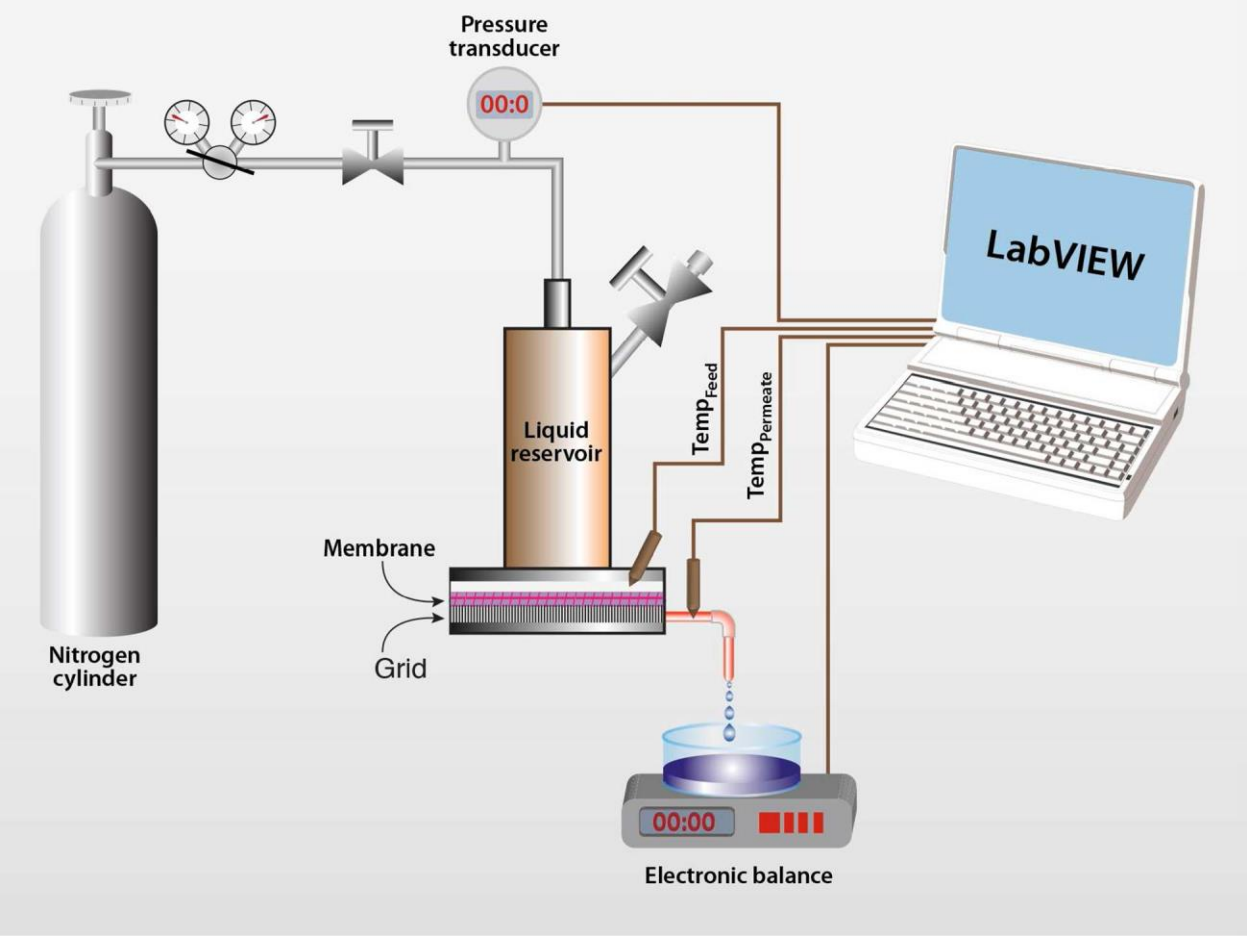

Figure B- 1. Schematic of the batch experimental setup.

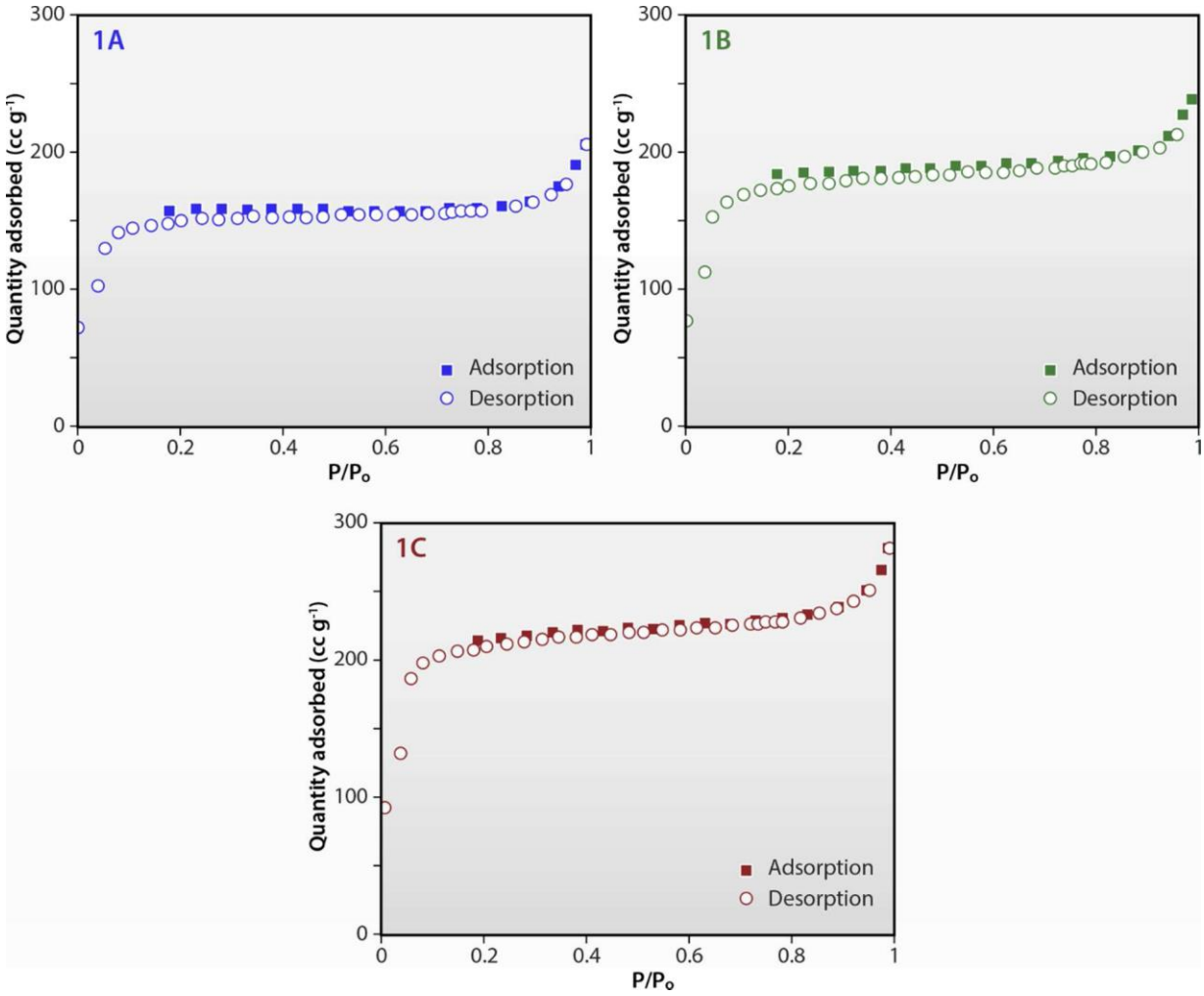

Figure B- 2. The BET plot of the MOF-808 materials.

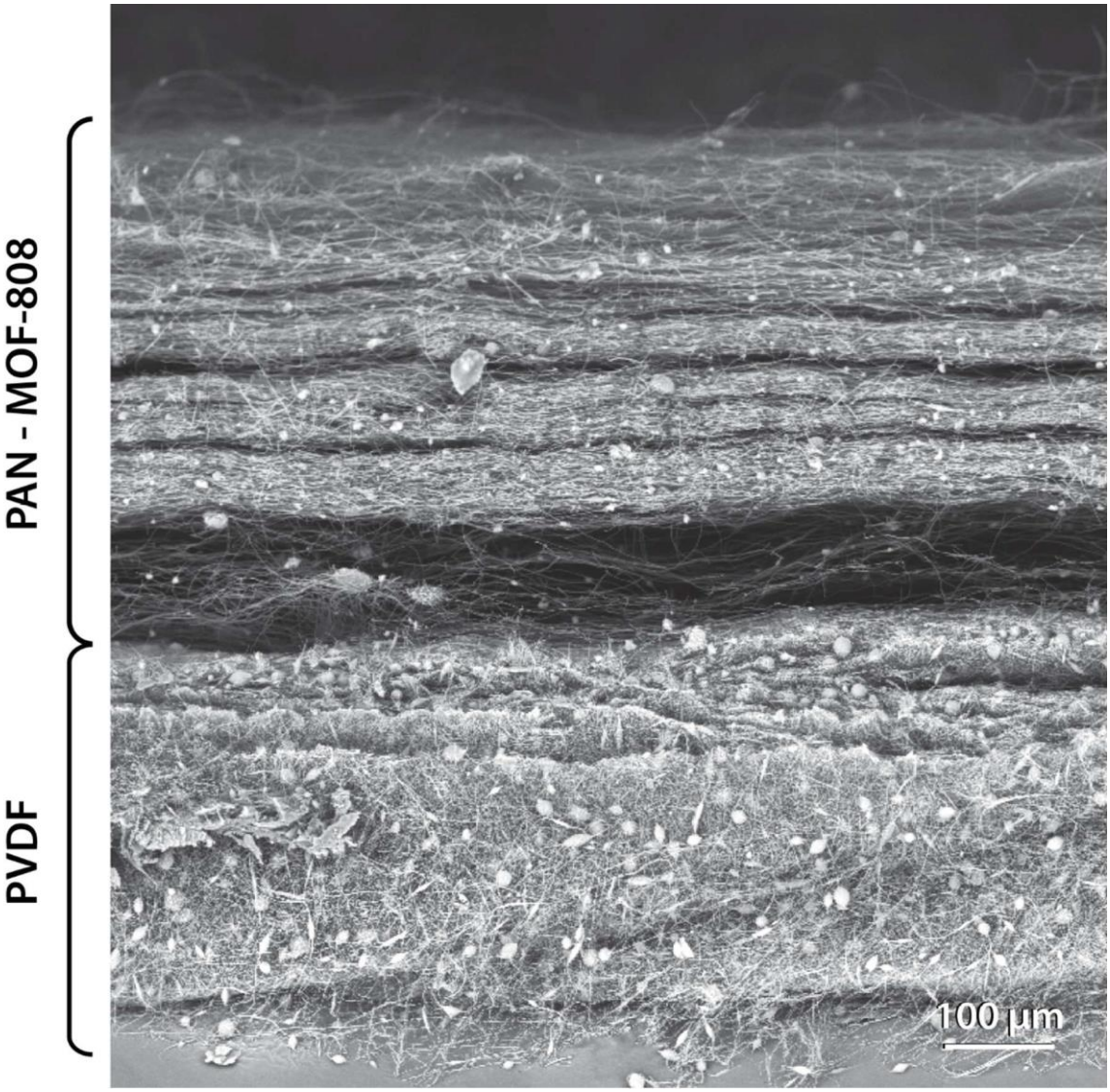

Figure B- 3. Multilayer nanofibrous membrane with top PAN with MOF-808, and bottom PVDF used for the filtration experiment.

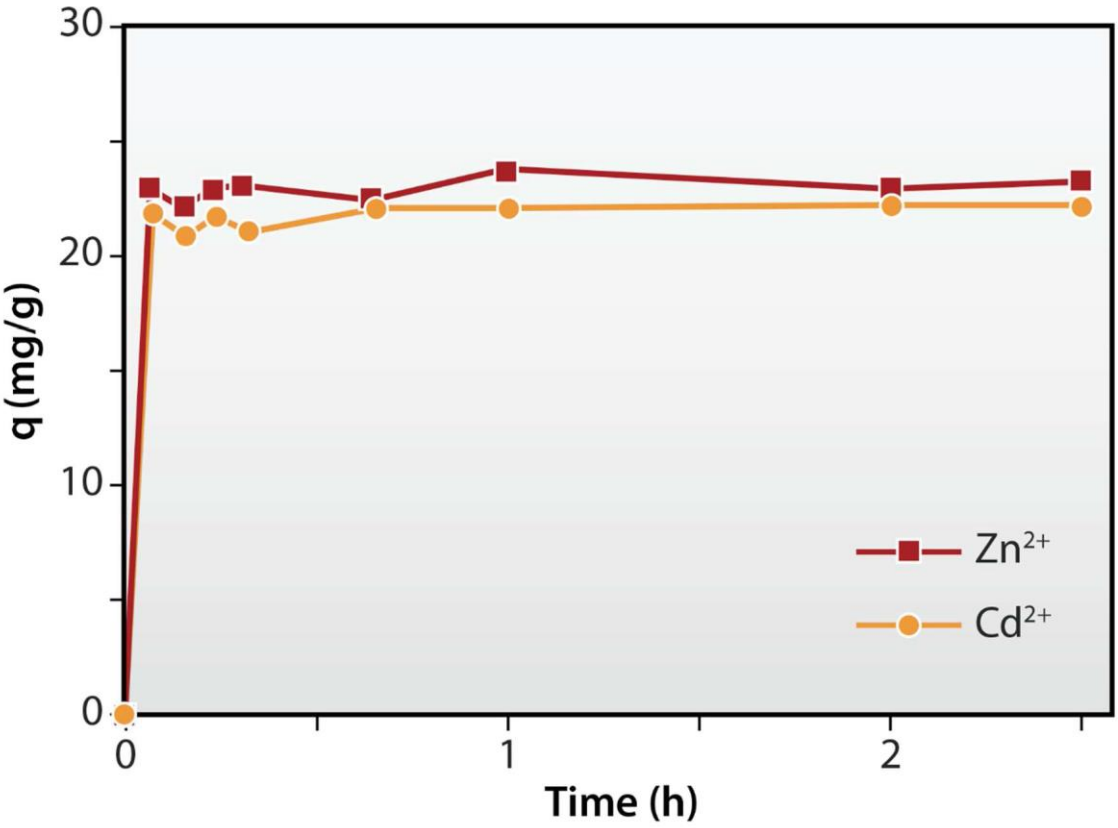

Figure B- 4. Kinetic experimental data showing equilibrium attained within 10 mins for MOF-808

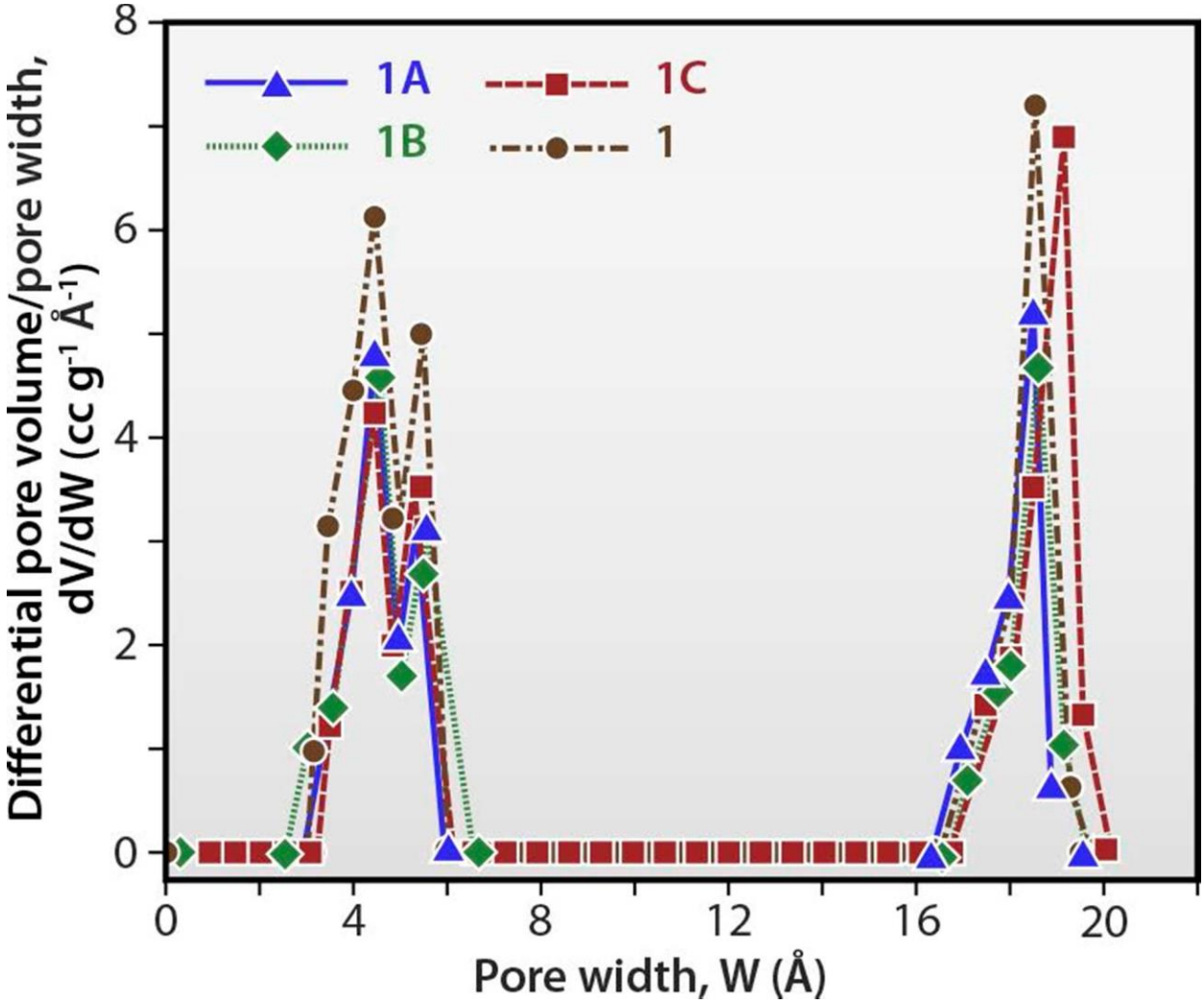

Figure B- 5. Differential pore volume / pore width versus pore width.

Table B- 1. Pore characteristics of MOFs.

Sample code	Surface area (m^2/g)	Pore volume (cm^3/g)	Average pore width (Å)
1	939	0.162	18.5
1A	748	0.124	18.1
1B	693	0.105	17.8
1C	1118	0.202	19.2

Table B- 2. Tensile properties of nanofibrous membranes measured at 25ºC and room temperature humidity.

Membrane	Young's modulus	Yield stress (MPa)	Yield strain (%)	Elongation at break (%)	Stress at break (MPa)
PAN nanofibers	127.3 ± 4.1	0.63 ± 0.11	30.6 ± 4.3	26.7 ± 4.1	0.26 ± 0.13
1a (PAN - MOF-808)	146.5 ± 6.2	1.61 ± 0.37	34.0 ± 7.8	43.3 ± 7.6	1.02 ± 0.74

Table B- 3. Kinetic parameter for Cd (II) and Zn (II) fitted with three models.

		First order			Second order			Intra-particle	
Adsorbate	Sorbent	k_1	q_e	R^2	k_2	q_e	R^2	k_{id}	R^2
Cd (II)	1	0.023	35.113	0.987	0.196	35.281	0.997	1.436	0.652
Zn (II)		0.047	39.031	0.756	0.853	2.89	0.998	0.149	0.483

k_1 [1/min], k_2 [mg/g min], k_{id} [mg/g min], and q_e [mg/g].

Table B- 4a. Freundlich model parameters for sorption of Cd (II).

Sorbent	k (mg/g (L/mg)$^{1/n}$)	n	R^2
PAN nanofibrous	0.693	1.908	0.958
1	3.161	1.761	0.905
1a	0.400	1.540	0.904

Table B-4b. Langmuir model parameters for sorption of Cd (II)

Sorbent	q_{max} (mg/g)	K_l (L/mg)	R_L	R^2
PAN nanofibrous	21.571	0.003	0.478	0.987
1	225.055	0.003	0.393	0.979
1a	43.901	0.002	0.481	0.951

Table B-4c. Temkin model parameters for sorption of Cd (II).

Sorbent	B	A_T (L/g)	b_T (J/mol)	R^2
PAN nanofibrous	6.533	0.028	379.249	0.984
1	34.273	0.05	72.289	0.968
1a	9.100	0.021	272.269	0.947

Table B-4d. Freundlich model parameters for sorption of Zn (II).

Sorbent	k (mg/g(L/mg)$^{1/n}$)	n	R^2
PAN nanofibrous	1.532	4.608	0.941
1	0.712	1.301	0.953
1a	0.226	1.512	0.919

Table B-4e. Langmuir model parameters for sorption of Zn (II).

Sorbent	q_{max} (mg/g)	K_l (L mg-1)	R^2
PAN nanofibrous	4.888	0.106	0.839
1	287.064	0.003	0.998
1a	56.667	0.021	0.840

Table B-4f. Temkin model parameters for Zn (II) sorption.

Sorbent	B	A_T (L/g)	b_T (J/mol)	R^2
PAN nanofibrous	0.897	1.281	2763.264	0.879
1	15.486	0.095	159.991	0.947
1a	3.090	0.088	801.773	0.865

Table B- 5. Selected peaks for activated PXRD spectra showing a shift in peak position in the either lower 2Θ or higher 2Θ.

	Simulated	1	1A	1B	1C
Peaks	2Θ(º)				
111	4.360	4.360	4.865	4.796	3.914
311	8.360	8.360	8.931	8.901	8.011
222	8.726	8.726	9.110	8.995	8.512
400	10.082	10.082	11.056	10.989	9.809
331	10.982	10.982	11.788	11.980	10.482
511	13.100	13.100	13.769	13.978	12.864

Table B- 6. The adsorption capacity, source of metal ion, pH, and time to adsorption equilibrium of Cd (II) and Zn (II).

Metal ion	Sorbent	Adsorption capacity [mg g-1]	Metal ion source	pH	Time to adsorption equilibrium [min]	Reference
Cd (II)	HKUST-1-	33	¶NA	7	80	Yang et al. [1]
	Cu-terepthalate MOF	100	Wastewater Cd salt / Sungun wastewater	7	120	Zou et al. [2]
	Manganese MOF	176	$Cd(NO_3)_2$	5	60	Qin et al. [3]
	TMU-5	43	$Cd(NO_3)_2$	10	15	Rahimi and Mohaghegh [4]
	UiO-66-	49	$Cd(NO_3)_2$	¶NA	240	Saleem et al. [5]
	1 (MOF-808)	225.06	$Cd(NO_3)_2$	4.5	10	This Work
	1A	160.86	$Cd(NO_3)_2$	4.5	10	This Work
	1C	247.51	$Cd(NO_3)_2$	4.5	10	This Work
	1a	43.90	$Cd(NO_3)_2$	4.5	60	This Work
Zn (II)	Cu-terepthalate MOF	150	Wastewater Zn salt / Sungun wastewater	7	120	Zou et al. [2]
	Activated carbon from *Ceiba*	24.1	¶NA	6	50	Rao et al. [6]
	Fe3O4@APS@AA-	43.4	$ZnCl_2$	5.5	45	Ge et al. [7]
	EDTA functionalized silica	74.1	¶NA	5.5	60	Kumar et al. [8]
	Fe3O4@MCM-41- NH2	82.0	¶NA	7	5	Mehdinia et al. [9]
	1 (MOF-808)	287.06	$ZnCl_2$	4.5	10	This work
	1A	206.64	$ZnCl_2$	4.5	10	This work
	1C	312.68	$ZnCl_2$	4.5	10	This work
	1a	56.67	$ZnCl_2$	4.5	60	This Work

¶NA: Not available

References

1. Yang, Q. X.; Zhao, Q. Q.; Ren, S. S.; Lu, Q. Q.; Guo, X. M.; Chen, Z. J. Fabrication of Core-Shell Fe3O4@MIL-100(Fe) Magnetic Microspheres for the Removal of Cr (VI) in Aqueous Solution. *J. Solid. State Chem*. 2016, *244*, 25–30.
2. Zou, F.; Yu, R.; Li, R.; Li, W. Microwave-Assisted Synthesis of HKUST-1 and Functionalized HKUST-1-@H3PW12O40: Selective Adsorption of Heavy Metal Ions in Water Analyzed with Synchrotron Radiation. *ChemPhysChem.* 2013, *14* (12), 2825–2832.
3. Qin, Q. D.; Wang, Q. Q.; Fu, D. F.; Ma, J. An Efficient Approach for Pb (II) and Cd (II) Removal using Manganese Dioxide formed *In Situ*. *Chem. Eng. J.* 2011, *172* (1), 68–74.
4. Rahimi, E.; Mohaghegh, N. Removal of Toxic Metal Ions from Sungun Acid Rock Drainage Using Mordenite Zeolite, Graphene Nanosheets, and a Novel Metal–Organic Framework. *Mine Water Environ*. 2015, *35* (1), 18–28.
5. Saleem, H.; Rafique, U.; Davies, R. P. Investigations on Post-Synthetically Modified UiO-66- NH2 for the Adsorptive Removal of Heavy Metal Ions from Aqueous Solution. *Microporous Mesoporous Mater*. 2016, *221*, 238–244.
6. Rao, M. M.; Chandra Rao, G. P.; Seshaiah, K.; Choudary, N.V.; Wang, M. C. Activated Carbon from *Ceiba pentandra* hulls, an Agricultural Waste, as an Adsorbent in the Removal of Lead and Zinc from Aqueous Solutions. *Waste Manage.* 2008, *28* (5), 849–858.
7. Ge, F.; Li, M.-M.; Ye, H.; Zhao, B.-X. Effective Removal of Heavy Metal Ions Cd2+, Zn2+, Pb2+, Cu2+ from Aqueous Solution by Polymer-Modified Magnetic Nanoparticles. *J. Hazard. Mater.* 2012, *211-212*, 366–372.

8. Kumar, R.; Barakat, M. A.; Daza, Y. A.; Woodcock, H. L.; Kuhn, J. N. EDTA Functionalized Silica for Removal of Cu (II), Zn (II) and Ni (II) from Aqueous Solution. *J. Colloid Interface Sci.* 2013, *408*, 200–205.
9. Mehdinia, A.; Shegefti, S.; Shemirani, F. Removal of Lead (II), Copper (II) and Zinc (II) Ions from Aqueous Solutions Using Magnetic Amine-Functionalized Mesoporous Silica Nanocomposites. *J. Braz. Chem. Soc.* 2015, *26* (11), 2249–2257.

Appendix C

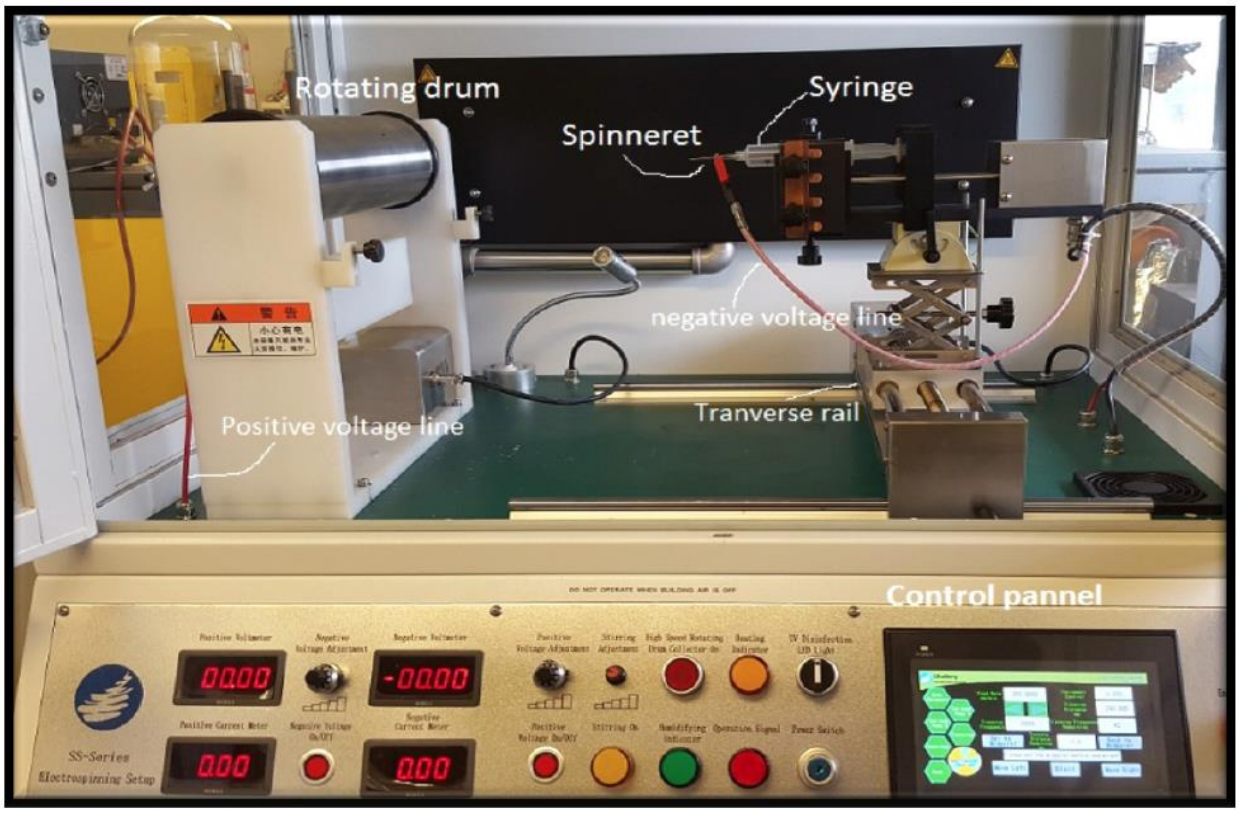

Figure C- 1. Photographic image of the laboratory electrospinning equipment.